HEAT TRANSFER AUGMENTATION IN A ROUND TUBE WITH WINGLET INSERTS

SURIYA CHOKPHOEMPHUN

A THESIS SUBMITTED IN PARTIAL FULFILLMENT
OF THE REQUIREMENT FOR THE DEGREE OF
DOCTOR OF ENGINEERING IN MECHANICAL ENGINEERING
FACULTY OF ENGINEERING
KING MONGKUT'S INSTITUTE OF TECHNOLOGY LADKRABANG

2014

HEAT TRANSFER AUGMENTATION IN A ROUND TUBE WITH WINGLET INSERTS

SURIYA CHOKPHOEMPHUN

A THESIS SUBMITTED IN PARTIAL FULFILLMENT
OF THE REQUIREMENT FOR THE DEGREE OF
DOCTOR OF ENGINEERING IN MECHANICAL ENGINEERING
FACULTY OF ENGINEERING
KING MONGKUT'S INSTITUTE OF TECHNOLOGY LADKRABANG
2014

KMITL-2014-EN-D-058-187

หัวข้อวิทยานิพนธ์	การเพิ่มการถ่ายเทความร้อนในท่อกลมโดยการสอดใส่แผ่นบาง
นักศึกษา	นายสุริยา โชคเพิ่มพูน
รหัสนักศึกษา	53610206
ปริญญา	วิศวกรรมศาสตรดุษฎีบัณฑิต
สาขาวิชา	วิศวกรรมเครื่องกล
พ.ศ.	2557
อาจารย์ที่ปรึกษาวิทยานิพนธ์	รศ.ดร.พงษ์เจต พรหมวงศ์

บทคัดย่อ

วิทยานิพนธ์นี้ได้ทำการศึกษาการเพิ่มการถ่ายเทความร้อนของเครื่องแลกเปลี่ยนความร้อนชนิดท่อกลม การทดสอบกระทำภายใต้สภาวะฟลักซ์ความร้อนที่ผิวคงที่ ในช่วงการไหลแบบปั่นป่วนที่เลขเรย์โนลด์ (*Re*) ระหว่าง 5300 ถึง 24,000 ผลการศึกษาการถ่ายเทความร้อนและการสูญเสียความดันแสดงอยู่ในพจน์เลขนัสเซิลท์ (Nu) และในพจน์ของตัวประกอบเสียดทาน (*f*) ตามลำดับ การศึกษาทดลองแบ่งออกเป็น 3 ส่วน ดังนี้

ส่วนที่ 1 การใช้ใบบิดที่มีจำนวนและการจัดเรียงที่แตกต่างกันซึ่งสามารถแบ่งเป็น 2 กลุ่ม ได้แก่ กลุ่มที่ 1 ใบบิดแบบหลวมใส่ไม่หนาแน่น (loose-fit twisted tapes) โดยใช้ใบบิดจำนวน 2 และ 3 ใบ โดยมีทิศทางการบิดแตกต่างกัน ที่อัตราส่วนการบิดเท่ากับ 4 และ 4.5 นำมาจัดเรียงในแนวตามแกนเดียวกัน กลุ่มที่ 2 ใบบิดแบบใส่แน่นเต็มท่อ (tight-fit twisted tapes) โดยใช้ใบบิดเดี่ยว ใบบิดคู่และใบบิดชุดจำนวน 3 และ 4 ใบ ที่มีอัตราส่วนการบิดเท่ากับ 4 เท่ากันแต่มีทิศทางการบิดที่แตกต่างกันมาจัดเรียงเป็นกลุ่มของใบบิดได้ทั้งหมด 8 รูปแบบ (2T1, 2T2, 3T1, 3T2, 4T1, 4T2, 4T3 และ 4T4) ผลการศึกษา พบว่าการถ่ายเทความร้อน การสูญเสียความดันและสมรรถนะเชิงความร้อนที่ได้จากกรณีการจัดเรียงใบบิดแบบวางทิศทางสลับกันมีค่าสูงกว่ากรณีการจัดเรียงใบบิดแบบวางทิศทางการบิดตามกัน โดยแนวโน้มของผลัพธ์มีค่าเพิ่มสูงขึ้นเมื่อจำนวนใบบิดที่ใช้มีจำนวนเพิ่มมากขึ้นและที่อัตราส่วนการบิดมีค่าลดลง การใช้ใบบิดกลุ่มที่ 1 (loose-fit twisted tapes) ให้ค่าสมรรถนะเชิงความร้อนสูงสุดมีค่าเท่ากับ 1.26 สำหรับกรณีการใช้ใบบิดจำนวน 3 ใบจัดเรียงแบบทิศทางการบิดสวนทางกันที่อัตราส่วนการบิดเท่ากับ 4 ซึ่งให้ค่าการถ่ายเทความร้อนและตัวประกอบความเสียดทานเพิ่มขึ้นประมาณ 1.52 และ 1.77 เท่าของท่อผิวเรียบ ตามลำดับ ในขณะที่การใช้ใบบิดกลุ่มที่ 2 (tight-fit twisted tapes) พบว่าค่าสมรรถนะเชิงความร้อนสูงสุดมีค่าเท่ากับ 1.33 เกิดขึ้นในกรณีการใช้ใบบิดจำนวน 4 ใบจัดเรียงแบบทิศทางการบิดสวนทางกันทั้งหมด (4T4) โดยให้ค่าการถ่ายเทความร้อนและตัวประกอบความเสียดทานเพิ่มสูงขึ้นกว่ากรณีท่อผิวเรียบประมาณ 2.12 และ 4.06 เท่าตามลำดับ

ส่วนที่ 2 การใช้ปีกเดี่ยวและปีกคู่รูปตัววีที่มีปลายวีชี้ทิศทางตามและทวนกระแสการไหล โดยจัดวางปีกให้มีมุมปะทะกับทิศทางการไหลหลักจำนวน 3 ค่า ได้แก่มุม 30° 45° และ 60° มีอัตราส่วนการขวางกั้นการไหลเท่ากับ 0.1 0.15 และ 0.2 ที่อัตราส่วนระยะพิตช์ของปีกจำนวน 4 ค่า ได้แก่ 0.5, 1.0, 1.5 และ 2.0 โดยการวางปีกขวางการไหลจะถูกติดตั้งบนโครงลวดครึ่งวงกลมและสอดใส่เข้าในท่อทดสอบโดยให้ปีกซึ่งวางต่อๆกันตามแนวยาวของท่อนั้นจะลอยอยู่บริเวณกลางหน้าตัดท่อตลอดเพื่อขวางและเบนการไหลหลัก ผลการศึกษา พบว่าค่าการถ่ายเทความร้อนและการสูญเสียความดันมีแนวโน้มเพิ่มสูงขึ้นเมื่ออัตราส่วนระยะพิตช์มีค่าลดลงในขณะที่อัตราส่วนการขวางกั้นการไหลและมุม

ปะทะการไหลมีค่าเพิ่มสูงขึ้น ภายใต้เงื่อนไขการทดลองเดียวกันจะเห็นได้ว่าการใช้ปีกคู่รูปตัววีชี้ทวนกระแสการไหลให้ค่าสมรรถนะเชิงความร้อนสูงสุดเท่ากับ 1.65 ในขณะที่กรณีปีกคู่รูปตัววีชี้ตามกระแสการไหลและกรณีปีกเดี่ยวมีค่าสมรรถนะเชิงความร้อนสูงสุดมีค่าเท่ากับ 1.47 และ 1.59 ตามลำดับ โดยเกิดขึ้นที่มุมปะทะการไหลเท่ากับ 30° อัตราส่วนการขวางกั้นการไหล 0.1 อัตราส่วนระยะพิตต์ 1.5 และเลขเรย์โนล์ดประมาณ 5300 สำหรับปีกทั้ง 3 รูปทรง รวมทั้งได้มีการนำเสนอถึงการศึกษาเชิงตัวเลขเพื่อแสดงพฤติกรรมการไหลและกลไกการเพิ่มการถ่ายเทความร้อนภายในท่อที่สอดใส่ปีกคู่รูปตัววีชี้ทวนกระแสการไหลที่มุมปะทะเท่ากับ 30° นอกจากนั้นทำการวิเคราะห์เพื่อหาสภาวะที่เหมาะสมที่สุดจากกรณีการสอดใส่ปีกคู่รูปตัววีชี้ทวนกระแสการไหลที่มุมปะทะการไหลเท่ากับ 30° พบว่าค่าสมรรถนะเชิงความร้อนสูงสุดมีค่าเท่ากับ 1.61 โดยเกิดขึ้นที่อัตราส่วนการขวางกั้นการไหล 0.13 อัตราส่วนระยะพิตต์ 1.4 และเลขเรย์โนล์ดประมาณ 5300

ส่วนที่ 3 การใช้ปีกเดี่ยวและปีกตัววีชี้เฉพาะทิศทางทวนกระแส โดยมีมุมปะทะการไหลเท่ากับ 30° เท่านั้น เนื่องจากให้ผลลัพธ์สมรรถนะที่ดีที่สุดตามที่รายงานในส่วนที่สอง กรณีนี้จะเหมือนกับกรณีในส่วนที่สองทุกประการ เว้นแต่ว่าปีกทั้งคู่จะวางบนผิวท่อเท่านั้นเพื่อเพิ่มกำลังการหมุนควงให้ชิดผิว รวมทั้งเพื่อลดแรงต้านและแรงเสียดทานการไหลจากการวางกลางท่อ โดยมีอัตราส่วนการขวางกั้นการไหลเท่ากับ 0.1, 0.15 และ 0.2 ที่อัตราส่วนระยะพิตต์ของปีกจำนวน 3 ค่า ได้แก่ 0.5, 1.0 และ 2.0 โดยปีกขวางการไหลมีการติดตั้งใน 2 ลักษณะได้แก่การติดตั้งบนโครงลวดครึ่งวงกลมเหมือนในส่วนที่สองและการติดตั้งบนแผ่นทึบบางแล้วสอดใส่เข้าในท่อทดสอบเพื่อให้ปีกอยู่ชิดติดผิวภายในท่อ ภายใต้ขอบเขตการศึกษานี้ พบว่าการถ่ายเทความร้อนและการสูญเสียความดันมีแนวโน้มเพิ่มสูงขึ้นเมื่ออัตราส่วนระยะพิตต์มีค่าลดลงและที่อัตราส่วนการขวางกั้นการไหลมีค่าเพิ่มสูงขึ้น กรณีการติดตั้งปีกทั้งสองลักษณะบนแผ่นทึบบางให้ค่าถ่ายเทความร้อนและการสูญเสียความดันที่สูงกว่ากรณีการติดตั้งบนโครงลวดครึ่งวงกลม โดยค่าค่าสมรรถนะเชิงความร้อนสูงสุดสำหรับกรณีปีกติดตั้งบนแผ่นทึบบาง ปีกติดตั้งบนโครงลวดครึ่งวงกลม ปีกตัววีติดตั้งบนแผ่นทึบบางและติดตั้งบนโครงลวดครึ่งวงกลมมีค่าเท่ากับ 1.75, 1.78, 1.77 และ 1.81 ตามลำดับ ที่เลขเรย์โนล์ดประมาณ 5300 อัตราส่วนการขวางกั้นการไหล 0.1 และอัตราส่วนระยะพิตต์ 0.5 ดังนั้นการจัดวางปีกที่ผิวท่อจึงให้สมรรถนะความร้อนเหนือกว่าการจัดวางตรงกลางท่อ

Thesis Title	Heat Transfer Augmentation in a Round Tube with Winglet Inserts
Student	Mr. Suriya Chokphoemphun
Student ID.	5361026
Degree	Doctor of Engineering
Program	Mechanical Engineering
Year	2014
Thesis Adviser	Assoc.Prof.Dr. Pongjet Promvonge

ABSTRACT

The thesis presents an experimental study on heat transfer enhancement in a round tube heat exchanger. The experiment was conducted in a uniform wall heat-fluxed tube by varying turbulent airflow for Reynolds number (*Re*) ranging from 5300 to 24,000. The present results on the heat transfer and flow friction characteristics are displayed in terms of Nusselt number (Nu) and friction factor (*f*), respectively. The layouts of the thesis are divided into three sections as follows:

Section 1 involves the different twisted-tape numbers and arrangements that can be classified into two groups. Group I: loose-fit twisted tape insert, deals with double and triple co- and counter-twisted tape inserts with two twist ratios, y/w=4 and 4.5 that are arranged by placing them along the axial plane. Group II: tight-fit twisted tape insert, is concerned with single, double, triple, and quadruple twisted-tape inserts at two twist ratios, y/w=4 and 5 for the single one while the rests at y/w=4 only are twisted in two different directions: left-twist (L_T) and right-twist (R_T), and arranged in 8 different forms (2T1, 2T2, 3T1, 3T2, 4T1, 4T2, 4T3 and 4T4). The experimental results reveal that the Nu, f and η obtained from counter-twisted tape arrangements higher than the co-twisted tape arrangements and tends to increase with the increment of tape numbers and the reduction of twist ratio. For the loose-fit twisted tapes, the maximum η is about 1.26 for the triple counter-twisted tape ($L_TR_TL_T$) insert at y/w=4 that yields the mean Nu and f of around 1.52 and 1.77 times the smooth tube, respectively. For the tight-fit twisted tapes, the maximum η is around 1.33 for the quadruple counter-twisted tape insert (4T4) that yields the mean Nu and f of about 2.12 and 4.06 times the smooth tube.

Section 2 is related to the winglet vortex generators (WVGs) arranged in angled and V-shaped winglets and placed along the core flow area. The V-winglet stems from a winglet pair formed in V-shape by letting V-tip point downstream (called VD-WVGs) and upstream (called VU-WVGs). The WVGs were arranged in the tube with three attack angles (α=30°, 45° and 60°), three winglet-height or blockage ratios ($B_R=e/D$=0.1 0.15 and 0.2) and four winglet-pitch ratios ($P_R=P/D$=0.5, 1.0, 1.5 and 2.0). The WVG elements were

tied together by putting two straight steel wires into the holes drilled on both end areas of the elements with two semicircular rod-supports on both ends of the wires. The experimental results show that the Nu and f values tend to increase with the reduction of P_R and the increment of B_R and α. At similar operating condition, the use of VU-WVGs leads to the highest η of about 1.65. The highest η values for the VD-WVGs and WVGs are, respectively, around 1.47 and 1.59, all at α=30°, B_R=0.1, P_R =1.5 and Re=5300. In addition, a numerical investigation is performed to study the flow structure and heat transfer enhancement mechanism in the tube inserted with 30° VU-WVGs. Also, the optimal condition analysis reveals that the maximum η around 1.61 is achieved for the 30° VU-WVGs with B_R=0.13 and P_R=1.4 at Re=5300.

Section 3 is concerned with the WVG modification in Section 2. The WVG and VU-WVG with α=30° were only selected due to its highest thermal performance and the modification is made by placing them on the inner tube wall. There were two types of WVG placements in the tube wall. One was similar method of using wire and rod-supports as in Section 2. The other was done by mounting the WVGs on the edges of a thin sheet or straight tape to keep WVGs placed tightly on the inner wall of test tube after insertion. Over the range investigated, the Nu and f increase with the reduction of P_R and the increment of B_R. The WVGs mounted on the straight tape provided the Nu and f higher than those on the wire supports. The η shows the increasing trend with the reduction of P_R and B_R. The maximum η for the WVGs-Wire, WVGs-Tape, VU-WVGs-Wire and VU-WVGs-Tape are, respectively, about 1.78, 1.75, 1.81 and 1.77 at Re=5300, B_R=0.1 and P_R=0.5. Therefore, the placement of WVGs on the inner tube wall provides higher thermal performance than that on the central core flow region.

ACKNOWLEDGEMENTS

It would not have been possible for writing up this doctoral thesis without the help and support of the kind people around me, to only some of whom it is possible to give particular mention here.

Above all, I would like to express my sincere gratitude to my thesis advisor, Assoc.Prof.Dr. Pongjet Promvonge, for his valuable help, teaching and advice; not only in the research methodologies but also in many other methodologies of life.

I warmly appreciate all lecturers and teachers at department of mechchanical engineering, faculty of engineering at King Mongkute Institute of Technology Ladkrabang for providing academic knowledge and guidance in the thesis.

I would like to thank my friends in Thermo-Fluid and CFD laboratory for suggestions and all their help throughout the period of this research.

In addition, I would like to acknowledge gratefully the Thailand Research Fund (TRF) for the financial support through the Royal Golden Jubilee Ph.D. program (Grant No. PhD/0143/2552).

Finally, I most gratefully acknowledge my family for their support of education and encouragement over the years.

CONTENTS

CONTENTS (cont'd)

CONTENTS (cont'd)

CONTENTS (cont'd)

LIST OF TABLES

LIST OF FIGURES

LIST OF FIGURES (cont'd)

LIST OF FIGURES (cont'd)

NOMENCLATURE

A	heat transfer surface area, m^2
B_R	blockage ratio
C_P	specific heat of fluid, $J.kg^{-1}.K^{-1}$
D	inner diameter of test tube, m
e	winglet width, m
f	friction factor
h	heat transfer coefficient, $W\ m^{-2}\ K^{-1}$
k	thermal conductivity of fluid, $W\ m^{-1}\ K^{-1}$
L	length of the test section, m
$\dot{m}$	mass flow rate, $kg\ s^{-1}$
Nu	Nusselt number
P	pitch length, m
P_R	pitch ratio
ΔP	pressure drop, Pa
Pr	Prandtl number
Q	heat transfer rate, W
Re	Reynolds number
$\tilde{T}$	mean temperature, K
T	temperature, K
η	thermal performance factor
U	mean air velocity, $m\ s^{-1}$
$\dot{V}$	volumetric flow rate, $m^3\ s^{-1}$
w	tape width, m
y	pitch length of twisted tape (180° rotation), m

Greek symbols

ρ	fluid density, $kg\ m^{-3}$
ν	kinematic viscosity, $m^2\ s^{-1}$

Subscripts

a	air
b	bulk
conv	convection
i	inlet

NOMENCLATURE (cont'd)

o	outlet
pp	pumping power
p	plain tube
s	swirl flow generator
w	tube wall

CHAPTER 1
INTRODUCTION

1.1 Statement and significance of the problem

A heat exchanger as an equipment to facilitate the convective heat transfer of fluid inside the tubes is frequently utilized in many industrial applications, such as chemical engineering process, heat recovery process, refrigeration systems, air conditioning systems, power plants and radiators for automobiles. Therefore, increasing the heat transfer coefficients and thermal performance of the heat exchangers can cause great impact in terms of saving the energy and reducing the material of the heat exchangers. Considering in business aspects, it is seen that the energy saving and material reduction leads to benefits in lower the operating cost and investment of the system.

Many researches have been carried out to investigate the influence of the different techniques/methods for increasing the thermal performance of heat exchangers, for decades. In general, heat transfer enhancement techniques can be classified into three categories. The first is the active method which requires external power sources, for example, fluid vibration, fluid injection and suction, and the use of electrostatic fields. The second is the passive method without stimulation by external power such as rough surfaces, extended surfaces and swirl flow devices to behave as turbulence promoter (sometimes called “turbulator”). The last is a combination of passive and active methods. Within the passive category, insertion of turbulator/swirl generator device is one of the most promising techniques. The major function of turbulator/swirl generator device is to reduce the thickness of the boundary layer and introducing better fluid mixing in ducts. These devices are considered to be advantageous compared with active techniques because the insert manufacturing process is simple and these techniques can be easily applied to existing heat exchangers.

Several turbulator devices have been employed for heat transfer augmentation in the heat transfer systems, both tubular and flat surface ducts/channels heat exchanger. For tubular heat exchangers, the wire coils, vortex rings, conical turbulators and especially the twisted/helical tapes have been widely used for enhancing heat transfer. Various configurations of twisted tapes are studied, such as typical twisted tapes with different twist ratios, tape numbers and tape-twist directions, and modified twisted-tapes with different geometries. In scrutiny of the maximum thermal performance factor for the inserted tubes, it was found in a range of some 0.9–1.2 for typical twisted-tape inserts and of about 1.1–1.5 for modified

twisted-tape inserts. For ducts/channels heat exchanger, the thermal performance can be enhanced mostly by the use of ribs, fins, winglets and baffles placed repeatedly on duct walls. There are several pertinent parameters that characterize the shape/geometry of the rib/winglet/baffle elements such as height (*e*), pitch length (*P*) and angle of attack (α). The optimum thermal performance factor for ribbed/baffled channels was much higher than that for the inserted tubes and was approximately 2.0 or above.

In the literature review above, it is commonly known that the twisted tapes has been widely used in enhancing the heat transfer in tubular heat exchangers, while other devices such as ribs/baffles/winglets have been extensively applied in flat-surfaced channel/duct heat exchangers. Therefore, the present research initiates the study on effect of various twisted-tape numbers for co- and counter-twist arrangements on enhanced heat transfer and pressure loss characteristics in a round tube. Then, two modifications of winglet vortex generators (WVG) placed repeatedly in the core flow and on the inner wall of tubular heat exchanger are experimentally investigated.

1.2 Goal and objective

The main aim of this work is to investigate the effect of insertion of multiple twisted-tapes with different tape-twist directions and modified winglet-type vortex generators on heat transfer and flow friction data of air heated in a round tube heat exchanger. In addition, the empirical correlations developed by relating the parameters of each turbulator used for guidance in the design and development of a high performance heat exchanger are determined.

1.3 Scope of the study

The thesis presents the experimentally investigation on the influence of various turbulator inserts on heat transfer (Nu), friction factor (*f*) and thermal performance enhancement (η) in a tubular heat exchanger. The experiment was carried out in a uniform wall heat-fluxed tube by varying turbulent airflow for Reynolds number ranging from 5300 to 24,000. The categories of turbulators can be divided into 3 sections as follows:

Section I : Multiple Twisted Tapes, The multiple twisted-tape inserts are investigated first and classified into 2 parts. In Part I, all twisted tapes made of 0.8 mm aluminum sheet were 1000 mm long and 8 mm width (*w*) with two different twist lengths (*y*): 32 and 36 mm (twist ratio, *y*/*w*=4 and 4.5). All the tapes were twisted in two different directions: left-twist (L_T) and right-twist (R_T), and were arranged in different forms. The double or triple small tapes were placed in the

same plane and held along the tube with straight steel wires having semicircular rod-supports at both ends. In Part II, all the twisted-tapes were inserted into the test tube with slightly tight fit and before insertion the multiple twisted-tapes were attached together by superglue. The twisted-tapes made of aluminum sheet were 1200 mm long and 0.8 mm thick. The typical single twisted-tape had a width (w) of 42 mm with two different twist lengths (y): 168 and 210 mm (twist ratio, y/w=4 and 5) while the rests were 21 mm wide with 84 mm twist-length (y/w=4). All the tapes were twisted in two different directions: left-twist (L_T) and right-twist (R_T), and were arranged in 8 different configurations (2T1, 2T2, 3T1, 3T2, 4T1, 4T2, 4T3 and 4T4).

Section II : Winglets Placed in Central Core Flow, Winglets in this section consist of winglets (WVGs) and winglet pairs that formed in V-shape elements arranged in two types: V-tip pointing downstream (VD-WVGs) and pointing upstream (VU-WVGs). All the WVGs made of aluminum strip were 0.3 mm thick with rounded ends. In the present work, the winglets with three different attack angles (α=30°, 45° and 60°), three different winglet-width (e) or blockage ratios ($B_R=e/D$=0.1, 0.15 and 0.2) and four different winglet pitch ratios ($P_R=P/D$=0.5, 1.0, 1.5 and 2.0) were offered. The WVG elements were tied together by putting two straight steel wires into the holes drilled on both end areas of the winglets with two semicircular rod-supports on both ends of the wires. The WVGs were inserted and mounted repeatedly along the central core flow of the test tube.

Section III : Winglets Placed on Inner Tube Wall, The winglets and winglet pairs (by letting V-tip point upstream) with an attack angle (α) of 30°. Three different winglet-width or blockage ratios ($B_R=e/D$=0.1 0.15 and 0.2) and winglet-pitch ratios ($P_R=P/D$=0.5, 1.0 and 2.0) were introduced. The WVGs were arranged in two types. One was that WVGs are tied together by putting two straight steel wires on both ends, similar to the case in section II. The other was mounting WVGs on edges of a thin sheet or straight tape to keep WVGs placed tightly on the inner wall of test tube after insertion.

1.4 Outlines of thesis

The thesis entitled “Heat transfer augmentation in a round tube with finned-tape insert” consists of 8 chapters. Chapter 1 presents the significance of the problems, goal and objective, scope of the study and thesis outlines. Chapter 2 describes the review of the past investigations on several turbulator devices used in tubular and duct/channel heat exchangers. Theories relevant to this research include fluid mechanics, heat transfer and principles of heat transfer enhancement as a basis for the study and understanding are explained in Chapter 3.

Chapter 4 deals with the facility, equipment, measuring tools and experimental set up. In addition, the turbulator geometry, methodology and data

processing are described in this chapter. Chapter 5 proposes the experimental result and discussion of heat transfer, friction factor and thermal performance factor obtained from using various twisted-tape turbulators.

Chapter 6 comprises the influence of winglet vortex generators (WVGs) with different geometry placed in the central core flow area on thermal performance enhancement. The optimal blockage ratio and pitch ratio for each of the winglets was determined in the last section. The experimental results of the winglets with/without straight tapes placed on the inner tube wall are presented in Chapter 7. Finally, the main conclusions of the results obtained in the present study are given in Chapter 8.

CHAPTER 2
LITERATURE REVIEW

2.1 Application of turbulators in tubular heat exchangers

For tubular heat exchanger systems, the twisted/helical tapes, wire coils, vortex rings and conical turbulators have been widely employed for enhancing the heat transfer in the system. The literature survey on different types of turbulators used in tubular heat exchangers is presented in Table 2.1

2.1.1 Twisted tapes

Twisted-tape inserts have been extensively investigated both experimentally and numerically for augmentation of the heat transfer rate in tube heat exchangers [1-25]. The insertion of twisted tapes in a tube is a simple passive technique for enhancing the heat transfer coefficient. For decades, many attempts have been made by focusing on the effect of geometry of twisted-tapes on heat transfer and flow friction in tubes with both typical and modified twisted-tapes. However, the typical twisted tapes have been adopted in different operating conditions in order to reduce pressure loss such as the work of Eiamsa-ard et al. [3] investigated the influence of the short-length typical twisted tapes with various tape-length ratios on Nu, f and thermal performance characteristics. The effect of typical twisted tapes with different twist ratios and clearance ratios was discussed by Bas and Ozceyhan [6]. Eiamsa-ard et al. [9] reported the heat transfer and pressure drop behaviors in a double pipe heat exchanger fitted with regularly-spaced twisted tape elements at different space ratios.

On the other hand, modifications of twisted tapes were made with a view to the increase in heat transfer rate rather than the reduction of friction loss. These can be divided into several categories such as tape-surface modification [2, 8, 15], tape-edge modification [5, 16, 20], helical left–right screw tapes [10, 11, 22], twisted tapes with wings [13, 17, 21] and alternate-axes twisted-tapes [14, 25]. The experimental investigation on Nu, f and thermal performance factor in a circular tube equipped with perforated twisted tape inserts with four different porosities was carried out by Bhuiya et al. [8]. Similar experimental work on twisted tapes consisting wire-nails with three different twist ratios fitted into a heat exchanger pipe was studied by Murugesan et al. [15]. Murugesan et al. [16, 20] also conducted experimentally on heat transfer rate and friction factor characteristics in a double pipe heat exchanger fitted with square-cut and V-cut twisted tapes.

Sivashanmugam and Suresh [10, 11] examined the heat transfer and friction factor characteristics in a tube inserted with regularly spaced helical screw-tape and full-length helical screw-tape inserts. Influences of the oblique delta-winglet twisted tape and straight delta-winglet twisted tape arranged by three different twist ratios and three wing-cut depth ratios were also described by Eiamsa-ard [17]. Wongcharee and Eiamsa-ard [21] employed the modified wing-formed twisted-tapes with three different shapes, namely, triangular, rectangular and trapezoidal wings on the tape edges for enhancing heat transfer in a tube.

Eiamsa-ard and Promvonge [14] performed an experimental work on turbulent flow and heat transfer characteristics in a tube equipped with two types of twisted tapes : (1) typical twisted tapes and (2) alternate clockwise and counterclockwise twisted-tapes. Nine different clockwise and counterclockwise twisted tapes with three twist ratios and three twist-angles were tested. Heat transfer enhancement in a tube using twisted tapes with both uniform and non-uniform alternate lengths at different alternate lengths in terms of alternate length to twist length ratio was studied by Eiamsa-ard [25].

2.1.2 Wire coils

Wire-coil insert is one of the heat transfer enhancement methods, which is extensively used in various heat exchanger systems [26-35]. The insertion of wire coils into a flow provides a swirling flow that helps improve fluid mixing between the core and the near-wall flow regions, thus the heat transfer is enhanced by rapid fluid mixing. Promvonge [27] investigated and compared the results between the effects of square cross-sectional and circular cross-sectional coil-wires on the heat transfer and flow friction characteristics in a tube having a uniform wall heat-flux and also, studied the wire coil insert in conjunction with a snail-type swirl generator mounted at the tube entrance as reported in Ref. [28]. Influences of wire coil inserts in common with twisted tapes on heat transfer and turbulent flow friction characteristics in a uniform heat-fluxed tube were examined by Promvonge [29]. In his work, the wire coil used as a turbulator was placed inside the test tube while the twisted tape was inserted into the wire coil to create a continuous impinging swirl flow along the tube wall.

Gunes et al. [30] presented the heat transfer enhancement and pressure drop of airflow in a tube heat exchanger inserted with an equilateral triangle cross-sectioned coiled-wire with three pitch ratios and two different ratio of equilateral triangle length side to tube diameter. Gunes et al. [31] again conducted an experimental work on heat transfer and pressure drop in a tube with coiled-wire inserts placed separately from the tube wall with three pitch ratios and two different

distances in turbulent flow regime. The heat transfer, friction factor and thermal performance behaviors in a tube equipped with combined devices between the twisted tape with two twist ratios and constant/periodically varying wire-coil pitch ratio were studied by Eiamsa-ard et al. [32]. The experimental results on thermal-hydraulic behaviors of three types of enhancement techniques based on artificial roughness as corrugated tubes, dimpled tubes and wire coils were reported by García et al. [35].

2.1.3 Other turbulators

Various styles of turbulator devices, apart from twisted tapes and wire coils, have been applied in order to improve the heat transfer rate in heat exchangers [36-50]. The effect of baffles with various ratios of pitch to tube diameter and baffle orientation angles on forced convection heat transfer for turbulent flow in a circular tube was investigated by Tandiroglu [37]. The heat transfer and flow friction characteristics in a uniform heat-fluxed tube with V-nozzle inserts for different pitch ratios were studied by Eiamsa-ard and Promvonge [38]. Promvonge [42] examined the effect of conical ring inserts with three different ring diameter ratios and for each ratio, the rings were placed with three different arrangements (converging conical ring, diverging conical ring and converging–diverging conical ring) on heat transfer enhancement in a tube.

Eiamsa-ard et al. [44] studied thermal characteristics in a concentric tube heat exchanger inserted with louvered strips with forward or backward arrangements at various inclination angles. The influences of using the propeller rotating freely with several blade numbers of the propeller and for different blade angles at several pitch ratios on heat transfer enhancement and pressure loss were reported by Eiamsa-ard et al. [45]. Kongkaitpaiboon et al. [46] presented the effect of the circular-ring turbulator arranged by various patterns, including three different diameter ratios and three different pitch ratios on the heat transfer and fluid friction characteristics in a heat exchanger tube. An experimental work was conducted by Eiamsa-ard and Promvonge [48] to investigate the heat transfer and friction factor characteristics in a tube fitted with diamond-shaped turbulators in tandem arrangements.

The convective heat transfer behaviors of turbulent tube flow through a straight tape with double-sided delta wings with forward/backward-wing arrangement and alternate axis were studied experimentally by Eiamsa-ard and Promvonge [49]. The augmentation of convective heat transfer in a single-phase turbulent flow by using helically corrugated tubes was experimentally investigated by Pethkool et al. [50]. Effects of pitch-to-diameter ratio and rib-height to diameter ratio of helically

corrugated tubes on the heat transfer enhancement, isothermal friction and thermal performance factor in a concentric tube heat exchanger were examined.

2.2 Application of turbulators in duct/channel heat exchangers

For duct/channel heat exchangers, the thermal performance can be elevated by the use of ribs, winglets and baffles as majority. Table 2.2 displays the literature survey of various turbulators used in duct/channel heat exchangers [51-90].

2.2.1 Ribs/Winglets/Baffles

For rib, winglet and baffle applications, Momin et al. [51] presented the results of an experimental investigation of the effect of geometrical parameters of V-shaped ribs on heat transfer and fluid flow characteristics of rectangular duct of solar air heater. The experimental investigation on heat transfer and friction factor behaviors in a rectangular duct roughened with repeated square cross-section split-ribs with a gap, on one broad wall arranged at an inclination with respect to the flow direction were also reported by Aharwal et al. [55]. The use of different cross-sections ribs (isosceles triangular, right-triangular wedge and rectangular shapes) with two rib arrangements, namely, in-line and staggered arrays to enhance heat transfer in a channel was introduced by Promvonge and Thianpong [58].

An experimental investigation on the heat transfer coefficient and friction factor by using artificial roughness in the form of specially prepared inverted U-shaped turbulators with different height ratios and pitch ratios on the absorber surface of an air heater duct was presented by Bopche and Tandale [61]. Promvonge et al. [66] experimentally studied the effect of combined ribs and winglet type vortex generators on convection heat transfer and friction loss behaviors for turbulent airflow through a constant heat-fluxed channel. Two rib arrangements, namely, in-line and staggered arrays, were introduced. Also, two pairs of the winglets with various attack angles were mounted on the duct entrance to create a longitudinal vortex flow through the test channel.

The heat and fluid flow characteristics of a rectangular duct having its one broad wall heated and roughened with periodic ‘discrete V-down rib’ in a turbulent region with several relative gap widths and relative gap positions were experimentally examined by Singh et al. [74]. Promvonge et al. [78] proposed a numerical investigation on laminar flow and heat transfer characteristics in a three dimensional isothermal wall square-channel fitted with inline 45° V-shaped baffles on two opposite walls and influences of different baffle height ratios and pitch ratios on thermal behaviors for a fully developed periodic condition were reported. The effect of zigzag-shaped baffles (Z-shaped baffle) placed on the isothermal-fluxed top wall

at three baffle- to channel-height ratios and pitch ratios on heat transfer augmentation in a rectangular channel was investigated experimentally and numerically by Sriromreun et al. [81].

2.2.2 Grooves

For groove applications, Jaurker et al. [52] carried out measurements to study the effect of rib-grooved artificial roughness with different relative roughness pitchs, relative roughness heights and relative groove positions on the heat transfer coefficient, friction factor and thermo-hydraulic performance of a solar air heater duct. An experimental work on Nu and f of a fully developed turbulent flow in a rectangular duct having repeated integral transverse chamfered rib-groove roughness on one broad wall with various relative roughness pitchs, chamfer angles, relative groove positions and relative roughness heights was performed by Layek et al. [54]. A numerical investigation of turbulent forced convection in a two dimensional channel with periodic transverse grooves on the lower channel wall with different groove-width to channel-height ratios while the groove pitch ratio and the depth ratio are fixed throughout was conducted by Eiamsa-ard and Promvonge [56].

Thereafter, Eiamsa-ard and Promvonge [59] examined the combined effects of rib-grooved turbulators on the turbulent forced convection heat transfer and friction characteristics in a rectangular duct having a uniform heat-flux boundary condition. In their work, three types of rib-groove arrangements: rectangular-rib and triangular-groove, triangular-rib and rectangular-groove and triangular-rib with triangular-groove were offered. Skullong et al. [89] presented an experimental study on turbulent flow and heat transfer characteristics in a solar air heater channel fitted with combined wavy-rib and groove turbulators. The results of wavy ribs placed at an attack angle of 45°, various rib-pitch to channel-height ratios, and a single rib-to-channel height ratio with three types of rib arrangements, namely, rib-groove on the upper wall only, inline rib-groove, and staggered rib inline groove on two principal walls were reported.

2.2.3 Other turbulators

For other turbulators, Effects of insertion of full-length wire coil and wire-coil elements with various free-space lengths used as turbulator on heat transfer and turbulent flow friction characteristics in a uniform heat-flux square duct were experimentally investigated by Eiamsa-ard et al. [79]. An experimental study was carried out to determine the heat transfer and flow characteristics of a solar air heater having roughened duct with dimple-shaped roughness arranged in angular fashion on the absorber plate were reported by Sethi et al. [83].

Table 2.1 Application of turbulators in tubular heat exchangers.

Authors	Conditions and results			Configuration
[1] 2007	Broken twisted tape			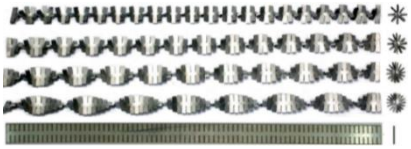
	Air : *Re*=1000–40,000			
	Twisted tapes with the twist ratios of 1, 1.5, 2, 2.5 and ∞			
	Nu/Nu_0	f/f_0	η	
	1.28–2.40	2.0–4.7	0.99–1.80	
[2] 2007	Serrated twisted tape			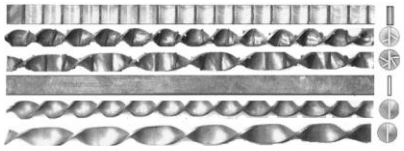
	Air : *Re*=5000–25,000			
	Twisted tape with twist ratio of 1.56, 1.88, 2.81 and ∞			
	Nu/Nu_0	f/f_0	η	
	1.31–4.80	2.0–78.0	0.65–1.60	
[3] 2009	Short-length twisted tape			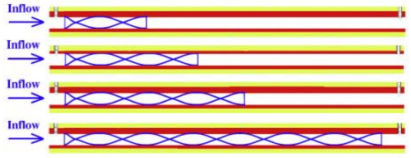
	Air : *Re*=4000–20,000			
	Twisted tape with several tape-length ratios 0.29, 0.43, 0.57 and 1.0			
	Nu/Nu_0	f/f_0	η	
	1.1–1.37	1.6–2.4	0.85–1.05	
[4] 2010	Dual twisted tape			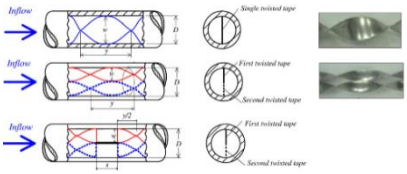
	Air : *Re*=4000–19,000			
	Single tape, full-length dual tapes and regularly-spaced dual tapes with 3 different space ratios			
	Nu/Nu_0	f/f_0	η	
	2.32–2.46	2.13–2.55	0.8–1.1	
[5] 2010	Serrated twisted tape			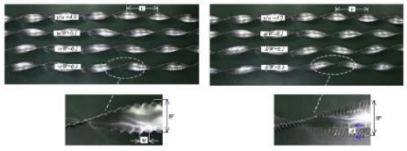
	Air : *Re*=4000–20,000			
	Twisted tape with different serration width ratio (0.1, 0.2 and 0.3) and serration depth ratio (0.1, 0.2 and 0.3)			
	Nu/Nu_0	f/f_0	η	
	1.32–1.42	2.49–3.33	0.97–1.17	

Table 2.1 (cont'd)

Authors	Conditions and results			Configuration
[6] 2012	Twisted tape separately from wall			
	Air : *Re*=5132–24,989			
	Twisted tape with twist ratio of 2, 2.5, 3, 3.5 and 4 and clearance ratios of 0.0178 and 0.0357			
	Nu/Nu_0	f/f_0	η	
	1.36–2.75	2.2–4.0	1.18–1.76	
[7] 2012	Helically twisted tapes			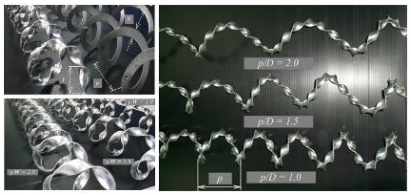
	Air : *Re*=6000–20,000			
	Helically twisted tape with twist ratios of 2, 2.5 and 3, and helical pitch ratios of 1, 1.5 and 2			
	Nu/Nu_0	f/f_0	η	
	1.73–2.72	4–46	0.6–1.3	
[8] 2013	Perforated twisted tape			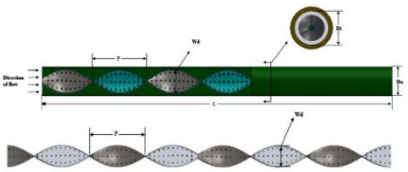
	Air : *Re*=7200–49,800			
	Perforated twisted tape with different porosities of 1.6, 4.5, 8.9 and 14.7%			
	Nu/Nu_0	f/f_0	η	
	2.1–4.4	2.1–4.6	1.28–1.59	
[9] 2006	Regularly spaced twisted tape			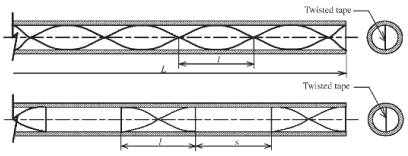
	Water : *Re*=2000–12,000			
	Twisted tape with twisted ratios of 6.0 and 8.0 and twisted tape with free space ratios 1.0, 2.0, and 3.0			
	Nu/Nu_0	f/f_0	η	
	2.21–2.79	1.94–4.26	0.63–1.05	
[10] 2007	Spaced helical screw-tape			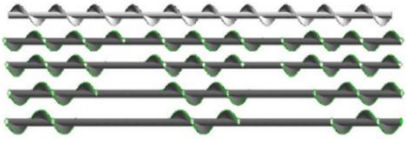
	Water : *Re*=6000–14,000			
	Helical screw with spacer length 100, 200, 300, and 400 mm			
	Nu/Nu_0	f/f_0	η	
	–	–	–	

Table 2.1 (cont'd)

Authors	Conditions and results			Configuration
[11] 2007	Helical screw-tape			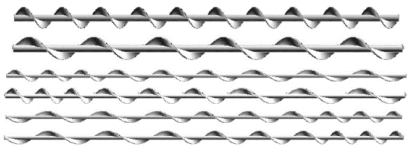
	Water : *Re*=2700–13,500			
	Full-length helical screw element of different twist ratio, and increasing and decreasing order of twist ratio			
	Nu/Nu_0	f/f_0	η	
	–	–	–	
[12] 2009	Modified twisted tape			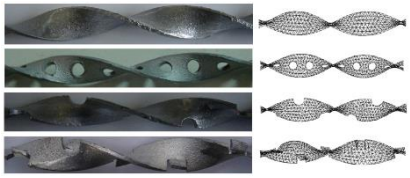
	Water : *Re*=2950–11,800			
	The classic and modified twisted tape (perforated, notched and jagged twisted tape)			
	Nu/Nu_0	f/f_0	η	
	1.33–2.49	4.4–8.7	0.9–1.22	
[13] 2010	Twisted tape with wings			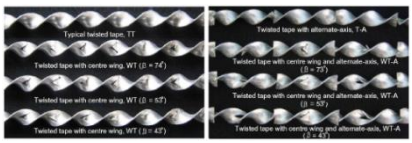
	Water : *Re*=5200–22,000			
	Twisted tape with wings along center line at different attack angles of 43° 53° and 74°			
	Nu/Nu_0	f/f_0	η	
	1.6–2.8	4.4–8.4	0.95–1.4	
[14] 2010	C-CC twisted tape			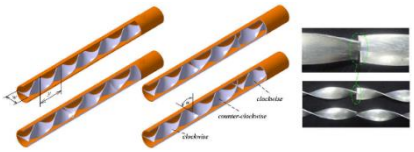
	Water : *Re*=3000–27,000			
	Typical, alternate clockwise and counterclockwise twisted tapes with different twist ratios and twist angles			
	Nu/Nu_0	f/f_0	η	
	1.27–1.91	3.42–5.1	0.96–1.4	
[15] 2010	Wire-nails twisted tape			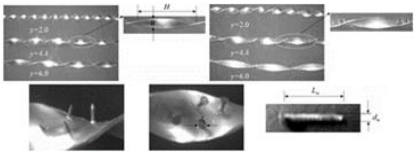
	Water : *Re*=2000–12,000			
	Twisted tape consisting wire nails and plain twisted tapes with twist ratios of 2.0, 4.4 and 6.0			
	Nu/Nu_0	f/f_0	η	
	1.47–1.98	3.22–4.26	1.0–1.32	

Table 2.1 (cont'd)

Authors	Conditions and results			Configuration
[16] 2010	Square-cut twisted tape			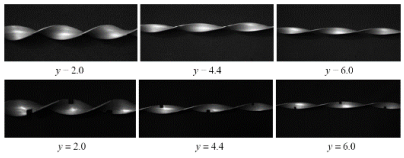
	Water : *Re*=2000–12,000			
	Square-cut twisted tapes and plain twisted tapes with twist ratios of 2.0, 4.4 and 6.0			
	Nu/Nu_0	f/f_0	η	
	1.05–1.81	2.45–3.81	0.98–1.27	
[17] 2010	Delta-winglet twisted tape			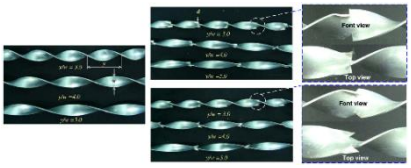
	Water : *Re*=3000–27,000			
	The oblique and straight delta winglet twisted tape with three twist ratios and three depth of wing cut ratios			
	Nu/Nu_0	f/f_0	η	
	1.10–2.55	2.50–7.02	0.88–1.24	
[18] 2010	Peripherally-cut twisted tape			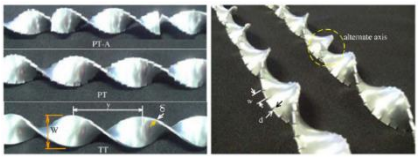
	Water : *Re*=5000–20,000			
	Peripherally-cut twisted tape with 3 different peripherally-cut width ratios (0.11, 0.22 and 0.33)			
	Nu/Nu_0	f/f_0	η	
	1.50–2.84	6–11	0.86–1.25	
[19] 2010	Peripherally-cut twisted tape			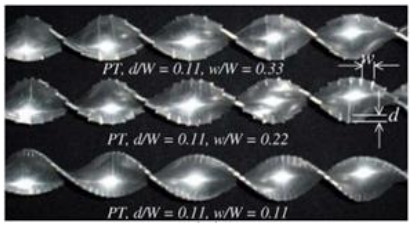
	Water : *Re*=1000–20,000			
	Peripherally-cut twisted tapes with different tape depth ratios, each with different tape width ratios			
	Nu/Nu_0	f/f_0	η	
	1.3–3.3	3.8–12.2	0.87–1.42	
[20] 2011	V-cut twisted tape			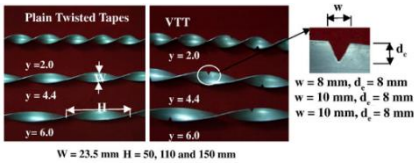
	Water : *Re*=2000–12,000			
	V-cut twisted tape with 3 twist ratios and 3 different combinations of depth and width ratios			
	Nu/Nu_0	f/f_0	η	
	1.36–2.46	2.49–5.86	1.07–1.27	

Table 2.1 (cont'd)

Authors	Conditions and results			Configuration
[21] 2011	Twisted tape with wings			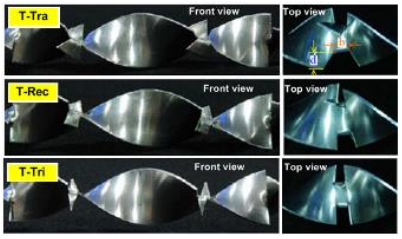
	Water : *Re*=5500–22,000			
	Twisted tapes with alternate-axes and wings with three different wing-chord ratios and constant twist ratio of 4.0			
	Nu/Nu_0	f/f_0	η	
	1.65–2.85	3.6–7.9	1.06–1.42	
[22] 2011	Helical screw-tape			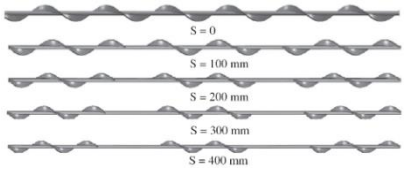
	Water : *Re*=570–1310			
	Full length helical screw element of different twist ratio and helical screw inserts with different spacer length			
	Nu/Nu_0	f/f_0	η	
	–	–	–	
[23] 2011	Jagged twisted tape			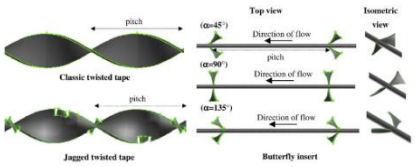
	Water : *Re*=3000–17,000			
	Three types of tube insert including butterfly, classic and jagged twisted tape.			
	Nu/Nu_0	f/f_0	η	
	–	–	–	
[24] 2012	Short-length twisted tapes			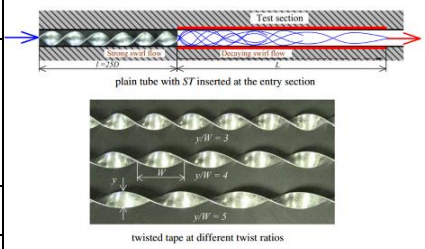
	Water : *Re*=5200–15,300			
	Short-length twisted tapes with three different twist ratios were applied at the entrance of the test section			
	Nu/Nu_0	f/f_0	η	
	1.05–1.66	–	0.93–1.03	
[25] 2013	Uniform/non-uniform twisted tape			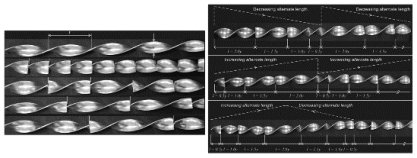
	Water : *Re*=5000–21,500			
	Twisted tapes with uniform and non-uniform alternate axes at different alternate lengths			
	Nu/Nu_0	f/f_0	η	
	1.25–2.95	3.3–10	0.89–1.38	

Table 2.1 (cont'd)

Authors	Conditions and results			Configuration
[26] 2008	Wire coils			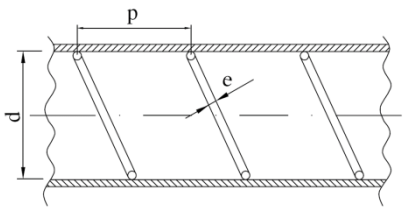
	Water : *Re*=80–90,000			
	Six wire coils within a geometrical range of helical pitch 1.17–2.68 and wire diameter 0.07-0.10			
	Nu/Nu_0	f/f_0	η	
	–	–	–	
[27] 2008	Coiled square wires			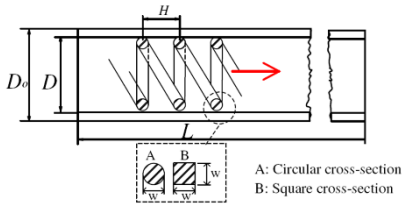
	Air : *Re*=5000–25,000			
	wires coil with two different spring coiled wire pitches			
	Nu/Nu_0	f/f_0	η	
	1.8–2.6	5–9	1.1–1.3	
[28] 2008	Coiled-wire with snail entry			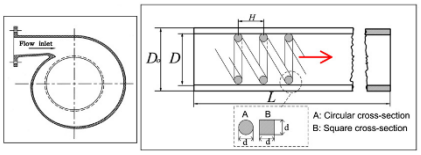
	Air : *Re*=5000–25,000			
	Square cross section wires coil with a snail-type swirl generator			
	Nu/Nu_0	f/f_0	η	
	3.4–3.9	42–50	0.9–1.1	
[29] 2008	Wire coil and twisted tape			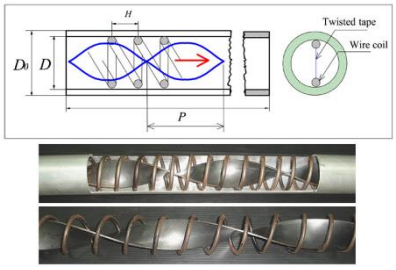
	Air : *Re*=3000–18,000			
	Wire coils with different coil pitch in conjunction with twisted tapes			
	Nu/Nu_0	f/f_0	η	
	3.0–6.5	27–75	0.85–1.53	
[30] 2010	Equilateral triangle coiled wire			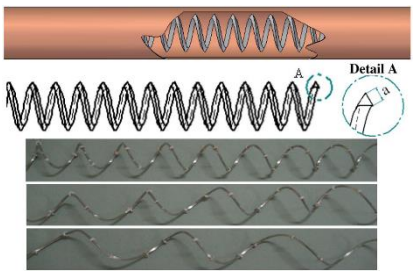
	Air : *Re*=3500–27,000			
	Equilateral triangular coiled wire with different pitch ratios and ratio of triangle length side to tube diameter			
	Nu/Nu_0	f/f_0	η	
	1.27–2.5	3–6	0.88–1.36	

Table 2.1 (cont'd)

Authors	Conditions and results			Configuration
[31] 2010	Coiled wire separately from tube wall			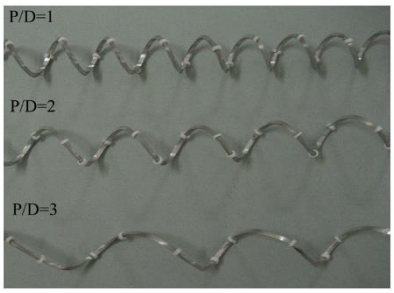
	Air : *Re*=4105–26,400			
	Coiled wire with three different pitch ratios and two different distances from tube wall			
	Nu/Nu_0	f/f_0	η	
	1.6–3.1	5–8	1–1.5	
[32] 2010	Non-uniform wire coil and twisted			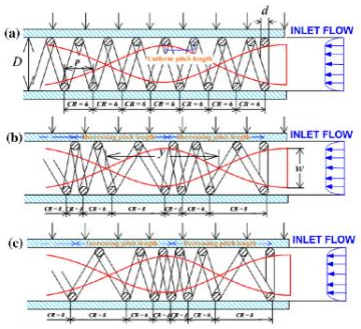
	Air : *Re*=4600–20,000			
	Twisted tape combined with constant and periodically varying wire coil pitch ratio			
	Nu/Nu_0	f/f_0	η	
	2.3–3.7	8–27	0.97–1.2	
[33] 2010	Helical wire coil			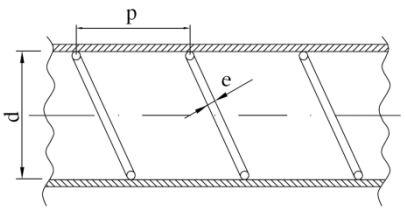
	Water : *Re*=4200–49,000			
	Wire coils with helical pitch in rang 0:156–0:354 and wire diameter in rang 0:027–0:094			
	Nu/Nu_0	f/f_0	η	
	–	–	–	
[34] 2011	Equilateral triangle coiled wire			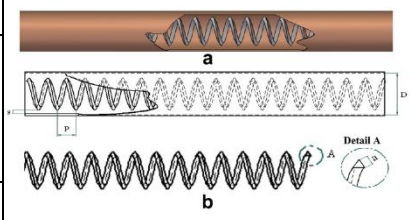
	Air : *Re*=13,200–19,800			
	Optimization of design parameters in a tube with coiled wire inserts by Taguchi method			
	Nu/Nu_0	f/f_0	η	
	–	–	–	
[35] 2012	Wire coils			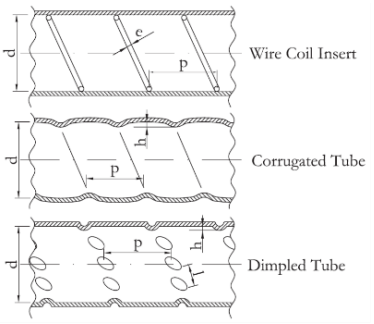
	Air : *Re*=20–20,000			
	The comparison of wire coils with corrugated tubes and dimpled tubes			
	Nu/Nu_0	f/f_0	η	
	–	–	–	

Table 2.1 (cont'd)

Authors	Conditions and results			Configuration
[36] 2004	Conical-ring turbulators			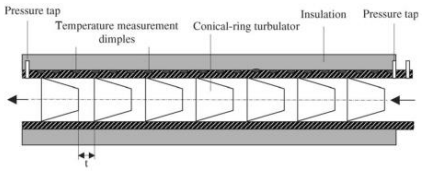
	Air : *Re*=5000–20,000			
	Conical-rings with 10, 20 and 30 mm pitches			
	Nu/Nu_0	f/f_0	η	
	–	–	0.86–1.17	
[37] 2006	Half circle baffled			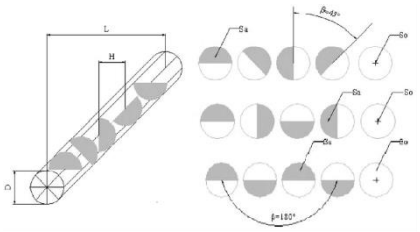
	Air : *Re*=3000–20,000			
	Baffle with different pitch to tube inlet diameter ratio and baffle orientation angle			
	Nu/Nu_0	f/f_0	η	
	–	–	–	
[38] 2006	V-nozzle turbulators			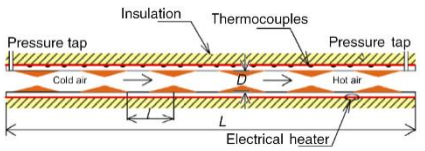
	Air : *Re*=8000–18,000			
	V-nozzle arrangements with different pitch ratios of 2.0, 4.0, and 7.0			
	Nu/Nu_0	f/f_0	η	
	3.16–3.70	–	0.85–1.19	
[39] 2007	Conical-nozzle turbulators			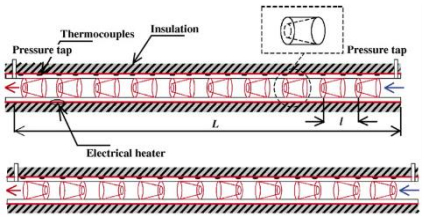
	Air : *Re*=8000–18,000			
	Diverging and converging nozzle arrangement with various pitch ratios of 2.0, 4.0, and 7.0.			
	Nu/Nu_0	f/f_0	η	
	3.36–4.44	–	–	
[40] 2007	V-nozzle turbulator and snail entry			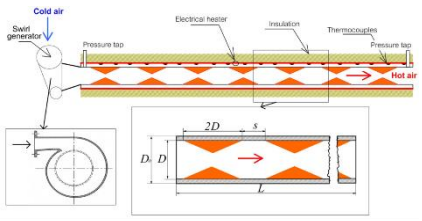
	Air : *Re*=8000–18,000			
	V-nozzles with three different pitch ratios of 2.0, 4.0, and 7.0 inserts in conjunction with a snail entry			
	Nu/Nu_0	f/f_0	η	
	3.44–3.94	22–61	0.7–1.15	

Table 2.1 (cont'd)

Authors	Conditions and results			Configuration
[41] 2007	Conical-nozzle and snail entry			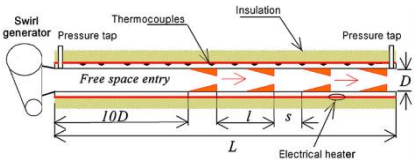
	Air : *Re*=8000–18,000			
	Free-spacing snail entry together with conical-nozzle turbulators with three different pitch ratios			
	Nu/Nu_0	f/f_0	η	
	–	–	0.65–1.19	
[42] 2008	Conical ring			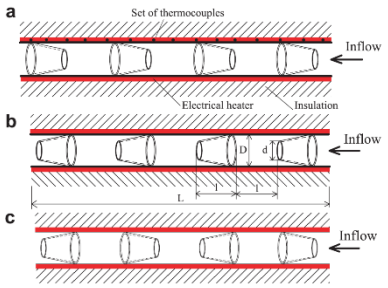
	Air : *Re*=6000–26,000			
	Conical rings with different diameter ratios of the ring to tube diameter and different arrangements			
	Nu/Nu_0	f/f_0	η	
	1.91–4.33	–	0.9–1.8	
[43] 2008	Circular cross sectional rings			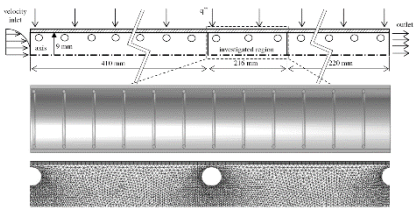
	Air : *Re*=4475–43,725			
	Circular cross sectional rings with five different spacings between the rings			
	Nu/Nu_0	f/f_0	η	
	–	–	0.95–1.18	
[44] 2008	Louvered strip			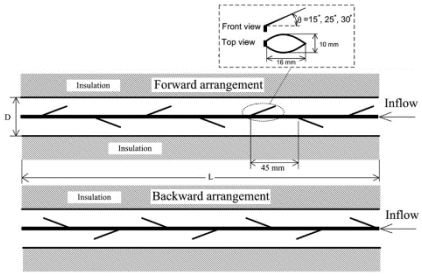
	Water : *Re*=6000–42,000			
	Louvered strips with forward or backward arrangements, and various inclined angles			
	Nu/Nu_0	f/f_0	η	
	1.2–4.4	1.1–8.7	0.9–2.6	
[45] 2009	Propeller type swirl generators			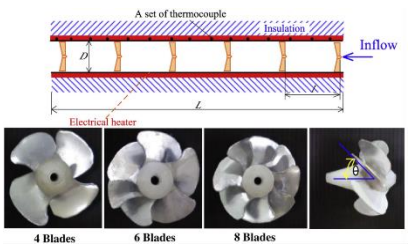
	Air : *Re*=4000–21,000			
	Propeller type swirl generators at several pitch ratios, blade numbers and blade angles			
	Nu/Nu_0	f/f_0	η	
	1.6–2.3	–	0.82–1.19	

Table 2.1 (cont'd)

Authors	Conditions and results			Configuration
[46] 2010	Circular-ring turbulator			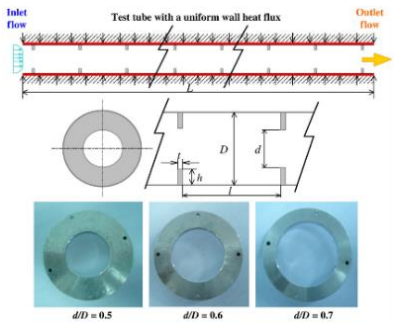
	Air : *Re*=4000–20,000			
	Circular-ring turbulator with different diameter ratios and different pitch ratios			
	Nu/Nu_0	f/f_0	η	
	1.6–2.9	5–70	0.55–1.07	
[47] 2010	Perforated conical-rings			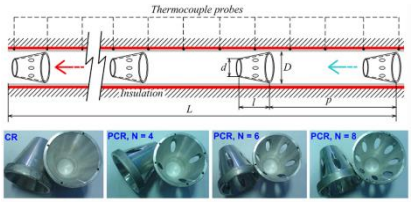
	Air : *Re*=4000–20,000			
	Perforated conical-rings used are of different pitch ratios and different numbers of perforated holes			
	Nu/Nu_0	f/f_0	η	
	1.65–3.39	2.3–7.0	0.54–0.92	
[48] 2010	Diamond-shaped			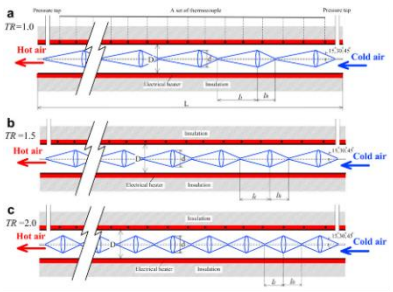
	Air : *Re*=3500–16,500			
	Tandem diamond-shaped turbulators with different cone angle and the tail length ratio			
	Nu/Nu_0	f/f_0	η	
	–	–	0.78–1.12	
[49] 2011	Double-sided Delta-wing Tape			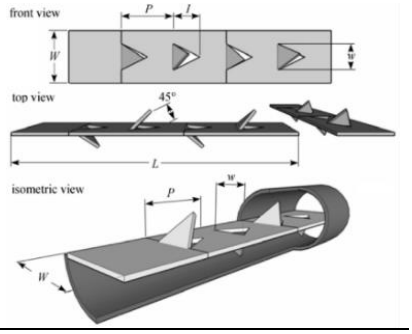
	Air : *Re*=4000–20,000			
	Straight tape with different double-sided delta wing arrangement, wing-width ratios and wing-pitch ratios			
	Nu/Nu_0	f/f_0	η	
	1.8–2.7	5–15	0.9–1.2	
[50] 2011	Helically corrugated tube			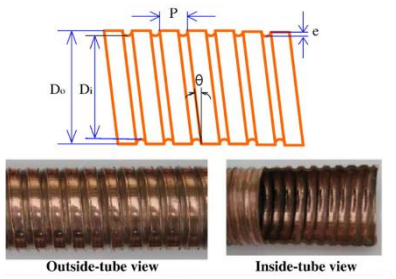
	Water : *Re*=5500–60,000			
	Helically corrugated tube with different pitch to diameter ratio and rib height to diameter ratio			
	Nu/Nu_0	f/f_0	η	
	1.1–3.0	1.45–2.15	1.0–2.35	

Table 2.2 Application of turbulators in duct/channel heat exchangers.

Authors	Conditions and results			Configuration
[51] 2002	V-shaped rib			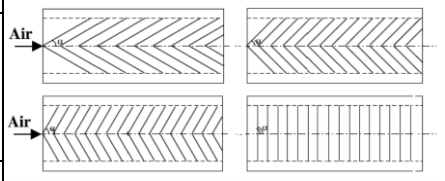
	Air : *Re*=2500–18,000			
	V-rib with relative roughness height of 0.02–0.034 and angle of attack of flow of 30°–90°			
	Nu/Nu_0	f/f_0	η	
	1.3–2.3	1.36–2.83	1.1–1.8	
[52] 2006	Rib-grooved			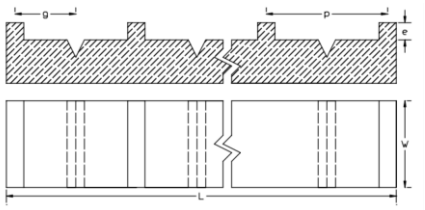
	Air : *Re*=3000–21,000			
	Rib with variation of relative roughness height and relative roughness pitch, groove position to			
	Nu/Nu_0	f/f_0	η	
	–	–	1.1–1.8	
[53] 2007	Metal grit ribs			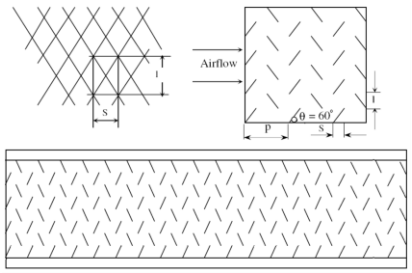
	Air : *Re*=4000–17,000			
	Metal grit ribs with different relative length, height and pitch			
	Nu/Nu_0	f/f_0	η	
	–	–	–	
[54] 2007	Transverse chamfered rib-groove			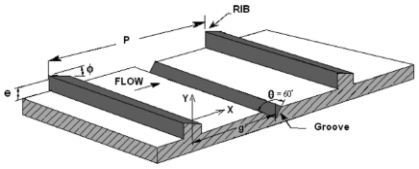
	Air : *Re*=3000–21,000			
	Rib with different relative pitch, relative height chamfer angle and groove position to pitch ratio			
	Nu/Nu_0	f/f_0	η	
	1.8–2.6	2.2–3.4	–	
[55] 2008	Inclined rib			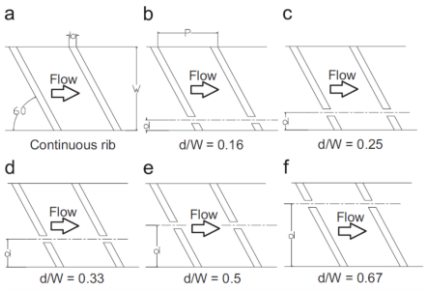
	Air : *Re*=3000–18,000			
	Square cross-section split-rib with gap width in the range of 0.5–2 and gap position in the range of 0.1667–0.667			
	Nu/Nu_0	f/f_0	η	
	1.48–2.59	2.26–2.9	1.0–1.8	

Table 2.2 (cont'd)

Authors	Conditions and results			Configuration
[56] 2008	Periodic grooves			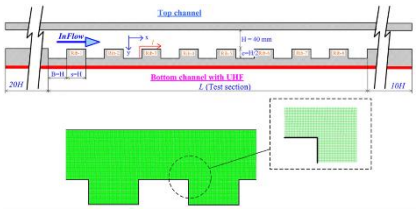
	Air : *Re*=6000–18,000			
	Periodic grooves with the groove-width to channel-height ratio of 0.5 to 1.75			
	Nu/Nu_0	f/f_0	η	
	2.45–2.58	–	0.95–1.32	
[57] 2008	Different shaped ribs			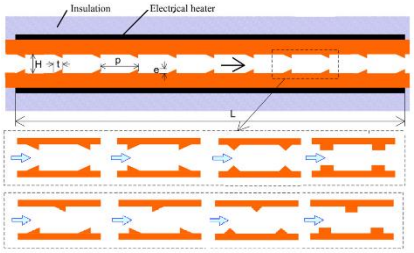
	Air : *Re*=4000–16,000			
	Triangular, wedge and rectangular shapes rib with in-line and staggered arrangements			
	Nu/Nu_0	f/f_0	η	
	2.7–4.4	20–70	0.78–1.1	
[58] 2008	Inclined and transverse ribs			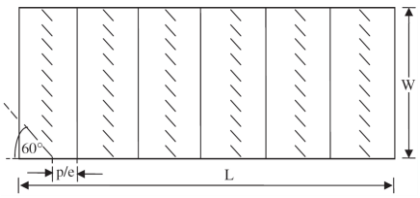
	Air : *Re*=2000–14,000			
	Inclined and transverse ribs with different relative roughness pitch and relative roughness height			
	Nu/Nu_0	f/f_0	η	
	–	–	–	
[59] 2009	Rib-grooved			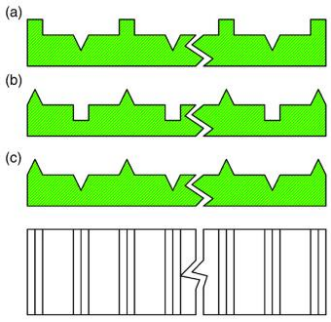
	Air : *Re*=3000–10,000			
	Rectangular-rib and triangular-groove, triangular-rib and rectangular-groove and triangular-rib at three pitch ratios			
	Nu/Nu_0	f/f_0	η	
	–	–	0.8–1.08	
[60] 2009	Isosceles triangular ribs			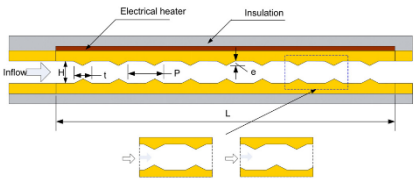
	Air : *Re*=5000–22,000			
	Isosceles triangle ribs with in-line and staggered arrangements at three uniform rib heights			
	Nu/Nu_0	f/f_0	η	
	1.6–4.2	2–86	0.88–1.34	

Table 2.2 (cont'd)

Authors	Conditions and results			Configuration
[61] 2009	Inverted U-shaped turbulators			
	Air : *Re*=3800–18,000			
	Inverted U-shaped turbulators with different height and pitch length			
	Nu/Nu_0	f/f_0	η	
	1.41–2.82	1.3–3.72	1.3–1.9	
[62] 2009	Discrete W-shaped roughness			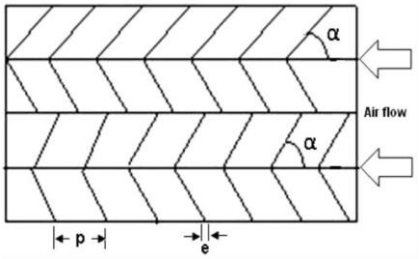
	Air : *Re*=3000–15,000			
	W-rib with relative roughness height in the range of 0.0168–0.0338 and the attack angle in the range of 30°–75°			
	Nu/Nu_0	f/f_0	η	
	1.44–2.16	1.53–2.75	–	
[63] 2009	Perforated baffles			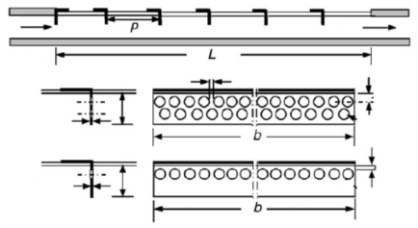
	Water : *Re*=2700–11,150			
	Fully and half perforated baffles at relative roughness pitch of 7.2–28.8 affixed to one of the broader walls			
	Nu/Nu_0	f/f_0	η	
	1.79–3.74	2.98–17.5	1.2–1.8	
[64] 2009	Diamond-shaped baffles			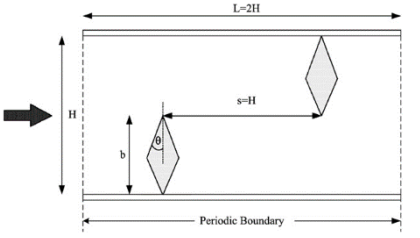
	Air : *Re*=100–600			
	Diamond baffle with different baffle tip angles			
	Nu/Nu_0	f/f_0	η	
	1.2–6.7	15–225	0.55–1.12	
[65] 2010	45° angled baffles			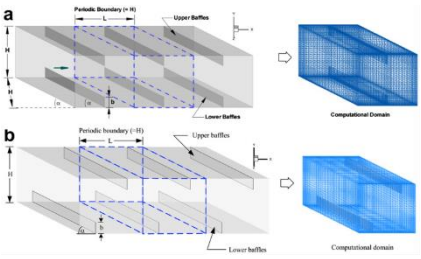
	Air : *Re*=100–1000			
	Inline arrangement 45° angled baffles with different baffle heights			
	Nu/Nu_0	f/f_0	η	
	1.2–9	2–66	1.2–2.6	

Table 2.2 (cont'd)

Authors	Conditions and results			Configuration
[66] 2010	Ribs and winglet			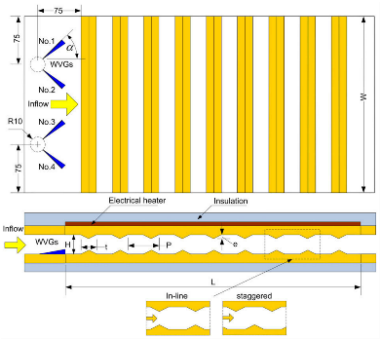
	Air : *Re*=5000–22,000			
	An isosceles triangle shape with inline and staggered arrangements combine with two pairs of the winglet			
	Nu/Nu_0	f/f_0	η	
	1.6–2.5	1.8–6	1.0–1.65	
[67] 2010	Multiple 60° V-baffles			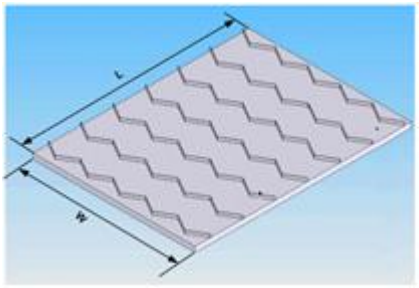
	Air : *Re*=5000–25,000			
	60° V-baffles with three different baffle blockage ratios and three baffle pitch spacing ratios			
	Nu/Nu_0	f/f_0	η	
	2.8–5.6	4–38	1.48–1.88	
[68] 2010	Wedge ribs and winglet			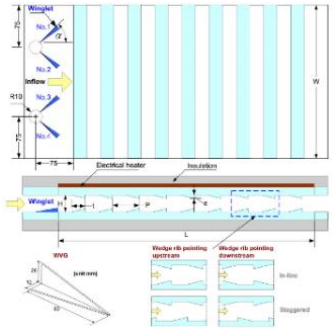
	Air : *Re*=5000–20,00			
	Wedge ribs pointing downstream and upstream with in-line and staggered arrangements combine with winglet			
	Nu/Nu_0	f/f_0	η	
	1.3–3.8	3–44	0.92–1.31	
[69] 2010	Multiple V-ribs			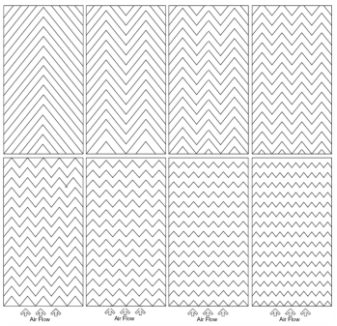
	Air : *Re*=2000–20,000			
	V-ribs with different relative height, relative pitch and relative width at angle of attack in a range of 30°–75°			
	Nu/Nu_0	f/f_0	η	
	–	–	–	
[70] 2011	Inline 60° V-shaped discrete thin ribs			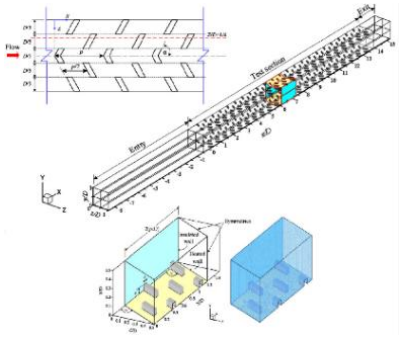
	Air : *Re*=10,000–25,000			
	Inline arrangement 60° V-shaped discrete thin ribs with different rib heights			
	Nu/Nu_0	f/f_0	η	
	2.7–4.7	6.5–29.5	1.13–1.81	

Table 2.2 (cont'd)

Authors	Conditions and results			Configuration
[71] 2011	W-rib			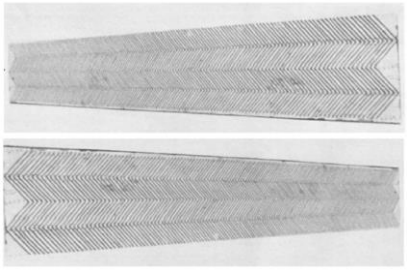
	Air : *Re*=2300–14,000			
	Downstream and upstream W rib with angle of attack of flow of 30°–75°			
	Nu/Nu_0	f/f_0	η	
	1.93–2.36	1.67–2.35	1.1–2.0	
[72] 2011	45° angled rib			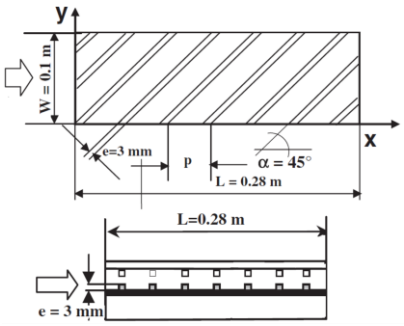
	Air : *Re*=9000–35,500			
	45° angled rib at rib height to hydraulic diameter was 0.09 with different four rib pitch-to-height ratios			
	Nu/Nu_0	f/f_0	η	
	1.6–2.5	2.5–14.8	–	
[73] 2011	Rib			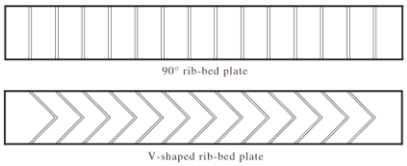
	Air : *Re*=6000–15,000			
	Channel with 90° ribs and V-shaped ribs were studied experimentally and numerically			
	Nu/Nu_0	f/f_0	η	
	–	–	0.75–2.0	
[74] 2011	Discrete V-down ribs			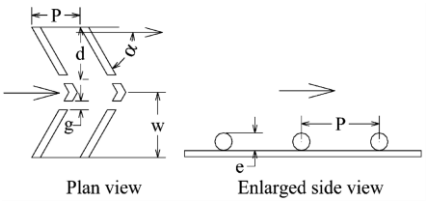
	Air : *Re*=3000-15,000			
	periodic discrete V-down rib with variation of relative pitch, angle of attack and relative height			
	Nu/Nu_0	f/f_0	η	
	–	–	–	
[75] 2011	W-shaped rib			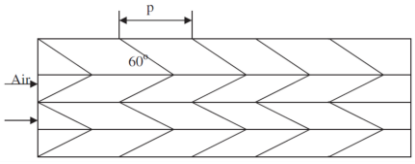
	Air : *Re*=2300–14,000			
	W-shaped rib with different roughness height (0.018–0.03375) and angle of attack of flow (30°–75°)			
	Nu/Nu_0	f/f_0	η	
	1.76–2.36	1.36–2.01	1.2–2.0	

Table 2.2 (cont'd)

Authors	Conditions and results			Configuration
[76] 2011	Ribs and delta-winglet			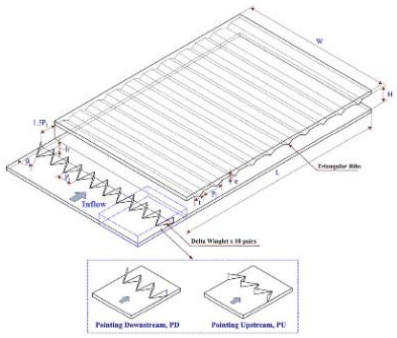
	Air : *Re*=5000–22,000			
	The combined triangular rib and the delta-winglet type vortex generators with three attack of 60°, 45° and 30°			
	Nu/Nu_0	Nu/Nu_0	Nu/Nu_0	
	2.3–2.55	2.3–2.55	2.3–2.55	
[77] 2012	V-down rib			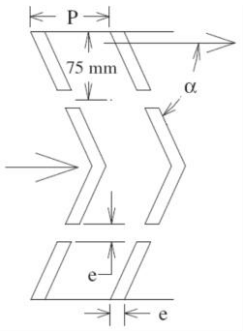
	Air : *Re*=3000–15,000			
	V-down rib having gap with variation of relative roughness height and flow-attack-angle			
	Nu/Nu_0	f/f_0	η	
	–	–	1.45–2.05	
[78] 2012	V-baffled			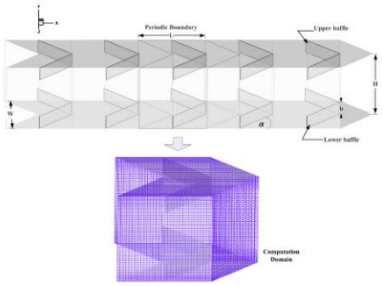
	Air : *Re*=200–2,000			
	Inline 45° V-baffles on the upper and lower walls with different blockage ratios and pitch ratios			
	Nu/Nu_0	f/f_0	η	
	1–21	1.1–225	1–3.8	
[79] 2012	Wire coil elements			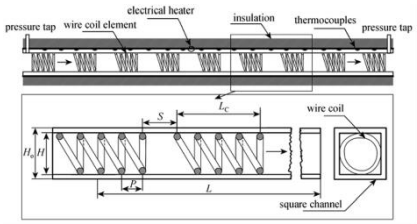
	Air : *Re*=4000–25,000			
	Wire coil elements with various free-space lengths			
	Nu/Nu_0	f/f_0	η	
	1.7–2.45	4.5–9.5	1.24–1.33	
[80] 2012	30° angle-finned tapes			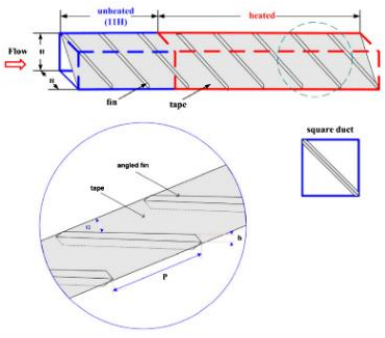
	Air : *Re*=4000–23,000			
	Diagonally 30° angle-finned tapes with three ratios of fin pitch to duct height and five fin-to-duct height ratios			
	Nu/Nu_0	f/f_0	η	
	3.9–6.3	14–109	1.05–1.8	

Table 2.2 (cont'd)

Authors	Conditions and results			Configuration
[81] 2012	Z-shaped baffles			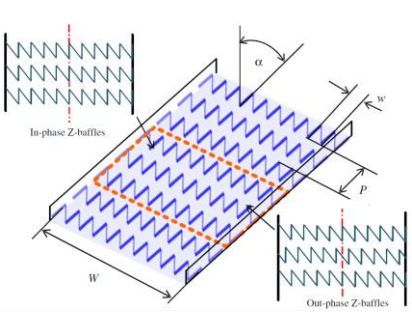
	Air : *Re*=4400–20,400			
	Baffles are placed in a zigzag shape at three baffle to channel height ratios and baffle pitch ratios			
	Nu/Nu_0	Nu/Nu_0	Nu/Nu_0	
	4.3–6.7	4.3–6.7	4.3–6.7	
[82] 2012	Multi V-shaped ribs			
	Air : *Re*=2000–20,000			
	Multi V-shaped ribs with various relative gap distance and relative gap width			
	Nu/Nu_0	f/f_0	η	
	4.1–6.3	3.8–5.6	2.4–3.6	
[83] 2012	Dimpled shape roughness			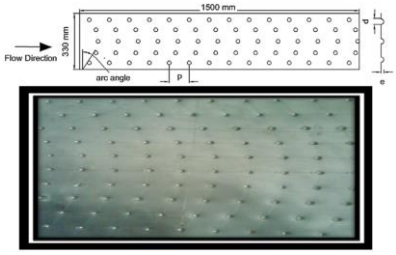
	Air : *Re*=3600–18,000			
	Dimpled shape with various relative roughness pitch, relative roughness height and arc angle			
	Nu/Nu_0	f/f_0	η	
	–	–	–	
[84] 2013	60° angled rib turbulators			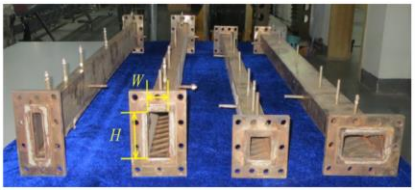
	Water : *Re*=10,000–80,000			
	Rib with different the rib height-to-hydraulic diameter ratio and rib pitch-to-rib height ratio			
	Nu/Nu_0	f/f_0	η	
	1.1–2.6	1.5–14	0.78–1.3	
[85] 2013	Discrete rib			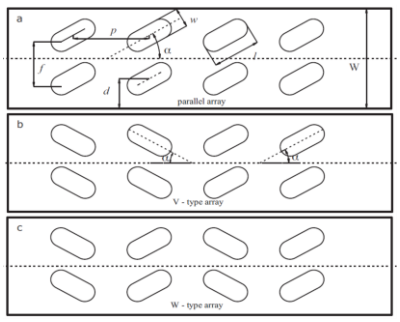
	Water : *Re*=6700–13,400			
	Inclined broken ribs for three kinds of rib arrays as parallel array, V-type array and W-type array			
	Nu/Nu_0	f/f_0	η	
	2.0–3.3	2.1–4.0	1.5–2.1	

Table 2.2 (cont'd)

Authors	Conditions and results			Configuration
[86] 2014	Inclined detached-ribs			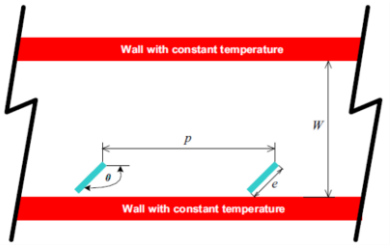
	Air : *Re*=4000–24,000			
	Inclined detached-ribs with different attack angles of 0°, 15°, 30°, 45°, 60°, 75°, 105°, 120°, 135°, 150° and 165°			
	Nu/Nu_0	f/f_0	η	
	–	–	0.73–1.22	
[87] 2014	Multiple arc shape			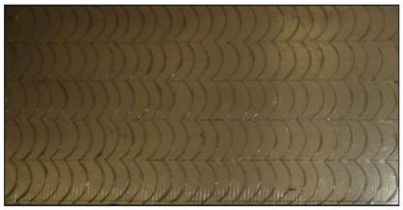
	Air : *Re*=2200–22,000			
	Arc shape with different relative height, relative width and relative pitch at arc angle range of 30°–75°			
	Nu/Nu_0	f/f_0	η	
	–	–	–	
[88] 2014	V-shaped perforated blocks			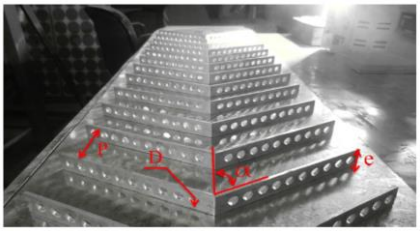
	Air : *Re*=2000–20,000			
	V blocks with relative blockage height of 0.4–1.0, relative pitch ratio of 4–12 and open area ratio of 5–25%			
	Nu/Nu_0	f/f_0	η	
	6.76	28.84	2.5–3.0	
[89] 2014	Rib-groove turbulators			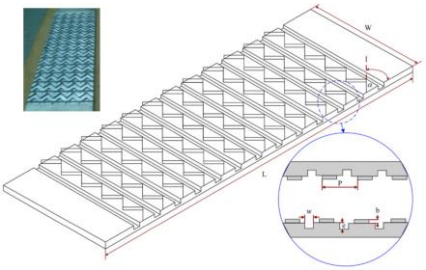
	Air : *Re*=4000–21,000			
	Wavy-rib with different pitch ratios at a single rib height ratio and transverse groove			
	Nu/Nu_0	f/f_0	η	
	4.40–7.69	14–135	1.1–1.8	
[90] 2014	Multiple arc shaped			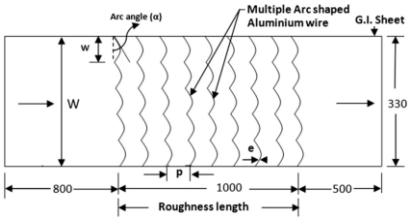
	Air : *Re*=2200–22,000			
	Arc shaped with different relative height, relative width, relative pitch and arc angle			
	Nu/Nu_0	f/f_0	η	
	1.2–5	2.3–3.5	0.7–3.4	

2.3 Concept of the research

According to the literature review above, various turbulence promoter devices have been used in the thermal systems both tubular and flat-surface duct/channel heat exchangers for heat transfer enhancement. Each turbulator is suitable for different applications indicating its advantages and disadvantages. Among turbulators, the winglet turbulator demonstrates the superiority of thermal performance in a duct/channel heat exchanger. This superiority lies in the ability of providing the heat transfer rate at lower flow resistance. The purpose of the present research is therefore to develop and modify the winglet tubulator for use in a tubular heat exchanger. The present research can be divided into 3 sections.

Section I : Multiple Twisted-Tapes

Twisted tapes belonging to one important group of swirl generators are mostly applied in heat transfer improvement in a tubular heat exchanger for both typical and modified twisted-tapes. Many investigations are mostly focused on the use of the modified single twisted-tapes, double and triple twisted-tapes. Both typical and modified tapes are used in a similar tape-twist direction while the effect of the multiple tapes with co- and counter-twist arrangements is reported later. Therefore, the utilization of double, triple and quadruple twisted-tapes in various forms of co- and counter-twist arrangements is offered as an enhancement device in this section. The experiments are performed using the left- and right-twisted tapes arranged in different forms of counter-twisted and co-twisted tape pairs. These test cases are employed as the base cases for comparison with the modified winglet cases being mentioned in the next section.

Section II : Winglets Placed in Central Core Flow

The application of winglets is more attractive than that of other vortex-flow devices due to lower pressure loss. However, the winglets cited above, in general, are used by placing on flat surfaces of ducts or channels and rarely found in round tubes. To employ winglets in a circular tube, the modification of winglet placements is needed by placing the winglet repeatedly on the central core flow along the tube. Therefore, the aim of the present work in this section is to examine the influence of the employed various winglet configurations with different attack angles, pitch lengths and winglet heights on enhanced heat transfer and flow characteristics in turbulent tube flow region. In the literature, the Nu and f increase with the rise of attack angles until about 60° before Nu shows a decreasing trend. The suggestion of small attack angles around 15°–30° is offered and therefore, the attack angle of winglets in the present research is considered only in a range of 30°–60°. In general, the heat transfer and pressure drop tends to increase with the reduction of pitch lengths but with the increase of winglet-heights. However, in the literature the

appropriate values of the pitch length and winglet-height did not mention because the results from both factors are also dependent of other parameters such as winglet geometry and angle of attack. Therefore, the pitch length and winglet-height are the key parameters determined by the suitability and limitations. These parameters will be defined as relative parameters normalized by the test tube diameter and presented in a range of 0.5–2.0 for the relative pitch or pitch ratio and of 0.1–0.2 for the relative height or winglet-height ratio.

Section III : Winglets Placed on Inner Tube Wall

The winglets and winglet pairs (by letting V-tip point upstream) with different pitch ratios and winglet-width ratios at a fixed optimal attack angle are selected for optimization. The selected winglet cases are considered from the optimum thermal performance cases obtained in section II. Those cases selected will be tested again by placing them on the inner tube wall instead of the central core. This placement is to reduce the very high pressure drop from disturbing the core flow. In this section work, the winglet elements will be tied together by putting two straight steel wires with semicircular-ring supports on both ends and be mounted on the tape edges to keep the winglets attached to the test tube surface. This modified winglet turbulator is expected to provide higher thermal performance than other turbuletors found in the literature.

CHAPTER 3
BASIC CONVECTIVE HEAT TRANSFER

3.1 Opening remarks

This chapter describes basic theory and principles of convective heat transfer involved, which include fluid mechanics [91, 92], heat transfer [93, 94] and heat transfer enhancement [95, 96]. For fluid mechanics, it starts with an explanation of the dimensionless Reynolds number and a general physical explanation of internal flow and the velocity boundary layer. Then, the characteristics of flow inside pipe/tubes and the head loss and friction factor correlations are introduced while the basic theory of heat transfer is focused on the internal forced convection. This section deals with characteristics of thermal boundary layer, calculation of the convective heat transfer coefficient and Nusselt number. Finally, a presentation of the principles of enhanced heat transfer is offered, which include the classification of enhancement techniques, the benefits of enhancement and thermal performance enhancement analysis.

3.2 Internal flow

3.2.1 Laminar and turbulent flow

Flow in a tube can be laminar or turbulent, depending on the flow condition. Fluid flow is streamlined and thus laminar at low velocities, but turns turbulent as the velocity is increased beyond a critical value. Transition from laminar to turbulent flow does not occur suddenly; rather, it occurs over some range of velocity where the flow fluctuates between laminar and turbulent flows before it becomes fully turbulent.

The transition from laminar to turbulent flow depends on the geometry, surface roughness, flow velocity, surface temperature, and type of fluid, among other things. After exhaustive experiments in 1880, Osborne Reynolds discovered that the flow regime depends mainly on the ratio of inertial forces to viscous forces in the fluid. This ratio is called the Reynolds number (*Re*) and is expressed for internal flow in a circular pipe as

$$\mathrm{Re} = UD/\nu \tag{3.1}$$

The Reynolds number at which the flow becomes turbulent is called the critical Reynolds number. The value of the critical Reynolds number is different for

different pipe/tube geometries and flow conditions. For internal flow in a circular pipe, the generally accepted value of the critical Reynolds number is 2300.

3.2.2 Velocity boundary layer

Considering a fluid entering a circular pipe at a uniform velocity, because of the no-slip condition, the fluid particles in the layer in contact with the surface of the pipe come to a complete stop. This layer also causes the fluid particles in the adjacent layers to slow down gradually as a result of friction. To make up for this velocity reduction, the velocity of the fluid at the midsection of the pipe has to increase to keep the mass flow rate through the pipe constant. As a result, a velocity gradient develops along the pipe.

The region of the flow in which the effects of the viscous shearing forces caused by fluid viscosity are felt is called the velocity boundary layer. The hypothetical boundary surface divides the flow in a pipe into two regions: the boundary layer region, in which the viscous effects and the velocity changes are significant, and the core flow region, in which the frictional effects are negligible and the velocity remains essentially constant in the radial direction.

The thickness of this boundary layer increases in the flow direction until the boundary layer reaches the pipe center and thus fills the entire pipe, as shown in Fig. 3.1. The region from the pipe inlet to the point at which the boundary layer merges at the centerline is called the hydrodynamic entrance region, and the length of this region is called the hydrodynamic entry length. Flow in the entrance region is called hydrodynamically developing flow since this is the region where the velocity profile develops. The region beyond the entrance region in which the velocity profile is fully developed and remains unchanged is called the hydrodynamically fully developed region. The flow is said to be fully developed when the normalized temperature profile remains unchanged as well.

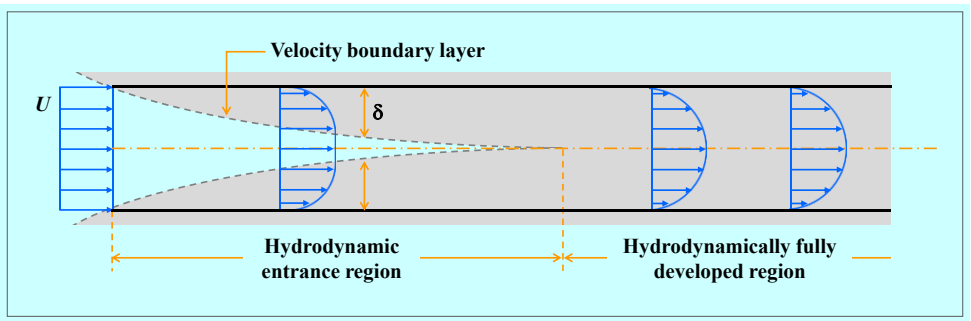

Figure 3.1 Development of the velocity boundary layer in a tube.

3.2.3 Mean velocity

In internal flow, there is no free stream and thus we need an alternative. The fluid velocity in a tube changes from zero at the surface because of the no-slip condition, to a maximum at the tube center. Therefore, it is convenient to work with an average or mean velocity, which remains constant for incompressible flow when the cross sectional area of the tube is constant.

The value of the mean velocity in a tube is determined from the requirement that the conservation of mass principle be satisfied (Figure 3.2). That is,

$$\dot{m} = \rho U A_{cross} \tag{3.2}$$

The mean velocity in actual heating and cooling applications may change somewhat because of the changes in density with temperature. But, in practice, the fluid properties are evaluated at some average temperature and treated as constants. The convenience in working with constant properties usually is more justified than the slight loss in accuracy.

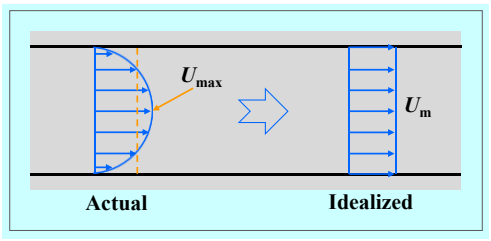

Figure 3.2 Actual and idealized velocity profiles for flow in a tube.

3.2.4 Head loss and friction factor

Calculating the losses of flow in pipes can be done by using the governing equations that are conservation of mass, conservation of momentum and conservation of energy equations. For incompressible fluid at steady state flow in a constant cross section area circular pipe, the control volume of the internal fluid flow shown in Figure 3.3, the calculation procedure includes:

Conservation of mass

The amount of mass flowing through a cross section per unit time is called the mass flow rate and is expressed as.

$$\dot{m} = \text{constant} = \rho_1 U_1 A_{1\,cross} = \rho_2 U_2 A_{2\,cross} \tag{3.3}$$

For steady flow, the mass flow is constant across every section of the tube and incompressible flow, the density is constant, then

$$U_1 = U_2 \tag{3.4}$$

Conservation of momentum

The momentum equation for the control volume in Figure. 3.3, accounting for applied forces due to pressure, gravity, and shear

$$\dot{m}(U_2 - U_1) = \sum F_x = (P_1 A_{1cross} - P_2 A_{2cross}) - (\tau_{\text{wall}} A_s) - (\rho g A_{cross} L \sin\phi) \tag{3.5}$$

For steady flow $U_1 = U_2$ from Eq. (3.4) and Eq. (3.5) $L\sin\phi = (z_1 - z_2)$, $A_s = 4\pi DL$ and $A_{cross} = \pi D^2/4$, Eq. (3.5) now reduces to a simple expression as

$$\frac{(P_1 - P_2)}{\rho g} + (z_1 - z_2) = \frac{\tau_{\text{wall}}}{\rho g}\frac{4L}{D} \tag{3.6}$$

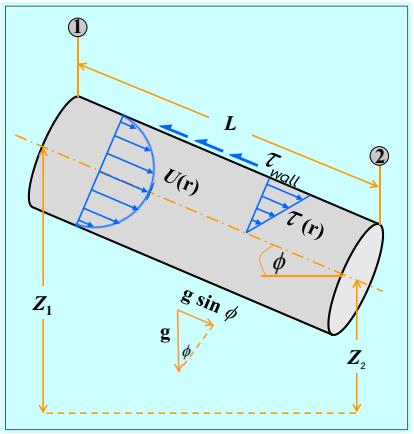

Figure 3.3 Control volume of steady and fully developed flow in an inclined pipe.

Conservation of energy

The energy equation for steady, incompressible one-dimensional flow and no mechanical work devices or heat-transfer effects in terms of heads as

$$\frac{P_1}{\rho g} + \frac{U_1^2}{2g} + z_1 = \frac{P_2}{\rho g} + \frac{U_2^2}{2g} + z_2 + h_{loss} \tag{3.7}$$

For steady flow $U_1 = U_2$ from Eq. (3.4), Eq. (3.7) now reduces to a simple expression for the friction-head loss

$$\frac{(P_1 - P_2)}{\rho g} + (z_1 - z_2) = h_{loss} \tag{3.8}$$

Combining Eqs. (3.6) and (3.8), the desired expression for finding pipe head loss is

$$h_{loss}=\frac{\tau_{\text{wall}}}{\rho g}\frac{4L}{D} \tag{3.9}$$

Friction factor

So far we have not assumed either laminar or turbulent flow. If we can correlate the shear wall stress with flow conditions, we have solved the problem of head loss in pipe flow. Functionally, we can assume that

$$\tau_{\text{wall}} = f^n(\rho,d,U,\mu,\varepsilon) \tag{3.10}$$

where ε is the wall-roughness height. Then dimensional analysis tells us that

$$f = f^n(\rho,d,U,\mu,\varepsilon) \equiv \frac{8\tau_{wall}}{\rho U^2} \tag{3.11}$$

The dimensionless parameter f is called the Darcy friction factor, after Henry Darcy (1803–1858), a French engineer whose pipe-flow experiments in 1857 first established the effect of roughness on pipe resistance.

Combining Eqs. (3.9) and (3.11), we obtain the desired expression for finding friction factor.

$$f = \frac{2gh_{loss}}{(L/D)U^2} \tag{3.12}$$

This is the Darcy-Weisbach equation, valid for duct flows of any cross section and for laminar and turbulent flow.

Our only remaining problem is to find the form of the function in Eq. (3.11) and plot it in the Moody chart.

3.3 Internal forced convection

3.3.1 Thermal boundary layer

Consider a fluid at a uniform temperature entering a circular tube whose surface is maintained at a different temperature. This time, the fluid particles in the layer in contact with the surface of the tube will assume the surface temperature is known as no-temperature-jump condition. This will initiate convection heat transfer in the tube and the development of a thermal boundary layer along the tube. The

thickness of this boundary layer also increases in the flow direction until the boundary layer reaches the tube center and thus fills the entire tube.

The region of flow over which the thermal boundary layer develops and reaches the tube center is called the thermal entrance region, and the length of this region is called the thermal entry length. Flow in the thermal entrance region is called thermally developing flow since this is the region where the temperature profile develops.The region beyond the thermal entrance region is called the thermally fully developed region. The region in which the flow is both hydrodynamically and thermally developed and thus both the velocity and dimensionless temperature profiles remain unchanged is called fully developed flow, as shown in Figure 3.4.

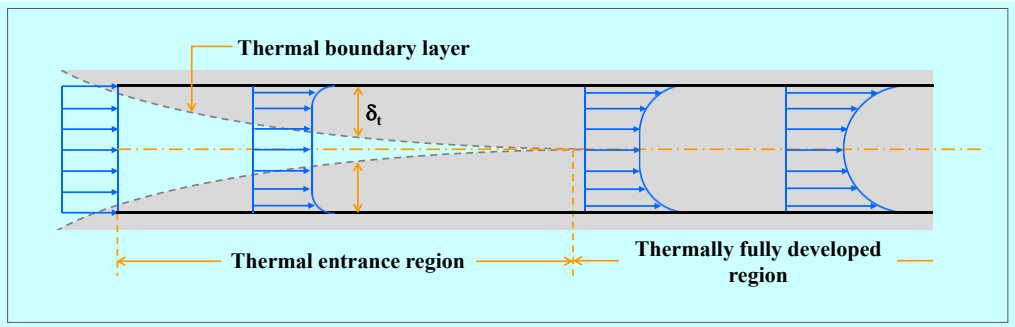

Figure 3.4 Development of the thermal boundary layer in a tube.

3.3.2 Mean temperature

When a fluid is heated as it flows through a tube, the temperature of the fluid at any cross section changes from surface temperature at the surface of the wall to some minimum at the tube center. In fluid flow it is convenient to work with an average or mean temperature that remains uniform at a cross section. The mean temperature will change in the flow direction whenever the fluid is heated.

The value of the mean temperature is determined from the requirement that the conservation of energy principle be satisfied. That is, the energy transported by the fluid through a cross section in actual flow must be equal to the energy that would be transported through the same cross section if the fluid were at a constant temperature. This can be expressed mathematically as depicted in Figure 3.5

$$E_{fluid} = \dot{m} C_p T_m \tag{3.13}$$

Note that the mean temperature of a fluid changes during heating. Also, the fluid properties in internal flow are usually evaluated at the bulk mean fluid

temperature, which is the arithmetic average of the mean temperatures at the inlet and the exit. That is,

$$T_b = (T_{m,i} + T_{m,o})/2 \tag{3.14}$$

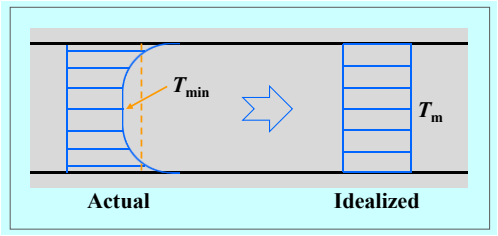

Figure 3.5 Actual and idealized temperature profiles for flow in a tube.

3.3.3 General thermal analysis

The rate of convection heat transfer is observed to be proportional to the temperature difference and is conveniently expressed by Newton's law of cooling as

$$Q = hA_s(T_w - T_b) \tag{3.15}$$

The conservation of energy equation for the steady flow of a fluid in a tube can be expressed as

$$Q = \dot{m}C_p(T_o - T_i) \tag{3.16}$$

The thermal conditions at the surface can usually be approximated with reasonable accuracy to be constant surface temperature or constant surface heat flux. For example, the constant surface temperature condition is realized when a phase change process such as boiling or condensation occurs at the outer surface of a tube. The constant surface heat flux condition is realized when the tube is subjected to radiation or electric resistance heating uniformly from all directions.

In the case of constant surface heat flux, the rate of heat transfer can also be expressed as

$$Q = \dot{q}A_s = \dot{m}C_p(T_o - T_i) \tag{3.17}$$

From Newton's law of cooling, the rate of heat transfer to or from a fluid flowing in a tube under the constant surface heat flux condition can be expressed as

$$Q = \dot{q}A_s = \dot{m}C_p(T_o - T_i) = hA_s(T_w - T_b) \tag{3.18}$$

In equation 3.18, it can be displayed in terms of convective heat transfer coefficient as shown in the equation below.

$$h = \frac{\dot{m}C_p(T_o - T_i)}{A_s(T_w - T_b)} \tag{3.19}$$

In convection studies, it is common practice to nondimensionalize the governing equations to combine the variables, which group together into dimensionless numbers in order to reduce the number of total variables. It is also common practice to nondimensionalize the heat transfer coefficient with the Nusselt number, defined as

$$Nu = \frac{hD}{k} \tag{3.20}$$

For the constant surface heat flux condition, the surface temperature in the entrance region normally increases abruptly from the inlet until reaching the fully developed region. In the fully developed region, the wall temperature T_w will also increase linearly in the flow direction since h is constant and thus $T_w - T_m$ constant (Figure 3.6). Of course this is true when the fluid properties remain constant during flow.

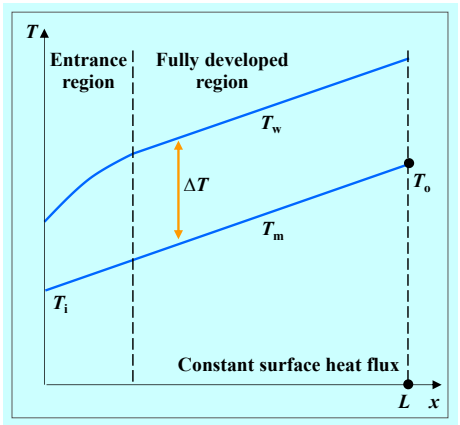

Figure 3.6 Axial temperature variation in a tube under constant surface heat flux.

3.3.4 Correlations in turbulent tube flow and heat transfer

Turbulent flow is commonly utilized in practice because of the higher heat transfer coefficients associated with it. Most correlations for the friction and heat transfer coefficients in turbulent flow are based on experimental studies because of the difficulty in dealing with turbulent flow theoretically.

Nuselt number correlation: Dittus-Boelter

$$Nu = 0.023\ \mathrm{Re}^{0.8}\ \mathrm{Pr}^{n} \qquad (0.1 \le \mathrm{Pr} \le 160,\ \mathrm{Re} > 10{,}000) \tag{3.21}$$

where n=0.4 for heating and n=0.3 for cooling of the fluid flowing in the tube.

Nuselt number correlation: Gnielinski

$$Nu = \frac{(f/8)(\mathrm{Re}-1000)\,\mathrm{Pr}}{1+12.7(f/8)^{0.5}(\mathrm{Pr}^{2/3}-1)} \qquad (0.5 \le \mathrm{Pr} \le 2000,\ 3\mathrm{x}10^{3} < \mathrm{Re} < 5\mathrm{x}10^{6}) \tag{3.22}$$

Friction factor correlation: Blasius

$$f = 0.316\ \mathrm{Re}^{-0.25} \qquad (3000 \le \mathrm{Re} \le 20{,}000) \tag{3.23}$$

Friction factor correlation: Petukhov

$$f = (0.790\ \ln \mathrm{Re} - 1.64)^{-2} \qquad (10^{4} < \mathrm{Re} < 10^{6}) \tag{3.24}$$

3.4 Principles of enhanced heat transfer

3.4.1 The overall heat transfer coefficient

A heat exchanger typically involves two flowing fluids separated by a solid wall. Heat is first transferred from the hot fluid to the wall by convection, through the wall by conduction, and from the wall to the cold fluid again by convection. In the analysis of heat exchangers, it is convenient to combine all the thermal resistances in the path of heat flow from the hot fluid to the cold one into a single resistance *R*, and to express the rate of heat transfer between the two fluids as

$$Q = \frac{\Delta T}{R} = UA\Delta T \tag{3.25}$$

where U is the overall heat transfer coefficient, whose unit is W/m^{2}°C. To illustrate the benefits of enhancement, we will multiply and divide Eq. 3.25 by the total tube length, L

$$Q = \frac{\Delta TL}{RL} = \frac{UA}{L} L\Delta T \tag{3.26}$$

The term L/UA is the overall thermal resistance per unit tube length, and is given by

$$\frac{L}{UA} = \frac{L}{h_i A_i} + \frac{L \ln(D_o / D_i)}{2\pi k L} + \frac{L}{h_o A_o} \tag{3.27}$$

The performance of heat exchanger will be enhanced if the term UA/L is increased. An enhanced surface geometry may be used to increase either or both of the terms, relative to that given by plain surfaces. This will reduce the thermal resistance per unit tube length. This reduced L/UA may be used for one of three objectives as

1. Size reduction : To make heat exchangers more compact in order to reduce their overall volume, and possibly their cost.
2. Reduced pumping power : To reduce the pumping power required for a given heat transfer process.
3. Increased UA : A higher UA value can be exploited in either of two ways :
   (1) To obtain an increased heat exchange rate for fixed fluid inlet temperatures.
   (2) To reduce the mean temperature difference for the heat exchange; this increases the thermodynamic process efficiency, which can result in a saving of operating costs.

3.4.2 Classification of enhancement techniques

In general, heat transfer enhancement techniques can be classified into three categories: active, passive and compound method.

Active techniques

These techniques are more complex from the use and design point of view as the method requires some external power input to cause the desired flow modification and improvement in the rate of heat transfer. It finds limited application because of the need of external power in many practical applications. In comparison to the passive techniques, these techniques have not shown much potential as it is difficult to provide external power input in many cases. Enhancement of heat transfer by this method can be achieved by: mechanical aids, surface vibration, fluid vibration, electrostatic fields, injection suction and jet impingement.

Passive method

These techniques generally use surface or geometrical modifications to the flow channel by incorporating inserts or additional devices. They promote higher heat transfer coefficients by disturbing or altering the existing flow behavior (except for extended surfaces) which also leads to increase in the pressure drop. In case of extended surfaces, effective heat transfer area on the side of the extended surface is increased. Passive techniques hold the advantage over the active techniques as any direct input of external power is not needed. These techniques do not require any

direct input of external power; rather they use it from the system itself which ultimately leads to an increase in fluid pressure drop. Heat transfer augmentation by these techniques can be achieved by using: treated surfaces, rough surfaces, extended surfaces, displaced enhancement devices, swirl flow devices, coiled tubes, surface tension devices, additives for liquids and additives for gases.

Compound techniques

A compound augmentation technique is the one where more than one of the above mentioned techniques is used in combination with the purpose of further improving the thermo-hydraulic performance of a heat exchanger. When any two or more of these techniques are employed simultaneously to obtain enhancement in heat transfer that is greater than that produced by either of them when used individually, is termed as compound enhancement. This technique involves complex design and hence has limited applications.

3.4.3 Mechanisms of enhancement of heat transfer

The mechanisms of heat transfer enhancement can be at least one of the following.

1. Use of a secondary heat transfer surface.
2. Disruption of the unenhanced fluid velocity.
3. Disruption of the laminar sublayer in the turbulent boundary layer.
4. Introducing secondary flows.
5. Promoting boundary-layer separation.
6. Promoting flow attachment/reattachment.
7. Enhancing effective thermal conductivity of fluid under static conditions
8. Enhancing effective thermal conductivity of fluid under dynamic conditions
9. Delaying the boundary layer development.
10. Thermal dispersion.
11. Increasing the order of the fluid molecules.
12. Redistribution of the flow.
13. Modification of radiative property of the convective medium.
14. Increasing the difference between the surface and fluid temperatures.
15. Increasing fluid flow rate passively.
16. Increasing the thermal conductivity of the solid phase using special nano technology fabrications

3.4.4 Benefits of enhancement

Special surface geometries provide enhancement by establishing a higher hA per unit base surface area. Clearly, there are three basic ways of accomplishing this

1. Increase the effective heat transfer surface area (A) per unit volume without appreciably changing the heat transfer coefficient (h). Plain fin surfaces enhance heat transfer in this manner.

2. Increase h without appreciably changing A. This is accomplished by using a special channel shape, such as a wavy or corrugated channel, which provides mixing due to secondary flows and boundary-layer separation within the channel. Vortex generators also increase h without a significant area increase by creating longitudinally spiraling vortices exchange fluid between the wall and core regions of the flow, resulting in increased heat transfer.

3. Increase both h and A. Interrupted fins (i.e. offset strip and louvered fins) act in this way. These surfaces increase the effective surface area, and enhance heat transfer through repeated growth and destruction of the boundary layers.

3.4.5 Thermal performance factor

The importance parameter for the heat transfer enhancement investigation is the thermal performance factor (η) which presents the relationship between the increasing of the heat transfer and the friction factor since it is relevant to operation cost. In the present work, the thermal performance factor (η) considered under constant pumping/blowing power between the plain tube and the inserted tube and constant fluid properties, can be made as follows:

$$(\dot{V}\rho g\Delta h)_{\mathrm{p}} = (\dot{V}\rho g\Delta h)_{\mathrm{s}} \tag{3.28}$$

The relationship between volume flow rate and Reynolds number can be expressed by multiplying and dividing the Reynolds number equation by volume flow rate.

$$\mathrm{Re} = \left(\frac{UD}{\nu}\right)\left(\frac{\dot{V}}{UA}\right) = \left(\frac{D}{\nu A}\right)(\dot{V}) = C(\dot{V}) \tag{3.29}$$

From Eq. 3.12 presented in the form of pipe head loss, the relationship between head loss and friction factor can be expressed by multiplying and dividing by the squared Reynolds number

$$\Delta h_{loss} = \left(f\frac{LU^2}{2gD}\right)\left(\frac{\mathrm{Re}^2}{(UD/\nu)^2}\right) = \left(\frac{L\nu^2}{2gD^3}\right)(f.\mathrm{Re}^2) = C(f.\mathrm{Re}^2) \tag{3.30}$$

Substituting Eqs. 3.29 and 3.30 into Eq. 3.28, it can be seen the relationship between friction factor ratio and Reynolds number at the same pumping power

$$\left(\frac{\mathrm{Re_s}}{\mathrm{Re_p}}\right)_{\mathrm{pp}} = \left(\frac{f_\mathrm{s}}{f_\mathrm{p}}\right)^{-1/3} \tag{3.31}$$

Thermal performance factor (η) is defined as ratio of the convective heat transfer coefficient of the inserted tube to that of the plain tube which can be expressed as

$$\eta = \left.\frac{h_\mathrm{s}}{h_\mathrm{p}}\right|_{\mathrm{pp}} = \left.\frac{\mathrm{Nu_s}}{\mathrm{Nu_p}}\right|_{\mathrm{pp}} = \left(\frac{\mathrm{Nu_s}}{\mathrm{Nu_p}}\right)\left(\frac{\mathrm{Re_s}}{\mathrm{Re_p}}\right) = \left(\frac{\mathrm{Nu_s}}{\mathrm{Nu_p}}\right)\left(\frac{f_\mathrm{s}}{f_\mathrm{p}}\right)^{-1/3} \tag{3.32}$$

where h_p and h_s stand for the heat transfer coefficients for the plain tube and the inserted tube, respectively.

CHAPTER 4
METHODOLOGY

4.1 Experimental setup

A schematic diagram of the experimental set-up is demonstrated in Figure 4.1. In the apparatus setting above, the inlet bulk air at 25 °C from a 1.5 kW blower was directed through a clam section to achieve a fully developed flow before being tested in the test tube. The airflow rate was measured by the orifice meter, built according to ASME standard [97] and calibrated by using a hot-wire anemometer to measure flow velocities across the tube section. Manometric fluid was used in an inclined-manometer with specific gravity (SG) of 0.826 to ensure reasonably accurate measurement of pressure drop across the orifice. The volumetric air flow rate was varied by adjusting motor speed of the blower through the inverter to achieve desired Reynolds number (*Re*) in the range of 5300 to 24,000. The inner (*D*) and outer diameters of the copper test tube was, respectively, 50.8 and 54.8 mm and the tube was 3000 mm long, included the test section (*L*) of 1000 mm. The test tube was heated by continually winding flexible electrical wire under a uniform wall heat-flux boundary condition. The electrical output power was controlled via a variac transformer. The outer surface of the test tube was well insulated to minimize convective heat loss to the surroundings. The inlet and outlet air temperatures in the test tube were measured by RTD PT100 type thermocouples with ±0.1 °C accuracy positioned around 50 mm upstream and downstream of the test tube while the surface temperatures (T_w) were measured by 12 type-K thermocouples located equally on each of the top wall and the sidewall along the test section. The totally 24 type-K thermocouples were embedded in holes drilled from the outer surface and centered of the tube walls with the respective junctions positioned within 1 mm of the inside wall and axial separation of the thermocouples was 90 mm apart and calibrated within ±0.2 °C deviation by thermostat before being used. All of the temperatures getting from the system were consistently recorded using a data logger. The pressure drop across the test section for calculation of the friction factor was measured at the isothermal condition by a digital manometer with accuracy ±0.5%. All physical properties of air, including density, viscosity and thermal conductivity were based on the overall bulk mean temperature which is an average value of the inlet and outlet temperatures. For each test run, the data of temperature, volumetric flow rate and pressure drop of the bulk air in the inserted tube were measured and recorded at steady state conditions in which the inlet air temperature was maintained at about 25 °C.

The uncertainty in the data calculation was based on ref. [98]. The maximum uncertainties of non-dimensional parameters were ±5% for Reynolds number, ±7.6% for Nusselt number and ±9.5% for friction. The uncertainty in the axial velocity measurement was estimated to be less than ±5%, and pressure has a corresponding estimated uncertainty of ±5%, whereas the uncertainty in temperature measurement at the tube wall was about ±0.5%.

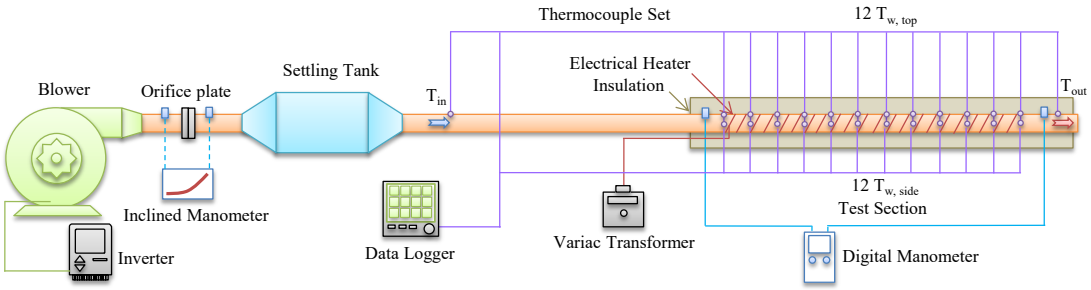

Figure 4.1 Schematic diagram of experimental apparatus.

4.2 Equipment and measuring instruments

4.2.1 The copper test tube

- The copper test tube has inner (*D*) and outer diameters of 50.8 and 54.8 mm, respectively and the tube was 3000 mm long, included the test section (*L*) of 1000 mm.
- Ceramic fiber insulation was used to prevent heat loss to the surrounding.

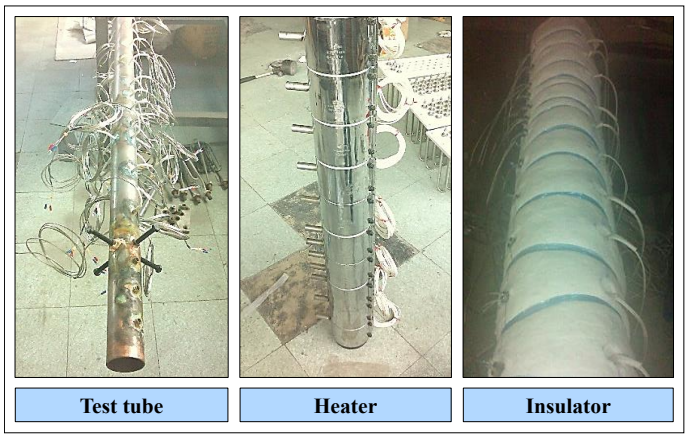

Figure 4.2 The copper test tube.

4.2.2 Air supply and controller set

- High pressure blower (HITACHI model VB-020-DN) was used for supplying air into the heat exchanger tube.
- Inverter (Novem model ND1-4-5A5 series) was employed for controlling

the speed of the blower to obtain the desired air volume flow rate.

- Orifice plate was used for measuring the airflow rate in the system.
- Inclined manometer (Dwyer mark II model No.25) was utilized for reading the pressure drop across the orifice plate and for the reference levels to adjust the airflow rate.
- Vane-type anemometer (Testo 445) was applied to measure the air velocity in the system according to the reference levels from the inclined manometer for calculation the air flow rate.

Figure 4.3 Supplied air and controller set.

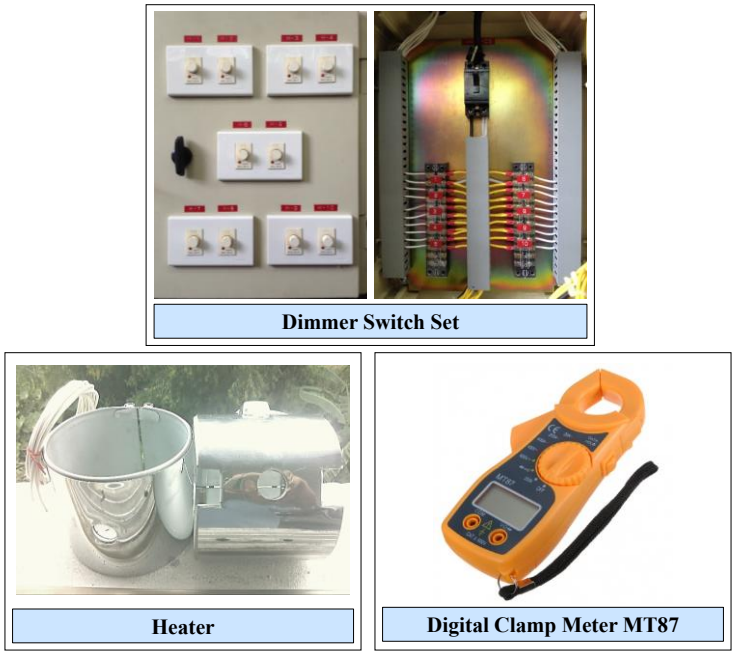

Figure 4.4 Heater and controller set.

4.2.3 Heater and controller set

- The 10 band heaters were used for heating the outer surface of the test tube in during the test under constant heat-flux conditions.
- The 10 dimmer switches were employed for adjusting the amount of power supplied to each heater collar band.
- The Digital clamp meter was utilized for measuring the quantity of electricity supplied to each band heater.

4.2.4 Data logger and thermocouple set

- The 24 type-K thermocouples were used to measure the surface temperatures in the test section.
- The 2 RTD PT-100 were employed to measure the inlet and outlet air temperatures at upstream and downstream of the test tube.
- The data logger (SUPCON model R3000 Series) was utilized to display and record the surface temperature on the top wall of test tube.
- The data logger (GRAPHTEC model GL820) was used to display and record the surface temperature on the side wall of test tube.

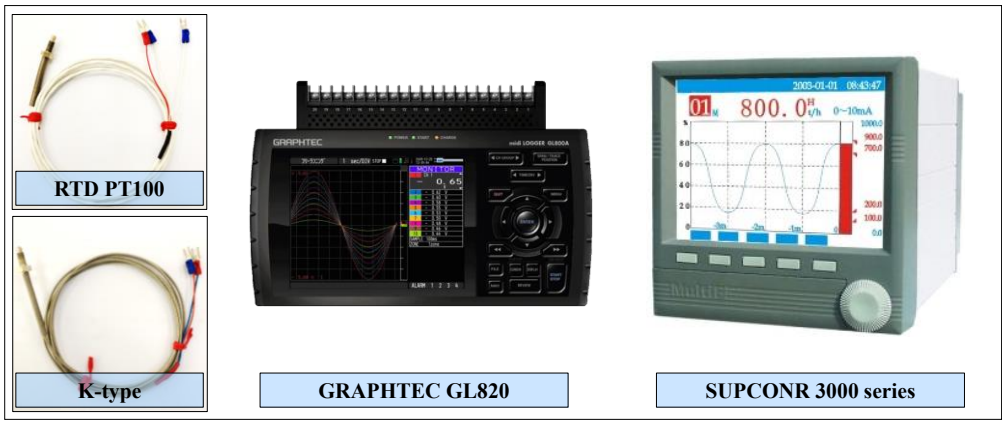

Figure 4.5 Data logger and thermocouple set.

Figure 4.6 Digital manometer.

4.2.5 Digital manometer

- Digital manometer (Dwyer model 475 Mark III) was used for measuring the pressure drop across the test tube in calculating the friction factor.

4.3 Geometry of turbulators

Several geometries of turbulators used in the present work can be divided into 3 types as follows :

(1) Multiple twisted-tapes

(2) Winglets placed in central core flow

(3) Winglets placed on inner tube wall

4.3.1 Multiple twisted tapes

Part I : Loose-fit multiple twisted-tapes (LF-TT), all twisted tapes made of 0.8 mm aluminum sheet were 1000 mm long and 8 mm width (w) with two different twist lengths (y) : 32 and 36 mm (twist ratio, y/w=4 and 4.5). All the tapes were twisted in two different directions: left-twist (L_T) and right-twist (R_T), and were arranged in different forms. The double or triple twisted-tapes were placed in the same plane and held along the tube length with straight steel wires having semicircular rod-supports at both wire ends, as demonstrated in Figure 4.7.

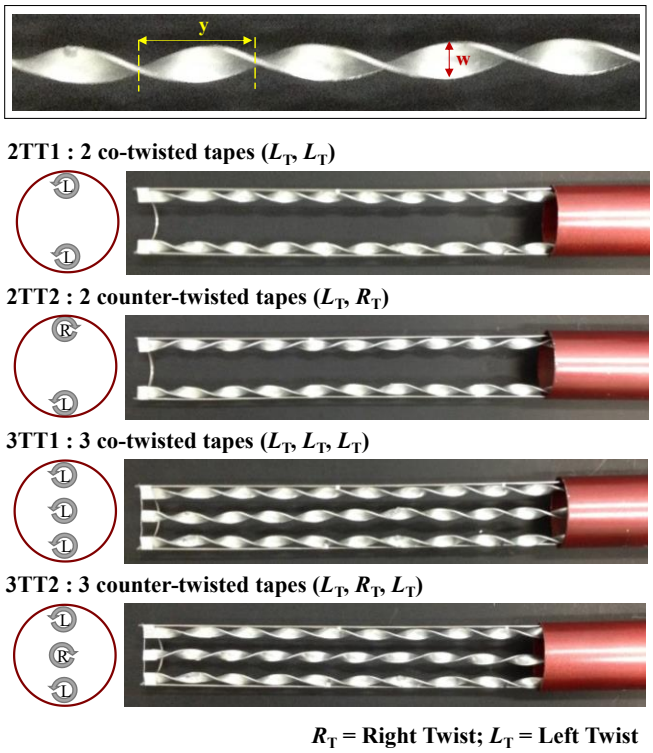

Figure 4.7 Loose-fit multiple twisted-tapes.

Part II : Tight-fit multiple twisted-tapes (TF-TT), all the twisted-tapes were inserted into the test tube with slightly tight fit and before insertion the multiple twisted-tapes were attached together by superglue. The twisted-tapes made of aluminum sheet were 1200 mm long and 0.8 mm thick. The typical single twisted-tape had a width (w) of 42 mm with two different twist lengths (y) : 168 and 210 mm (twist ratio, y/w=4 and 5) while the rests were 21 mm wide with 84 mm twist-length (y/w=4). All the tapes were twisted in two different directions : left-twist (L_T) and right-twist (R_T), and were arranged in 8 different configurations (2T1, 2T2, 3T1, 3T2, 4T1, 4T2, 4T3 and 4T4), as shown in Figure 4.8

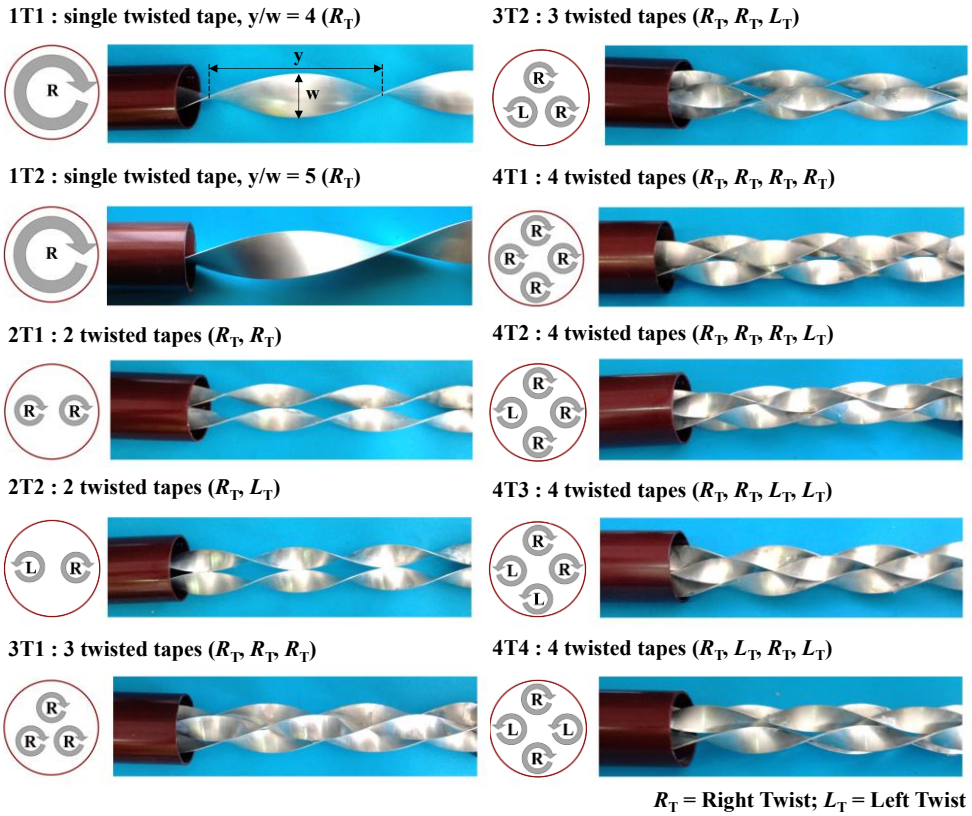

Figure 4.8 Tight-fit multiple twisted-tapes.

4.3.2 Winglets placed in central core flow

The WVG elements were tied together by putting two straight steel wires into the holes drilled on both end areas of the winglets with two semicircular rod-supports on both ends of the wires. The WVGs were inserted and mounted repeatedly along the central core flow of the test tube. Winglets in this section consisted of :

Part I : Winglets as depicted in Figure 4.9.

Part II : Winglet pairs with V-tip pointing downstream as shown in Figure 4.10.

Part III : Winglet pairs with V-tip pointing upstream as displyed in Figure 4.11.

All the WVGs made of aluminum strip were 0.3 mm thick with rounded ends. In the present work, the winglets with three different attack angles (α=30°, 45° and 60°), three different winglet-width (e) of 5, 7.5 and 10 mm (or blockage ratios $B_R=e/D$=0.1, 0.15 and 0.2) and four different winglet pitch length of 25, 50, 75 and 100 mm (or pitch ratios $P_R=P/D$=0.5, 1.0, 1.5 and 2.0) were offered.

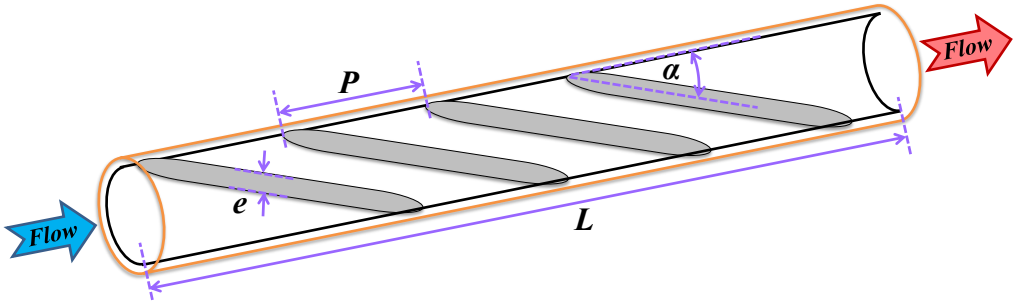

Figure 4.9 Winglets placed in the central core flow.

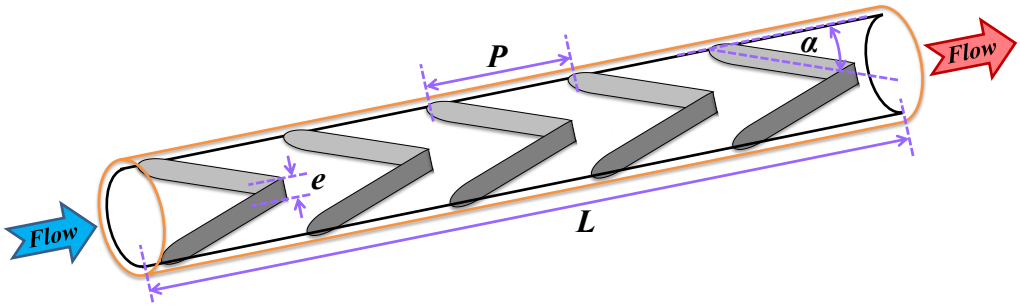

Figure 4.10 V-downstream winglets placed in the central core flow.

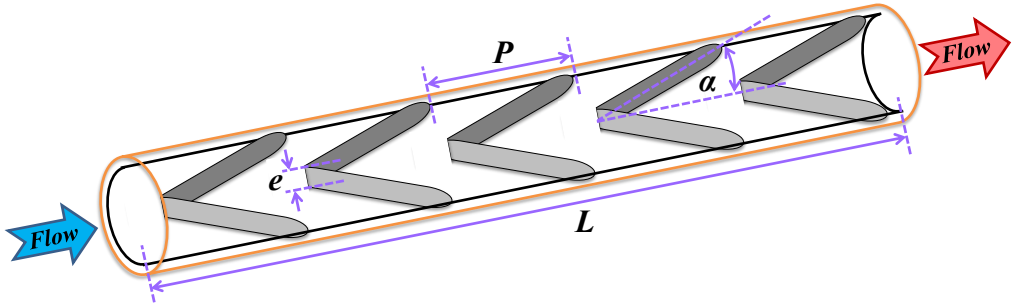

Figure 4.11 V-upstream winglets placed in the central core flow.

4.3.3 Winglets placed on inner tube wall

The WVG elements were placed tightly on the inner wall of test tube after insertion. Winglets in this section consisted of :

Part I : Winglets depicted in Figures 4.12 and 4.13

Part II : Winglet pairs with V-upstream shown in Figures 4.14 and 4.15

All the WVGs made of aluminum strip were 0.3 mm thick with rounded ends. In the present work, the winglets with only the attack angle (α) of 30° at three winglet-widths (e) of 5, 7.5 and 10 mm (or blockage ratio, B_R=e/D=0.1, 0.15 and 0.2) and three winglet pitches of 25, 50 and 100 mm (or pitch ratio, PR=P/D=0.5, 1.0 and 2.0) were introduced.

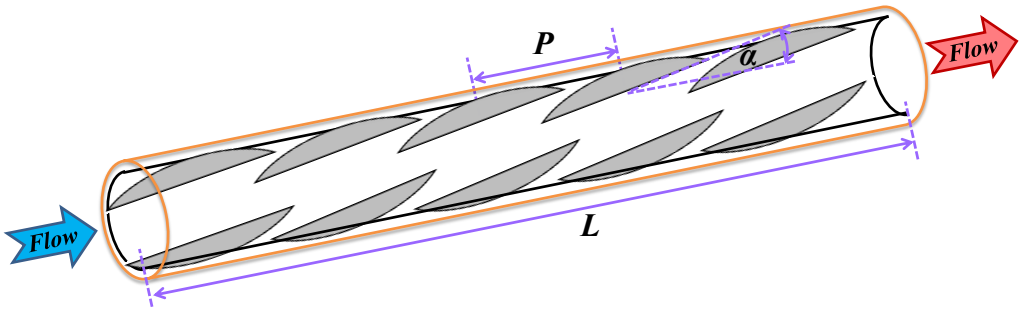

Figure 4.12 Winglets with straight wires placed on the inner wall.

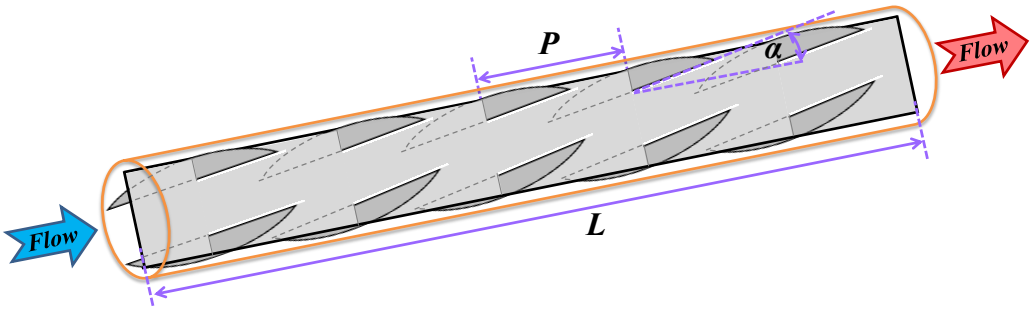

Figure 4.13 Winglets with straight tape placed on the inner wall.

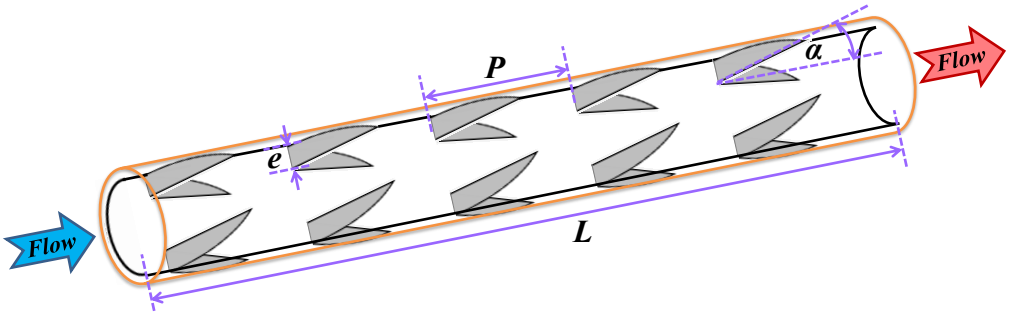

Figure 4.14 V-upstream winglets with straight wires placed on the inner wall.

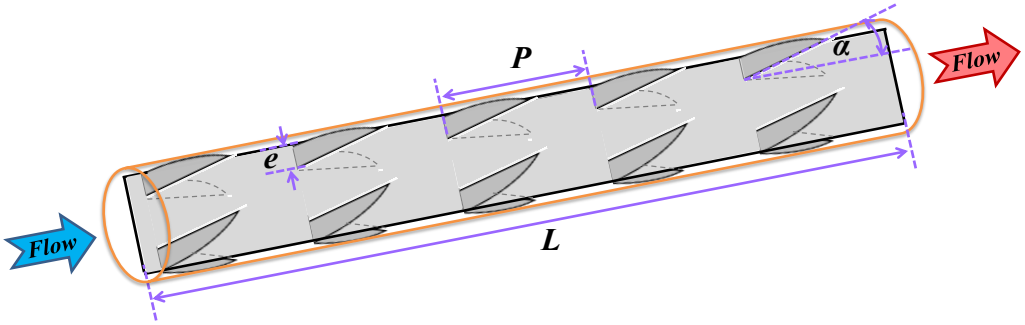

Figure 4.15 V-upstream winglets with straight tape placed on the inner wall.

4.4 Data processing

4.4.1 Heat transfer

In the present work, the air used as the test fluid flowed through a uniform heat-fluxed and insulated tube. The steady state heat transfer rate is assumed to be equal to the heat loss in the test section, which can be expressed as

$$Q_{\mathrm{a}} = Q_{\mathrm{conv}} \tag{4.1}$$

where

$$Q_{\mathrm{a}} = \dot{m} C_{\mathrm{p,a}} \left(T_{\mathrm{o}} - T_{\mathrm{i}} \right) \tag{4.2}$$

The heat supplied by the electrical winding in the test tube is found to be 3-5% higher than the heat absorbed by the fluid for the thermal equilibrium test due to convection and radiation heat losses from the test section to the surrounding. Thus, only the heat transfer rate absorbed by the fluid is taken for the internal convective heat transfer coefficient calculation. The convection heat transfer in the test tube can be written as

$$Q_{\mathrm{conv}} = hA\left(\widetilde{T}_{\mathrm{w}} - T_{\mathrm{b}} \right) \tag{4.3}$$

The average heat transfer coefficient (h) is estimated as follows:

$$h = \dot{m} C_{\mathrm{p,a}} \left(T_{\mathrm{o}} - T_{\mathrm{i}} \right) / A\left(\widetilde{T}_{\mathrm{w}} - T_{\mathrm{b}} \right) \tag{4.4}$$

where $\dot{m}$ is mass flow rate, kg.s^{-1}
$C_{\mathrm{p,a}}$ is specific heat of air, J.kg^{-1}.K^{-1}
T_{o} is outlet temperature, K
T_{i} is inlet temperature, K
A is heat transfer surface area, m^2
$\widetilde{T}_{\mathrm{w}}$ is mean wall temperature, K
T_{b} is bulk temperature, K

in which

$$\widetilde{T}_{\mathrm{w}} = \sum T_{\mathrm{w}} / 24 \tag{4.5}$$

$$T_{\mathrm{b}} = (T_{\mathrm{o}} + T_{\mathrm{i}}) / 2 \tag{4.6}$$

The heat transfer is calculated from the Nusselt number which can be obtained by

$$Nu = \frac{hD}{k} \tag{4.7}$$

where h is heat transfer coefficient, $W.m^{-2}.K^{-1}$
D is inner diameter of test tube, m
k is thermal conductivity of fluid, $W.m^{-1}.K^{-1}$

4.4.2 Friction factor

The friction factor (*f*) computed by pressure drop across the test tube length (*L*) is written as

$$f = \frac{2}{(L/D)}\frac{\Delta P}{\rho U^2} \tag{4.8}$$

where ΔP is pressure drop, $kg.m^{-1}.s^{-2}$
L is length of test section, m
D is inner diameter of test tube, m
ρ is air density, $kg.m^{-3}$
U is mean air velocity, $m.s^{-1}$

4.4.3 Thermal performance factor

In thermal performance evaluation, the thermal enhancement factor (η) is defined as the ratio of the heat transfer coefficient for the inserted tube (h_s) to that of the plain tube (h_p) at the same level of pumping power and can be expressed as follows

$$\eta = \left.\frac{h_s}{h_p}\right|_{pp} = \left.\frac{Nu_s}{Nu_p}\right|_{pp} = \left(\frac{Nu_s}{Nu_p}\right)\left(\frac{f_s}{f_p}\right)^{-1/3} \tag{4.9}$$

4.4.4 Parameters

Reynolds number

The Reynolds number based on tube diameter is given by

$$Re = UD/\nu \tag{4.10}$$

Twist ratio

The twist ratio (*Y*) is defined as the pitch length (180° rotation) of twisted tape

(*y*) to the tape width (*w*) is written as

$$Y = y/w \tag{4.11}$$

Blockage ratio

The blockage ratio (B_R) is defined as the ratio of winglet width (*e*) to the test tube diameter (*D*) can be written as

$$B_R = e/D \tag{4.12}$$

Pitch ratio

The pitch ratio (P_R) is defined as the ratio of pitch lengths (*P*) to the test tube diameter (*D*) which can be expressed as

$$P_R = P/D \tag{4.13}$$

4.5 Validation of smooth tube

The present experimental results on the heat transfer and friction characteristics in a smooth wall tube were first validated in terms of Nusselt number (Nu) and friction factor (*f*). The Nu obtained from the present smooth tube was compared with that from correlations of Dittus-Boelter and Gnielinski while the *f* was compared with data from correlations of Blasius and Petukhov found in the open literature [93] for turbulent flow in circular tube.

Correlation of Dittus-Boelter:

$$\mathrm{Nu} = 0.023\,\mathrm{Re}^{0.8}\,\mathrm{Pr}^{0.4} \tag{4.14}$$

Correlation of Gnielinski:

$$\mathrm{Nu} = \frac{(f/8)(\mathrm{Re}-1000)\mathrm{Pr}}{1+12.7(f/8)^{1/2}\left(\mathrm{Pr}^{2/3}-1\right)} \tag{4.15}$$

Correlation of Blasius:

$$f = 0.316\,\mathrm{Re}^{-0.25} \tag{4.16}$$

Correlation of Petukhov:

$$f = (0790 \ln \mathrm{Re} - 1.64)^{-2} \tag{4.17}$$

Figure 4.16 shows a comparison of the Nu and f obtained from the present work with those from correlations from previous works available for steady state flow conditions for smooth tube. As shown in the figure, the present results are in good agreement with those from available correlations within ±6% and ±10% in comparison with Dittus-Boelter and Gnielinski correlations, respectively, for Nu and ±6% with both Blasius and Petukhov for f.

In addition, the correlations of the measured data for Nu and f in the present work are provided in Eqs. (4.18) and (4.19), respectively.

Correlation of Nu for smooth tube :

$$\mathrm{Nu} = 0.0435\ \mathrm{Re}^{0.738}\ \mathrm{Pr}^{0.4} \tag{4.18}$$

Correlation of f for smooth tube :

$$f = 0.4424\ \mathrm{Re}^{-0.28} \tag{4.19}$$

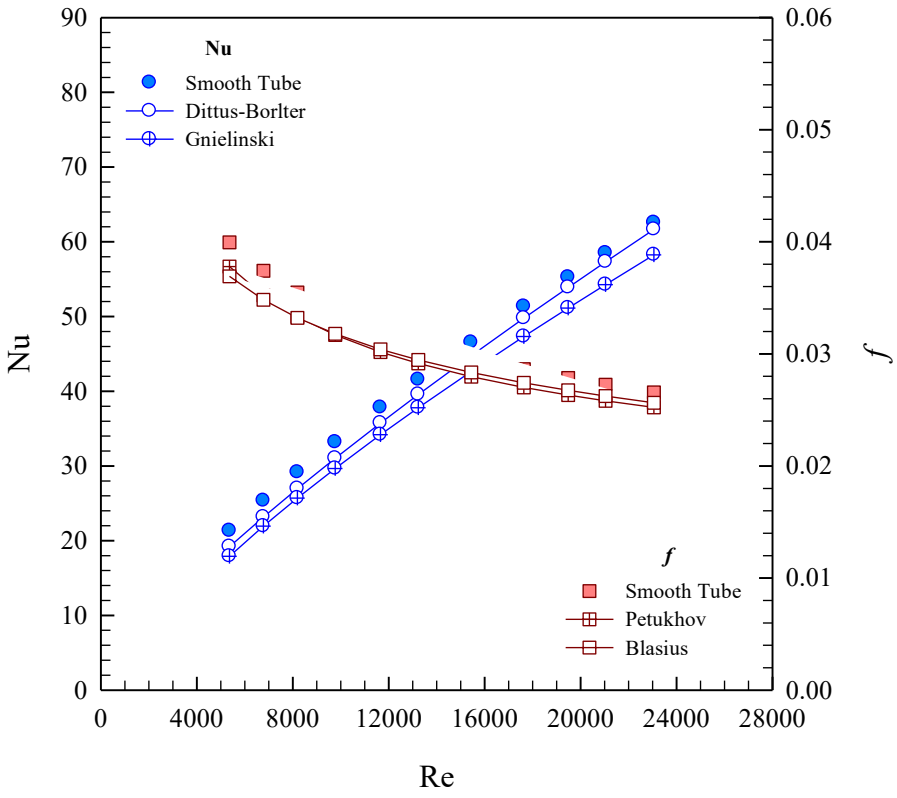

Figure 4.16 Verification of Nusselt number and friction factor for smooth tube.

4.6 Wall temperature distribution

The axial wall temperature distribution along the tube at each thermocouple location for smooth tube and a tube with quadruple counter-twisted tape insert (TF-TT, 4T4) is depicted in Figure. 4.17. The wall temperature variation is found to gradually increase downstream of the inlet until x/D≈5–6 and then increased slightly to the exit. However, in the region near the exit, the wall temperature drops slightly from location x/D≈18 to the outlet due to the exit loss effect, similar trend as found in ref. [1, 48] if it is presented in the form of local Nu_x. The wall temperature and the temperature difference between the inlet and outlet of air at low Re are seen to be higher than those at high *Re*.

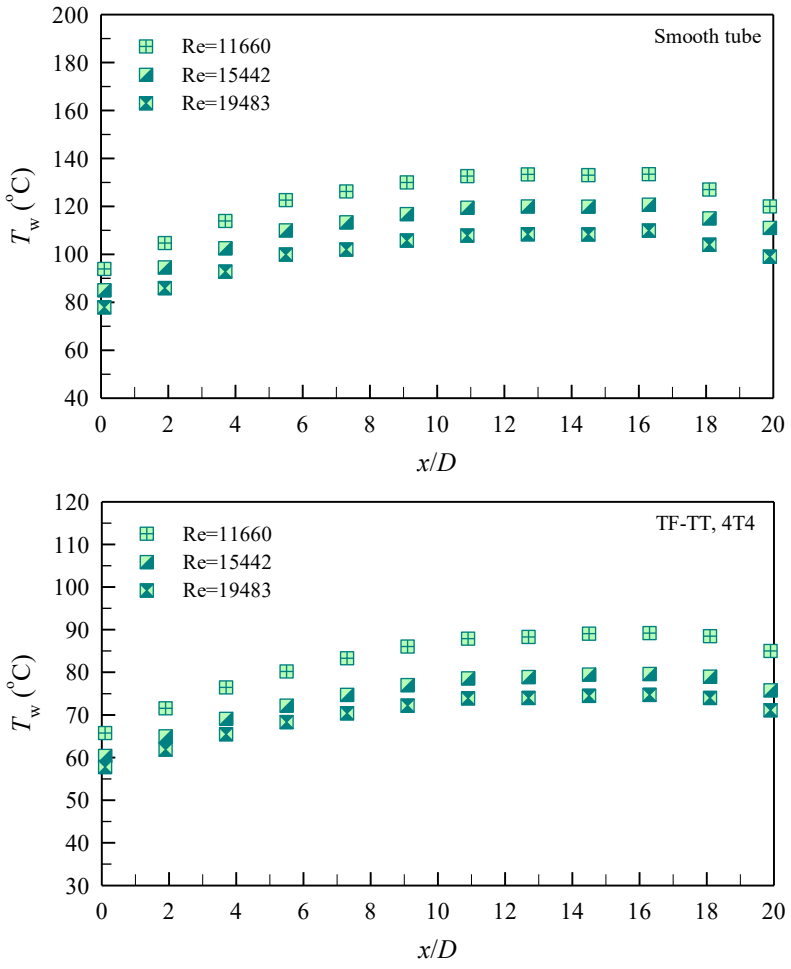

Figure 4.17 Axial wall temperature distribution along test tube.

CHAPTER 5
MULTIPLE TWISTED-TAPES

5.1 Opening remarks

This chapter presents an experimental investigation on enhanced heat transfer and pressure loss characteristics by using multiple twisted-tapes inserted into a round tube having a uniform heat-fluxed wall. The investigation has been conducted in the heat exchanger tube with various twisted-tape numbers of co- and counter-twist arrangements for turbulent air flow, Reynolds number (*Re*) from 5300 to 24,000. The experimental results of heat transfer and pressure drop are presented in terms of Nusselt number (Nu) and friction factor (*f*), respectively. The multiple twisted-tapes are classified into 2 parts :

Part I : Loose-fit twisted-tapes (LF-TT), the double and triple small twisted-tapes with twist ratios of y/w=4.0 and 4.5 were placed in the same parallel plane along the axial length of tube, held with straight steel wires which has semicircular rod-supports on both ends.

Part II : Tight-fit twisted-tapes (TF-TT) were inserted into the test section with slightly tight fit and multiple twisted-tapes were attached together by superglue.

The twisted-tapes in each part yielding the maximum thermal enhancement factor are compared with the different modified twisted-tapes in previous work.

5.2 Loose-fit twisted-tapes

5.2.1 Effect of LF-TT on heat transfer

The mean heat transfer (Nu) of the tube inserted with loose-fit multiple twisted-tapes is depicted in Figure 5.1. It is found that the Nu increases with the rise of *Re* for all twisted-tapes employed. In the figure, the heat transfer rate of the inserted tube is found to be considerably higher than that of the plain tube. This can be attributed to the strong swirl enhancing the flow turbulence intensity, leading to higher convection heat transfer than the axial flow in the plain tube. Thus, the stronger vortex flow, the greater Nu becomes. The combination of L_T and R_T tapes is called “counter-twisted tape” while that of L_T and L_T tapes is called “co-twisted tape”. The Nu increases with the increment of tape number (*N*) but with decreasing twist ratio due to the increase of swirl intensity imparted to the flow at the tube wall. The triple twisted-tapes provide mean heat transfer higher than double twisted-tapes about 13% and 11% for y/w=4.0 and 4.5, respectively. The counter-twisted tapes yield considerable Nu in comparison with co-twisted tapes about 3% for *N*=2 and about 5% for *N*=3.

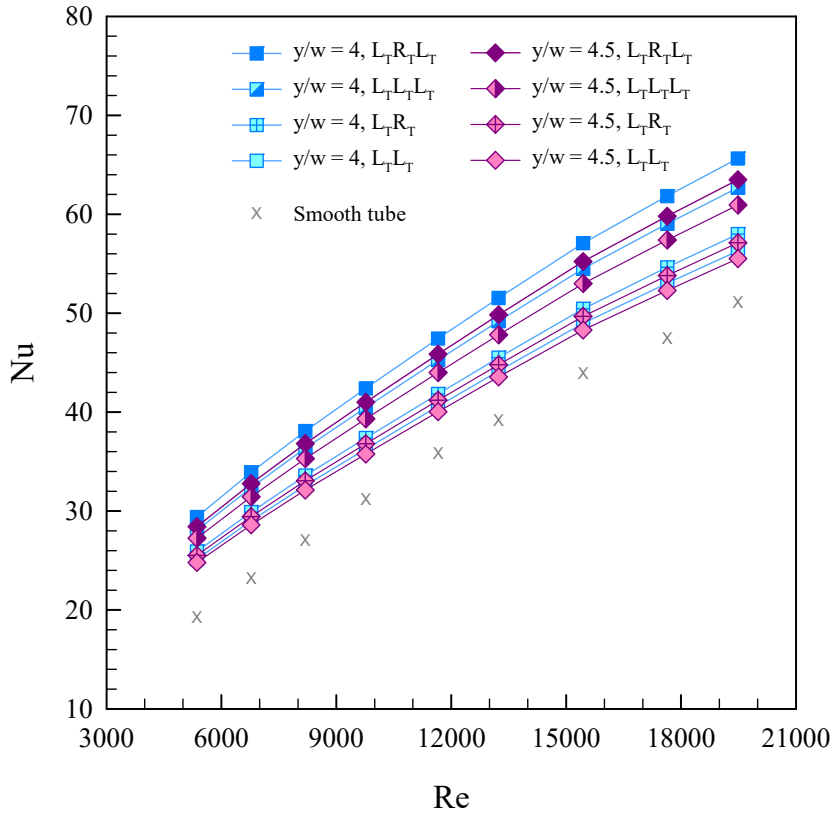

Figure 5.1 Effect of LF-TT on Nusselt number.

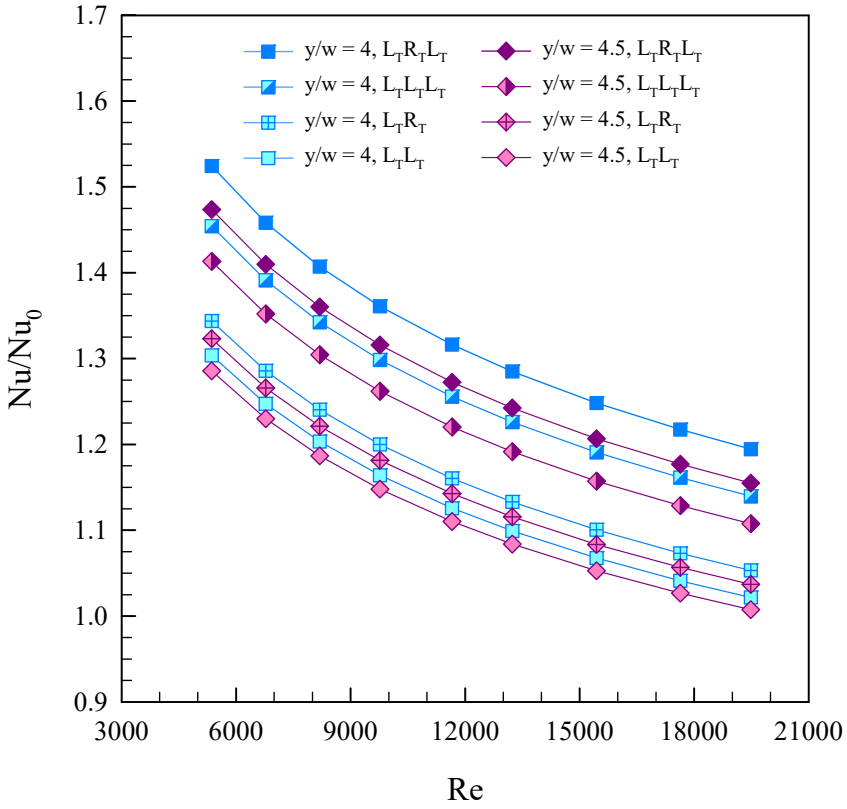

Figure 5.2 Effect of LF-TT on Nusselt number ratio.

The Nu/Nu_0 defined as a ratio of augmented Nu to Nu of plain tube, shows decreasing trend with the rise of *Re* for all cases studied as can be seen in Figure 5.2. Under the present measurement, the Nu/Nu_0 values for the L_TL_T, L_TR_T, $L_TL_TL_T$ and $L_TR_TL_T$ tapes are, respectively, in a range of 1.02–1.30, 1.05–1.34, 1.14–1.45 and 1.19–1.52 at y/w=4 and 1.01–1.29, 1.04–1.32, 1.11–1.41 and 1.15–1.47 at y/w=4.5, depending on the *Re* value.

5.2.2 Effect of LF-TT on friction factor

The influence of the twisted-tape number and arrangement on the *f* characteristics against the *Re* is depicted in Figure 5.3. It is interesting to note in the figure that the application of twisted tapes gives rise to the *f* considerably higher than that of the plain tube with no insert. This can be attributed to dissipation of the dynamic pressure of the fluid due to higher surface area and flow blockage of the twisted tape along the tube wall. The *f* decreases with the increment of y/w but the reduction of *N*. The triple twisted-tapes provide mean *f* higher than the double twisted-tapes about 21% for both twist ratios. The *f* values for the counter-twisted tapes are seen to be higher than those for the co-twisted ones about 5%.

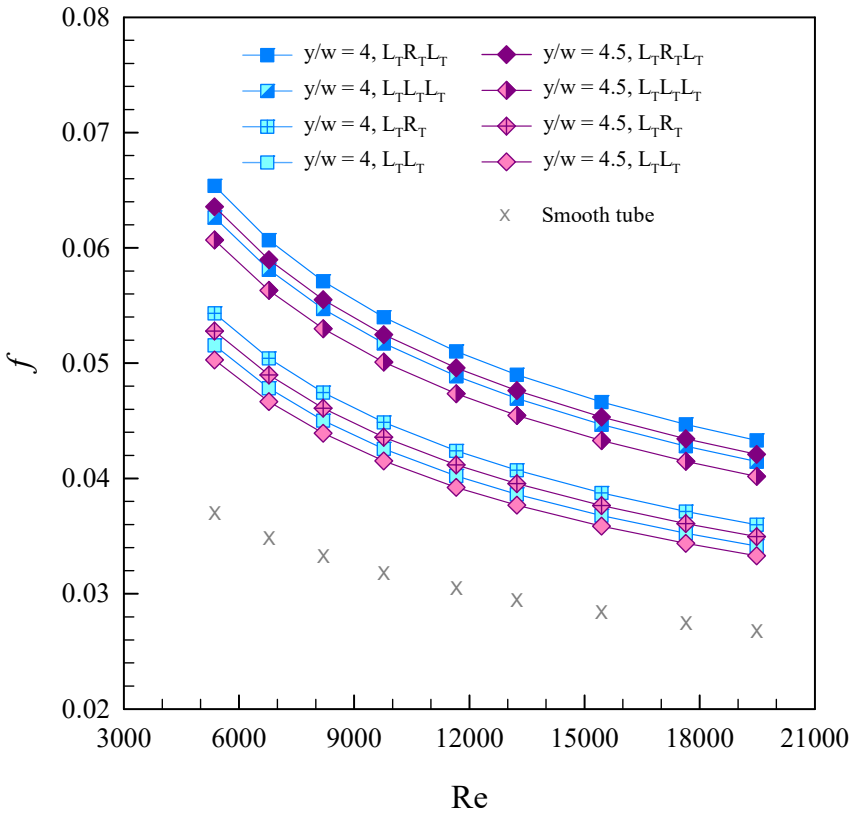

Figure 5.3 Effect of LF-TT on friction factor.

The f/f_0 defined as a ratio of augmented f to f of plain tube shows the decreasing trend with the rise of Re for all cases studied as can be seen in Figure 5.4. The f/f_0 values for the L_TL_T, L_TR_T, $L_TL_TL_T$ and $L_TR_TL_T$ tapes are, respectively, in a range of 1.28–1.40, 1.35–1.47, 1.55–1.70 and 1.62–1.77 for y/w=4 and of 1.24–1.36, 1.31–1.43, 1.50–1.64 and 1.57–1.72 for y/w=4.5.

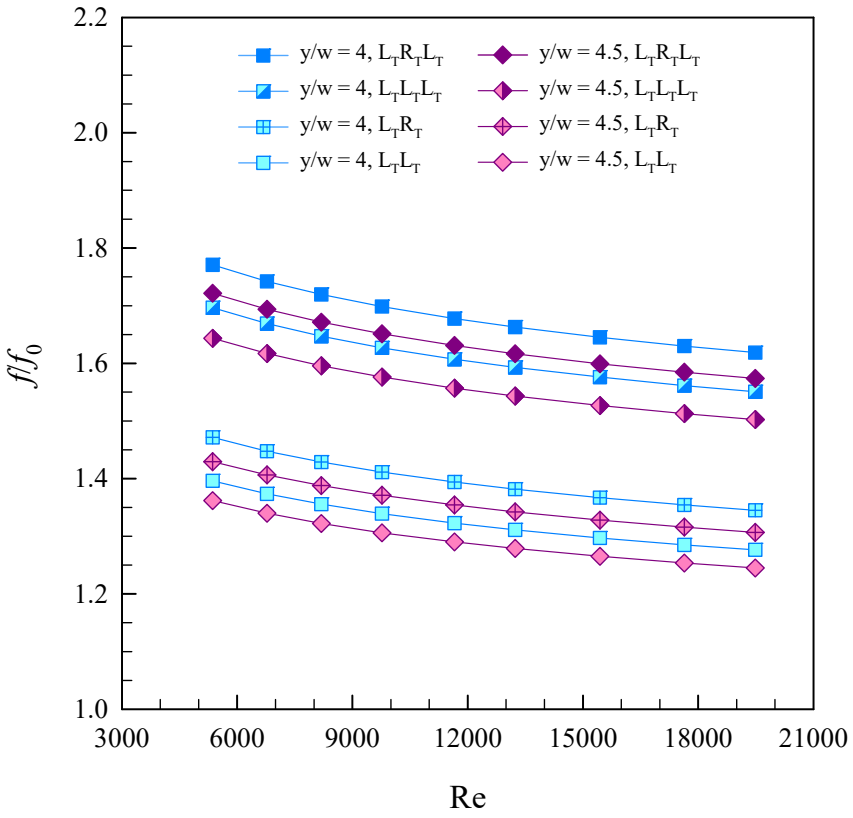

Figure 5.4 Effect of LF-TT on friction factor ratio.

5.2.3 Effect of LF-TT on thermal performance factor

Figure 5.5 depicts the effect of different twisted-tape numbers and arrangements on thermal performance factor (η). For all, the data obtained by the measured Nu and f values are compared at similar pumping power conditions. In the figure, the η decreases with the increase of Re for all the tapes studied. The counter-twisted tapes provide higher η than the co-twisted ones. The η values for the L_TL_T, L_TR_T, $L_TL_TL_T$ and $L_TR_TL_T$ tapes are, respectively, in a range of 0.94–1.17, 0.95–1.18, 0.98–1.22 and 1.02–1.26 for y/w=4 and of 0.94–1.16, 0.95–1.17, 0.97–1.20 and 0.99–1.23 for y/w=4.5. The maximum η is found to be about 1.26 for the triple counter-twisted tapes ($L_TR_TL_T$) at y/w=4. It is interesting to note that the η tends to increase with the increment of N.

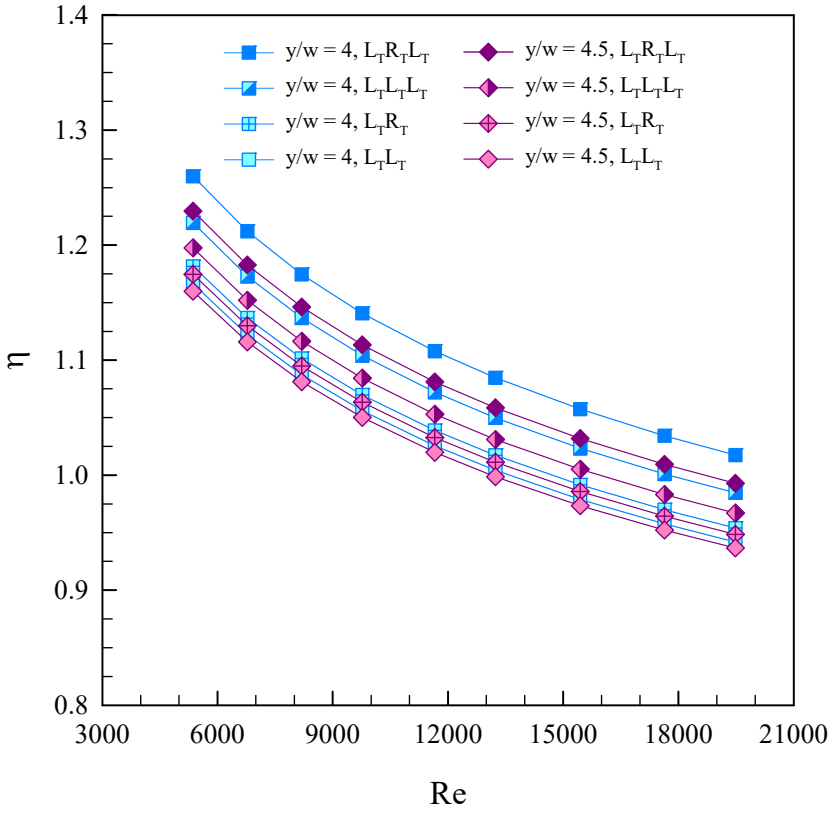

Figure 5.5 Effect of LF-TT on thermal performance factor.

Table 5.1 Experimental results of loose-fit multiple twisted-tapes.

Tape Types	Results		
	Nu/Nu_0	f/f_0	η
y/w=4.0, $L_TR_TL_T$	1.52–1.19	1.77–1.62	1.26–1.02
y/w=4.5, $L_TR_TL_T$	1.47–1.15	1.72–1.57	1.23–0.99
y/w=4.0, $L_TL_TL_T$	1.45–1.14	1.70–1.55	1.22–0.98
y/w=4.5, $L_TL_TL_T$	1.41–1.11	1.64–1.50	1.20–0.97
y/w=4.0, L_TR_T	1.34–1.05	1.47–1.35	1.18–0.95
y/w=4.5, L_TR_T	1.32–1.04	1.43–1.31	1.17–0.95
y/w=4.0, L_TL_T	1.30–1.02	1.40–1.28	1.17–0.94
y/w=4.5, L_TL_T	1.29–1.01	1.36–1.24	1.16–0.94

5.3 Tight-fit twisted-tapes

5.3.1 Effect of TF-TT on heat transfer

The variations of Nu and Nusselt number ratio, Nu/Nu_0 with Re for the tube inserted with tight-fit multiple twisted-tapes are depicted in Figures 5.6 and 5.7, respectively. It is visible that all the tapes yield considerable heat transfer with a similar trend in comparison with the plain tube. For a single twisted tape, the heat transfer rate increases with decreasing the twist ratio as already mentioned in the literature. Due to the increase of swirl intensity imparted to the flow at tube wall, the heat transfer rate of the inserted tube is found to be considerably higher than that of the plain tube with no insert. This can be attributed to stronger swirl enhancing turbulence intensity, leading to higher convection heat transfer than axial flow in the plain tube. Thus, the higher vortex flow, the greater Nusselt number becomes. In scrutiny of Figure 5.6, the Nu obtained from the combined R_T and L_T tapes (called counter-twisted tapes) is seem to be higher than that from the combined R_T and R_T, or L_T and L_T ones (called co-twisted tapes). For double twisted-tapes, the counter-twisted tapes (2T2) perform better than the co-twisted ones (2T1) and also the triple counter-twisted tapes (3T2) yield higher Nu than the triple co-twisted ones (3T1). For quadruple twisted tapes, it is noted that the four counter-swirl pairs, 4T4 and four co-swirl pairs, 4T1 provide, respectively, the highest and lowest heat transfer rate. The 4T3 consisting of two counter-swirl pairs performs better than the 4T2 comprising the counter-swirl and co-swirl pairs.

The Nusselt number ratio (Nu/Nu_0) shows a decrease trend with the rise of *Re* as seen in Figure 5.7. Under the present study, the Nu/Nu_0 values for the 4T4, 4T3, 4T2, 4T1; 3T2, 3T1; 2T2, 2T1; and 1T1 tapes are, respectively, in a range of 1.70–2.12, 1.67–2.08, 1.65–2.06, 1.63–2.02; 1.53–1.90, 1.51–1.88; 1.23–1.53, 1.18–1.47; and 1.15–1.43, depending on *Re* values. The mean Nu/Nu_0 increases for *N*=4(4T4), 3(3T2), 2(2T2) and 1(1T1) are about 87%, 68%, 35% and 27% above the plain tube.

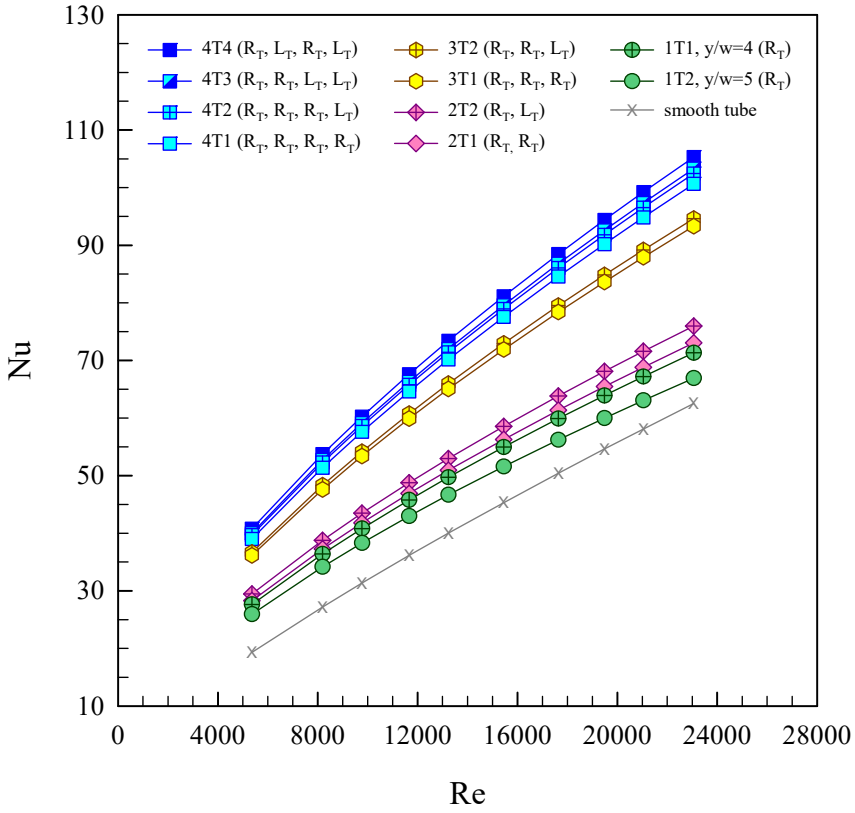

Figure 5.6 Effect of TF-TT on Nusselt number.

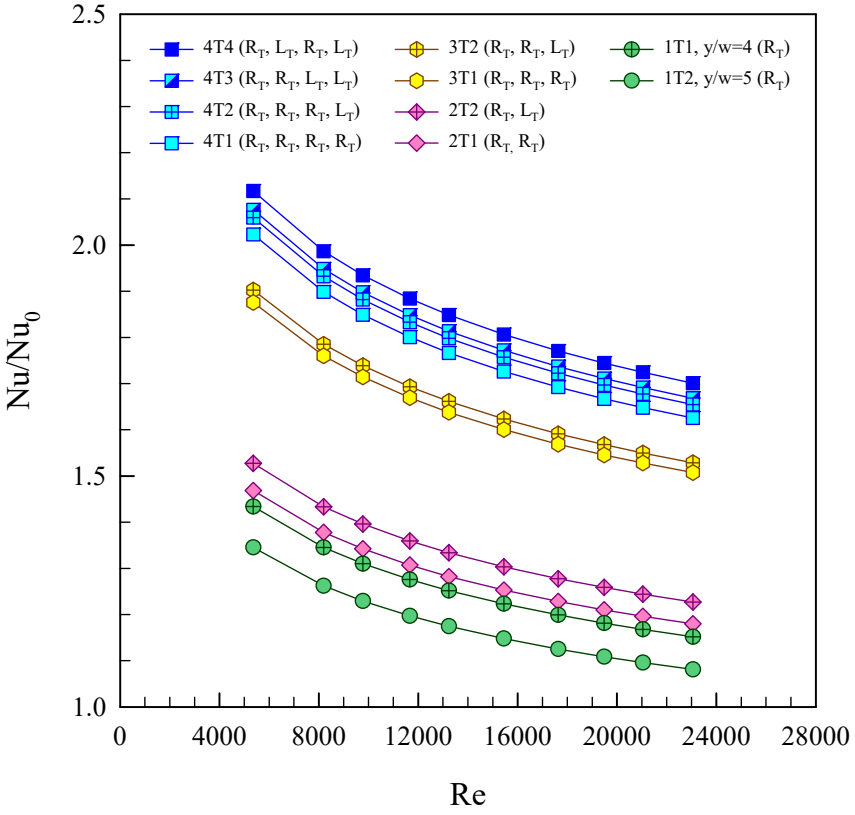

Figure 5.7 Effect of TF-TT on Nusselt number ratio.

5.3.2 Effect of TF-TT on friction factor

The influence of different twisted-tape numbers and arrangements on f and f/f_0 characteristics against Re is displayed in Figures 5.8 and 5.9, respectively. It is observed in the figure that the application of twisted tapes gives rise to the f considerably higher than that of the plain tube with no insert. The higher friction loss mainly comes from the increased surface area and higher swirl intensity. The f of single twisted-tape increases with the reduction of twist ratio and is about 2 times above that of the plain tube. The f values for double and triple counter-twisted tapes (2T2 and 3T2) are seen to be higher than those for double and triple co-twisted ones (2T1 and 3T1) and are around 5% and 50% above that for the single twisted-tape. For quadruple twisted-tapes, the highest and lowest f values are, respectively, found for four counter-twisted (4T4) and four co-twisted (4T1) tapes while the f of two counter-twisted tapes (4T3) is slightly larger than that of two co-twisted ones (4T2). This indicates a significant effect of multiple twisted-tape arrangements on thermal performance.

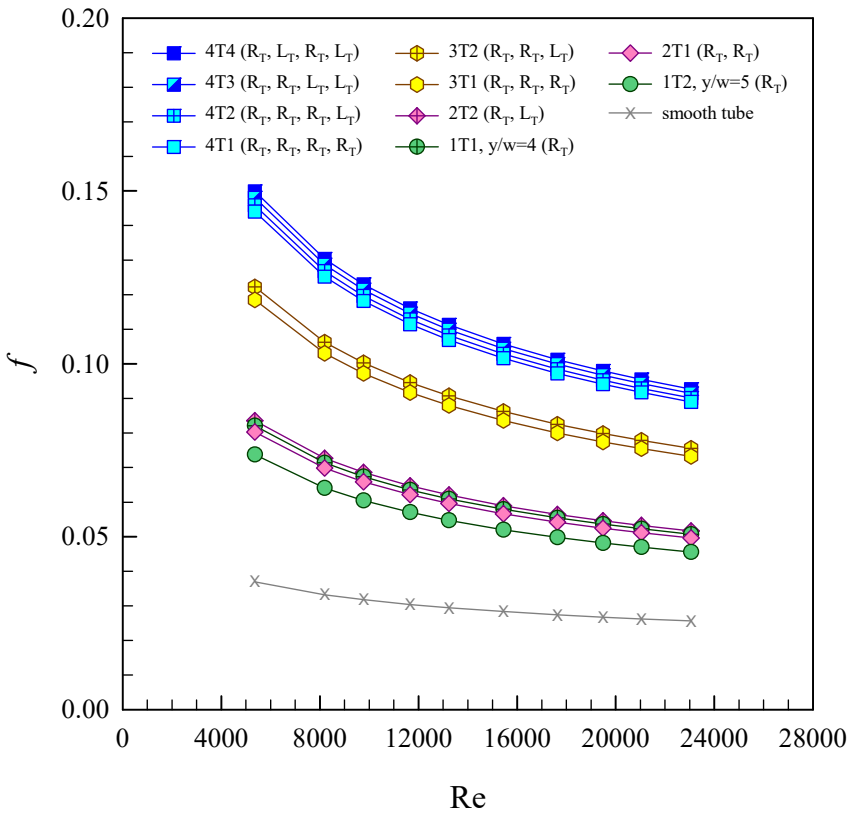

Figure 5.8 Effect of TF-TT on friction factor.

In Figure 5.9, it is visible that the f/f_0 shows decreasing tendency pattern with the increment of Re. The f/f_0 values for the 4T4, 4T3, 4T2, 4T1; 3T2, 3T1; 2T2, 2T1; and 1T1 tapes are, respectively, ranging from 3.61–4.06, 3.57–4.01, 3.51–3.95, 3.47–

3.90; 2.95–3.31, 2.86–3.21; 2.01–2.26, 1.94–2.18; and 1.98–2.22, depending on the *Re*. The mean f/f_0 increases for *N*=4(4T4), 3(3T2), 2(2T2) and 1(1T1) are about 278%, 208%, 111% and 107% above the plain tube.

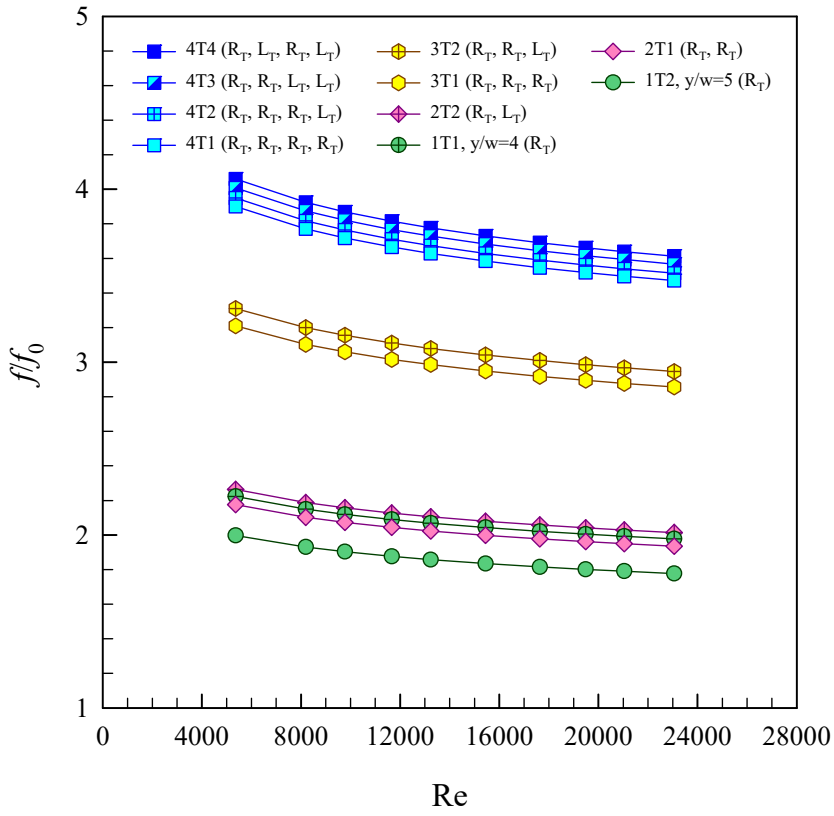

Figure 5.9 Effect of TF-TT on friction factor ratio.

5.3.3 Effect of TF-TT on thermal performance factor

Figure 5.10 portrays the variation of the thermal performance factor (η) with *Re*. For all, the data obtained by the measured Nu and *f* values are compared at the same pumping power. It is seen in the figure that the η values generally are above unity for all the inserted tubes while are below unity only for the single twisted (1T1 and 1T2) and double co-twisted tapes (2T1) at higher *Re* values. The η tends to decrease as *Re* increases for all tapes studied. Counter-twisted tapes provide higher η than co-twisted ones and the maximum η of about 1.33 is found for quadruple counter-twisted tapes (4T4) at lower *Re*. It is noted that the η displays increasing trend with the increment of *N*. To obtain higher η, the use of counter-twisted tapes at *N*>2 is recommended. The application of counter-twisted tapes leads to the increase in mean η of about 20%, 15% and 5% for *N*=4(4T4), 3(3T2) and 2(2T2), respectively.

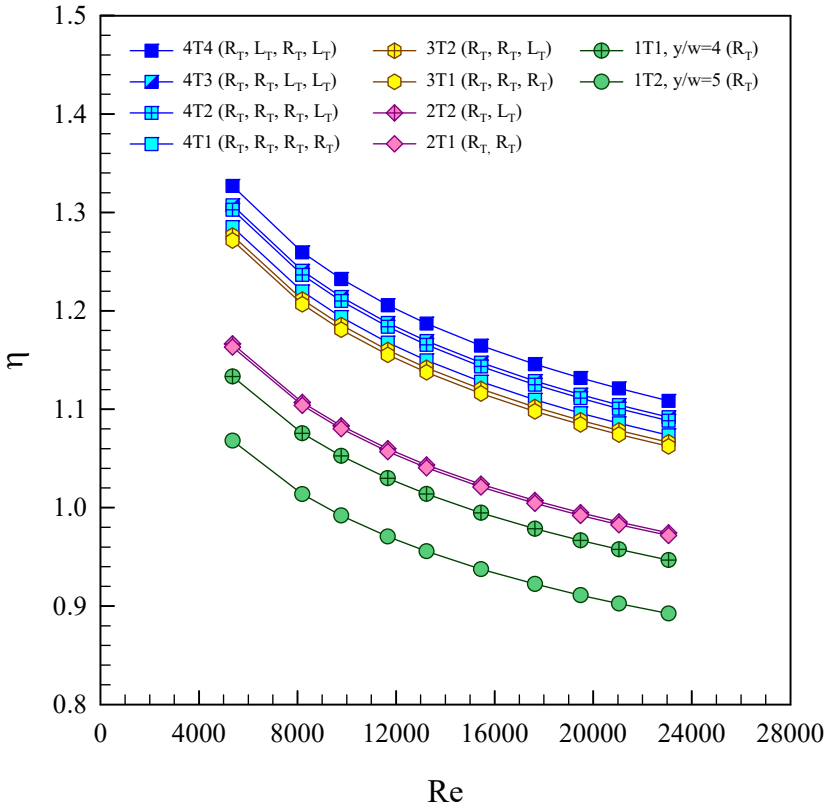

Figure 5.10 Effect of TF-TT to thermal performance factor.

Table 5.2 Experimental results of tight-fit multiple twisted-tapes.

Tape Types	Results		
	Nu/Nu_0	f/f_0	η
4T4	2.12–1.70	4.06–3.61	1.33–1.11
4T3	2.08–1.67	4.01–3.57	1.31–1.09
4T2	2.06–1.65	3.95–3.51	1.30–1.09
4T1	2.02–1.63	3.90–3.47	1.29–1.07
3T2	1.90–1.53	3.31–2.95	1.28–1.07
3T1	1.88–1.51	3.21–2.86	1.27–1.06
2T2	1.53–1.23	2.26–2.01	1.16–0.97
2T1	1.47–1.18	2.18–1.94	1.13–0.95
1T2	1.37–1.07	2.00–1.78	1.07–0.88
1T1	1.43–1.15	2.22–1.98	1.10–0.92

5.4 Comparison with previous work

The comparison of thermal performance factors of different modified twisted tapes from previous work and multiple twisted tapes in the present work is shown in Table 5.3.

The previous investigations included the broken twisted tapes with twist ratio of 2 [1], the helically twisted tapes (HTT) with *y/w*=3 and helical pitch ratio, *p/D*=2 [7], the alternate-axes twisted tapes with centre wings (WT-A) at attack angle, β=74° [13], the alternate clockwise and counterclockwise twisted tapes (C-CC) with *y/w*=3.0 and twist angle, θ=90° [14], twisted tape with wire-nails (WN-TT) at *y/w*=2.0 [15], square-cut twisted tape (STT) with *y/w*=2.0 [16], the oblique delta-winglet twisted tape (O-DWT) with *y/w*=3 and wing-cut depth ratio of 0.32 [17], The peripherally-cut alternate-axes twisted tape (PT-A) with peripherally-cut width ratio, *w/W*=0.11 [18], the peripherally-cut twisted tape (PT) with depth ratio, *d/W*=0.33 and width ratio, *w/W*=0.11 [19], the V-cut twisted tape (VTT) with *y/w*=2.0, depth and width ratio, *DR*=0.43 and *WR*=0.34 [20]. The alternate-axes twisted tapes with trapezoidal wings (T-Tra) with wing-chord ratio, *d/W*=0.3 [21]. The uniform alternate length twisted tape (TA) with *y/w*=3.0 at ratio of alternate length to twist length (*l/y*) of 0.5 [25].

For the present work, the triple counter-twisted tapes ($L_TR_TL_T$) at *y/w*=4.0 and the quadruple counter-twisted tapes (4T4) are offered for comparison. The comparison of thermal performance factors in tubes equipped with multiple twisted tape and various modified twisted tapes from previous work in the range of *Re*=4000–20,000 is depicted in Figure 5.7. The general trend found for all twisted-tape turbulators is that the η increases with decreasing Reynolds number. The η values obtained in the present work are moderate in a range of values in previous work.

Table 5.3 Comparison of thermal performance factor with previous work.

Ref.	Case study	η
[1]	Broken twisted tape, *y/w*=2	1.41–0.99
[25]	TA, *l/y*=0.5, *y/w*=3	1.41–0.98
[21]	T-Tra, *d/W*=0.3	1.40–1.04
[13]	WT-A, β=74°	1.40–1.03
present work	TF-TT, 4T4	1.33–1.09
[7]	HTT, *y/w*=3, *p/D*=2	1.32–1.05
[14]	C-CC, *y/w*=3.0, θ=90°	1.31–1.16
[15]	WN-TT *y/w*=2.0	1.30–1.19
[19]	PT, *d/W*=0.33, *w/W*=0.11	1.30–0.97
present work	LF-TT, *y/w*=4, $L_TR_TL_T$	1.27–0.97
[20]	VTT *y/w*=2.0, *DR*=0.43, *WR*=0.34	1.25–1.20
[16]	STT *y/w*=2.0	1.24–1.16
[18]	PT-A, w/W=0.11	1.22–0.89
[17]	O-DWT, y/W=3, d/w=0.32	1.21–1.12

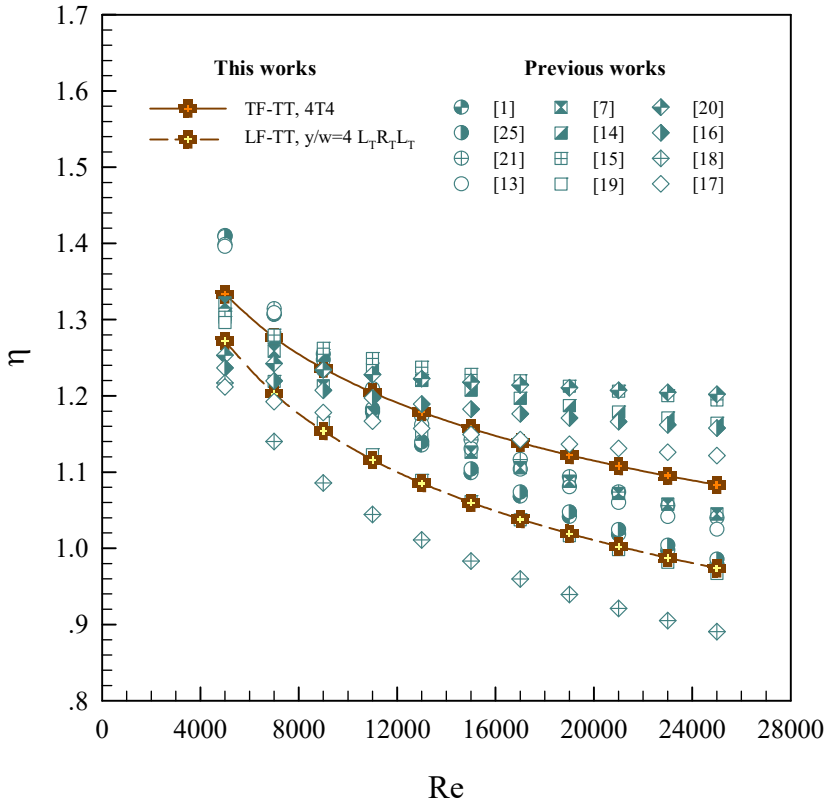

Figure 5.11 Comparison of thermal performance factor with previous work.

5.5 Conclusions

An experimental study has been performed to investigate the air flow friction and heat transfer characteristics in a round tube inserted with loose-fit and tight-fit multiple twisted-tapes with different tape numbers and twist directions for the turbulent regime, *Re*=5300–24,000 under a uniform heat-flux condition. From the experimental results of the present study, the following conclusions can be drawn.

For using loose-fit multiple twisted-tapes, the mean Nu and *f* values are higher than the plain tube around 1.01–1.52 and 1.24–1.77 times, respectively. Both the Nu and *f* show the increasing trend with the increment of *N* but with the reduction of twist ratio. The counter-twisted tapes provide Nu and *f* higher than the co-twisted ones. The maximum η of about 1.26 is obtained for the triple counter-twisted tapes ($L_TR_TL_T$) at *y/w*=4. It is noted that the η shows increasing tendency pattern with the increment of *N*.

For the tight-fit multiple twisted-tapes, Nu and *f* values are, respectively, in a range of 1.15–2.12 and 1.94–4.06 times above the plain tube. Both the Nu and *f* are seen to increase with the increment of *N* and with counter-twist arrangements. The η tends to decrease with the increase in *Re* but with decreasing *N*. The highest η is found to be about 1.33 for quadruple counter-twisted tapes (4T4).

CHAPTER 6
WINGLETS PLACED IN CENTRAL CORE FLOW

6.1 Opening remarks

This chapter describes the influence of different winglet geometry placed in the flow core region on heat transfer and pressure drop in a tubular heat exchanger. The winglet vortex generators are classified into 3 parts :

Part I : Winglets (WVGs),

Part II : Winglet pairs with V-tip pointing downstream (VD-WVGs),

Part III : Winglet pairs with V-tip pointing upstream (VU-WVGs).

The experiment was carried out in a uniform heat-fluxed tube by varying turbulent airflow for Reynolds number ranging from 5300 to 24,000. In the present work, the WVGs were mounted periodically in the tube with different three attack angles (α=30°, 45° and 60°) at four winglet-pitch ratios (P_R=P/D=0.5, 1.0, 1.5 and 2.0) and three winglet-width or blockage ratios (B_R=e/D=0.1, 0.15 and 0.2).

The experimental results of heat transfer and pressure drop are, respectively, presented in terms of Nusselt number ratio (Nu/Nu_0) and frictiom factor ratio (f/f_0). The empirical correlations for Nusselt number (Nu) and friction factor (f) for the turbulators with different geometry in the present work are also determined. The winglet geometry that provides the maximum thermal enhancement factor is compared to the numerical results and the flow structure and heat transfer mechanisms are explored. Finally, the optimization analysis for the winglet geometry parameters is made to obtain the optmal thermal enhancement factor.

6.2 Winglets

6.2.1 Effect of WVGs on heat transfer

The effect of four different pitch ratios (P_R=0.5, 1, 1.5 and 2) and three blockage ratios (B_R=0.1, 0.15 and 0.2) on the heat transfer is examined and presented in the form of Nu and Nu/Nu_0. The variations of Nu/Nu_0 with Re are displayed in Figures 6.1, 6.2 and 6.3 for the WVGs with α=30°, 45° and 60°, respectively. In the figures, the Nu/Nu_0 tends to decrease slightly with the rise of Re for all cases studied. The heat transfer value of the tube with WVGs is found to be better than that of the smooth tube because the WVGs provide the stronger mixing or turbulence intensity leading to destruction of thermal boundary layer and also the vortex flow creating better flow mixing between fluid at the core and the tube wall. Both flow phenomena promote an increase in the tangential and radial turbulent fluctuation or the turbulence intensity, thinning the boundary layer, and therefore cause the rise in

heat transfer rate inside the tube. The heat transfer shows the uptrend with the reduction of P_R due to higher turbulence intensity imparted to the flow between winglet elements, resulting in higher temperature gradients near the tube wall. The experimental results also reveal that the heat transfer tends to increase with the increment of B_R. This is because a larger winglet width can generate stronger vortex flow, giving higher turbulence intensity and better fluid mixing leading to higher heat transfer rate than a smaller one.

For 30° WVGs, at P_R=0.5, 1, 1.5 and 2, the average Nu values are about 218, 208, 200 and 186%; 234, 222, 215 and 202%; and 251, 240, 229 and 217% above the smooth tube for B_R=0.1, 0.15 and 0.2, respectively. The mean Nu for P_R=0.5 is about 5, 9 and 16% higher than that for P_R=1.0, 1.5 and 2.0, respectively and that is about 204, 219 and 235% above the smooth tube for B_R=0.1, 0.15 and 0.2. The mean Nu for B_R=0.2 is at some 7 and 15% higher than that for B_R=0.15 and 0.1.

For 45° WVGs, at P_R=0.5, 1, 1.5 and 2, the average Nu values are about 235, 219, 205 and 193%; 257, 237, 223 and 210%; and 276, 258, 241 and 226% above the smooth tube for B_R=0.1, 0.15 and 0.2, respectively. The mean Nu for P_R=0.5 is around 7, 14 and 22% higher than that for P_R=1.0, 1.5 and 2.0, respectively while that for B_R=0.1, 0.15 and 0.2 is approximately 213, 232 and 250% over the smooth tube. The Nu for B_R=0.2 is about 8 and 17% higher than those of B_R=0.15 and 0.1.

For 60° WVGs, at P_R=0.5, 1, 1.5 and 2, the average Nu values are about 254, 229, 216 and 207%; 273, 246, 232 and 220%; and 296, 270, 257 and 240% above the smooth tube for B_R=0.1, 0.15 and 0.2, respectively. The P_R=0.5 yields the mean Nu higher than the P_R=1.0, 1.5 and 2.0 at about 11, 17 and 24%. The average Nu values of B_R=0.1, 0.15 and 0.2 are, respectively, about 227, 243 and 266% above the smooth tube whereas those of B_R=0.2 are some 9 and 19% above that for B_R=0.15 and 0.1.

6.2.2 Effect of WVGs on friction factor

Figures 6.4, 6.5 and 6.6 depict the variations of friction factor ratio (f/f_0) with *Re* for WVGs with α=30°, 45° and 60°, respectively. It is clearly observed in the figures that the f/f_0 tends to increase slightly with the increment of *Re* for all the WVGs applied. The WVGs provides a substantial increase in f over the smooth tube. This can be attributed to the dissipation of dynamic pressure of the fluid due to higher surface area and the reverse/swirl flow. The f values obtained from three pitch ratios are in a similar trend pattern and increased with the decreasing P_R but the rise in B_R.

For 30° WVGs, at P_R=0.5, 1, 1.5 and 2, the average f/f_0 values are, respectively, about 3.53, 2.89, 2.37 and 2.07; 4.46, 3.62, 3.02 and 2.74; and 5.61, 4.60, 3.80 and 3.43 times for B_R=0.1, 0.15 and 0.2. The mean f for P_R=0.5 is about 22, 47 and 66% higher than that for P_R=1.0, 1.5 and 2.0, respectively while that for B_R=0.1, 0.15 and

0.2 is about 2.72, 3.46 and 4.36 times above the smooth tube. The mean f for B_R=0.2 is approximately 25 and 60% above that for B_R=0.15 and 0.1, respectively.

For 45° WVGs, at P_R=0.5, 1, 1.5 and 2, the average f/f_0 values are about 5.91, 4.26, 3.41 and 2.74; 8.74, 6.12, 4.93 and 4.06; and 11.10, 8.30, 6.44 and 5.19 times for B_R=0.1, 0.15 and 0.2, respectively. The P_R=0.5 provides the mean f at about 39, 74 and 115% higher than the P_R=1.0, 1.5 and 2.0, respectively. The average f for B_R=0.1, 0.15 and 0.2 is about 4.08, 5.96 and 7.76 times above the smooth tube whereas that for B_R=0.2 is around 27 and 89% higher than that for B_R=0.15 and 0.1, respectively.

For 60° WVGs, at P_R=0.5, 1, 1.5 and 2, the average f/f_0 values are, respectively, 7.94, 5.23, 4.22 and 3.67; 12.05, 8.06, 6.38 and 5.38; and 16.23, 11.16, 9.22 and 7.33 times for B_R=0.1, 0.15 and 0.2. The mean f for P_R=0.5 is about 49, 86 and 121% higher than that for P_R=1.0, 1.5 and 2.0 while that for B_R=0.1, 0.15 and 0.2 is around 5.26, 7.97 and 10.98 times above the smooth tube, respectively. The B_R=0.2 yields the mean f at about 38 and 104% higher than the B_R=0.15 and 0.1.

6.2.3 Effect of WVGs on thermal performance factor

In thermal performance evaluation, the thermal performance factor (η) under a constant pumping power is taken into account by using Eq. (4.9). The variation of η with Re is depicted in Figures 6.7, 6.8 and 6.9 for WVGs with α=30°, 45° and 60°, respectively. It is seen in the figures that the η values generally are above unity for all the inserts, indicating that the use of WVGs is advantageous over the smooth tube. The η shows the downtrend pattern with increasing Re because Nu/Nu_0 tends to reduce with increasing Re while f/f_0 gives the reversing trend.

For 30° WVGs, the maximum η is between 1.45–1.59 for B_R=0.1 and P_R=1.5 while the minimum is from 1.35–1.49 for B_R=0.2 and P_R=0.5. The η values for B_R=0.1, 0.15 and 0.2 are, respectively, about 1.39–1.59, 1.37–1.57 and 1.35–1.56. At a given B_R, the P_R=1.5 yields the maximum η and the P_R=1 and 2 give similar η values while the lowest η is at P_R=0.5. The highest η around 1.59 is found for B_R=0.1 and P_R=1.5.

For 45° WVGs, the maximum η is in a range of 1.31–1.48 for B_R=0.1 and P_R=2.0 while the minimum is between 1.17–1.33 for B_R=0.2 and P_R=0.5. The η values for B_R=0.1, 0.15 and 0.2 are, respectively, about 1.23–1.48, 1.18–1.42 and 1.17–1.40. The P_R=2.0 yields the optimum η while the P_R=0.5 provides the lowest η. The highest η seen at B_R=0.1 and P_R=2.0 is 1.48.

For 60° WVGs, the maximum η lies between 1.26–1.47 for B_R=0.1 and P_R=2.0 while the minimum is 1.10–1.28 for B_R=0.2 and P_R=0.5. The η values for B_R=0.1, 0.15 and 0.2 are, respectively, about 1.20–1.47, 1.12–1.37 and 1.10–1.35. At a given B_R, the highest η is seen at P_R=2.0 and P_R=1.5 while the lowest η is at P_R=0.5. The highest η found at B_R=0.1 and P_R=2.0 is 1.47.

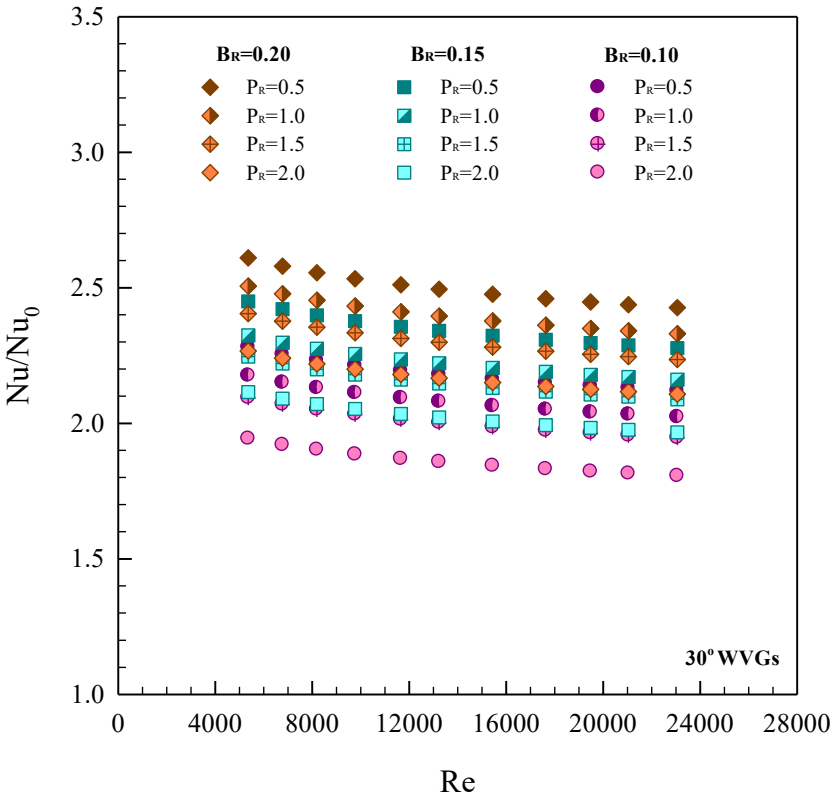

Figure 6.1 Effect of 30° WVGs on Nu/Nu_0.

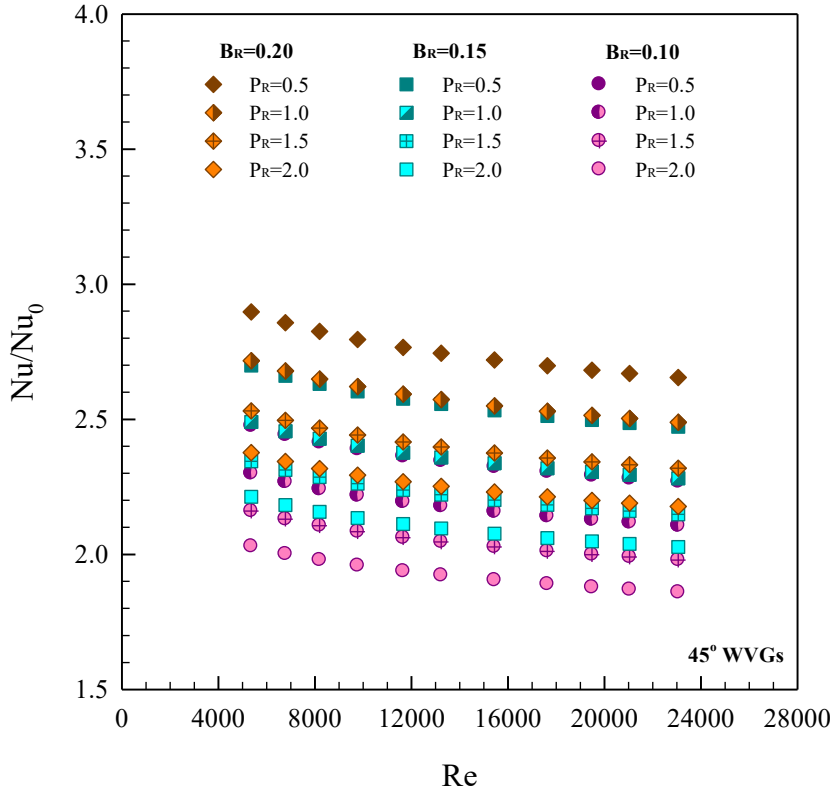

Figure 6.2 Effect of 45° WVGs on Nu/Nu_0.

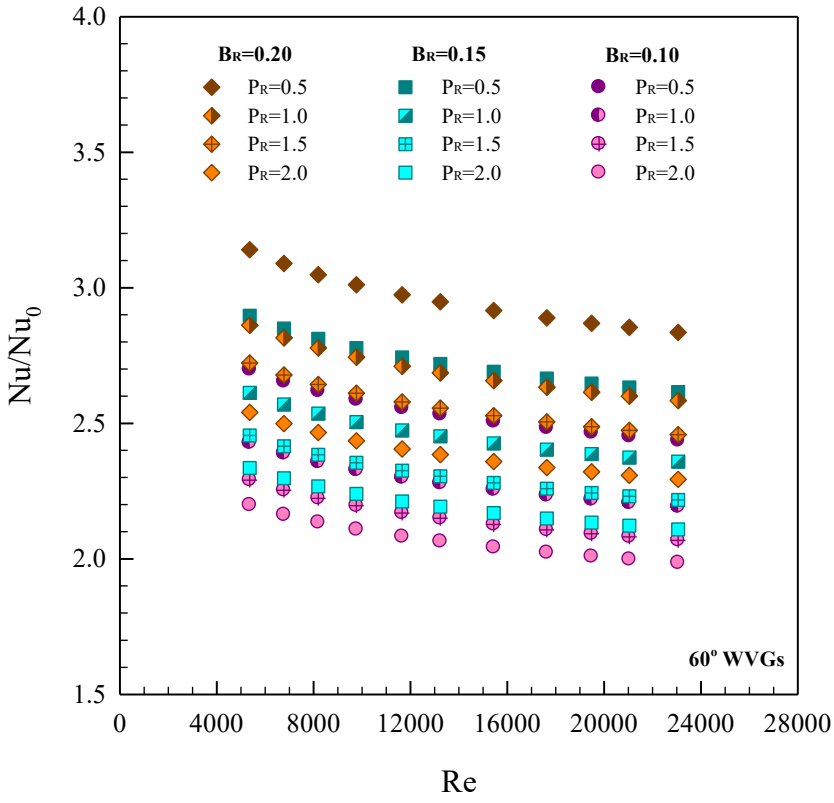

Figure 6.3 Effect of 60° WVGs on Nu/Nu_0.

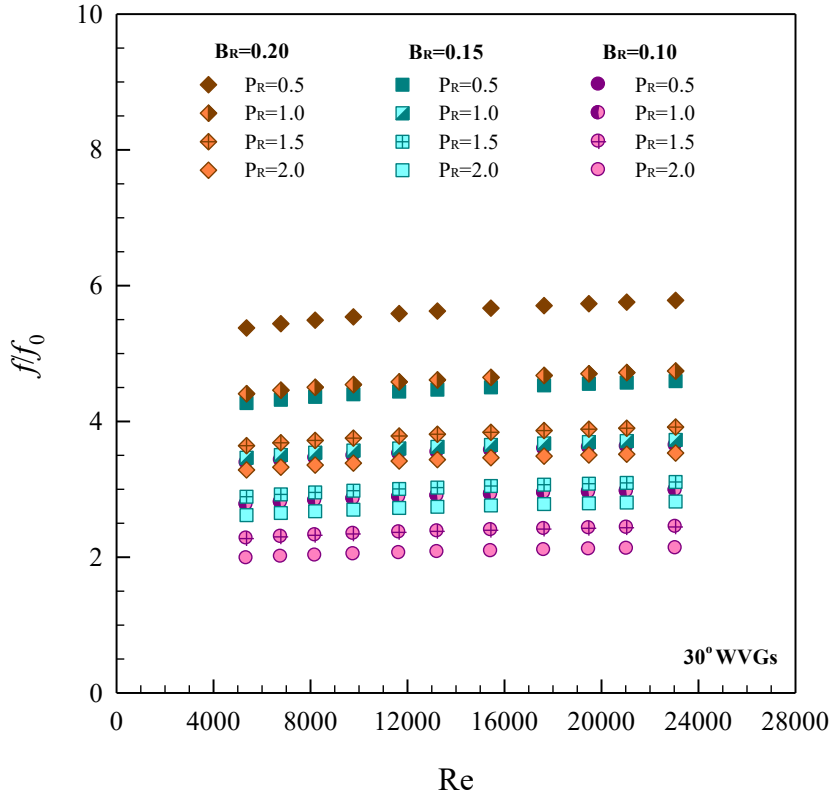

Figure 6.4 Effect of 30° WVGs on f/f_0.

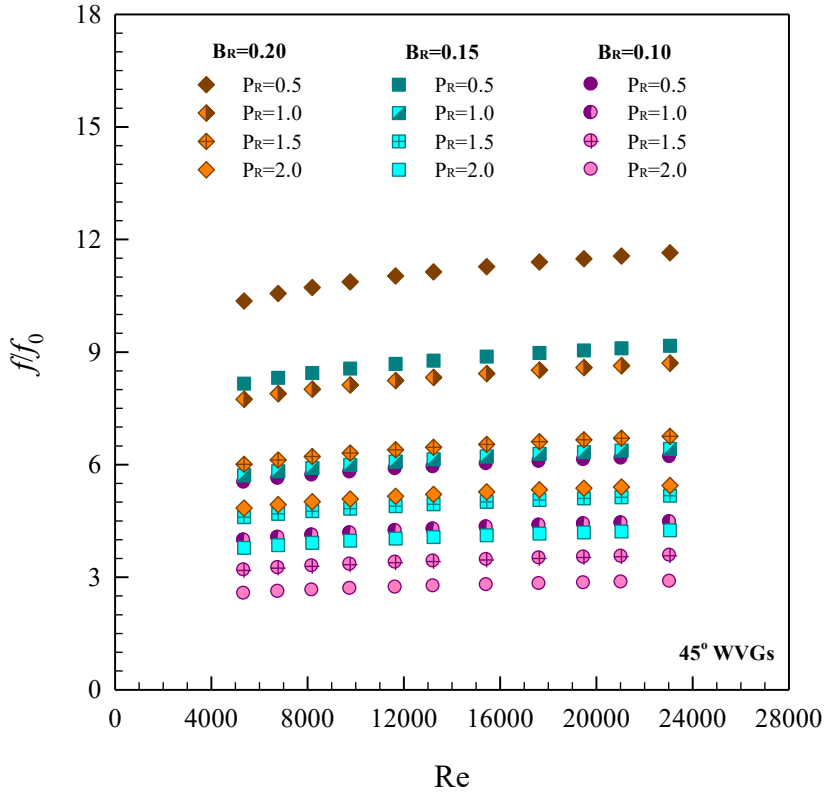

Figure 6.5 Effect of 45° WVGs on f/f_0.

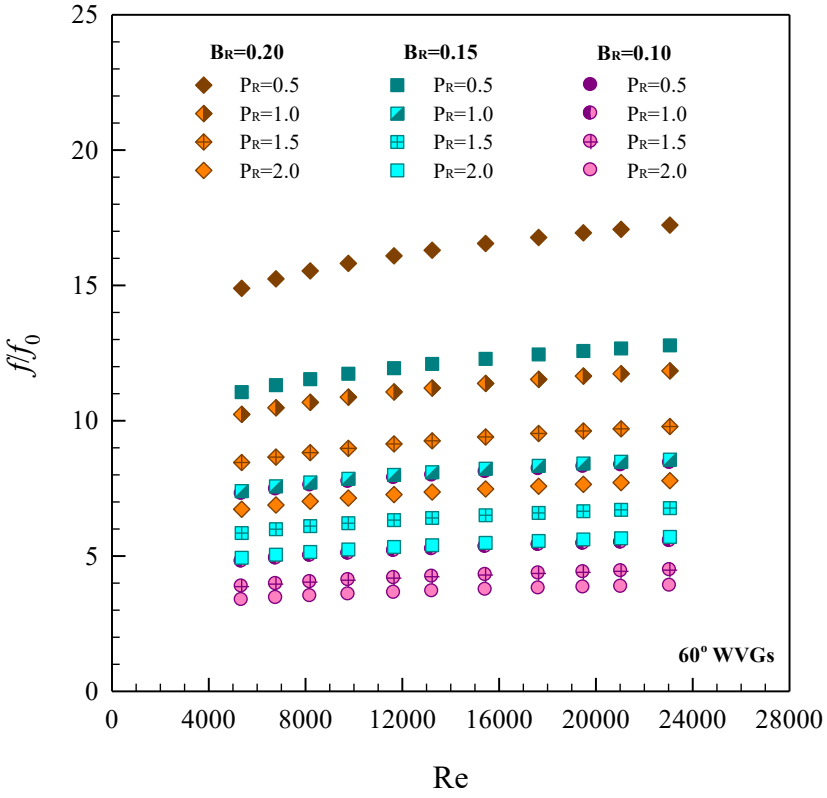

Figure 6.6 Effect of 60° WVGs on f/f_0.

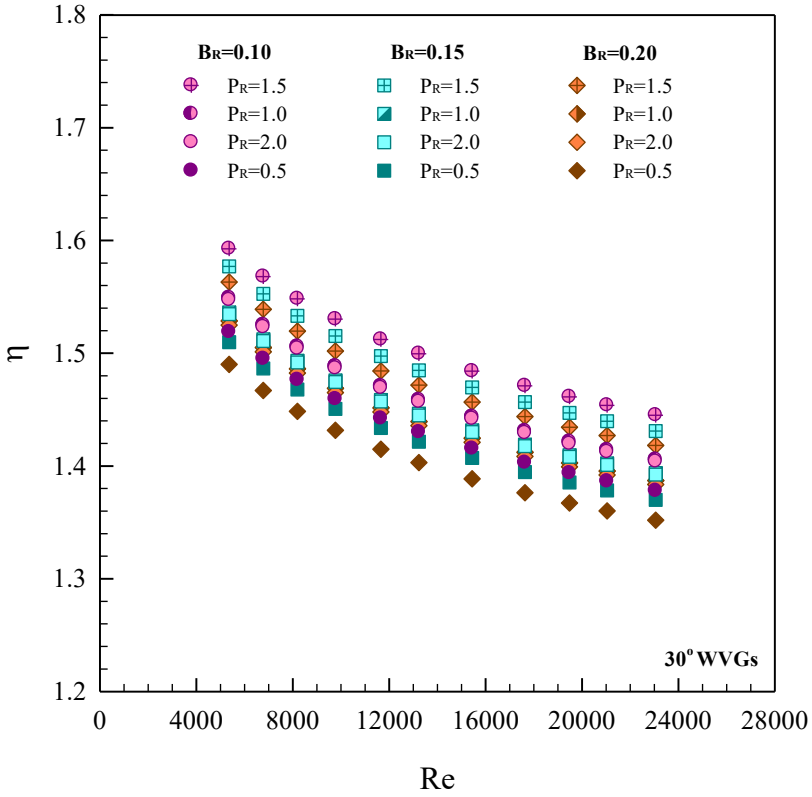

Figure 6.7 Effect of 30° WVGs on thermal performance.

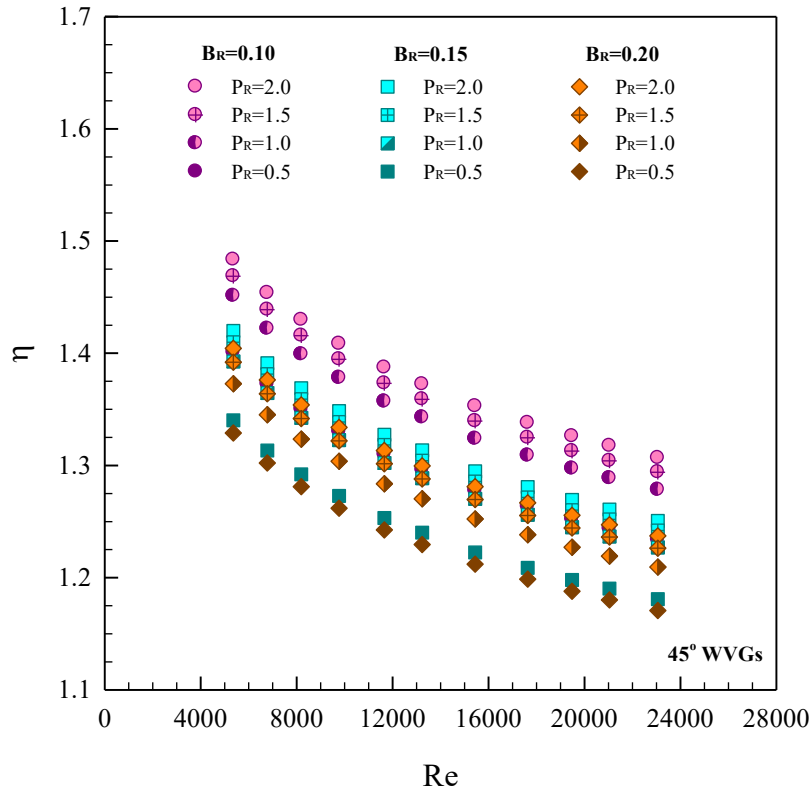

Figure 6.8 Effect of 45° WVGs on thermal performance.

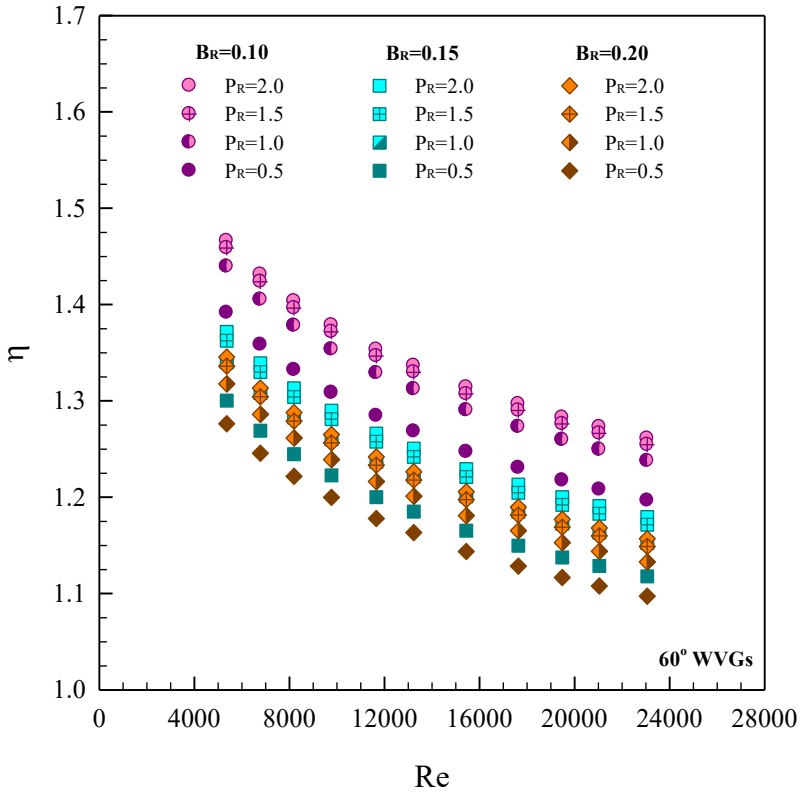

Figure 6.9 Effect of 60° WVGs on thermal performance.

Table 6.1 Experimental results of 30° WVGs.

WVGs			Results		
α	B_R	P_R	Nu/Nu$_0$	f/f_0	η
30°	0.10	0.5	2.28–2.12	3.38–3.64	1.52–1.39
		1.0	2.18–2.02	2.77–2.98	1.55–1.41
		1.5	2.09–1.95	2.27–2.45	1.59–1.45
		2.0	1.94–1.81	1.98–2.13	1.55–1.40
	0.15	0.5	2.45–2.28	4.27–4.59	1.51–1.37
		1.0	2.32–2.16	3.46–3.73	1.54–1.39
		1.5	2.25–2.09	2.89–3.11	1.57–1.43
		2.0	2.12–1.97	2.62–2.82	1.53–1.39
	0.20	0.5	2.61–2.43	5.38–5.78	1.49–1.35
		1.0	2.51–2.33	4.41–4.74	1.53–1.39
		1.5	2.40–2.24	3.64–3.92	1.56–1.42
		2.0	2.27–2.11	3.28–3.53	1.52–1.38
Optimal results			η=1.59 at Re≈5300, B_R=0.10 and P_R=1.5		

Table 6.2 Experimental results of 45° WVGs.

WVGs			Results		
α	B_R	P_R	Nu/Nu$_0$	f/f_0	η
45°	0.10	0.5	2.48–2.27	5.52–6.21	1.40–1.23
		1.0	2.30–2.11	3.98–4.48	1.45–1.28
		1.5	2.16–1.98	3.18–3.58	1.47–1.29
		2.0	2.03–1.86	2.56–2.88	1.48–1.31
	0.15	0.5	2.70–2.47	8.17–9.18	1.34–1.18
		1.0	2.49–2.28	5.72–6.43	1.39–1.23
		1.5	2.34–2.15	4.60–5.18	1.41–1.24
		2.0	2.21–2.03	3.79–4.26	1.42–1.25
	0.20	0.5	2.90–2.65	10.37–11.66	1.33–1.17
		1.0	2.72–2.49	7.75–8.72	1.37–1.21
		1.5	2.53–2.32	6.01–6.77	1.39–1.23
		2.0	2.38–2.18	4.85–.45	1.40–1.24
Optimal results			η=1.48 at Re≈5300, B_R=0.10 and P_R=2.0		

Table 6.3 Experimental results of 60° WVGs.

WVGs			Results		
α	B_R	P_R	Nu/Nu$_0$	f/f_0	η
60°	0.10	0.5	2.70–2.44	7.29–8.45	1.39–1.2
		1.0	2.43–2.19	4.80–5.56	1.44–1.24
		1.5	2.29–2.07	3.87–4.48	1.46–1.25
		2.0	2.20–1.99	3.37–3.90	1.47–1.26
	0.15	0.5	2.90–2.62	11.06–12.81	1.30–1.12
		1.0	2.61–2.36	7.40–8.57	1.34–1.15
		1.5	2.46–2.22	5.85–6.78	1.36–1.17
		2.0	2.34–2.11	4.93–5.71	1.37–1.18
	0.20	0.5	3.14–2.84	14.90–17.25	1.28–1.10
		1.0	2.86–2.58	10.24–11.86	1.32–1.13
		1.5	2.72–2.46	8.46–9.80	1.34–1.15
		2.0	2.54–2.29	6.73–7.79	1.35–1.16
Optimal results			η=1.47 at Re≈5300, B_R=0.10 and P_R=2.0		

6.3 Winglet pairs with V-tip pointing downstream

6.3.1 Effect of VD-WVGs on heat transfer

The relationships between Nu/Nu_0 and *Re* of the tube inserted with 30°, 45° and 60° VD-WVGs are depicted in Figures 6.10, 6.11 and 6.12, respectively. According to the figure, the VD-WVGs provide the heat transfer enhancement much higher than the smooth tube. The Nu/Nu_0 tends to slightly decrease with the increase of *Re* and B_R but the reduction of P_R for all cases, similar to the WVG inserts.

For 30° VD-WVGs, at P_R=0.5, 1, 1.5 and 2, the average Nu values are about 197, 178, 169 and 148%; 226, 207, 192 and 180%; and 245, 226, 209 and 198% above the plain tube for B_R=0.1, 0.15 and 0.2, respectively. The mean Nu for P_R=0.5 is around 9, 16 and 27% higher than that for P_R=1.0, 1.5 and 2.0 while that for B_R=0.1, 0.15 and 0.2 is some 173, 201 and 219% above the smooth tube and the B_R=0.2 performs better than the B_R=0.15 and 0.1 at about 9 and 24%, respectively.

For 45° VD-WVGs, at P_R=0.5, 1, 1.5 and 2, the average Nu values are around 209, 192, 182 and 160%; 253, 230, 216 and 190%; and 271, 247, 231 and 210% above the plain tube for B_R=0.1, 0.15 and 0.2, respectively. The P_R=0.5 provides the mean Nu higher than the P_R=1.0, 1.5 and 2.0 at about 9, 15 and 31%, respectively. The average Nu for B_R=0.1, 0.15 and 0.2 is around 186, 222 and 240% above the smooth tube and that for B_R=0.2 is some 7 and 30% higher than that for B_R=0.15 and 0.1, respectively.

For 60° VD-WVGs, at P_R=0.5, 1, 1.5 and 2, the average Nu values are some 226, 205, 190 and 170%; 268, 246, 224 and 201%; and 291, 266, 245 and 221% above the plain tube for B_R=0.1, 0.15 and 0.2, respectively. The P_R=0.5 provides the mean Nu around 10, 19 and 33% higher than the P_R=1.0, 1.5 and 2.0 while the average Nu for B_R=0.1, 0.15 and 0.2 is about 198, 235 and 256%, above the smooth tube and that for B_R=0.2 is around 9 and 30% over that for B_R=0.15 and 0.1, respectively.

6.3.2 Effect of VD-WVGs on friction factor

Figures 6.13, 6.14 and 6.15 display the relationships between f/f_0 with *Re* for using 30°, 45° and 60° VD-WVGs, respectively. It is observed that the f/f_0 shows the downtrend pattern with raising *Re* for all VD-WVGs used. The VD-WVGs provides a substantial increase in *f* over the smooth tube. The *f* increases with decreasing P_R but the rise of B_R values, similar to the WVG inserts.

For 30° VD-WVGs, at P_R=0.5, 1, 1.5 and 2, the avearge f/f_0 values are about 3.57, 2.49, 1.99 and 1.42; 5.59, 3.97, 3.04 and 2.65; and 7.30, 5.82, 4.20 and 3.58 times for B_R=0.1, 0.15 and 0.2, respectively. The P_R=0.5 gives the mean *f* higher than the P_R=1.0, 1.5 and 2.0 at about 40, 81 and 121%, respectively. At a given P_R, the average

f/f_0 for B_R=0.1, 0.15 and 0.2 is around 2.37, 3.81 and 5.04 and that for B_R=0.2 is some 32 and 112% higher than that for B_R=0.15 and 0.1, respectively.

For 45° VD-WVGs, at P_R=0.5, 1, 1.5 and 2, the avearge f/f_0 values are around 5.32, 3.54, 2.82 and 2.07; 10.16, 6.54, 4.99 and 3.72; and 13.31, 8.53, 6.39 and 5.38 for B_R=0.1, 0.15 and 0.2, respectively. The P_R=0.5 gives the mean f/f_0 around 53, 100 and 159% higher than the P_R=1.0, 1.5 and 2.0, respectively while that for B_R=0.1, 0.15 and 0.2 is about 3.44, 6.35 and 8.40. The B_R=0.2 yields the average f/f_0 of some 33 and 144% above the B_R=0.15 and 0.1, respectively.

For 60° VD-WVGs, at P_R=0.5, 1, 1.5 and 2, the avearge f/f_0 values are some 7.89, 5.29, 3.88 and 3.09; 13.87, 9.61, 6.74 and 5.28; and 18.91, 13.09, 9.44 and 7.50 for B_R=0.1, 0.15 and 0.2, respectively. The mean f/f_0 for P_R=0.5 is some 46, 103 and 156% higher than that for P_R=1.0, 1.5 and 2.0 while that for B_R=0.1, 0.15 and 0.2 is about 5.04, 8.87 and 12.23 times, respectively. The B_R=0.2 provides the average f/f_0 of around 39 and 143% over the B_R=0.15 and 0.1.

6.3.3 Effect of VD-WVGs on thermal performance factor

Figures 6.16, 6.17 and 6.18 show the relationships between the thermal performance factor (η) with *Re* for the tube inserted with 30°, 45° and 60° VD-WVGs, respectively. It is seen that the η values generally are above unity, indicating that the employ of VD-WVG turbulators is superior to the plain tube.

For 30° VD-WVGs, the maximum η lies between 1.26–1.47 at B_R=0.1 and P_R=1.5 while the minimum is 1.18–1.38 at B_R=0.2 and P_R=0.5. The η values are, respectively, about 1.21–1.47, 1.19–1.45 and 1.18–1.43 at B_R=0.1, 0.15 and 0.2. For a given B_R, the P_R=1.5 yields the highest η and the P_R=1 and 2 give similar η values, while the lowest η is at P_R=0.5. The highest η found to be 1.47 is seen at B_R=0.1 and P_R=1.5.

For 45° VD-WVGs, the maximum η is between 1.21–1.41 at B_R=0.1 and P_R=1.5 while the minimum is in a range of 1.07–1.25 at B_R=0.2 and P_R=0.5. The η values are, respectively, about 1.12–1.41, 1.09–1.38 and 1.07–1.36 at B_R=0.1, 0.15 and 0.2. For a given B_R, the P_R=1.5 gives the maximum η and the P_R=1 and 2 provide the similar η values, whereas the lowest η is found at P_R=0.5. The highest η of 1.41 is seen at B_R=0.1 and P_R=1.5.

For 60° VD-WVGs, the maximum η is in a range of 1.14–1.31 for B_R=0.1, P_R=1.5 while the minimum lies in 1.03–1.19 for B_R=0.2 and P_R=0.5. The η values are, respectively, about 1.07–1.31, 1.05–1.29 and 1.03–1.26 for B_R=0.1, 0.15 and 0.2. For a given B_R, the P_R=2.0 provides the maximum η and the P_R=1 and 2 yield the same η values while the lowest η is at P_R=0.5. The highest η for this case is 1.31 and found at B_R=0.1 and P_R=1.5.

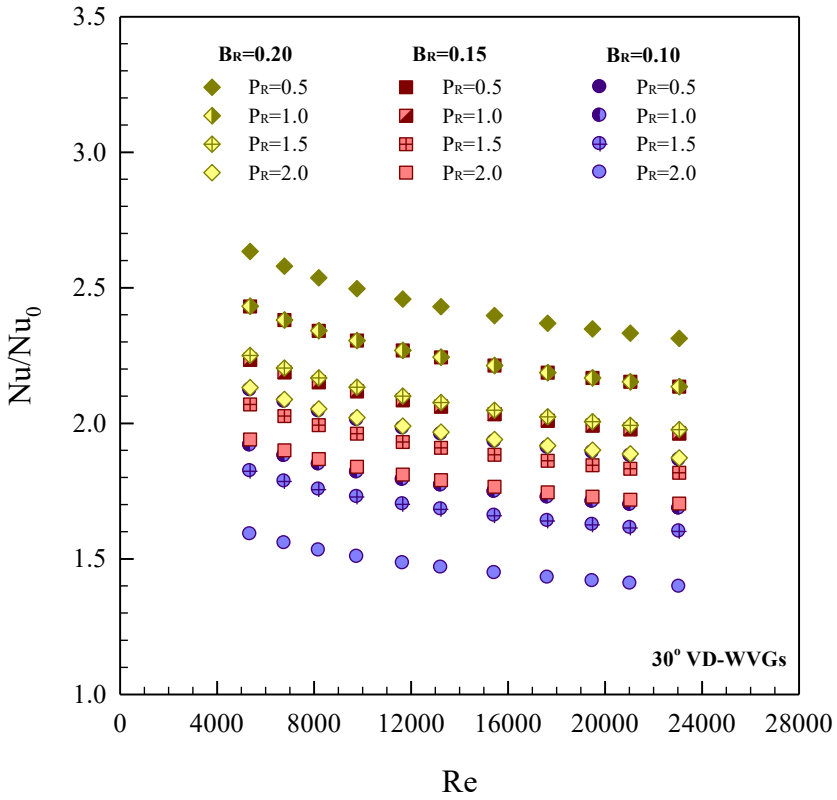

Figure 6.10. Effect of 30° VD-WVGs on Nu/Nu_0.

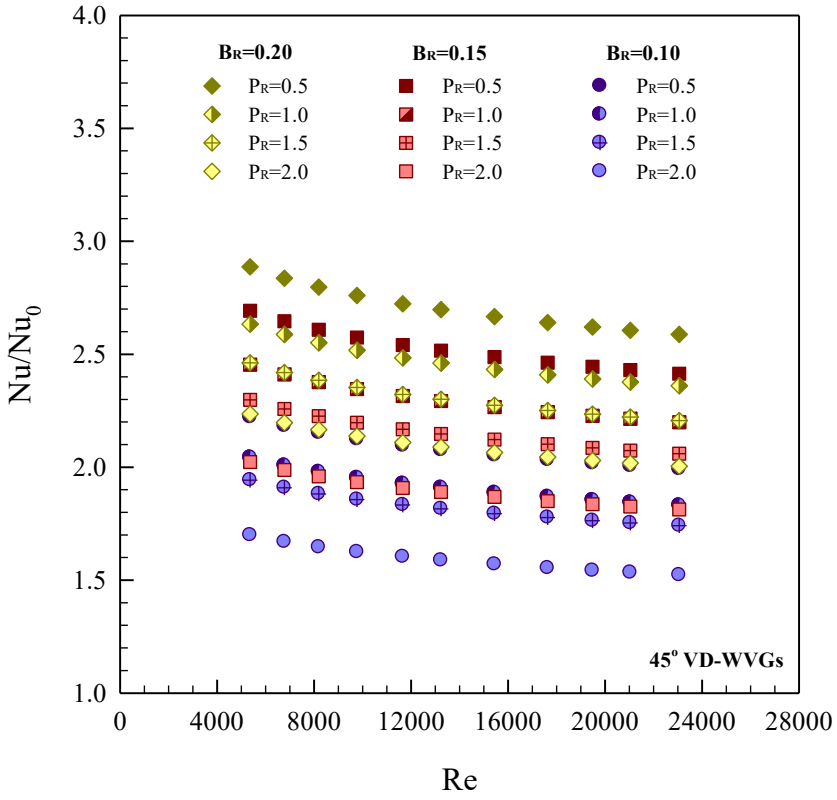

Figure 6.11. Effect of 45° VD-WVGs on Nu/Nu_0.

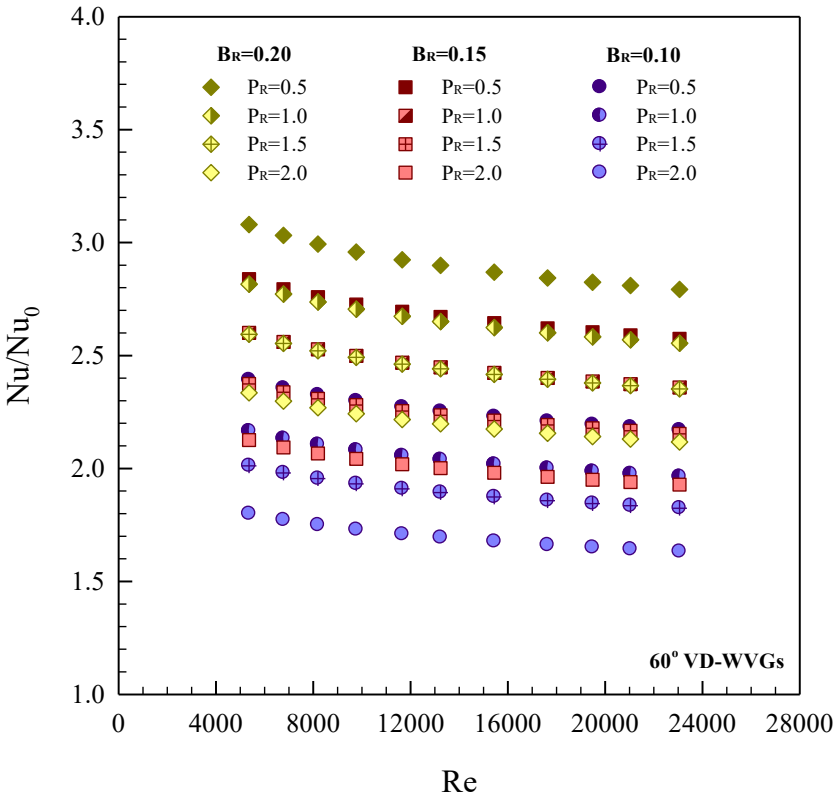

Figure 6.12. Effect of 60° VD-WVGs on Nu/Nu_0.

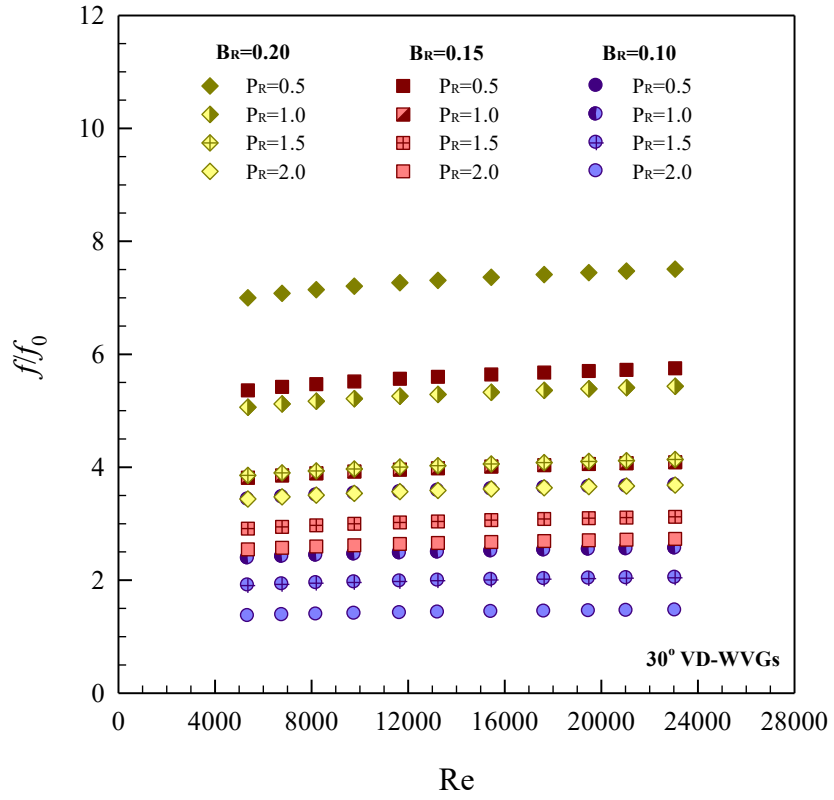

Figure 6.13. Effect of 30° VD-WVGs on f/f_0.

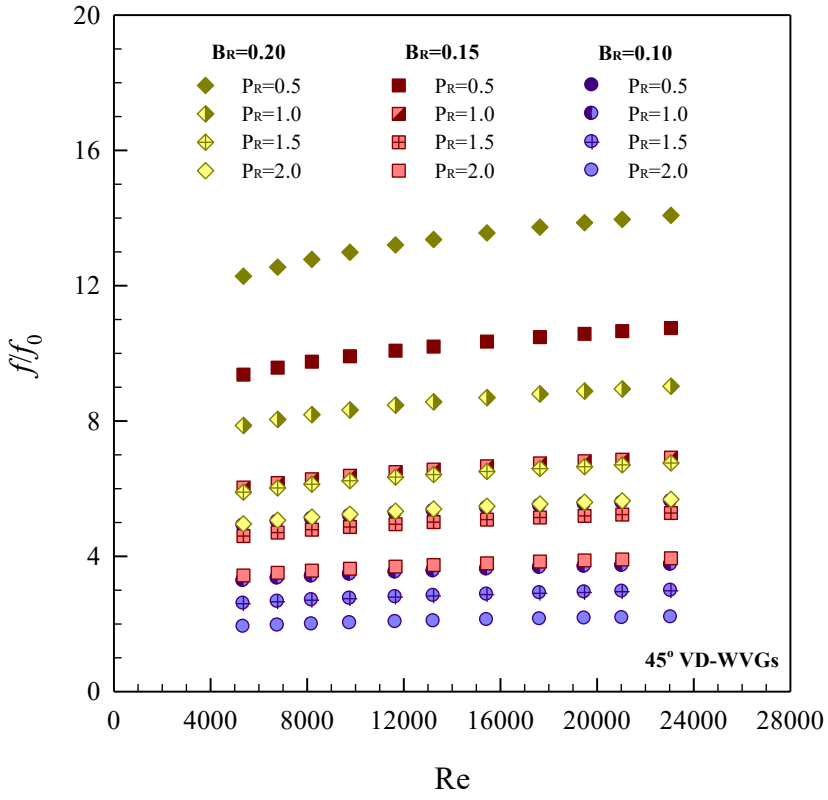

Figure 6.14. Effect of 45° VD-WVGs on f/f_0.

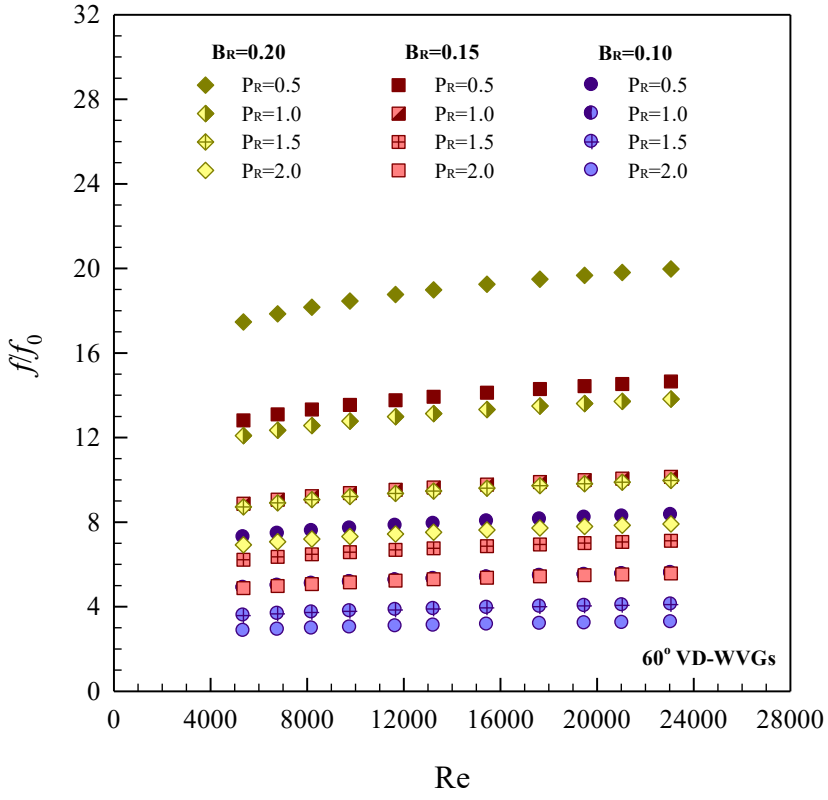

Figure 6.15. Effect of 60° VD-WVGs on f/f_0.

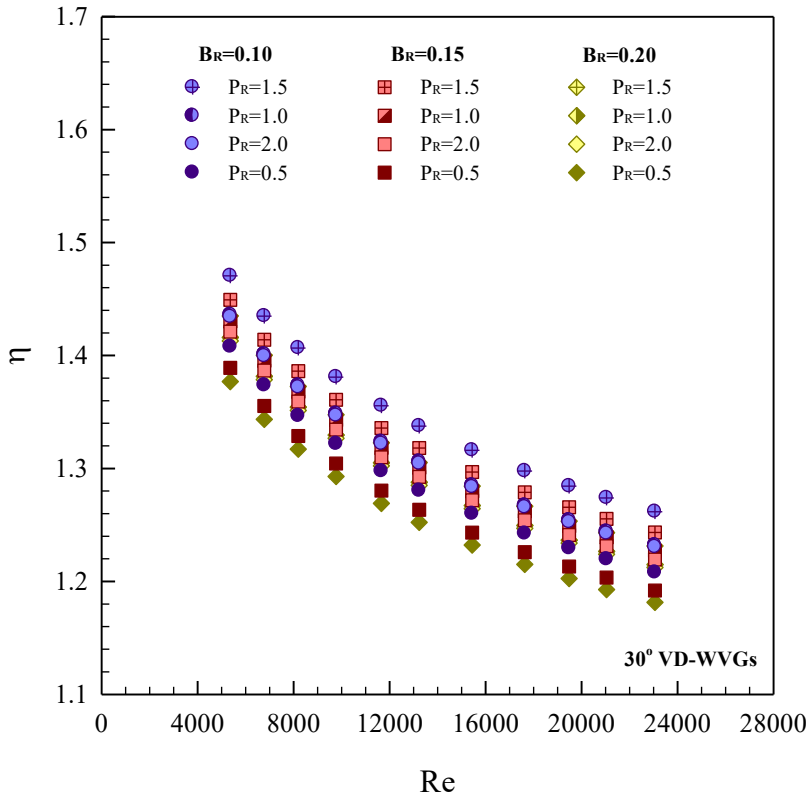

Figure 6.16. Effect of 30° VD-WVGs on thermal performance.

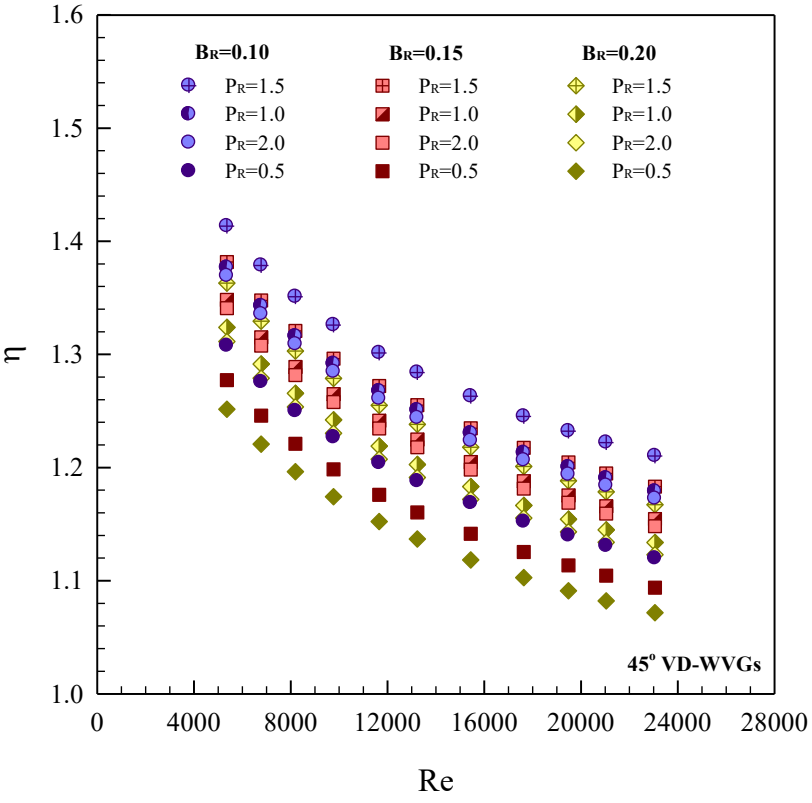

Figure 6.17. Effect of 45° VD-WVGs on thermal performance.

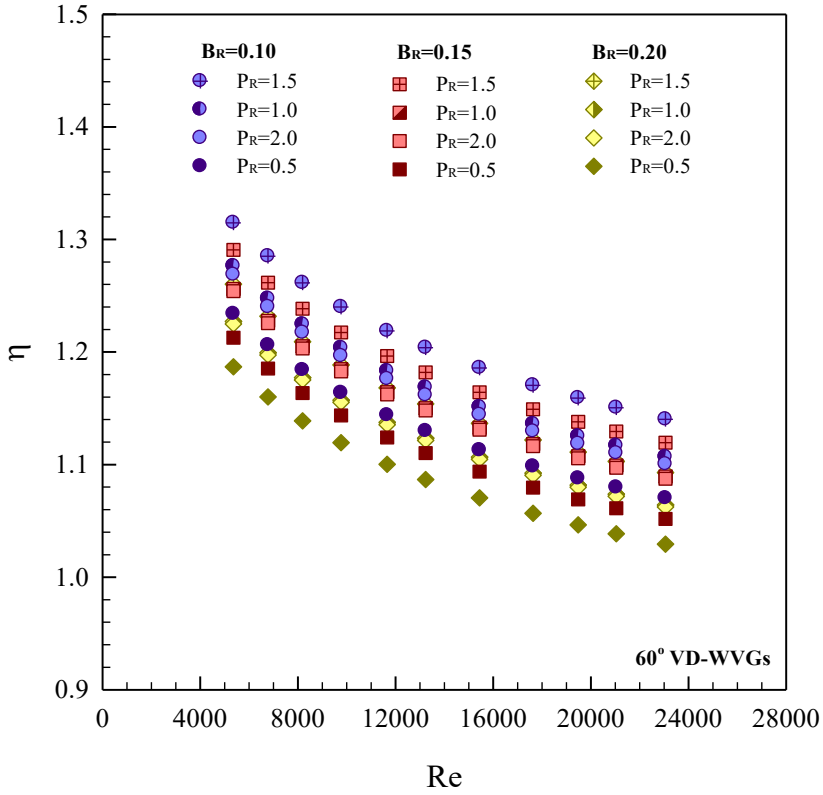

Figure 6.18. Effect of 60° VD-WVGs on thermal performance.

Table 6.4 Experimental results of 30° VD-WVGs.

VD-WVGs			Results		
α	B_R	P_R	Nu/Nu$_0$	f/f_0	η
30°	0.10	0.5	2.12–1.86	3.43–3.68	1.41–1.21
		1.0	1.92–1.69	2.39–2.56	1.44–1.23
		1.5	1.82–1.60	1.91–2.05	1.47–1.26
		2.0	1.59–1.40	1.36–1.46	1.43–1.23
	0.15	0.5	2.43–2.14	5.37–5.76	1.39–1.19
		1.0	2.23–1.96	3.82–4.10	1.43–1.23
		1.5	2.07–1.82	2.91–3.13	1.45–1.24
		2.0	1.94–1.70	2.55–2.73	1.42–1.22
	0.20	0.5	2.63–2.31	7.01–7.52	1.38–1.18
		1.0	2.43–2.14	5.07–5.44	1.42–1.21
		1.5	2.25–1.98	3.86–4.14	1.43–1.23
		2.0	2.13–1.87	3.44–3.69	1.41–1.21
Optimal results			η=1.47 at Re≈5300, B_R=0.10 and P_R=1.5		

Table 6.5 Experimental results of 45° VD-WVGs.

VD-WVGs			Results		
α	B_R	P_R	Nu/Nu$_0$	f/f_0	η
45°	0.10	0.5	2.22–1.99	4.91–5.63	1.31–1.12
		1.0	2.04–1.83	3.27–3.75	1.38–1.18
		1.5	1.94–1.74	2.60–2.98	1.41–1.21
		2.0	1.70–1.52	1.91–2.20	1.37–1.17
	0.15	0.5	2.69–2.41	9.37–10.76	1.28–1.09
		1.0	2.45–2.20	6.03–6.93	1.35–1.15
		1.5	2.30–2.06	4.60–5.29	1.38–1.18
		2.0	2.02–1.81	3.44–3.95	1.34–1.15
	0.20	0.5	2.89–2.59	12.28–14.10	1.25–1.07
		1.0	2.63–2.39	7.87–9.04	1.32–1.13
		1.5	2.46–2.21	5.89–6.77	1.36–1.17
		2.0	2.24–2.00	4.96–5.70	1.31–1.12
Optimal results			η=1.41 at Re≈5300, B_R=0.10 and P_R=1.5		

Table 6.6 Experimental results of 60° VD-WVGs.

VD-WVGs			Results		
α	B_R	P_R	Nu/Nu$_0$	f/f_0	η
60°	0.10	0.5	2.39–2.17	7.29–8.34	1.23–1.07
		1.0	2.17–1.96	4.89–5.60	1.28–1.11
		1.5	2.01–1.82	3.59–4.10	1.31–1.14
		2.0	1.80–1.63	2.86–3.27	1.27–1.10
	0.15	0.5	2.84–2.57	12.82–14.68	1.21–1.05
		1.0	2.60–2.36	8.88–10.16	1.26–1.09
		1.5	2.37–2.15	6.23–7.13	1.29–1.12
		2.0	2.13–1.93	4.88–5.58	1.25–1.09
	0.20	0.5	3.08–2.79	17.48–20.01	1.19–1.03
		1.0	2.82–2.55	12.09–13.85	1.23–1.06
		1.5	2.59–2.35	8.72–9.98	1.26–1.09
		2.0	2.33–2.12	6.93–7.93	1.22–1.06
Optimal results			η=1.31 at Re≈5300, B_R=0.10 and P_R=1.5		

6.4 Winglet pairs with V-tip pointing upstream

6.4.1 Effect of VU-WVGs on heat transfer

The effect of 30°, 45° and 60° VU-WVGs with different P_R and B_R values on Nu/Nu_0 plotted against the *Re* is displayed in Figures 6.19, 6.20 and 6.21, respectively. In the figure, the VU-WVGs yield the considerable heat transfer enhancement higher than the plain tube. The Nu/Nu_0 shows the slight downtrend with the increase of *Re* and B_R but the reduction of P_R for all cases studied.

For 30° VU-WVGs with P_R=0.5, 1, 1.5 and 2, the average Nu values are about 234, 219, 206 and 188%; 264, 249, 236 and 212%; and 297, 282, 266 and 240% above the plain tube for B_R=0.1, 0.15 and 0.2, respectively. The mean Nu for P_R=0.5 is some 6, 12 and 24% higher the P_R=1.0, 1.5 and 2.0, respectively while that for B_R=0.1, 0.15 and 0.2 is around 212, 240 and 271% above the smooth tube. The mean Nu for B_R=0.2 is about 13 and 28% higher than that for B_R=0.15 and 0.1, respectively.

For 45° VU-WVGs with P_R=0.5, 1, 1.5 and 2, the average Nu values are around 254, 240, 231 and 212%; 294, 278, 258 and 240%; and 325, 306, 285 and 265% above the plain tube for B_R=0.1, 0.15 and 0.2, respectively. The mean Nu for P_R=0.5 is about 6, 13 and 22% above that for P_R=1.0, 1.5 and 2.0, respectively whereas that for B_R=0.1, 0.15 and 0.2 is some 234, 268 and 295% above the smooth tube. The mean Nu for B_R=0.2 is about 10 and 26% higher than that for B_R=0.15 and 0.1.

For 60° VU-WVGs with P_R=0.5, 1, 1.5 and 2, the average Nu values are about 274, 250, 238 and 219%; 318, 288, 273 and 251%; and 346, 316, 305 and 282% above the plain tube for B_R=0.1, 0.15 and 0.2, respectively. The mean Nu for P_R=0.5 is around 9, 15 and 25% higher than that for P_R=1.0, 1.5 and 2.0, respectively while that for B_R=0.1, 0.15 and 0.2 is approximately 245, 282 and 312% above the smooth tube. The mean Nu for B_R=0.2 is around 11 and 27% higher than that for B_R=0.15 and 0.1.

6.4.2 Effect of VU-WVGs on friction factor

Figures 6.22, 6.23 and 6.24 display the effect of 30°, 45° and 60° VU-WVGs at different P_R and B_R values on f/f_0 plotted against the *Re*, respectively. It is observed that the f/f_0 displays the downtrend pattern with rising *Re* for all cases. The VU-WVGs provide the substantial increase in f over the smooth tube. The f/f_0 increases with decreasing P_R but rising B_R, similar to the WVGs and VD-WVGs inserts.

For 30° VU-WVGs, at P_R=0.5, 1, 1.5 and 2 the average f/f_0 values are about 4.59, 3.30, 2.47 and 2.15; 6.79, 5.05, 3.83 and 3.22; and 10.01, 7.48, 5.65 and 4.84 for B_R=0.1, 0.15 and 0.2, respectively. The mean f/f_0 for P_R=0.5 is some 36, 80 and 110% higher than that for P_R=1.0, 1.5 and 2.0, respectively while that for B_R=0.1, 0.15 and 0.2 is around 3.13, 4.72 and 6.99 and the B_R=0.2 gives the f around 48 and 125% higher than the B_R=0.15 and 0.1.

For 45° VU-WVGs, at P_R=0.5, 1, 1.5 and 2, the average f/f_0 values are about 6.84, 4.62, 3.64 and 3.34; 11.04, 7.37, 5.22 and 4.94; and 17.07, 11.54, 8.27 and 7.77 for B_R=0.1, 0.15 and 0.2, respectively. The mean f/f_0 for P_R=0.5 is about 49, 102 and 116% higher than that for P_R=1.0, 1.5 and 2.0, respectively while that for B_R=0.1, 0.15 and 0.2 is about 4.61, 7.15 and 11.16 times and the B_R=0.2 is seen to be higher than that for B_R=0.15 and 0.1 at about 57 and 140%.

For 60° VU-WVGs, at P_R=0.5, 1, 1.5 and 2, the average f/f_0 about 8.61, 5.86, 4.69 and 4.26; 14.61, 9.83, 7.83 and 6.93; and 20.55, 14.12, 11.85 and 10.84 times for B_R=0.1, 0.15 and 0.2, respectively. The mean f/f_0 for P_R=0.5 is higher than that for P_R=1.0, 1.5 and 2.0 at about 47, 81 and 101%, respectively while that with B_R=0.1, 0.15 and 0.2 is around 5.85, 9.80 and 14.34 times and that for B_R=0.2 is about 56 and 139% higher than that for B_R=0.15 and 0.1.

6.4.3 Effect of VU-WVGs on thermal performance factor

Figures 6.25, 6.26 and 6.27 present the effect of 30°, 45° and 60° VU-WVGs with different P_R and B_R on the η plotted against *Re* values, respectively. The measured Nu and f values in those figures are compared at the same pumping power. It is seen in the figures that the η generally are all above unity, indicating that the merits of VU-WVGs over the smooth tube.

For 30° VU-WVGs, the maximum η is between 1.44–1.65 for B_R=0.1 and P_R=1.5 while the minimum is 1.30–1.49 for B_R=0.2 and P_R=0.5. The η values are, respectively, about 1.33–1.65, 1.31–1.63 and 1.30–1.61 at B_R=0.1, 0.15 and 0.2. At a given B_R, the P_R=1.5 yields the maximum η and the P_R=1 and 2 give similar η values while the lowest η is found at P_R=0.5. The highest η is found to be 1.65 at B_R=0.1 and P_R=1.5.

For 45° VU-WVGs, the maximum η lies between 1.41–1.63 for B_R=0.1 and P_R=1.5 while the minimum is 1.19–1.38 for B_R=0.2 and P_R=0.5, similar to the case of 30°. The η values are, respectively, about 1.26–1.63, 1.24–1.62 and 1.19–1.53 for B_R=0.1, 0.15 and 0.2. At a given B_R, the P_R=1.5 yields the maximum η while the lowest η is at P_R=0.5. The highest η is around 1.63 at B_R=0.1 and P_R=1.5.

For 60° VU-WVGs, the maximum η is in a range of 1.37–1.50 for B_R=0.1 and P_R=1.5 while the minimum is between 1.21–1.33 for B_R=0.2 and P_R=0.5. The η values are, respectively, about 1.29–1.50, 1.25–1.45 and 1.21–1.41 for B_R=0.1, 0.15 and 0.2. At a given B_R, the P_R=2.0 yields the maximum η whereas the lowest η is at P_R=0.5. The highest η around 1.50 is at B_R=0.1 and P_R=1.5.

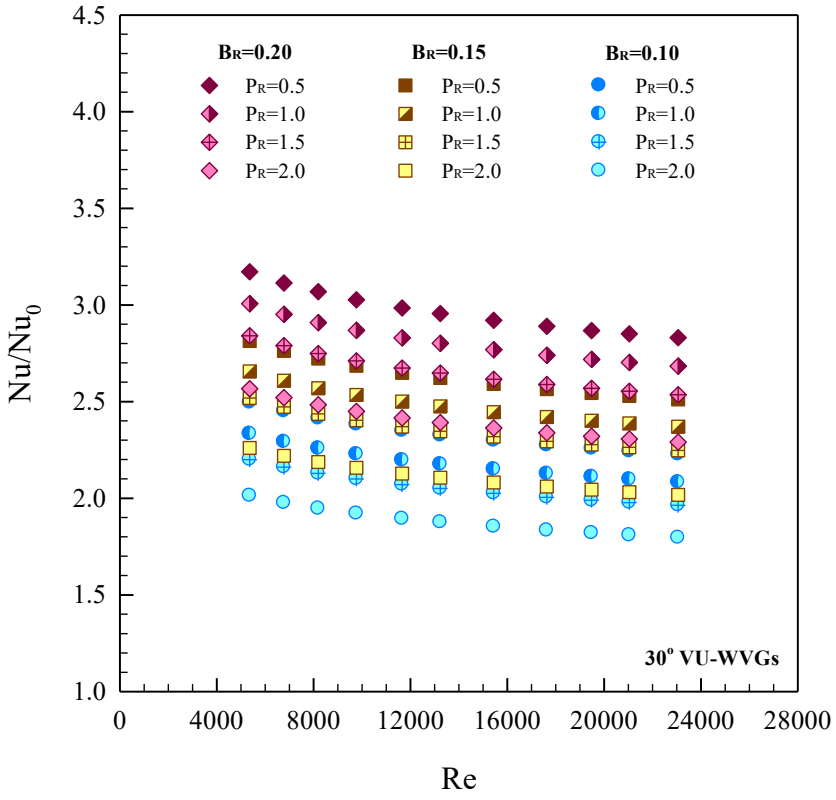

Figure 6.19. Effect of 30° VU-WVGs on Nu/Nu_0.

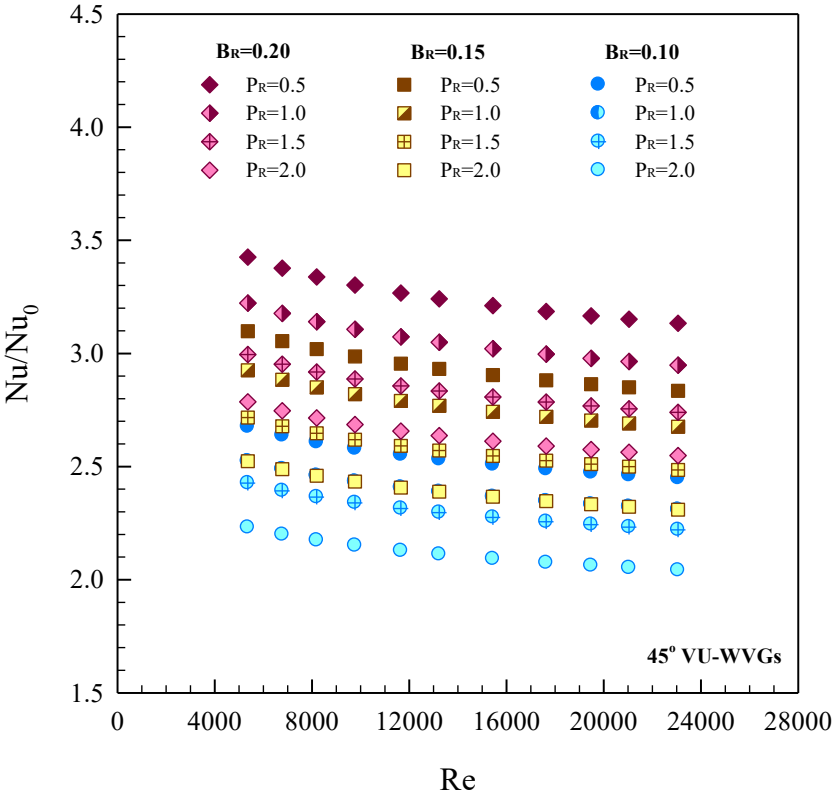

Figure 6.20 Effect of 45° VU-WVGs on Nu/Nu_0.

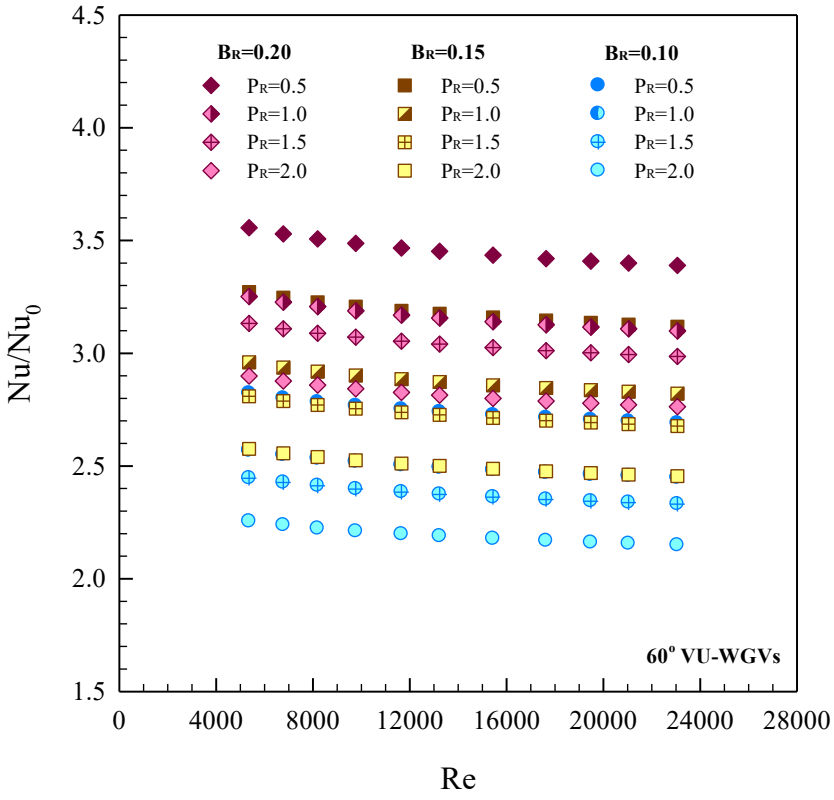

Figure 6.21 Effect of 60° VU-WVGs on Nu/Nu_0.

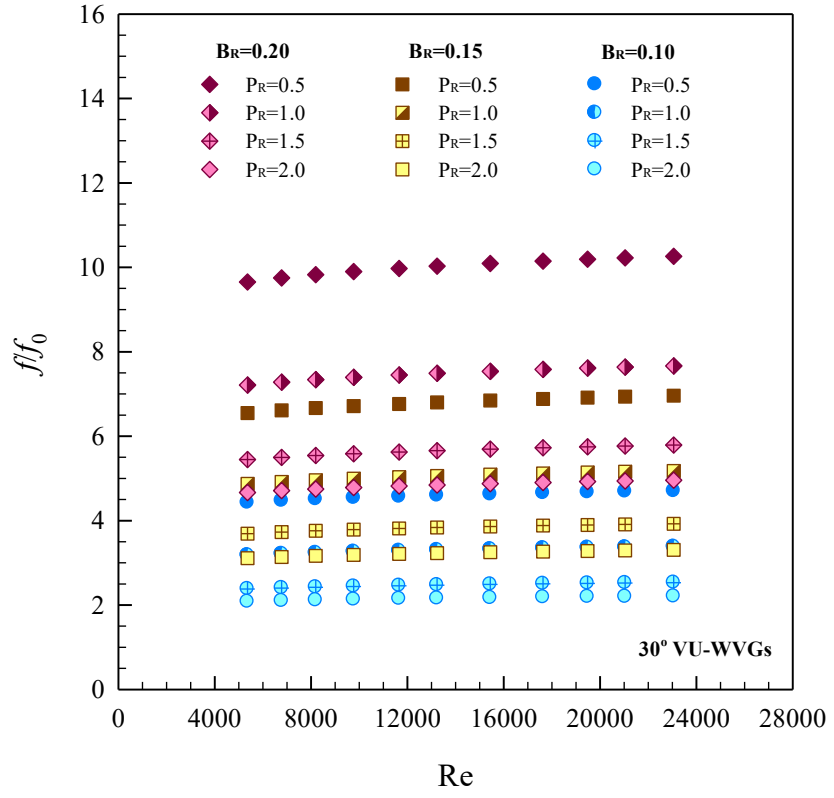

Figure 6.22 Effect of 30° VU-WVGs on f/f_0.

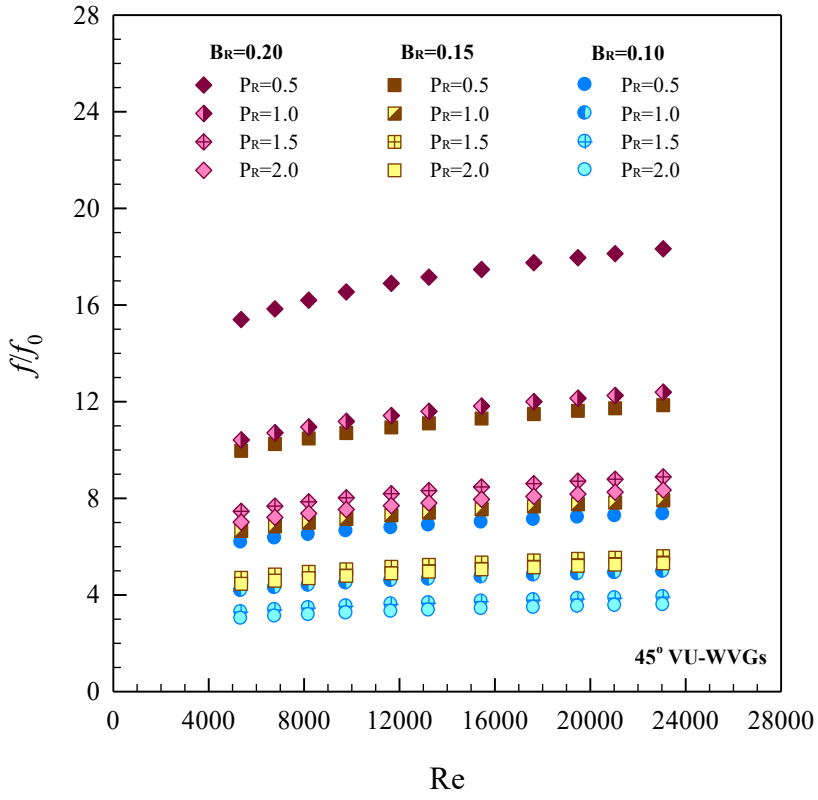

Figure 6.23 Effect of 45° VU-WVGs on f/f_0.

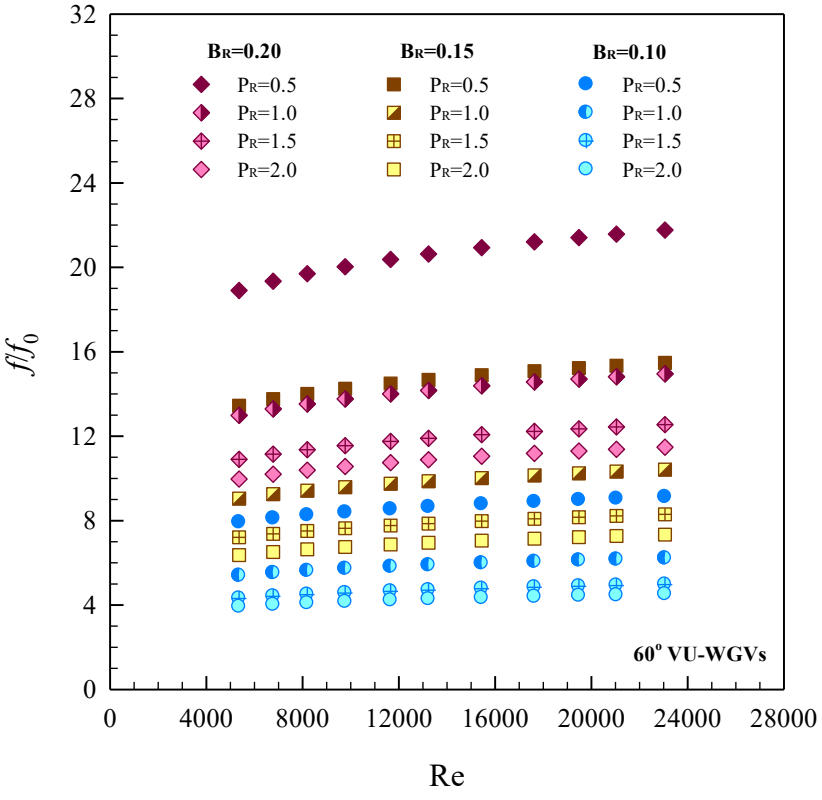

Figure 6.24 Effect of 60° VU-WVGs on f/f_0.

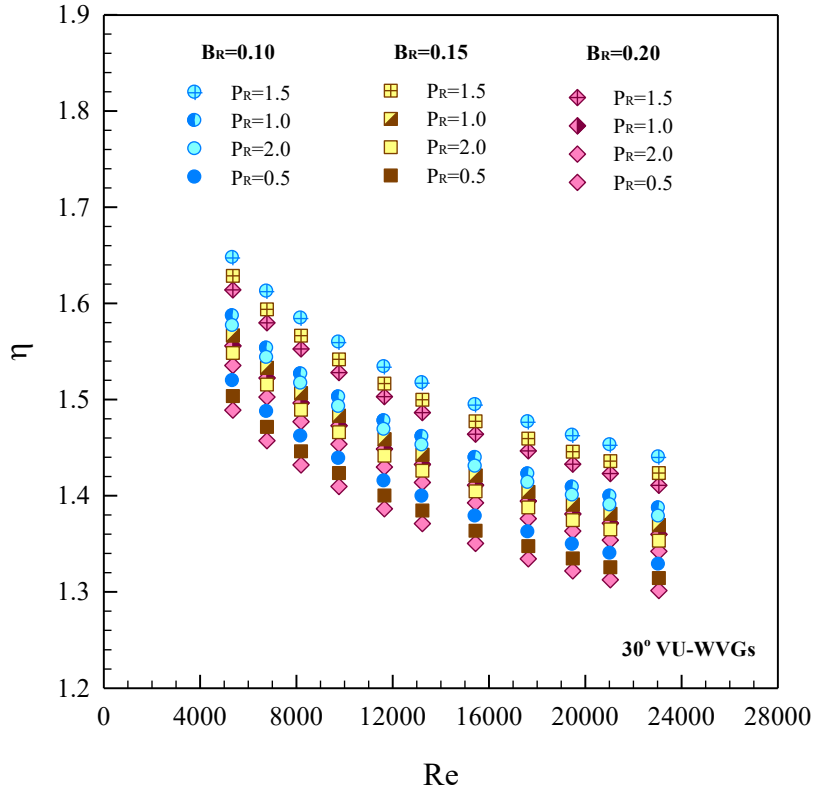

Figure 6.25 Effect of 30° VU-WVGs on thermal performance.

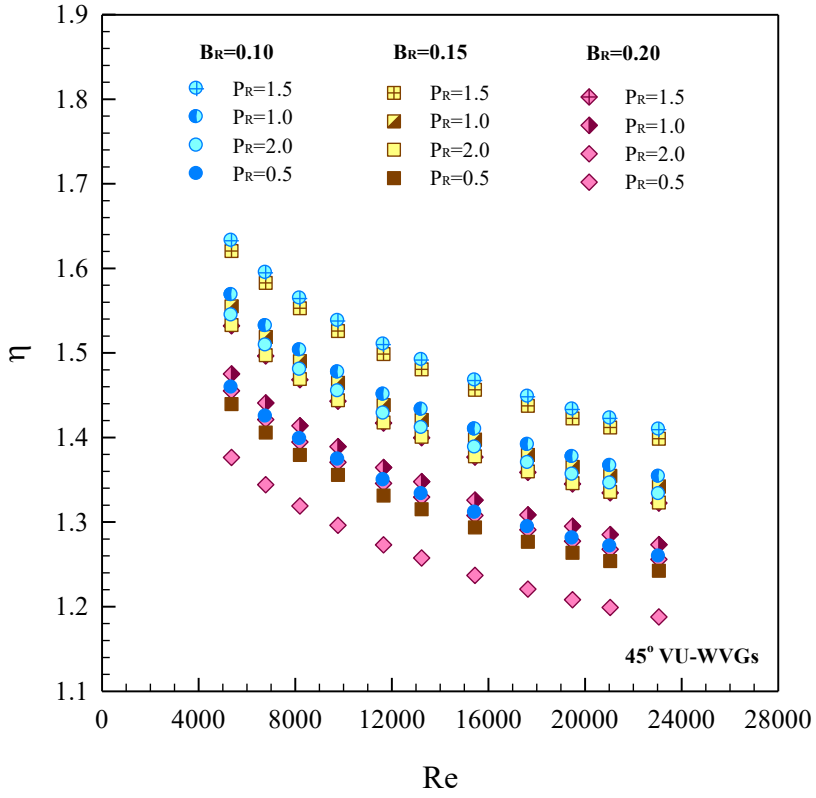

Figure 6.26 Effect of 45° VU-WVGs on thermal performance.

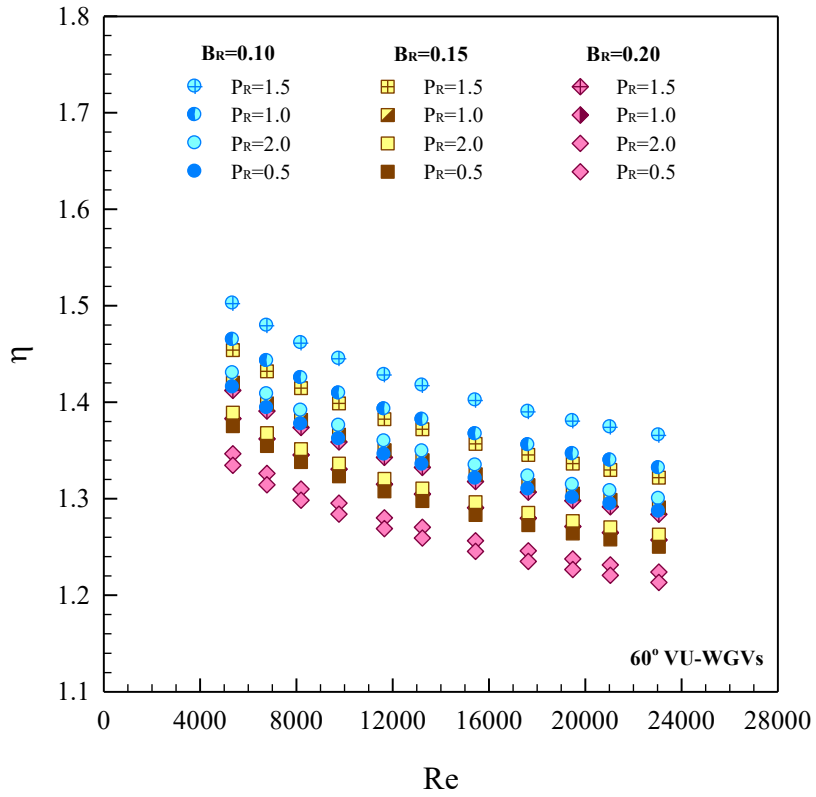

Figure 6.27 Effect of 60° VU-WVGs on thermal performance.

Table 6.7 Experimental results of 30° VU-WVGs.

VU-WVGs			Results		
α	B_R	P_R	Nu/Nu$_0$	f/f_0	η
30°	0.10	0.5	2.50–2.23	4.43–4.71	1.52–1.33
		1.0	2.33–2.08	3.18–3.39	1.59–1.39
		1.5	2.20–1.96	2.38–2.54	1.65–1.44
		2.0	2.01–1.80	2.08–2.21	1.58–1.38
	0.15	0.5	2.81–2.51	6.55–6.97	1.50–1.31
		1.0	2.66–2.37	4.87–5.19	1.57–1.37
		1.5	2.52–2.25	3.70–3.93	1.63–1.42
		2.0	2.26–2.02	3.11–3.31	1.55–1.35
	0.20	0.5	3.17–2.83	9.66–10.28	1.49–1.30
		1.0	3.01–2.68	7.21–7.68	1.56–1.36
		1.5	2.84–2.54	5.45–5.80	1.61–1.41
		2.0	2.57–2.29	4.67–4.97	1.54–1.34
Optimal results			η=1.65 at Re≈5300, B_R=0.10 and P_R=1.5		

Table 6.8 Experimental results of 45° VU-WVGs.

VU-WVGs			Results		
α	B_R	P_R	Nu/Nu$_0$	f/f_0	η
45°	0.10	0.5	2.68–2.45	6.17–7.35	1.46–1.26
		1.0	2.52–2.31	4.17–4.96	1.57–1.35
		1.5	2.43–2.22	3.28–3.91	1.63–1.41
		2.0	2.23–2.04	3.01–3.59	1.54–1.33
	0.15	0.5	3.10–2.83	9.97–11.88	1.44–1.24
		1.0	2.93–2.68	6.66–7.93	1.56–1.34
		1.5	2.72–2.49	4.71–5.61	1.62–1.40
		2.0	2.52–2.31	4.46–5.32	1.53–1.32
	0.20	0.5	3.43–3.13	15.41–18.36	1.38–1.19
		1.0	3.22–2.95	10.42–12.41	1.48–1.24
		1.5	2.99–2.74	7.47–8.89	1.53–1.32
		2.0	2.79–2.55	7.02–8.36	1.46–1.26
Optimal results			η=1.63 at Re≈5300, B_R=0.10 and P_R=1.5		

Table 6.9 Experimental results of 60° VU-WVGs.

VU-WVGs			Results		
α	B_R	P_R	Nu/Nu$_0$	f/f_0	η
60°	0.10	0.5	2.82–2.69	7.92–9.13	1.42–1.29
		1.0	2.57–2.45	5.40–6.22	1.46–1.33
		1.5	2.45–2.33	4.32–4.97	1.50–1.37
		2.0	2.25–2.15	3.92–4.52	1.43–1.30
	0.15	0.5	3.27–3.12	13.46–15.50	1.38–1.25
		1.0	2.96–2.82	9.05–10.43	1.42–1.29
		1.5	2.81–2.68	7.21–8.31	1.45–1.32
		2.0	2.58–2.46	6.38–7.35	1.39–1.26
	0.20	0.5	3.56–3.39	18.92–21.80	1.33–1.21
		1.0	3.25–3.10	13.00–14.98	1.38–1.26
		1.5	3.13–2.99	10.91–12.57	1.41–1.28
		2.0	2.90–2.76	9.98–11.50	1.35–1.22
Optimal results			η=1.50 at Re≈5300, B_R=0.10 and P_R=1.5		

6.5 Empirical correlations

The empirical correlations for Nusselt number (Nu) and friction factor (*f*) for various turbulator geometries in the present work are presented in Table 6.10 and 6.11, respectively. The resultant correlations reveal that Nusselt number is related to Reynolds number (*Re*), Prandtl number (*Pr*), blockage ratio (B_R) and pitch ratio (P_R) while the friction factor is dependent of Reynolds number (*Re*), blockage ratio (B_R) and pitch ratio (P_R). Evidently, the predicted Nusselt number and friction factor are, respectively, within ±6 and ±7 deviation with experimental data under the conditions; Re=5300–24,000, P_R=0.5–2.0 and B_R=0.1–0.2.

Table 6.10 Heat transfer correlations.

Correlations		$Nu = \mathrm{a}(Re^{\mathrm{b}})(Pr^{0.4})(B_{\mathrm{R}}^{\mathrm{c}})(P_{\mathrm{R}}^{\mathrm{d}})$			
		a	b	c	d
WVGs	30°	0.1206	0.7500	0.2036	-0.1008
	45°	0.1482	0.7400	0.2294	-0.1401
	60°	0.1707	0.7300	0.2245	-0.1498
VD-WVGs	30°	0.2087	0.7110	0.3471	-0.1678
	45°	0.2108	0.7250	0.3754	-0.1812
	60°	0.2078	0.7330	0.3749	-0.1950
VU-WVGs	30°	0.2321	0.7220	0.3546	-0.1444
	45°	0.2090	0.7390	0.3327	-0.1364
	60°	0.1745	0.7670	0.3482	-0.1521

Table 6.11 Friction factor correlations.

Correlations		$f = \mathrm{a}(Re^{\mathrm{b}})(B_{\mathrm{R}}^{\mathrm{c}})(P_{\mathrm{R}}^{\mathrm{d}})$			
		a	b	c	d
WVGs	30°	2.5858	-0.2000	0.6809	-0.3672
	45°	5.2005	-0.1700	0.9276	-0.5436
	60°	7.4735	-0.1501	1.0594	-0.5662
VD-WVGs	30°	6.3774	-0.2019	1.1229	-0.5686
	45°	9.2056	-0.1559	1.3009	-0.6734
	60°	13.2179	-0.1580	1.2893	-0.6782
VU-WVGs	30°	9.5231	-0.2081	1.1580	-0.5419
	45°	8.3051	-0.1308	1.2477	-0.5796
	60°	14.9555	-0.1535	1.2997	-0.5109

6.6 Numerical simulation

6.6.1 Winglet geometry and mathematical modeling

The detail of the tube inserted with full-length 30° VU-WVGs and a module of one periodic flow, computational domain and its grid is shown in Figure 6.28. The periodic flow tube attains a periodical fully developed flow and thermal condition where the velocity field and heat transfer pattern repeats itself from one module to another. The concept of periodical fully developed flow and its solution procedure have been described in ref. [99]. To investigate the flow structure and heat transfer mechanism, the 30° VU-WVGs with B_R=0.1, 0.15 and 0.2 at P_R=1 and 1.5 are introduced and their results are validated with measurements of the present work.

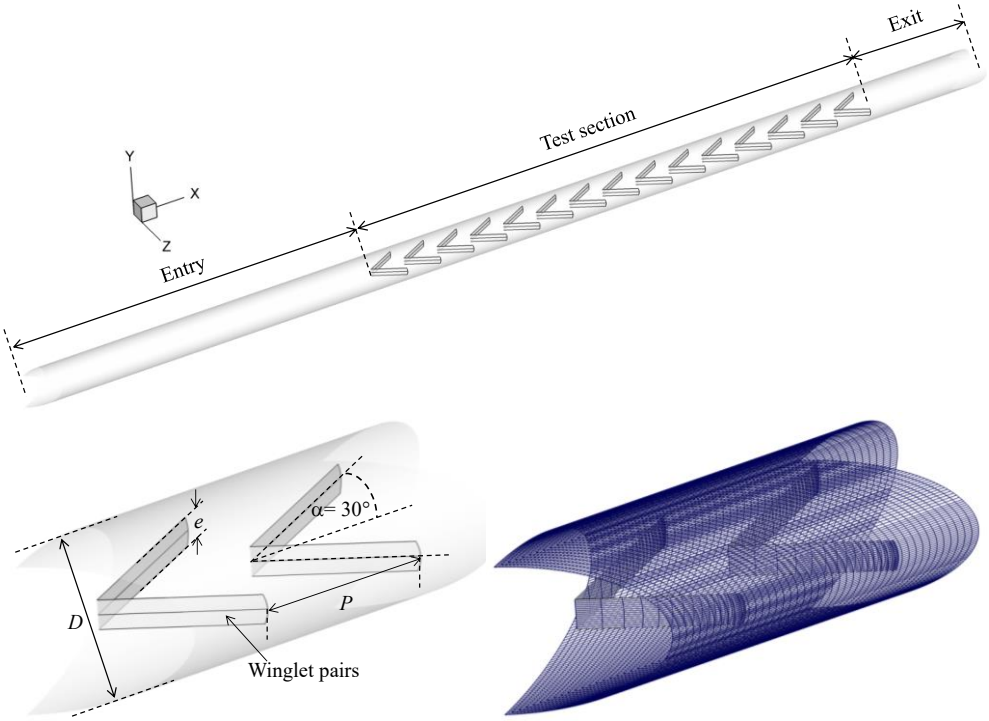

Figure 6.28. Full-length tube geometry and computational domain of periodic flow.

The numerical model for fluid flow and heat transfer in the inserted tube is developed under the following assumptions : steady, three-dimensional, turbulent and incompressible flow; constant fluid properties; and ignored body forces, viscous dissipation and radiation heat transfer. Based on the above assumptions, the tube flow model is governed by the Reynolds averaged Navier–Stokes (RANS) equations with the RNG k-ε turbulence model and the energy equation. The details on mathematical modeling can be found in ref. [70].

6.6.2 Boundary conditions

For a full-length circular tube fitted with 30° VU-WVGs, a uniform air velocity was introduced at the inlet while a pressure outlet condition was applied at the exit. For a periodic flow module, periodic boundaries were used for the inlet and outlet of the flow domain. Constant mass flow rate of air at 300 K was assumed in the flow direction. The physical properties of the air were assumed to remain constant at mean bulk temperature. Impermeable boundary and no–slip wall conditions were implemented inside the tube wall as well as the winglet surface. The constant wall heat-flux of the tube was maintained at 600 W/m^2 while the winglet strip was assumed at adiabatic wall condition.

6.6.3 Grid independence test

The computational domain of a periodic flow module is resolved by regular Cartesian elements or hexahedron elements. A grid independence procedure was implemented by using Richardson extrapolation technique over grids with different numbers of cells, about 32,000, 64,000, 128,000 and 255,000. The variation in *Nu* and *f* values is found to be less than 0.3% for the increment of the number of cells from 128,000 to 255,000. With consideration in both computing time and solution precision, the grid of 128,000 cells was adopted while similar grid density was also applied for the full-length flow model.

6.6.4 Numerical results of inserted-tube flow

The flow and vortex coherent structure in the inserted tube is displayed by streamlines superimposed at various locations in transverse planes as depicted in Figure 6.29 and streamlines of impinging jet are shown in Figure 6.30. The streamlines of the VU-WVG flow model are presented for Re=10,000, P_R=1.0 and B_R=0.2. It is visible in the figure that there are four main counter-rotating vortex flows appear on the lower and upper parts along the tube. In the lower and upper parts of the tube, the common-flow-up vortices appear and however, considering the left and right halfsides, there are two common-flow-down vortices that generally provide higher heat transfer in this region of the tube wall. The appearance of the four vortex flows can help increase higher heat transfer in the tube because of higher transporting the fluid from the central core to the near-wall regimes as can be observed from the major change in the temperature field over the tube.

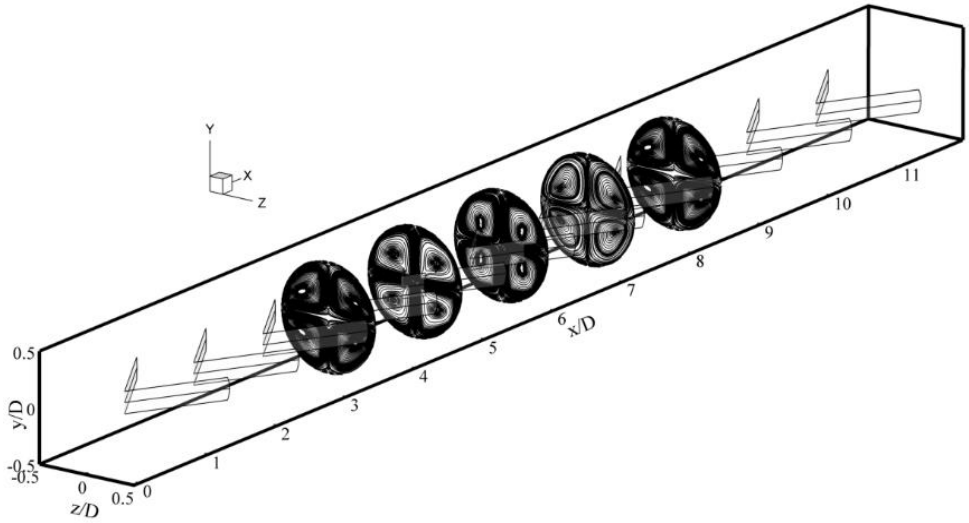

Figure 6.29 Streamlines in transverse planes for 30° VU-WVGs inserted at *Re*=10,000, P_R=1.0 and B_R=0.2.

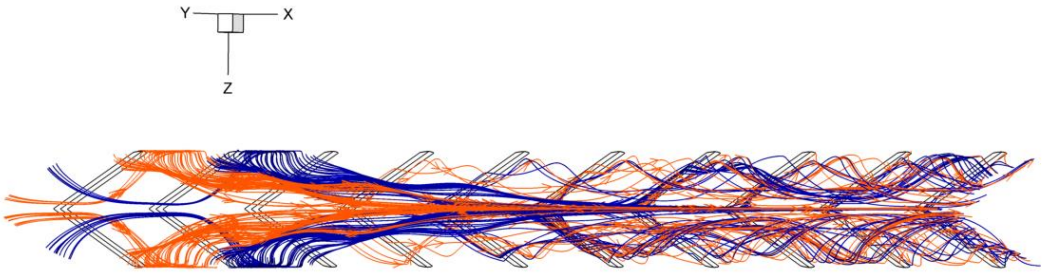

Figure 6.30 Streamlines of impinging jet for 30° VU-WVGs inserted at *Re*=10,000, P_R=1.0 and B_R=0.2.

The contour plots of temperature field in transverse planes of the 30° VU-WVGs inserted at *Re*=10,000, P_R=1.0 and B_R=0.2 are presented in Figure 6.31. The figure shows that there is a major change in the temperature field over the tube for using the VU-WVGs. This means that the vortex flows provide a significant influence on the temperature field, because it can induce better fluid mixing between the wall and the core flow regions, leading to a higher temperature gradient over the heating wall.

Figure 6.32 displays the local Nu contours on a sidewall for 30° VU-WVGs inserted at *Re*=10,000, P_R=1.0 and B_R=0.2. In the figure, it is apparent that the high Nu values for the inserted tube are seen in large areas over the tube sidewall. The peaks can be observed in the sidewall area around the downstream winglet-end where the red area shows the impingement region of the secondary flow providing higher heat transfer rate than other areas. This means that the vortex-induced impingement flow is responsible to heat transfer enhancement in the tube, apart from fast fluid mixing between the core and the near-wall regions.

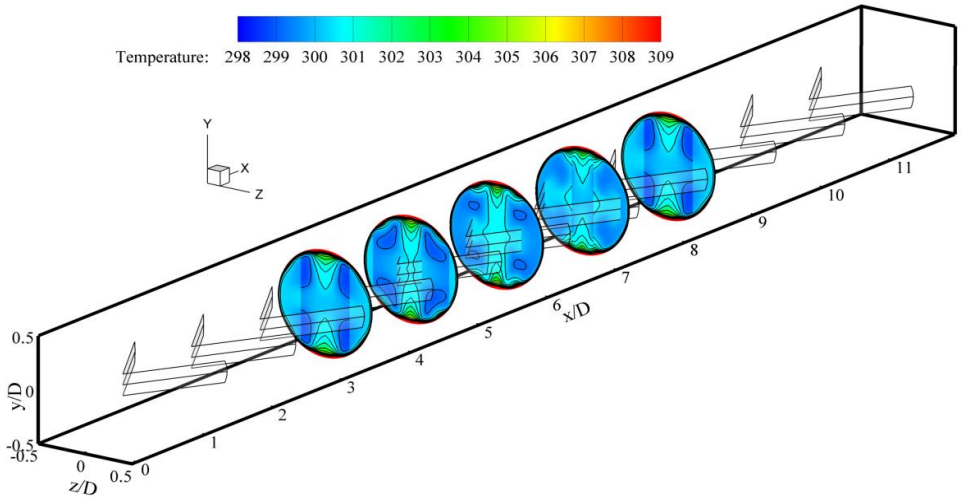

Figure 6.31 Temperature contours in transverse planes for 30° VU-WVGs inserted at *Re*=10,000, P_R=1.0 and B_R=0.2.

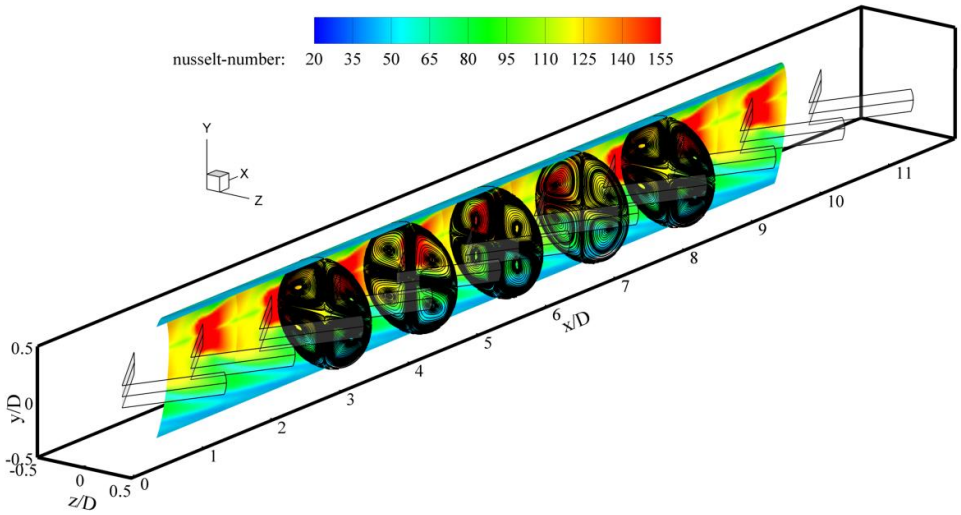

Figure 6.32 Local Nu contours on sidewall for 30° VU-WVGs inserted at *Re*=10,000, P_R=1.0 and B_R=0.2.

The results of heat transfer (Nu/Nu_0) and friction factor ratio (f/f_0) of the tube fitted with 30° VU-WVGs at P_R=1.0 and 1.5 for B_R=0.1, 0.15 and 0.2 from the simulation are validated by comparison with experimental data under similar operating conditions as shown in Figures 6.33 and 6.34, respectively. It is worth noting that the numerical results are in good agreement with measurements. The average deviations of the results are less than ±7% for heat transfer and ±6% for friction factor.

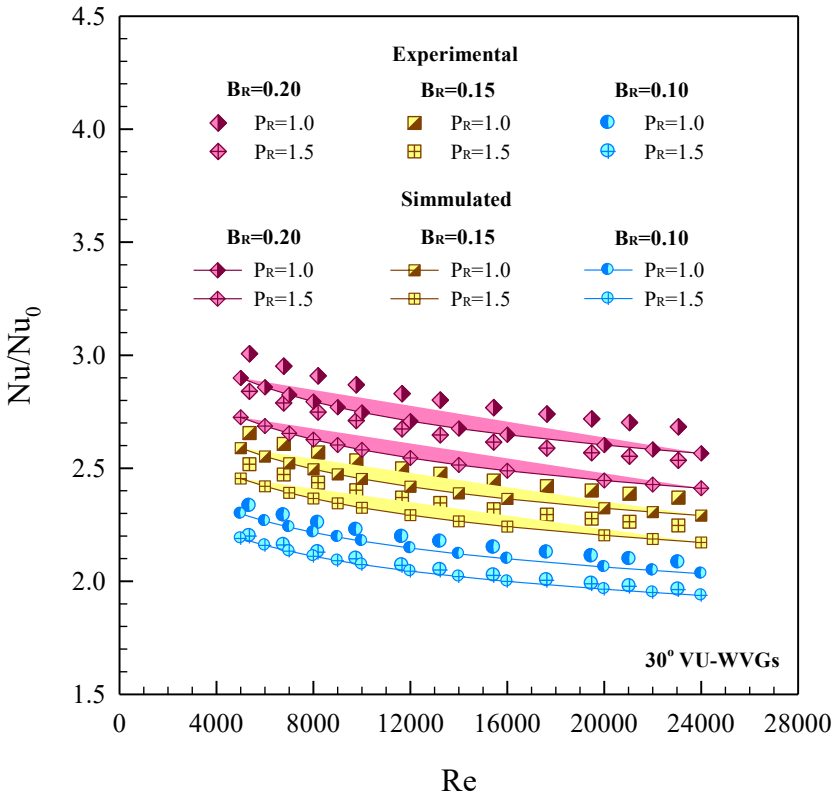

Figure 6.33 Comparison between experimental and predicted Nu/Nu_0 values.

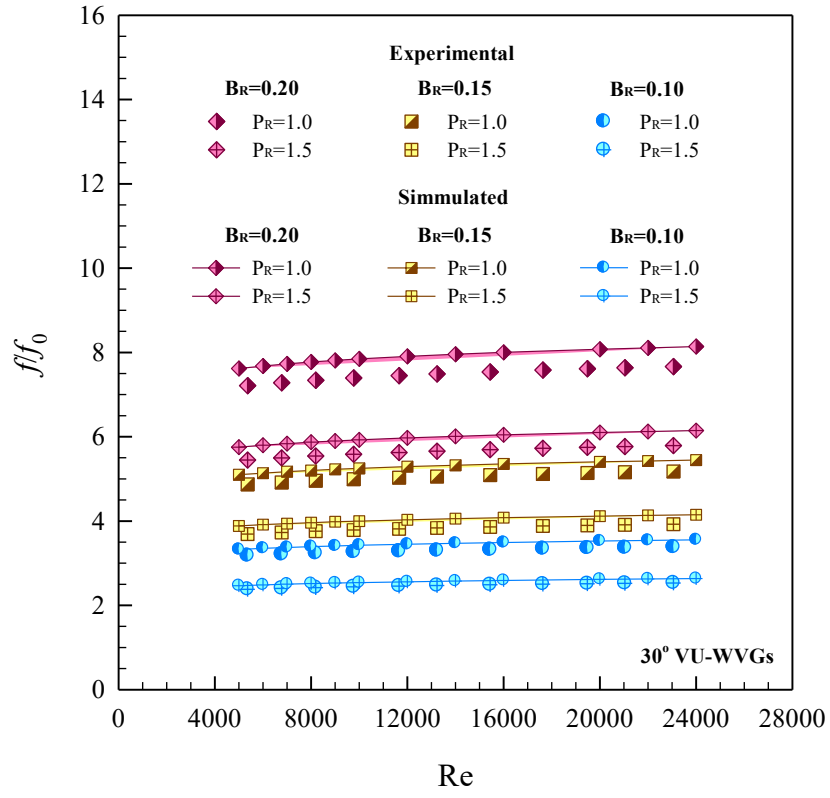

Figure 6.34 Comparison between experimental and simulated f/f_0 values.

6.7 Optimal condition analysis

The results from the experimental investigations of the WVG, VD-WVG and VU-WVG inserts with different three attack angles (α=30°, 45° and 60°) at four winglet pitch ratios (P_R=0.5, 1.0, 1.5 and 2.0) and three blockage ratios (B_R=0.1, 0.15 and 0.2) are examined. It is visible that the maximum thermal enhancement factor is obtained for the 30° VU-WVGs at P_R=1.5, and B_R=0.1. Thus, these conditions have been extended to study effect of B_R=0.05 on its thermal performance while other parameters were kept constant. The analytical method for evaluation of the optimal parameters to achieve the optimal thermal enhancement factor is the response surface method (RSM) by acting at *Re*=5300.

The result obtained from the RSM is displayed in Figure 6.35. In the figure, the maximum η is about 1.61 for the 30° VU-WVGs with B_R=0.13 and P_R=1.4 while the minimum is 1.48 for the one with B_R=0.2 and P_R=0.5.

The variations of Nu/Nu_0 with f/f_0 values at corresponding conditions for various P_R and B_R values are presented in Figure 6.36. In the figure, it is apparent that the slope of the Nu/Nu_0 with respect to the f/f_0 values tends to increase with the reduction of B_R.

Figures 6.37 and 6.38 depict the variation of the η with Nusselt number and friction factor ratios, rescpectively. For all, the data of Nusselt number, friction factor and η are obtain from an optimal analysis.

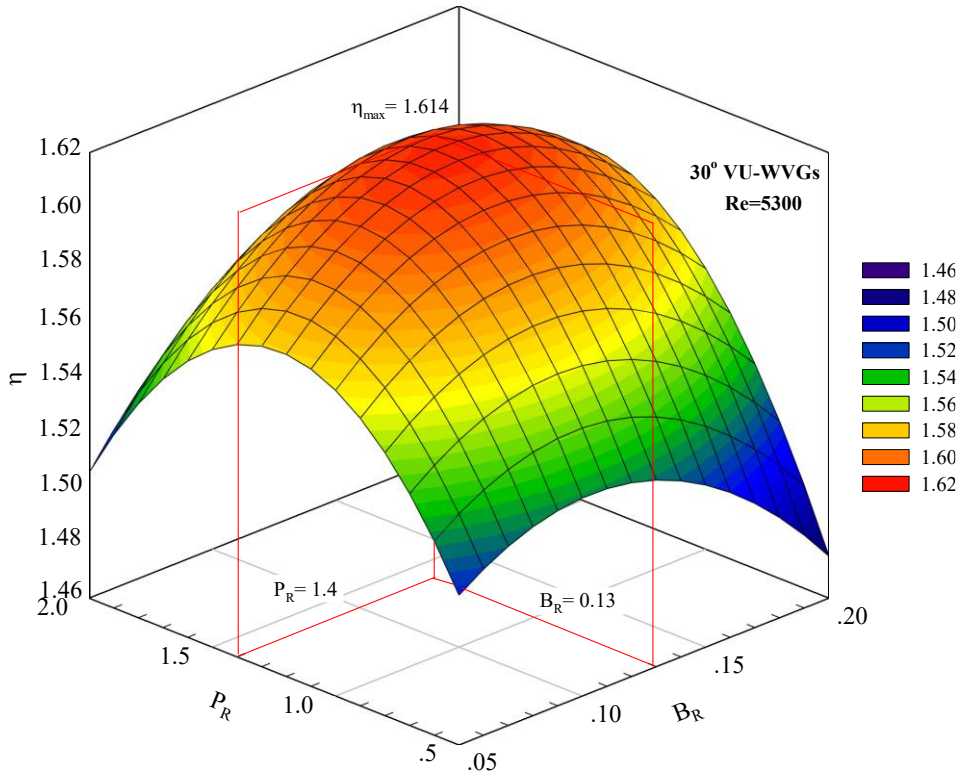

Figure 6.35 Variation of η with B_R and P_R values.

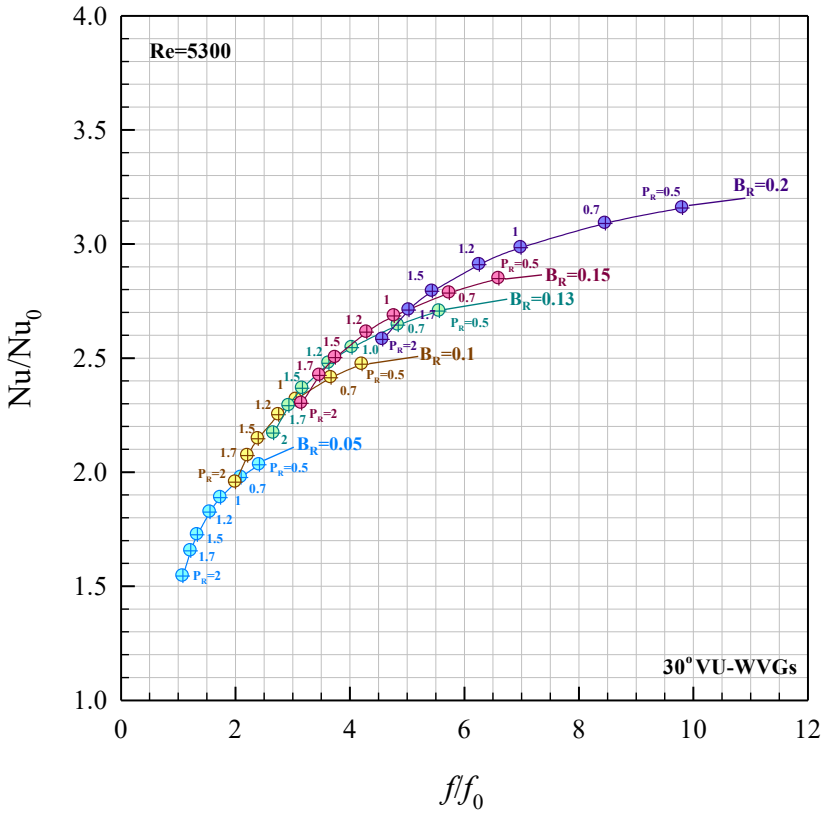

Figure 6.36 Nu/Nu$_0$ against friction f/f_0 for various B_R and P_R.

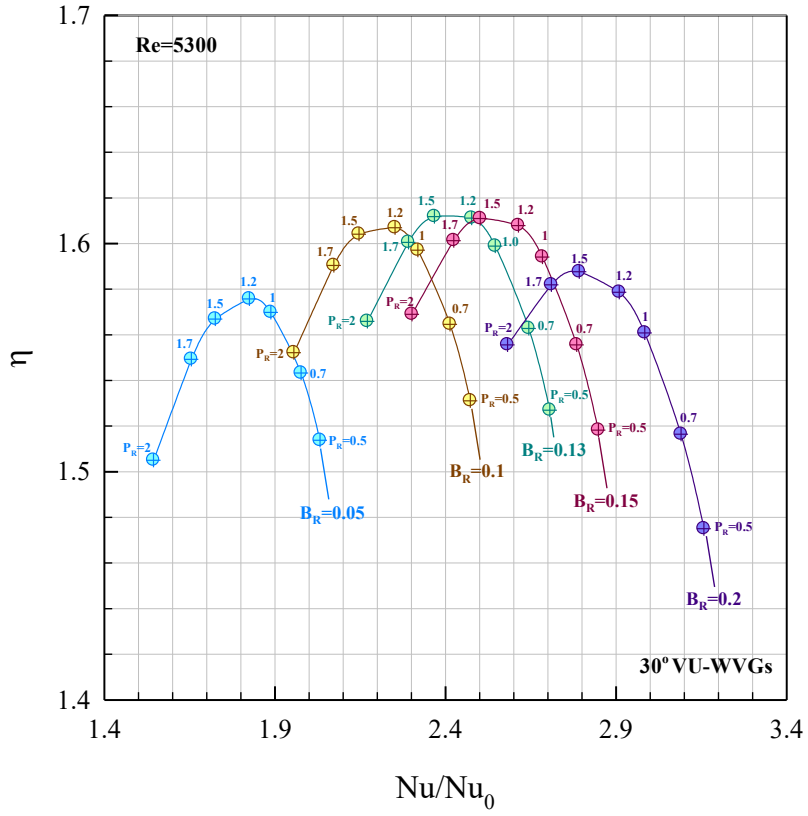

Figure 6.37 Variation of η with Nu/Nu$_0$.

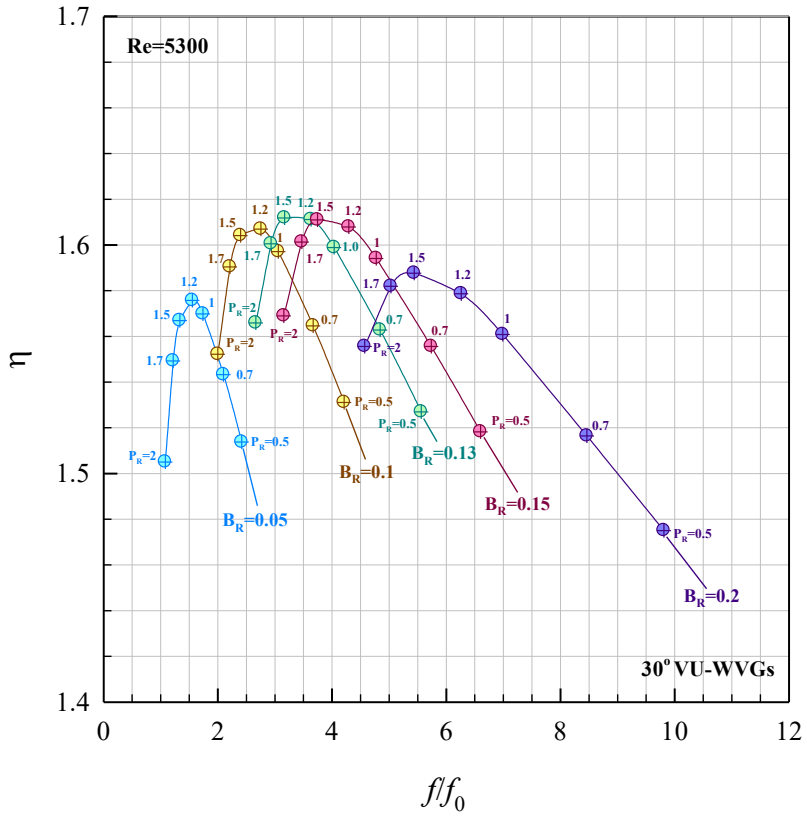

Figure 6.38. Variation of η with f/f_0.

6.8 Conclusions

The heat transfer and the friction factor characteristics in a round tube inserted with WVGs, VD-WVGs and VU-WVGs at three attack angles, four winglet pitch ratios, and three blockage ratios have been investigated for the turbulent regime, *Re*=5300–24,000 under a uniform heat-flux condition. In the present study, The Nu increases with the increment of B_R but the reduction of P_R. The WVGs, VD-WVGs and VU-WVGs provide the average increases in Nu at about 181–314%, 140–308% and 180–356% above the smooth tube, respectively while the *f* increases with the increment of B_R but the reduction of P_R. The WVG, VD-WVG and VU-WVG yeild the mean *f* around 1.98–17.25, 1.36–20.01 and 2.08–21.80 times above the smooth tube, respectively. The η for the WVG, VD-WVG and VU-WVG are, respectively, about 1.10–1.59, 1.03–1.47 and 1.21–1.65. At similar operating condition, the VU-WVG give the highest η while the WVG performs higher than the VD-WVG.

CHAPTER 7
WINGLETS PLACED ON INNER TUBE WALL

7.1 Opening remarks

The chapter describes heat transfer, friction factor and thermal performance behaviors in a tube heat exchanger equipped with winglet vortex generators. Two support-types of holding up winglet elements are offered. One is that the winglets are tied together by putting two straight steel wires on both winglet end areas with semicircular-rod supports on both ends of the wires. The other is the attachment of winglets on double-sided tape edges. The winglets used in this chapter are placed on the inner wall of the test tube after insertion and can be classified into 2 parts:

Part I : Winglets on wires (WVGs-Wire) and on tape-edges (WVGs-Tape)

Part II : Winglet pairs with V-tip pointing upstream on wires (VU-WVGs-Wire) and on tape edges (VU-WVGs-Tape)

The experiment was conducted in the test tube having a uniform heat-fluxed wall for turbulent air flow with Reynolds number in a range of 5300 to 24,000. Only the winglet elements with the attack angle of 30° were inserted into the test tube at three different pitch ratios (P_R=0.5, 1.0 and 2) and blockage ratios (B_R= 0.1, 0.15 and 0.2). The experimental results of heat transfer enhancement and pressure drop are, respectively, presented in terms of Nusselt number ratio (Nu/Nu_0) and friction factor ratio (f/f_0).

7.2 Heat transfer

7.2.1 Effect of winglet vortex generators

The influence of WVGs-Wire, WVGs-Tape, VU-WVGs-Wire and VU-WVGs-Tape with three blockage ratios (B_R=0.1, 0.15 and 0.2) and pitch ratios (P_R=0.5, 1.0 and 2.0) on Nu/Nu_0 against *Re* is demonstrated in Figure 7.1. In the figure, the heat transfer enhancement for the inserted tube is higher than that for the plain tube and shows the slight downtrend pattern with the rise of *Re* for all cases studied. The WVGs-Tape and the VU-WVGs-Tape provide the mean Nu/Nu_0 at about 7% higher than the WVGs-Wire and the VU-WVGs-Wire, respectively. The heat transfer increase in the tube with VU-WVGs is about 5% above that with WVGs.

The average increases in heat transfer for the WVGs-Wire with P_R=0.5, 1.0 and 2.0 are, respectively, 139–173%, 117–148% and 106–136%; 158–195%, 136–170% and 124–157%; and 189–231%, 164–203% and 151–188% for B_R=0.1, 0.15 and 0.2.

The average increases in heat transfer for the WVGs-Tape with P_R=0.5, 1.0 and 2.0 are, respectively, 160–198%, 131–165% and 121–153%; 175–215%, 153–190% and 138–174%; and 208–253%, 186–228% and 167–206% for B_R=0.1, 0.15 and 0.2.

The average increases in heat transfer for the VU-WVGs-Wire with P_R=0.5, 1.0 and 2.0 are, respectively, 151–188%, 127–160% and 116–148%; 170–209%, 148–184% and 136–170%; and 203–247%, 178–218% and 164–202% for B_R=0.1, 0.15 and 0.2.

The average increases in heat transfer for the VU-WVGs-Tape with P_R=0.5, 1.0 and 2.0 are, respectively, 170–209%, 143–179% and 132–166%; 189–231%, 165–204% and 152–189%; and 223–270%, 197–240% and 182–223% for B_R=0.1, 0.15 and 0.2.

7.2.2 Effect of pitch ratio

The influence of three pitch ratios (P_R=0.5, 1.0 and 2.0) for the WVGs-Wire, WVGs-Tape, VU-WVGs-Wire and VU-WVGs-Tape on the heat transfer enhancement is depicted in Figure 7.2. It is seen that the Nu/Nu_0 tends to increase with the reduction of P_R. The P_R=0.5, 1.0 and 2.0 provide the mean increase in heat transfer rate at 139–231%, 117–203% and 106–188%; 160–253%, 131–228% and 121–206%; 151–247%, 127–218% and 116–202%; and 170–270%, 143–240% and 132–223% for the WVGs-Wire, WVGs-Tape, VU-WVGs-Wire and VU-WVGs-Tape, respectively. The quantitative results reveal that the mean heat transfer rate in the inserted tube with P_R=0.5 is around 10–11% and 13–15% higher than with P_R=1.0 and 2.0, respectively.

7.2.3 Effect of blockage ratio

Effect of three blockage ratios (B_R=0.1, 0.15 and 0.2) on the increase in heat transfer rate for the WVGs-Wire, WVGs-Tape, VU-WVGs-Wire and VU-WVGs-Tape is displayed in Figure 7.3. Obviously, the larger B_R winglets provide higher heat transfer rate than the smaller one. The mean increases in Nu values for B_R=0.1, 0.15 and 2.0 are, respectively, about 106–173%, 124–195% and 151–231%; 121–198%, 138–215% and 167–253%; 116–188%, 136–209% and 164–247%; and 132–209%, 152–231% and 182–270% for the WVGs-Wire, WVGs-Tape, VU-WVGs-Wire and VU-WVGs-Tape. The B_R=0.2 provides the highest heat transfer rate around 10–13% and 19-21% over the B_R=0.15 and 0.1, respectively, for all cases studied.

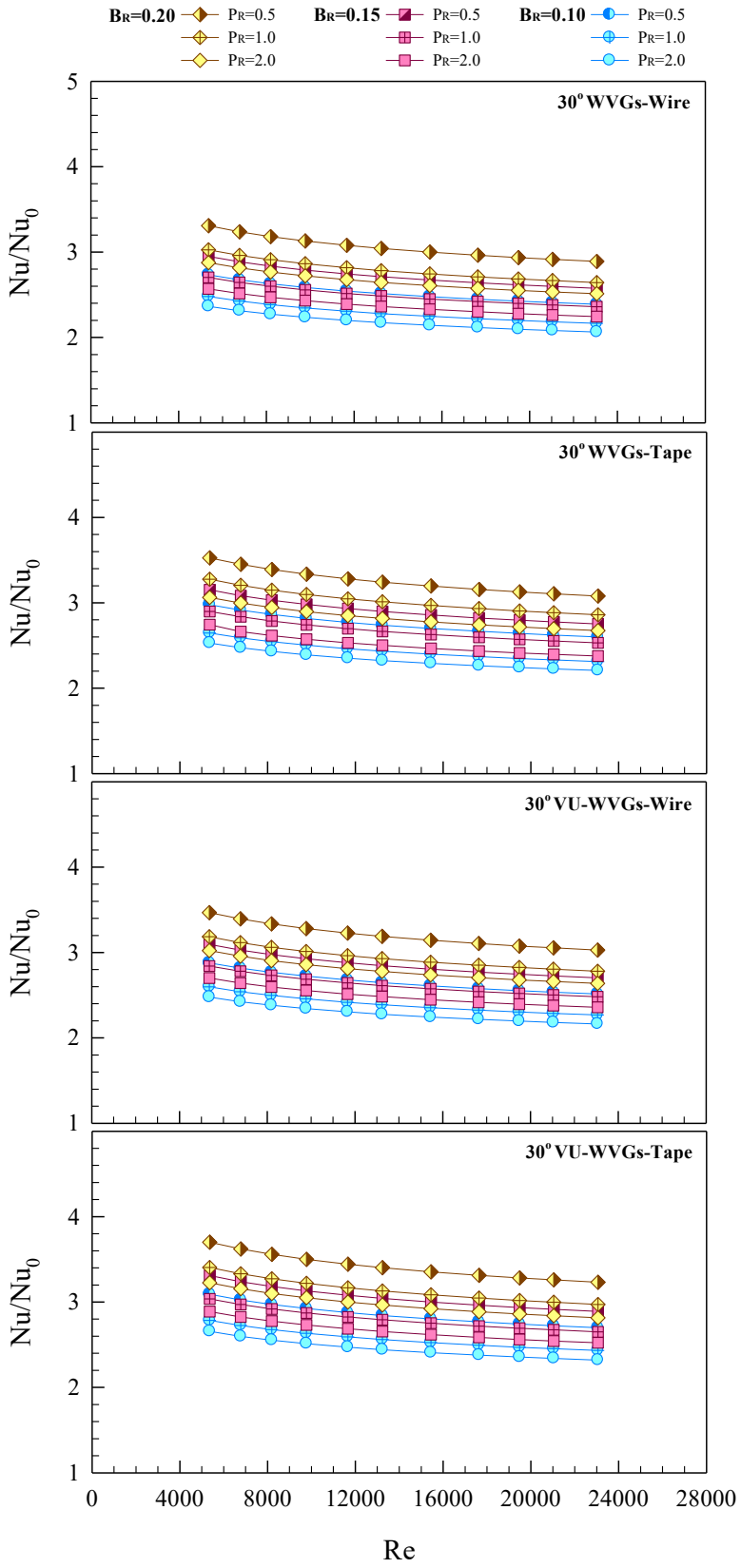

Figure 7.1 Sensitivity of all WVG types to heat transfer enhancement.

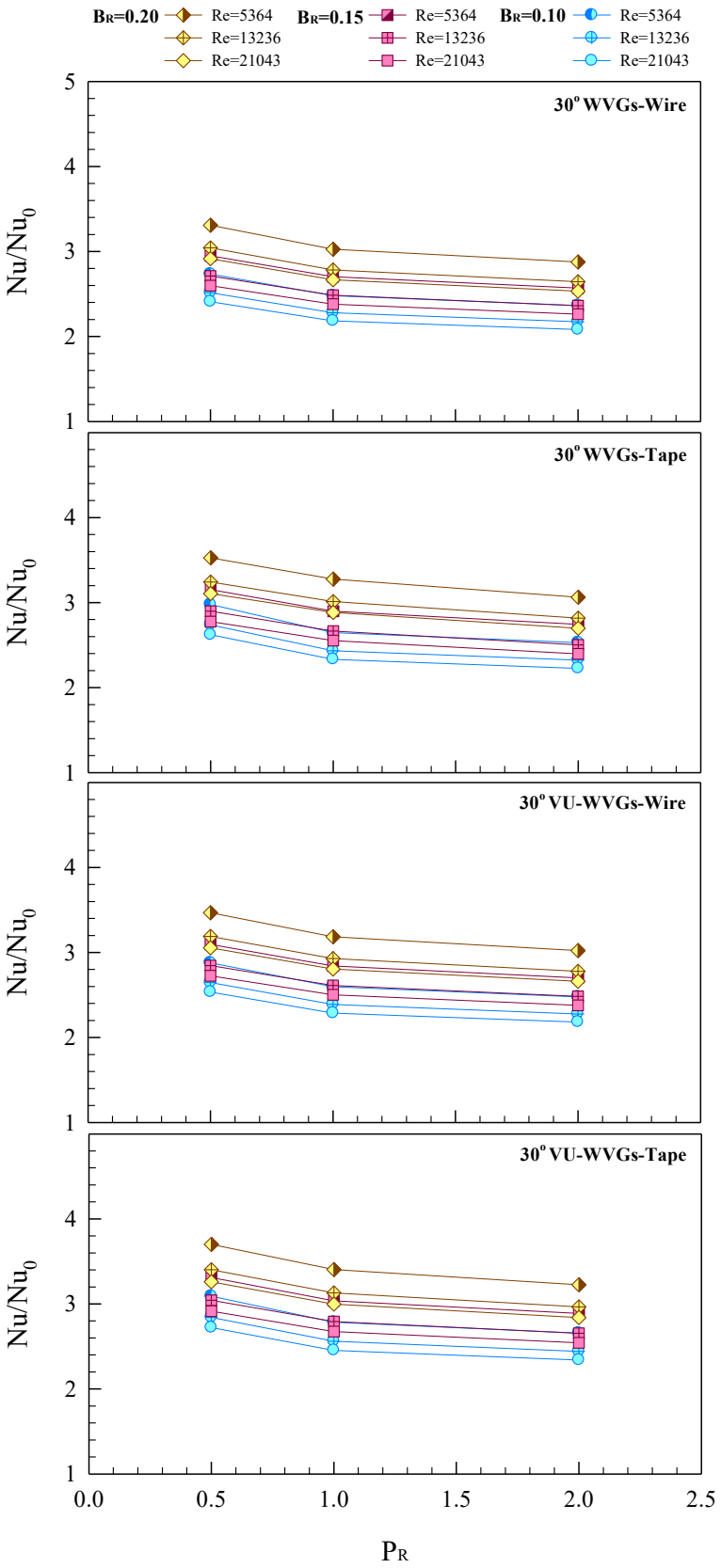

Figure 7.2 Sensitivity of pitch ratio to heat transfer enhancement.

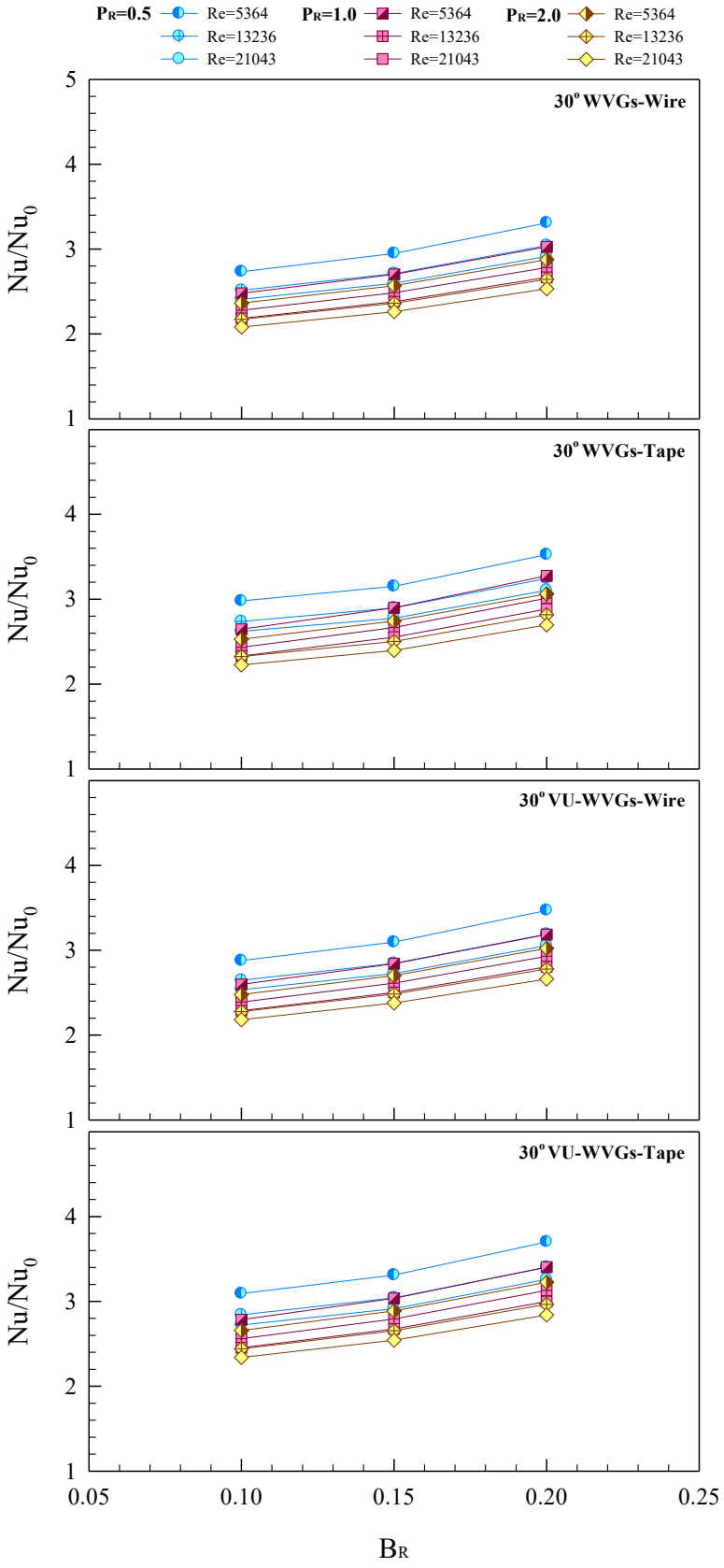

Figure 7.3 Sensitivity of blockage ratio to heat transfer enhancement.

7.3 Friction factor

7.3.1 Effect of winglet vortex generators

Figure 7.4 presents the variation of friction factor ratio (f/f_0) with *Re* for the WVGs-Wire, WVGs-Tape, VU-WVGs-Wire and VU-WVGs-Tape inserts at three blockage ratios (B_R=0.1, 0.15 and 0.2) and pitch ratios (P_R=0.5, 1.0 and 2.0). It is clearly observed in the figure that the winglet vortex generators provide the substantial increase in f over the smooth tube. The f/f_0 displays the uptrend with the rise of *Re* for all cases. The mean f for the WVGs-Tape and VU-WVGs-Tape is about 28% and 31% higher than the WVGs-Wire and VU-WVGs-Wire, respectively and that for the VU-WVGs is about 9% and 12% higher than that for the WVGs-Wire and the WVGs-Tape.

The increases of f/f_0 for the WVGs-Wire with P_R=0.5, 1.0 and 2.0 are 3.65–4.02, 3.16–3.49 and 2.91–3.21; 5.22–5.75, 4.58–5.05 and 4.15–4.58; and 7.70–8.50, 6.95–7.66 and 6.24–6.88 times for B_R=0.1, 0.15 and 0.2, respectively.

The increases of f/f_0 for the WVGs-Tape with P_R=0.5, 1.0 and 2.0 are 4.97–5.48, 4.04–4.45 and 3.72–4.11; 6.65–7.33, 5.81–6.41 and 5.22–5.76; and 9.91–10.93, 8.80–9.71 and 7.91–8.27 times for B_R=0.1, 0.15 and 0.2, respectively.

The increases of f/f_0 for the VU-WVGs-Wire with P_R=0.5, 1.0 and 2.0 are 4.04–4.46, 3.47–3.83 and 3.19–3.52; 5.72–6.31, 5.02–5.54 and 4.55–5.02; and 8.46–9.34, 7.63–8.41 and 6.84–7.55 times for B_R=0.1, 0.15 and 0.2, respectively.

The increases of f/f_0 for the VU-WVGs-Tape with P_R=0.5, 1.0 and 2.0 are 5.37–5.93, 4.59–5.07 and 4.18–4.61; 7.40–8.17, 6.55–7.23 and 5.94–6.56; and 11.07–12.21, 9.96–10.99 and 8.94–9.86 times for B_R=0.1, 0.15 and 0.2, respectively.

7.3.2 Effect of pitch ratio

The influence of three pitch ratios (P_R=0.5, 1.0 and 2.0) for the WVGs-Wire, WVGs-Tape, VU-WVGs-Wire and VU-WVGs-Tape on friction factor ratio (f/f_0) is displayed in Figure 7.5. It is seen that the f/f_0 tends to decrease with the rise of P_R. At P_R=0.5, 1.0 and 2.0, the mean f/f_0 are, respectively, about 3.65–8.50, 3.16–7.66 and 2.91–6.88; 4.97–10.93, 4.04–9.71 and 3.72–8.72; 4.04–9.34, 3.47–8.41 and 3.19–7.55; and 5.37–12.21, 4.59–10.99 and 4.18–9.86 for the WVGs-Wire, WVGs-Tape, VU-WVGs-Wire and VU-WVGs-Tape. The quantitative results reveal that the mean f/f_0 for P_R=0.5 is around 11–15% and 25–30% higher than that for P_R=1.0 and 2.0, respectively for all cases studied.

7.3.3 Effect of blockage ratio

The variations of f/f_0 with *Re* for the WVGs-Wire, WVGs-Tape, VU-WVGs-Wire and VU-WVGs-Tape for various B_R are exhibited in Figure 7.6. It is visible that the larger B_R winglet provides higher friction loss than the smaller one. The mean f/f_0

values at B_R=0.1, 0.15 and 2.0 are about 2.91–4.02, 4.15–5.75 and 6.24–8.50; 3.72–5.48, 5.22–7.33 and 7.91–10.93; 3.19–4.46, 4.55–6.31 and 6.84–9.34; and 4.18–5.93, 5.94–8.17 and 8.94–12.21 times for the WVGs-Wire, WVGs-Tape, VU-WVGs-Wire and VU-WVGs-Tape, respectively. The B_R=0.2 provides the highest friction loss of about 19–22% and 48–50% higher than the B_R=0.15 and 0.1, respectively.

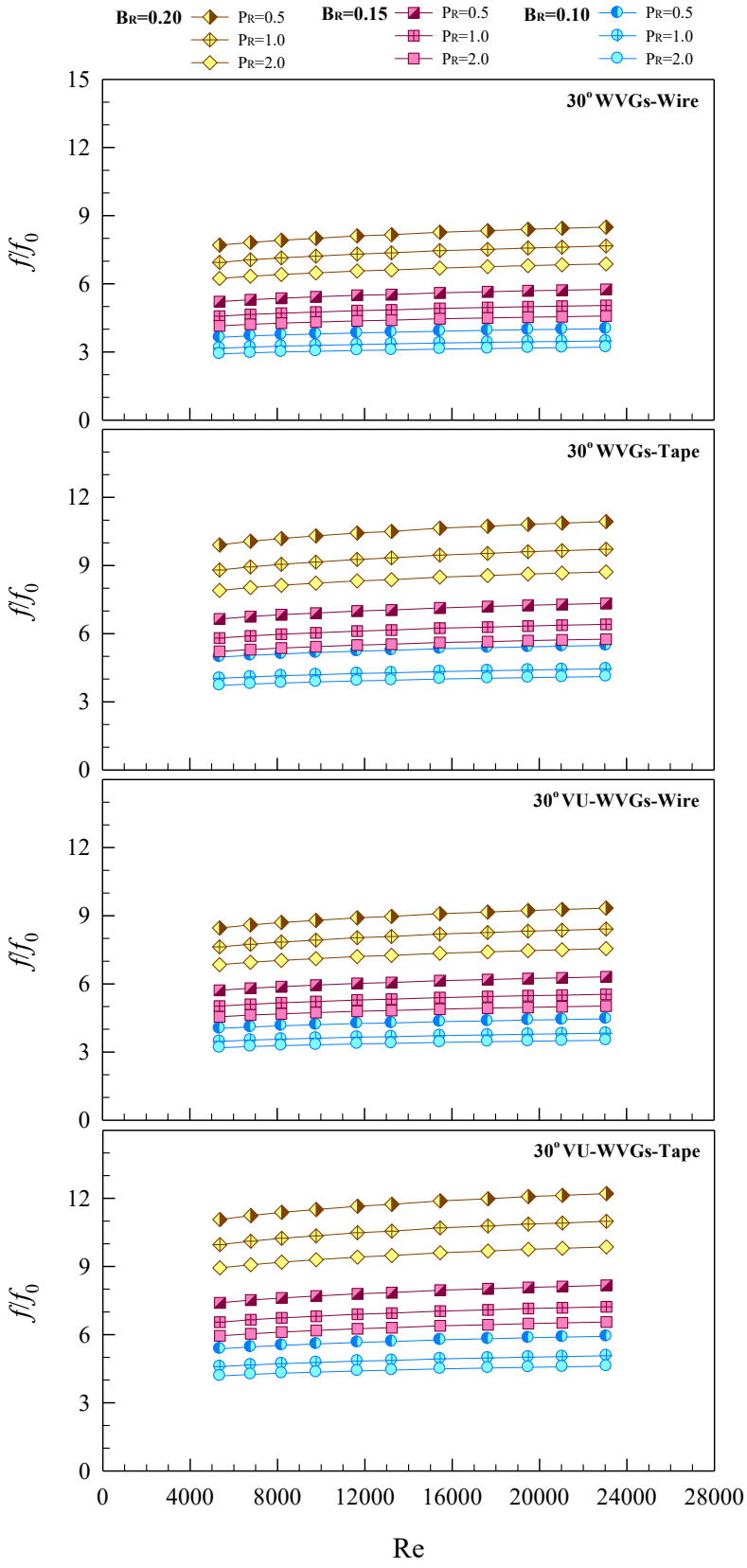

Figure 7.4 Effect of all WVG types on friction factor ratio.

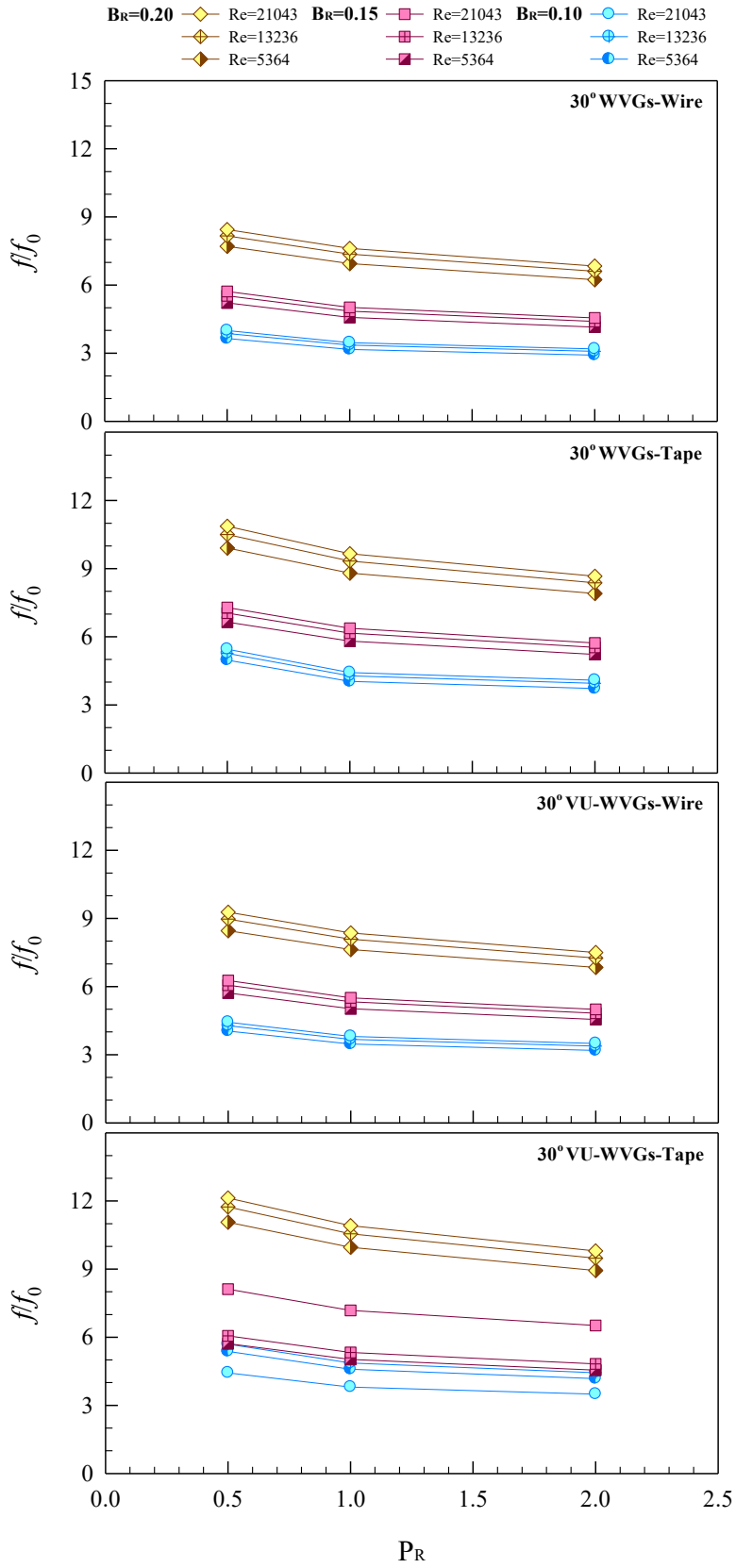

Figure 7.5 Effect of pitch ratio on friction factor ratio.

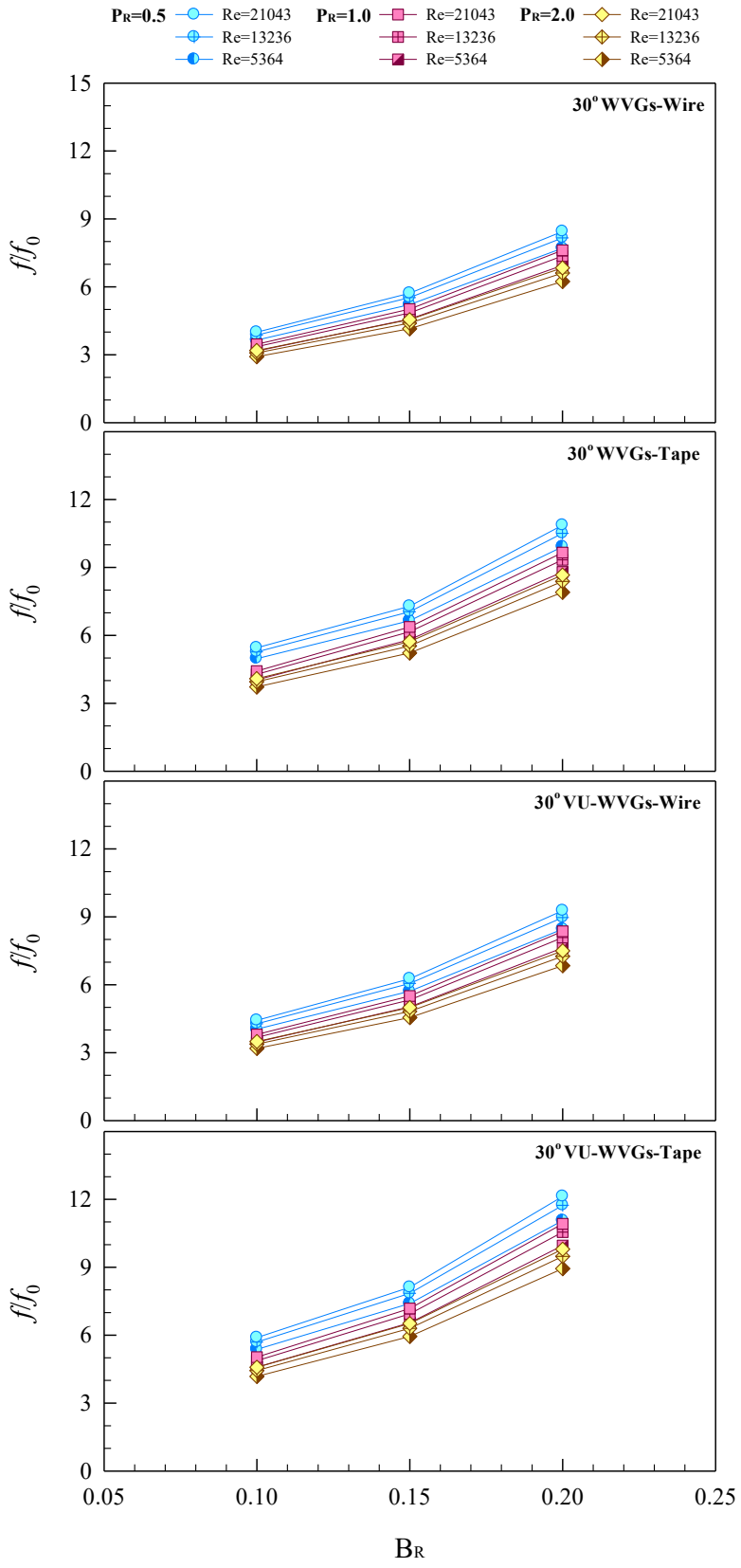

Figure 7.6 Effect of blockage ratio on friction factor ratio.

7.4 Thermal performance factor

7.4.1 Effect of winglet vortex generators

The variation of η with *Re* is depicted in Figure 7.7. It is seen in the figure that all η values generally are above unity, indicating the use of all WVG-types is advantageous over the smooth tube. The η shows the downtrend pattern with the increase of *Re* for all winglets investigated.

The η values for the WVGs-Wire at P_R=0.5, 1.0 and 2.0 are around 1.50–1.78, 1.43–1.69 and 1.40–1.66; 1.44–1.70, 1.38–1.63 and 1.35–1.60; and 1.42–1.68, 1.34–1.59 and 1.32–1.56 for B_R=0.1, 0.15 and 0.2, respectively.

The η values for the WVGs-Tape at P_R=0.5, 1.0 and 2.0 are about 1.47–1.75, 1.40–1.66 and 1.38–1.63; 1.42–1.68, 1.36–1.61 and 1.33–1.58; and 1.39–1.64, 1.33–1.58 and 1.30–1.54 for B_R=0.1, 0.15 and 0.2, respectively.

The η values for the VU-WVGs-Wire at P_R=0.5, 1.0 and 2.0 are some 1.53–1.81, 1.45–1.72 and 1.42–1.68; 1.46–1.73, 1.40–1.66 and 1.38–1.63; and 1.44–1.70, 1.37–1.62 and 1.34–1.59 for B_R=0.1, 0.15 and 0.2, respectively.

The η values for the VU-WVGs-Tape at P_R=0.5, 1.0 and 2.0 are approximately 1.49–1.77, 1.42–1.68 and 1.39–1.65; 1.44–1.70, 1.37–1.62 and 1.35–1.59; and 1.40–1.66, 1.34–1.58 and 1.31–1.55 for B_R=0.1, 0.15 and 0.2, respectively.

7.4.2 Effect of pitch ratio

The effect of three pitch ratios (P_R=0.5, 1.0 and 2.0) on η is displayed in Figure 7.8. It is apparent that the small P_R winglet yields higher η than the larger one. The quantitative results reveal that the mean η for P_R=0.5 is around 5% and 7% higher than that for P_R=1.0 and 2.0, respectively for all. The mean η values for P_R=0.5, 1.0 and 2.0 are, respectively, about 1.42–1.78, 1.34–1.69 and 1.32–1.66; 1.39–1.75, 1.34–1.66 and 1.30–1.63; 1.44–1.81, 1.37–1.72 and 1.34–1.68; and 1.40–1.77, 1.34–1.68 and 1.31–1.65 for the WVGs-Wire, WVGs-Tape, VU-WVGs-Wire and VU-WVGs-Tape.

7.4.3 Effect of blockage ratio

The influence of B_R on η is presented in Figure 7.9. It is seen that the η shows the downtrend pattern with the increase of B_R for all cases. The B_R=0.1 provides the highest η and is about 4% and 6% higher than the B_R=0.15 and 0.2, respectively. The mean η values at B_R=0.1, 0.15 and 2.0 are about 1.40–1.78, 1.35–1.70 and 1.32–1.68; 1.38–1.75, 1.33–1.68 and 1.30–1.64; 1.42–1.81, 1.38–1.73 and 1.34–1.70; and 1.39–1.77, 1.35–1.70 and 1.31–1.66 for the WVGs-Wire, WVGs-Tape, VU-WVGs-Wire and VU-WVGs-Tape, respectively.

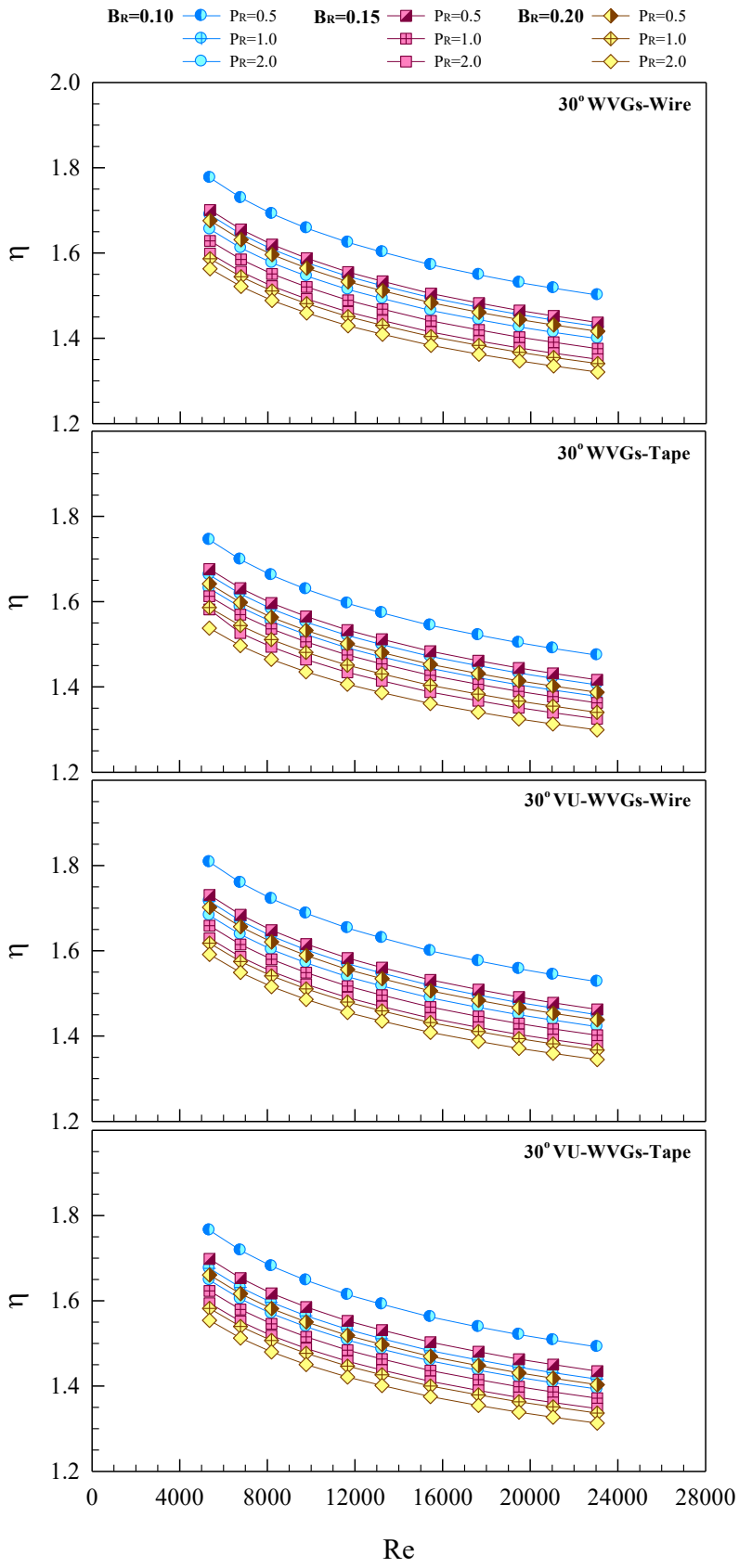

Figure 7.7 Effect of all WVG-types on thermal performance.

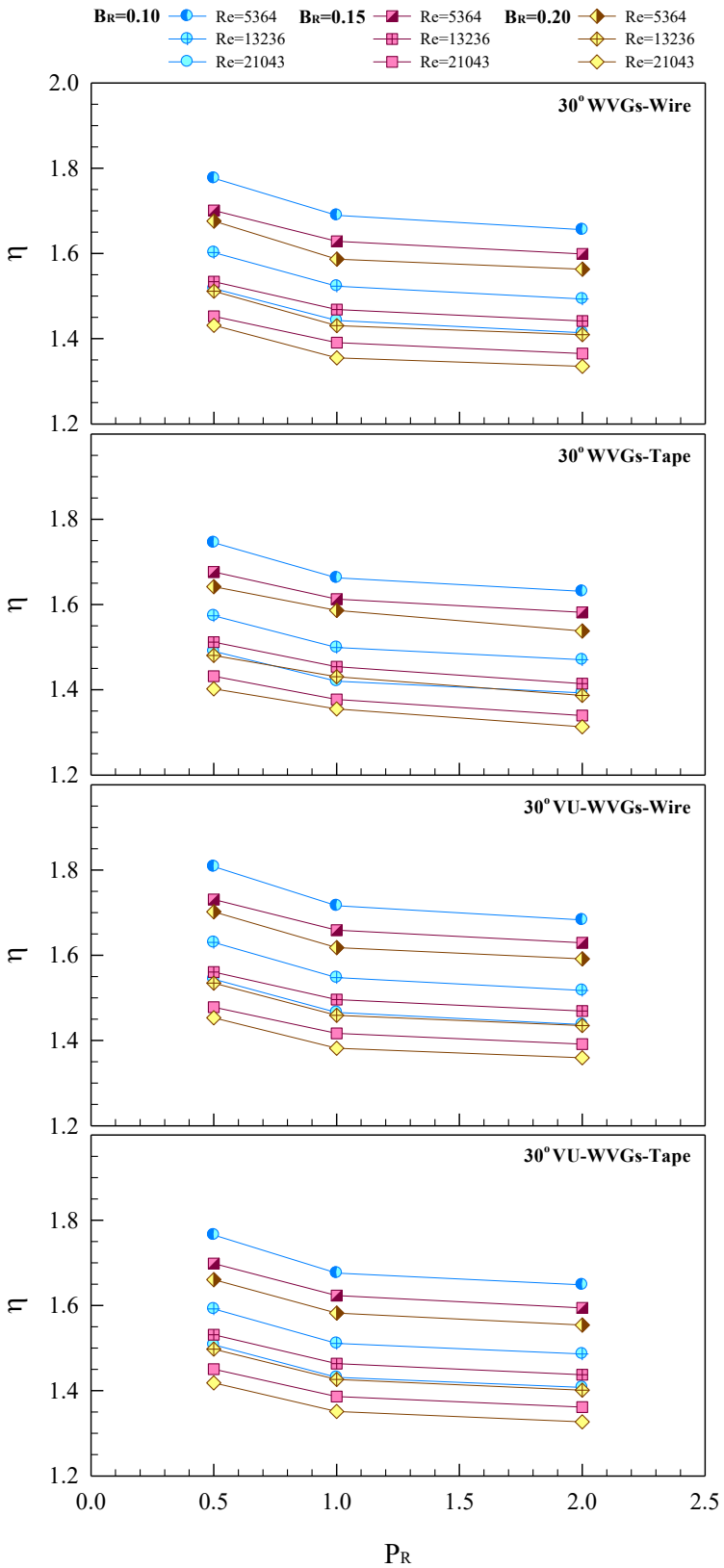

Figure 7.8 Effect of pitch ratio on thermal performance.

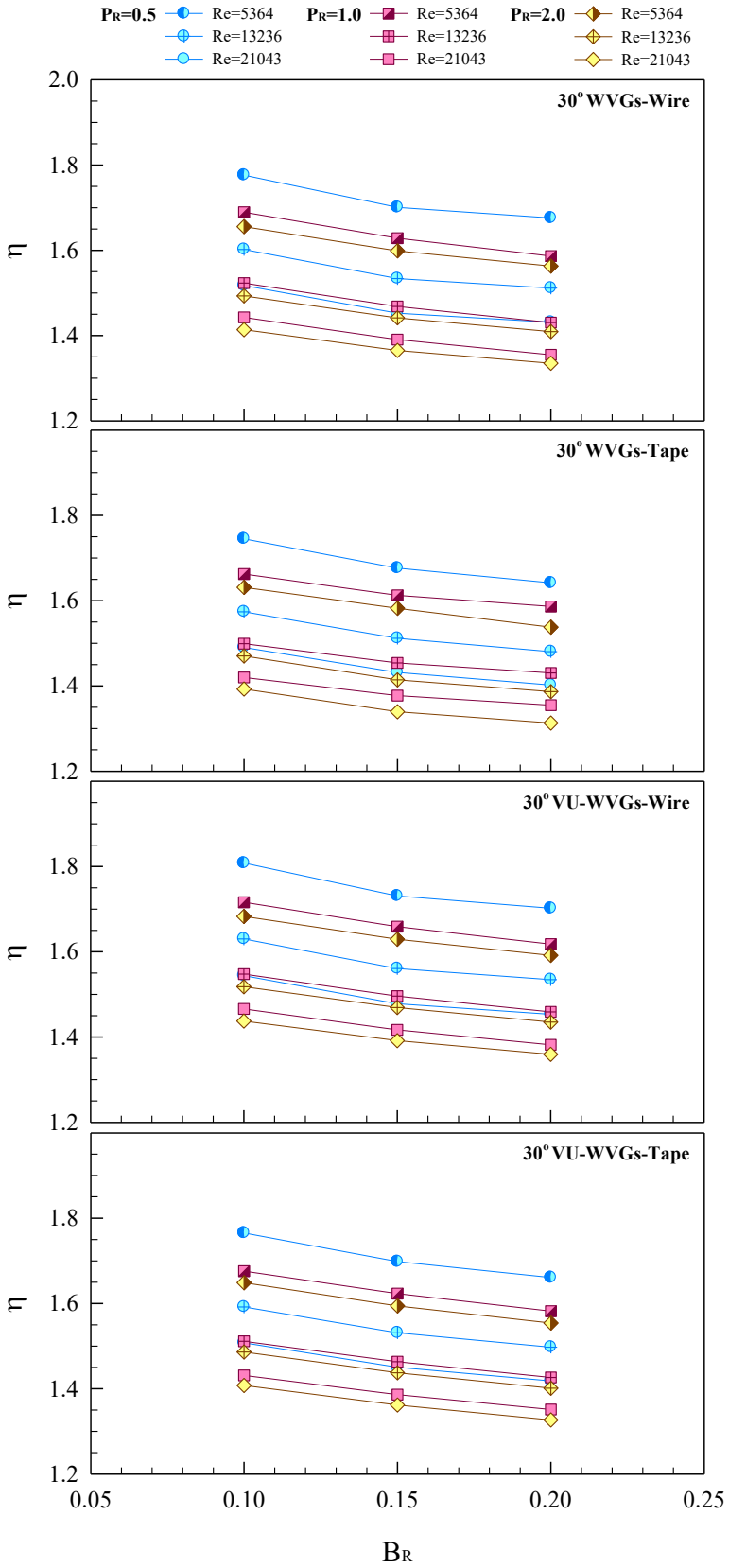

Figure 7.9 Effect of blockage ratio on thermal performance.

Table 7.1 Experimental results of WVGs-Wire.

WVGs-Wire		Results		
B_R	P_R	Nu/Nu$_0$	f/f_0	η
0.10	0.5	2.73–2.39	3.65–4.02	1.78–1.50
	1.0	2.48–2.17	3.16–3.49	1.69–1.43
	2.0	2.36–2.06	2.91–3.21	1.66–1.40
0.15	0.5	2.95–2.58	5.22–5.75	1.70–1.44
	1.0	2.70–2.36	4.58–5.05	1.63–1.38
	2.0	2.57–2.24	4.15–4.58	1.60–1.35
0.20	0.5	3.31–2.89	7.70–8.50	1.68–1.42
	1.0	3.03–2.64	6.95–7.66	1.59–1.34
	2.0	2.88–2.51	6.24–6.88	1.56–1.32
Optimal results		η=1.78 at Re≈5300, B_R=0.10 and P_R=0.5		

Table 7.2 Experimental results of WVGs-Tape.

WVGs-Tape		Results		
B_R	P_R	Nu/Nu$_0$	f/f_0	η
0.10	0.5	2.98–2.60	4.97–5.48	1.75–1.47
	1.0	2.65–2.31	4.04–4.45	1.66–1.40
	2.0	2.53–2.21	3.72–4.11	1.63–1.38
0.15	0.5	3.15–2.75	6.65–7.33	1.68–1.42
	1.0	2.90–2.53	5.81–6.41	1.61–1.36
	2.0	2.74–2.38	5.22–5.76	1.58–1.33
0.20	0.5	3.53–3.08	9.91–10.93	1.64–1.39
	1.0	3.28–2.86	8.80–9.71	1.59–1.34
	2.0	3.06–2.67	7.91–8.72	1.54–1.30
Optimal results		η=1.75 at Re≈5300, B_R=0.10 and P_R=0.5		

Table 7.3 Experimental results of VU-WVGs-Wire.

VU-WVGs-Wire		Results		
B_R	P_R	Nu/Nu$_0$	f/f_0	η
0.10	0.5	2.88–2.51	4.04–4.46	1.81–1.53
	1.0	2.60–2.27	3.47–3.83	1.72–1.45
	2.0	2.48–2.16	3.19–3.52	1.68–1.42
0.15	0.5	3.09–2.70	5.72–6.31	1.73–1.46
	1.0	2.84–2.48	5.02–5.54	1.66–1.40
	2.0	2.70–2.36	4.55–5.02	1.63–1.38
0.20	0.5	3.47–3.03	8.46–9.34	1.70–1.44
	1.0	3.18–2.78	7.63–8.41	1.62–1.37
	2.0	3.02–2.64	6.84–7.55	1.59–1.34
Optimal results		η=1.81 at Re≈5300, B_R=0.10 and P_R=0.5		

Table 7.4 Experimental results of VU-WVGs-Tape.

VU-WVGs-Tape		Results		
B_R	P_R	Nu/Nu$_0$	f/f_0	η
0.10	0.5	3.09–2.70	5.37–5.93	1.77–1.49
	1.0	2.79–2.43	4.59–5.07	1.68–1.42
	2.0	2.66–2.32	4.18–4.61	1.65–1.39
0.15	0.5	3.31–2.89	7.40–8.17	1.70–1.44
	1.0	3.04–2.65	6.55–7.23	1.62–1.37
	2.0	2.89–2.52	5.94–6.56	1.59–1.35
0.20	0.5	3.70–3.23	11.07–12.21	1.66–1.40
	1.0	3.40–2.97	9.96–10.99	1.58–1.34
	2.0	3.23–2.82	8.94–9.86	1.55–1.31
Optimal results		η=1.59 at Re≈5300, B_R=0.10 and P_R=1.5		

7.5 Empirical correlations

The empirical correlations for various turbulator geometries developed by relating Reynolds number (*Re*), blockage ratio (B_R) and pitch ratio (P_R) together are compared with experimental data under the conditions; Re=5300–24,000, P_R=0.5–2.0 and B_R=0.1–0.2. The predicted Nusselt number and friction factor are, respectively, within ±4 and ±6 deviation with experimental results.

Table 7.5 Heat transfer correlations.

Correlations	$Nu = a(Re^b)(Pr^{0.4})(B_R^c)(P_R^d)$			
	a	b	c	d
WVGs-Wire	0.2426	0.7071	0.2769	-0.1018
WVGs-Tape	0.2572	0.7067	0.2699	-0.1085
VU-WVGs-Wire	0.2552	0.7072	0.2779	-0.1021
VU-WVGs-Tape	0.2695	0.7070	0.2710	-0.1024

Table 7.6 Friction factor correlations.

Correlations	$f = a(Re^b)(B_R^c)(P_R^d)$			
	a	b	c	d
WVGs-Wire	6.8581	-0.1823	1.0903	-0.1598
WVGs-Tape	8.1692	-0.1825	1.0525	-0.1819
VU-WVGs-Wire	7.4904	-0.1822	1.0876	-0.1627
VU-WVGs-Tape	9.4688	-0.1824	1.0696	-0.1644

7.6 Conclusions

Experimental investigations have been conducted to examine the effect of the pitch length and the blockage ratios of the WVGs-Wire, WVGs-Tape, VU-WVGs-Wire and VU-WVGs-Tape inserts on heat transfer rate and flow friction characteristics in a uniform heat-fluxed tube using air as the test fluid for the turbulent regime, *Re*=5300–24,000. The application of the winglet elements results in a considerable increase in the heat transfer rate (Nu) and friction loss (*f*) that both the Nu and *f* show the uptrend pattern with the increment of B_R but the reduction of P_R. For the WVGs-Wire, WVGs-Tape, VU-WVGs-Wire and VU-WVGs-Tape, the average Nu/Nu_0 values are about 2.06–3.31, 2.21–3.53, 2.16–3.47 and 2.32–3.70, respectively while the average f/f_0 are around 2.91–8.50, 3.72–10.93, 3.19–9.34 and 4.18–12.21, depending on *Re*, B_R and P_R values. The maximum η for the WVGs-Wire, WVGs-Tape, VU-WVGs-Wire and VU-WVGs-Tape are, respectively, about 1.78, 1.75, 1.81 and 1.77, all at *Re*=5300, B_R=0.1 and P_R=0.5.

CHAPTER 8
CONCLUSIONS AND SUGGESTIONS

8.1 Conclusions

The thesis presents the experimental investigation on the influence of various turbulator inserts on heat transfer (Nu), friction factor (*f*) and thermal performance factor (η) in a tubular heat exchanger. The experiment was carried out in a uniform wall heat-fluxed tube by varying turbulent airflow for Reynolds number ranging from 5300 to 24,000. The categories of turbulators can be divided into 3 sections as follows:

Section I : Multiple twisted-tapes

Part I : Loose-fit multiple twisted-tapes (LF-TT)

Part II : Tight-fit multiple twisted-tapes (TF-TT)

Section II : Winglets Placed in Central Core Flow

Part I : Winglets (WVGs)

Part II : Winglet pairs with V-tip pointing downstream (VD-WVGs)

Part III : Winglet pairs with V-tip pointing upstream (VU-WVGs)

Section III : Winglets Placed on Inner Tube Wall

Part I : Winglets on wires (WVGs-Wire) and on tape-edges (WVGs-Tape)

Part II : Winglet pairs with V-tip pointing upstream on wires (VU-WVGs-Wire) and on tape edges (VU-WVGs-Tape)

From the experimental results of the present study, the following conclusions can be drawn.

The present research initiates the study on the effect of various twisted-tape numbers (*N*) with co- and counter-twist arrangements. The experimental results reveal that both the Nu and *f* tends to increase with the increment of *N* and the reduction of twist ratio. The counter-twisted tape arrangements provide Nu and *f* higher than the co-twisted tape arrangements. The loose-fit and tight-fit multiple twisted-tapes yield the mean Nu of around 1.01–1.52 and 1.15–2.12 while the mean *f* of about 1.24–1.77 and 1.94–4.06 times the smooth tube, respectively. It is interesting to note that the η shows the uptrend pattern with the increment of *N*. The counter-twisted tapes also give higher η than the co-twisted tapes. The maximum η for the loose-fit twisted tapes is about 1.26 for the triple counter-twisted tapes ($L_TR_TL_T$) at y/w=4 while that for the tight-fit one is about 1.33 for the quadruple counter-twisted tapes (4T4) at lower *Re*. The highest η for both tape types in this section are taken to compare of thermal enhancement factors with the different shape/modification of twisted tape from previous available works. Found that, the η

obtained from the present work are in a moderate range of the values from previous works.

Then, the modifications of winglets (WVGs) and winglet pairs (VD-WVGs and VU-WVGs) placed repeatedly in the core flow are studied. Over the range investigated, the Nu and f tend to increase with the reduction of P_R and the increment of B_R and α. The mean increases of Nu and f for the WVGs, VD-WVGs and VU-WVGs are about 1.81–3.14, 1.40–3.08 and 1.80–3.56; and 1.98–17.25, 1.36–20.01 and 2.08–21.80 times above the smooth tube, respectively. The η shows the uptrend with the reduction of B_R and α. At similar operating condition, the use of VU-WVGs leads to higher η than that of WVGs and VD-WVGs. The highest η values in this section are, respectively, around 1.47, 1.59 and 1.65 for the VD-WVGs, WVGs and VU-WVGs. In addition, the optimal condition analysis for prediction of the maximum η reveals that the maximum η around 1.61 is achieved for the 30° VU-WVGs with B_R=0.13 and P_R=1.4 at Re=5300 while in the experimental data, the maximum η around 1.65 is obtained for the 30° VU-WVGs with B_R=0.1 and P_R=1.5 at Re=5300.

Finally, two winglet-types: winglets and V-upstream winglet pairs, each tied together by putting two straight steel wires on both winglet ends (WVGs-Wire and VU-WVGs-Wire) and by attachment on edges of a thin sheet (tape) are experimentally examined. Both winglet-types are placed on the inner tube wall after insertion. The results show that the Nu and f increase with the reduction of P_R and the increment of B_R. The mean increases in Nu and f are about 2.06–3.31, 2.21–3.53, 2.16–3.47 and 2.32–3.70; and 2.91–8.50, 3.72–10.93, 3.19–9.34 and 4.18–12.21 times above the smooth tube for the WVGs-Wire, WVGs-Tape, VU-WVGs-Wire and VU-WVGs-Tape, respectively, depending on Re, B_R and P_R values. The η shows the increasing trend with the reduction of P_R and B_R. The maximum η for the WVGs-Tape, VU-WVGs-Tape, WVGs-Wire and VU-WVGs-Wire are, respectively, about 1.75, 1.77, 1.78 and 1.81 at Re=5300, B_R=0.1 and P_R=0.5.

8.2 Suggestions for future work

The author recommends the guidance for future work on increasing the thermal performance of a heat exchanger as follows:

1. Investigate the effect of the same turbulator, parameters and conditions of the present research, but the test fluid is changed to water/nano fluid.
2. Study the influence of other parameters such as attack angle, winglet-pitch length and winglet-width of the V-upstream winglets pair placed tightly on the inner wall, etc. that affect the performance of the heat exchanger.
3. Investigate the influence of insertion of twisted tapes in conjunction with winglet vortex generators, especially, a combination of multiple counter-

twisted tapes and V-upstream winglet pairs under the same condition with the present work.

4. Improve the turbulator in section III by using the wing mounted on the wavy surface tape instead of the plain tape.

REFERENCES

[1] Chang, S.W. Yang, T.L. and Liou, J.S. 2007. "Heat Transfer and Pressure Drop in Tube with Broken Twisted Tape Insert." *Experimental Thermal and Fluid Science*. 32 : 489–501.

[2] Chang, S.W. Jan, Y.J. and Liou, J.S. 2007. "Turbulent Heat Transfer and Pressure Drop in Tube Fitted with Serrated Twisted Tape." *International Journal of Thermal Sciences*. 46 : 506–518.

[3] Eiamsa-ard, S. Thianpong, C. Eiamsa-ard, P. and Promvonge, P. 2009. "Convective Heat Transfer in a Circular Tube with Short-length Twisted Tape Insert." *International Communications in Heat and Mass Transfer*. 36 : 365–371.

[4] Eiamsa-ard, S. Thianpong, C. Eiamsa-ard, P. and Promvonge, P. 2010. "Thermal Characteristics in a Heat Exchanger Tube Fitted with Dual Twisted Tape Elements in Tandem." *International Communications in Heat and Mass Transfer*. 37 : 39–46.

[5] Eiamsa-ard, S. and Promvonge, P. 2010. "Thermal Characteristics in Round Tube Fitted with Serrated Twisted Tape." *Applied Thermal Engineering*. 30 : 1673–1680.

[6] Bas, H. and Ozceyhan, V. 2012. "Heat Transfer Enhancement in a Tube with Twisted Tape Inserts Placed Separately from the Tube Wall." *Experimental Thermal and Fluid Science*. 41 : 51–58.

[7] Eiamsa-arda, S. Yongsiri, K. Nanan, K. and Thianpong, C. 2010. "Heat Transfer Augmentation by Helically Twisted Tapes as Swirl and Turbulence Promoters." *Chemical Engineering and Processing*. 60 : 58–65.

[8] Bhuiya, M.M.K. Chowdhury, M.S.U. Saha, M. and Islam, M.T. 2013. "Heat Transfer and Friction Factor Characteristics in Turbulent Flow Through a Tube Fitted with Perforated Twisted Tape Inserts." *International Communications in Heat and Mass Transfer*. 43 : 49–57.

[9] Eiamsa-ard, S. Thianpong, C. and Promvonge, P. 2006. "Experimental Investigation of Heat Transfer and Flow Friction in a Circular Tube Fitted with Regularly Spaced Twisted Tape Elements." *International Communications in Heat and Mass Transfer*. 33 : 1225–1233.

[10] Sivashanmugam, P. and Suresh, S. 2007. "Experimental Studies on Heat Transfer and Friction Factor Characteristics of Turbulent Flow Through a Circular Tube Fitted with Regularly Spaced Helical Screw-tape Inserts." *Applied Thermal Engineering*. 27 : 1311–1319.

[11] Sivashanmugam, P. and Suresh, S. 2007. "Experimental Studies on Heat Transfer and Friction Factor Characteristics of Turbulent Flow Through a Circular Tube Fitted with Helical Screw-tape Inserts." *Chemical Engineering and Processing*. 46 : 1292–1298.

[12] Rahimi, M. Shabanian, S.R. and Alsairafi, A.A. 2009. "Experimental and CFD Studies on Heat Transfer and Friction Factor Characteristics of a Tube Equipped with Modified Twisted Tape Inserts." *Chemical Engineering and Processing*. 48 : 762–770.

[13] Eiamsa-ard, S. Wongcharee, K. Eiamsa-ard, P. and Thianpong, C. 2010. "Thermohydraulic Investigation of Turbulent Flow Through a Round Tube Equipped with Twisted Tapes Consisting of Centre Wings and Alternate-axes." *Experimental Thermal and Fluid Science*. 34 : 1151–1161.

[14] Eiamsa-ard, S. and Promvonge, P. 2010. "Performance Assessment in a Heat Exchanger Tube with Alternate Clockwise and Counter-clockwise Twisted-tape Inserts." *International Journal of Heat and Mass Transfer*. 52 : 1364–1372.

[15] Murugesan, P. Mayilsamy, K. and Suresh, S. 2010. "Heat Transfer and Friction Factor Studies in a Circular Tube Fitted with Twisted Tape Consisting of Wire-nails." *Chinese Journal of Chemical Engineering*. 18(6) : 1034–1042.

[16] Murugesan, P. Mayilsamy, K. and Suresh, S. 2010. "Turbulent Heat Transfer and Pressure Drop in Tube Fitted with Square-cut Twisted Tape." *Chinese Journal of Chemical Engineering*. 18(4) : 609–617.

[17] Eiamsa-ard, S. Wongcharee, K. Eiamsa-ard, P. and Thianpong, C. 2010. "Heat Transfer Enhancement in a Tube Using Delta-winglet Twisted Tape Inserts." *Applied Thermal Engineering*. 30 : 310–318.

[18] Seemawute, P. and Eiamsa-ard, S. 2010. "Thermohydraulics of Turbulent Flow Through a Round Tube by a Peripherally-cut Twisted Tape with an Alternate Axis." *International Communications in Heat and Mass Transfer*. 37 : 652–659.

[19] Eiamsa-ard, S. Seemawute, P. and Wongcharee, K. 2010. "Influences of Peripherally-cut Twisted Tape Insert on Heat Transfer and Thermal Performance Characteristics in Laminar and Turbulent Tube Flows." *Experimental Thermal and Fluid Science*. 34 : 711–719.

[20] Murugesan, P. Mayilsamy, K. Suresh, S. and Srinivasan, P.S.S. 2011. "Heat Transfer and Pressure Drop Characteristics in a Circular Tube Fitted with and without V-cut Twisted Tape Insert." *International Communications in Heat and Mass Transfer*. 38 : 329–334.

[21] Wongcharee, K. and Eiamsa-ard, S. 2011. "Heat Transfer Enhancement by Twisted Tapes with Alternate-axes and Triangular, Rectangular and Trapezoidal Wings." *Chemical Engineering and Processing*. 50 : 211–219.

[22] Ibrahim, E.Z. 2011. "Augmentation of Laminar Flow and Heat Transfer in Flat Tubes by Means of Helical Screw-tape Inserts." *Energy Conversion and Management*. 52 : 250–257.

[23] Shabanian, S.R. Rahimi, M. Shahhosseini, M. and Alsairafi, A.A. 2011. "CFD and Experimental Studies on Heat Transfer Enhancement in an Air Cooler Equipped with Different Tube Inserts." *International Communications in Heat and Mass Transfer*. 38 : 383–390.

[24] Eiamsa-ard, S. and Seemawute, P. 2012. "Decaying Swirl Flow in Round Tubes with Short-length Ttwisted Tapes." *International Communications in Heat and Mass Transfer*. 39 : 649–656.

[25] Eiamsa-ard, S. Somkleang, P. Nuntadusit, C. and Thianpong, C. 2013. "Heat Transfer Enhancement in Tube by Inserting Uniform/non-uniform Twisted-tapes with Alternate Axes: Effect of Rotated-axis Length." *Applied Thermal Engineering*. 54 : 289–309.

[26] Garcia, A. Vicente, P.G. and Viedma, A. 2005. "Experimental Study of Heat Transfer Enhancement with Wire Coil Inserts in Laminar-transition-turbulent Regimes at Different Prandtl Numbers." *International Journal of Heat and Mass Transfer*. 48 : 4640–4651.

[27] Promvonge, P. 2008. "Thermal Performance in Circular Tube Fitted with Coiled Square Wires." *Energy Conversion and Management*. 49 : 980–987.

[28] Promvonge, P. 2008. "Thermal Enhancement in a Round Tube with Snail Entry and Coiled-wire Inserts." *International Communications in Heat and Mass Transfer*. 35 : 623–629.

[29] Promvonge, P. 2008. "Thermal Augmentation in Crcular Tube with Twisted Tape and Wire Coil Turbulators." *Energy Conversion and Management*. 49 : 2949–2955.

[30] Gunes, S. Ozceyhan, V. and Buyukalaca, O. 2010. "Heat Transfer Enhancement in a Tube with Equilateral Triangle Cross Sectioned Coiled Wire Inserts." *Experimental Thermal and Fluid Science*. 34 : 684–691.

[31] Gunes, S. Ozceyhan, V. and Buyukalaca, O. 2010. "The Experimental Investigation of Heat Transfer and Pressure Drop in a Tube with Coiled Wire Inserts Placed Separately from the Tube Wall." *Applied Thermal Engineering*. 30 : 1719–1725.

[32] Eiamsa-ard, .S Nivesrangsan, P. Chokphoemphun, S. and Promvonge, P. 2010. "Influence of Combined Non-uniform Wire Coil and Twisted Tape Inserts on Thermal Performance Characteristics." *International Communications in Heat and Mass Transfer*. 37 : 850–856.

[33] Nasr, M.R.J. Khalaj, A.H. and Mozaffari, S.H. 2010. "Modeling of Heat Transfer Enhancement by Wire Coil Inserts Using Artificial Neural Network Analysis." *Applied Thermal Engineering*. 30 : 143–151.

[34] Gunes, S. Manay, E. Senyigit, E. and Ozceyhan, V. 2011. "A Taguchi Approach for Optimization of Design Parameters in a Tube with Coiled Wire Inserts." *Applied Thermal Engineering*. 31 : 2568–2577.

[35] Garcia, A. Solano, J.P. Vicente, P.G. and Viedma, A. 2012. "The Influence of Artificial Roughness Shape on Heat Transfer Enhancement : Corrugated Tubes, Dimpled Tubes and Wire Coils." *Applied Thermal Engineering*. 35 : 196–201.

[36] Yakut, K. Sahin, B. and Canbazoglu, S. 2004. "Performance and Flow-induced Vibration Characteristics for Conical-ring Turbulators." *Applied Energy*. 79 : 65–76.

[37] Tandiroglu, A. 2006. "Effect of Flow Geometry Parameters on Transient Heat Transfer for Turbulent Flow in a Circular Tube with Baffle Inserts." *International Journal of Heat and Mass Transfer*. 49 : 1559–1569.

[38] Eiamsa-ard, S. and Promvonge, P. 2006. "Experimental Investigation of Heat Transfer and Friction Characteristics in a Crcular Tube Fitted with V-nozzle Turbulators." *International Communications in Heat and Mass Transfer*. 33 : 591–600.

[39] Promvonge, P. and Eiamsa-ard, S. 2007. "Heat Transfer and Turbulent Flow Friction in a Circular Tube Fitted with Conical-nozzle Turbulators." *International Communications in Heat and Mass Transfer*. 34 : 72–82.

[40] Promvonge, P. and Eiamsa-ard , S. 2007. "Heat Transfer Augmentation in a Circular Tube Using V-nozzle Turbulator Inserts and Snail Entry." *Experimental Thermal and Fluid Science*. 32 : 332–340.

[41] Promvonge, P. and Eiamsa-ard, S. 2007. "Heat Transfer in a Circular Tube Fitted with Free-spacing Snail Entry and Conical-nozzle Turbulators." *International Communications in Heat and Mass Transfer*. 34 : 838–848.

[42] Promvonge, P. 2008. "Heat Transfer Behaviors in Round Tube with Conical Ring Inserts." *Energy Conversion and Management*. 49 : 8–15.

[43] Ozceyhan, V. Gunes, S. Buyukalaca, O. and Altuntop, N. 2008. "Heat Transfer Enhancement in a Tube Using Circular Cross Sectional Rings Separated from Wall." *Applied Energy*. 85 : 988–1001.

[44] Eiamsa-ard, S. Pethkool, S. Thianpong, C. and Promvonge, P. 2008. "Turbulent Flow Heat Transfer and Pressure Loss in a Double Pipe Heat Exchanger with Louvered Strip Inserts." *International Communications in Heat and Mass Transfer*. 35 : 120–129.

[45] Eiamsa-ard, S. Rattanawong, S and Promvonge, P. 2009. "Turbulent Convection in Round Tube Equipped with Propeller Type Swirl Generators." *International Communications in Heat and Mass Transfer*. 36 : 357–364.

[46] Kongkaitpaiboon, V. Nanan, K. and Eiamsa-ard, S. 2010. "Experimental Investigation of Convective Heat Transfer and Pressure Loss in a Round Tube Fitted with Circular-ring

Turbulators." *International Communications in Heat and Mass Transfer*. 37 : 568–574.

[47] Kongkaitpaiboon, V. Nanan, K. and Eiamsa-ard, S. 2010. "Experimental Investigation of Heat Transfer and Turbulent Flow Friction in a Tube Ftted with Perforated Conical-rings." *International Communications in Heat and Mass Transfer*. 37 : 560–567.

[48] Eiamsa-ard, S. and Promvonge, P. 2010. "Thermal Characterization of Turbulent Tube Flows over Diamond-shaped Elements in Tandem." *International Journal of Thermal Sciences*. 49 : 1051–1062.

[49] Eiamsa-ard, S. and Promvonge, P. 2011. "Influence of Double-sided Delta-wing Tape Insert with Alternate-axes on Flow and Heat Transfer Characteristics in a Heat Exchanger Tube." *Chinese Journal of Chemical Engineering*. 19(3) : 410–423.

[50] Pethkool, S. Eiamsa-ard, S. Kwankaomeng, S. and Promvonge, P. 2011. "Turbulent Heat Transfer Enhancement in a Heat Exchanger Using Helically Corrugated Tube." *International Communications in Heat and Mass Transfer*. 38 : 340–347.

[51] Momin, A.M.E. Saini, J.S. and Solanki, S.C. 2002. "Heat Transfer and Friction in Solar Air Heater Duct with V-shaped Rib Roughness on Absorber Plate." *International Journal of Heat and Mass Transfer*. 45 : 3383–3396.

[52] Jaurker, A.R. Saini, J.S. and Gandhi, B.K. 2006. "Heat Transfer and Friction Characteristics of Rectangular Solar Air Heater Duct Using Rib-grooved Artificial Roughness." *Solar Energy*. 80 : 895–907.

[53] Karmare, S.V. and Tikekar, A.N. 2007. "Heat Transfer and Friction Factor Correlation for Artificially Roughened Duct with Metal Grit Ribs." *International Journal of Heat and Mass Transfer*. 50 : 4342–4351.

[54] Layek, A. Saini, J.S. and Solanki, S.C. 2007. "Heat Transfer and Friction Characteristics for Artificially Roughened Ducts with Compound Turbulators." *International Journal of Heat and Mass Transfer*. 50 : 4845–4854.

[55] Aharwal, K.R. Gandhi, B.K. and Saini, J.S. 2008. "Experimental Investigation on Heat Transfer Enhancement due to a Gap in an Inclined Continuous Rib Arrangement in a Rectangular Duct of Solar Air Heater." *Renewable Energy*. 33 : 585–596.

[56] Eiamsa-ard, S. and Promvonge, P. 2008. "Numerical Study on Heat Transfer of Turbulent Channel Flow over Periodic Grooves." *International Communications in Heat and Mass Transfer*. 35 : 844–852.

[57] Promvonge, P. and Thianpong, C. 2008. "Thermal Performance Assessment of Turbulent Channel Flows over Different Shaped Ribs." *International Communications in Heat and Mass Transfer*. 35 : 1327–1334.

[58] Varun, Saini, R.P. and Singal, S.K. 2008. "Investigation of Thermal Performance of Solar Air Heater having Roughness Elements as a Combination of Inclined and Transverse Ribs on the Absorber Plate." *Renewable Energy*. 33 : 1398–1405.

[59] Eiamsa-ard, S. and Promvonge, P. 2009. "Thermal Characteristics of Turbulent Rib-grooved Channel Flows." *International Communications in Heat and Mass Transfer*. 36 : 705–711.

[60] Thianpong, C. Chompookham, T. Skullong, S. and Promvonge, P. 2009. "Thermal Characterization of Turbulent Flow in a Channel with Isosceles Triangular Ribs." *International Communications in Heat and Mass Transfer*. 36 : 712–717.

[61] Bopche, S.B. and Tandale, M.S. 2009. "Experimental Investigations on Heat Transfer and Frictional Characteristics of a Turbulator Roughened Solar Air Heater Duct." *International Journal of Heat and Mass Transfer*. 52 : 2834–2848.

[62] Kumar, A. Bhagoria, J.L. and Sarviya, R.M. 2009. "Heat Transfer and Friction Correlations for Artificially Roughened Solar Air Heater Duct with Discrete W-shaped Ribs" *Energy Conversion and Management*. 50 : 2106–2117.

[63] Karwa, R. and Maheshwari B.K. 2009. "Heat Transfer and Friction in an Asymmetrically Heated Rectangular Duct with Half and Fully Perforated Baffles at Different Pitches." *International Communications in Heat and Mass Transfer*. 36 : 264–268.

[64] Sripattanapipat, S. and Promvonge, P. 2009. "Numerical Analysis of Laminar Heat Transfer in a Channel with Diamond-shaped Baffles." *International Communications in Heat and Mass Transfer*. 36 : 32–38.

[65] Promvonge, P. Sripattanapipat, S. and Kwankaomeng, A. 2010. "Laminar Periodic Flow and Heat Transfer in Square Channel with 45° Inline Baffles on Two Opposite Walls." *International Journal of Thermal Sciences*. 49 : 963–975.

[66] Promvonge, P. Chompookham, T. Kwankaomeng, S. and Thianpong, C. 2010. "Enhanced Heat Transfer in a Triangular Ribbed Channel with Longitudinal Vortex Generators." *Energy Conversion and Management*. 51 : 1242–1249.

[67] Promvonge, P. 2010. "Heat Transfer and Pressure Drop in a Channel with Multiple 60° V-baffles." *International Communications in Heat and Mass Transfer*. 37 : 835–840.

[68] Chompookham, T. Thianpong, C. Kwankaomeng, S. and Promvonge, P. 2010. "Heat Transfer Augmentation in a Wedge-ribbed Channel Using Winglet Vortex Generators." *International Communications in Heat and Mass Transfer*. 37 : 163–169.

[69] Hans, V.S. Saini, R.P. and Saini, J.S. 2010. "Heat Transfer and Friction Factor Correlations for a Solar Air Heater Duct Roughened Artificially with Multiple V-ribs." *Solar Energy*. 84 : 898–911.

[70] Promvonge, P. Changcharoen, W. Kwankaomeng, S. and Thianpong, C. 2011. "Numerical Heat Transfer Study of Turbulent Square-duct Flow Through Inline V-shaped Discrete Ribs." *International Communications in Heat and Mass Transfer*. 38 : 1392–1399.

[71] Lanjewar, A. Bhagoria, J.L. and Sarviya, R.M. 2011. "Experimental Study of Augmented Heat Transfer and Friction in Solar Air Heater with Different Orientations of W-Rib Roughness." *Experimental Thermal and Fluid Science*. 35 : 986–995.

[72] Tanda, G 2011. "Effect of Rib Spacing on Heat Transfer and Friction in a Rectangular Channel with 45° Angled Rib Turbulators on One/Two Walls." *International Journal of Heat and Mass Transfer*. 54 : 1081–1090.

[73] Peng, W. Jiang, P.X. Wang, Y.P. and Wei, B.Y. 2011. "Experimental and Numerical Investigation of Convection Heat Transfer in Channels with Different Types of Ribs." *Applied Thermal Engineering*. 31 : 2702–2708.

[74] Singh, S. Chander, S. Saini, J.S. 2011. "Heat Transfer and Friction Factor Correlations of Solar Air Heater Ducts Artificially Roughened with Discrete V-down Ribs." *Energy*. 36 : 5053–5064.

[75] Lanjewar, A. Bhagoria, J.L. and Sarviya, R.M. 2011. "Heat Transfer and Friction in Solar Air Heater Duct with W-shaped Rib Roughness on Absorber Plate" *Energy*. 36 : 4531–4541.

[76] Promvonge, P. Khanoknaiyakarn, C. Kwankaomeng, S. and Thianpong, C. 2011. "Thermal Behavior in Solar Air Heater Channel Fitted with Combined Rib and Delta-winglet." *International Communications in Heat and Mass Transfer*. 38 : 749–756.

[77] Singh, S. Chander, S. and Saini, J.S. 2012. "Investigations on Thermo-hydraulic Performance due to Flow-attack-angle in V-down Rib with Gap in a Rectangular Duct of Solar Air Heater." *Applied Energy*. 97 : 907–912.

[78] Promvonge, P. Jedsadaratanachai, W. Kwankaomeng, S. and Thianpong, C. 2012. "3D Simulation of Laminar Flow and Heat Transfer in V-baffled Square Channel." *International Communications in Heat and Mass Transfer*. 39 : 85–93.

[79] Eiamsa-ard, S. Koolnapadol, N. and Promvonge, P. 2012. "Heat Transfer Behavior in a Square Duct with Tandem Wire Coil Element Insert." *Chinese Journal of Chemical Engineering*. 20(5) : 863–869.

[80] Promvonge, P. Skullong, S. Kwankaomeng, S. and Thiangpong, C. 2012. "Heat Transfer in Square Duct Fitted Diagonally with Angle-finned Tape-Part 1: Experimental Study." *International Communications in Heat and Mass Transfer*. 39 : 617–624.

[81] Sriromreun, P. Thianpong, C. and Promvonge, P. 2012. "Experimental and Numerical Study on Heat Transfer Enhancement in a Channel with Z-shaped Baffles." *International Communications in Heat and Mass Transfer*. 39 : 945–952.

[82] Kumar, A. Saini, R.P. and Saini, J.S. 2012. "Experimental Investigation on Heat Transfer and Fluid Flow Characteristics of Air Flow in a Rectangular Duct with Multi V-shaped Rib with Gap Roughness on the Heated Plate." *Solar Energy*. 86 : 1733–1749.

[83] Sethi, M. Varun and Thakur. N.S. 2012. "Correlations for Solar Air Heater Duct with Dimpled Shape Roughness Elements on Absorber Plate." *Solar Energy*. 86 : 2852–2861.

[84] Shui, L. Gao, J. Shi, X. and Liu, J. 2013. "Effect of Duct Aspect Ratio on Heat Transfer and Friction in Steam-cooled Ducts with 60° Angled Rib Turbulators." *Experimental Thermal and Fluid Science*. 49 : 123–134.

[85] Tang, X.Y. and Zhu, D.S. 2013. "Flow Structure and Heat Transfer in a Narrow Rectangular Channel with Different Discrete Rib Arrays" *Chemical Engineering and Processing*. 69 : 1–14.

[86] Yongsiri, K. Eiamsa-ard, P. Wongcharee, K. and Eiamsa-ard, S. 2014. "Augmented Heat Transfer in a Turbulent Channel Flow with Inclined Detached-ribs." *Case Studies in Thermal Engineering*. 3 : 1–10.

[87] Singh, A.P. Varun and Siddhartha. 2014. "Heat Transfer and Friction Factor Correlations for Multiple Arc Shape Roughness Elements on the Absorber Plate Used in Solar Air Heaters." *Experimental Thermal and Fluid Science*. 54 : 117–126.

[88] Alam, T. Saini, R.P. and Saini, J.S. 2014. "Experimental Investigation on Heat Transfer Enhancement due to V-shaped Perforated Blocks in a Rectangular Duct of Solar Air Heater." *Energy Conversion and Management*. 81 : 374–383.

[89] Skullong, S. Kwankaomeng, S. Thianpong, C. and Promvonge, P. 2014. "Thermal Performance of Turbulent Flow in a Solar Air Heater Channel with Rib-groove Turbulators." *International Communications in Heat and Mass Transfer*. 50 : 34–43.

[90] Singh, A.P. Varun and Siddhartha. 2014. "Effect of Artificial Roughness on Heat Transfer and Friction Characteristics having Multiple Arc Shaped Roughness Element on the Absorber Plate." *Solar Energy*. 105 : 479–493.

[91] Cengel, Y.A. and Cimbala, J.M. © 2006. *Fluid Mechanics : Fundamentals and Applications*. 1st ed. New York : Mc Graw-Hill.

[92] White, F.M. 1999. *Fluid Mechanics*. 4th ed. New York : Mc Graw-Hill.

[93] Incropera, F.P. Dewitt, D.P. Bergman, T.L. and Lavine, A.S. © 2007. *Fundamentals of Heat and Mass Transfer*. 6th ed. Asia : John Wiley & Sons.

[94] Cengel, Y.A. © 2003. *Heat Transfer: A Practical Approach*. 2nd ed. New York : Mc Graw-Hill.

[95] Webb, R.L. and Kim, N.H. © 2005. *Principles of Enhanced Heat Transfer*. 2nd ed. New York : Taylor & Francis.

[96] Gupta, A. and Uniyal, M. 2012. "Review of Heat Transfer Augmentation Through Different Passive Intensifier Methods." *IOSR Journal of Mechanical and Civil Engineering*. 1(4) : 14-21.

[97] ASME. 1984. *Standard Measurement of fluid flow in pipes using orifice, nozzle and venture*. New York : United Engineering Center.

[98] ANSI/ASME. 1986. *Measurement uncertainty*. PTC 19. Part I. 1–1985. New York : ASME.

[99] Patankar, S.V., Liu, C.H., and Sparrow, E.M. 1998. "Fully developed flow and heat transfer in ducts having streamwise-periodic variations of cross-sectional area." *ASME Journal of Heat Transfe*r. 98 : 1109–1151.

APPENDIX

Publications of the author

Publications

International Journal

1. Chokphoemphun, S. Pimsarn, M. Thianpong, C. and Promvonge, P. "Heat Transfer Augmentation in a Circular Tube with Winglet Vortex Generators." has been accepted by *Chinese Journal of Chemical Engineering*. at 2014-04-18
2. Chokphoemphun, S. Pimsarn, M. Thianpong, C. and Promvonge, P. "Thermal Performance of Tubular Heat Exchanger with Multiple Twisted-tape Inserts." has been accepted by *Chinese Journal of Chemical Engineering*. at 2014-07-5
3. Chokphoemphun, S. Tongyote, P. Promvonge, P. Jedsadaratanachai, W and Chompookham, T. 2014. "Heat transfer augmentation in a round tube with 60° Winglet Pair inserts." *Advanced Materials Research*. 931-932 : 1188-1192.
4. Chokphoemphun, S. Hinthao, C. Eiamsa-ard, S. Promvonge, P. and Thianpong. C. 2014. "Thermal Performance in Circular Tube with Co/Counter-Twisted tapes." *Advanced Materials Research*. 931-932 : 1198-1202.

National Journal

1. Chokphoemphun, S. Chompookham, T. and Promvonge. P. 2014 "Heat Transfer Enhancement in a Tube Heat Exchanger with a V-Shape Winglet Turbulator." *KKU Research Journal*. 19(2) : 333-343

International Conference

1. Chokphoemphun, S. Skullong S. and Promvonge. P. 2011 "Thermal Characteristics in Square Channel with 45° U-Shaped Ribs." *1st International Symposium on Technology for Sustainability (ISTS)*. 26-29 January 2012, KMITL, Bangkok, Thailand
2. Chokphoemphun, S. Chompookham, T. Skullong, S.and Promvonge. P. 2012. "Heat Transfer in Solar Air Heater Channel with Inline 45° Wavy-Ribs." *International Conference on Green and Sustainable Innovation (ICGSI)*. 24-26 May 2012, Chiang Mai, Thailand.
3. Chokphoemphun, S. Skullong, S. Chompookham, T. Limkul T. and Promvonge. P. 2012. "Turbulent Heat Transfer in a Channel with Rib-Groove Turbulators." *The 3rd TSME International Conference on Mechanical Engineering (ICoME)*. October 2012, Chiang Rai, Thailand.
4. Chokphoemphun, S. Tongyote, P. Chompookham, T. Skullong, S. Promvonge P. and Jansangsuk. D. 2013. "Experimental study on Heat transfer augmentation in a round tube with V-shaped ribs." *International Conference on Interdisciplinary Research and Development in ASEAN Universities (ICIRD)*. 8-10 August 2013, Imperial Mae Ping Hotel, Chiang Mai, Thailand.

5. Hinthao, C. Chokphoemphun, S. Promvonge, P. Thianpong, C. Skullong, S. Chingtoaytong W. and Chompookham. T. 2013. “Heat transfer augmentation in square duct with 30° V–finned tape inserts.” *Joint Symposium on Mechanical-Industrial Engineering, and Robotics (MIER).* 14-17 November 2013, Centara Duangtawan Hotel, Chiang Mai, Thailand.

Certificate of Acceptance

To whom it may concern:

Article "*Thermal Performance of Tubular Heat Exchanger with Multiple Twisted-tape Inserts*" authored by Suriya Chokphoemphun, Monsak Pimsarn, Chinaruk Thianpong and Pongjet Promvonge (*Department of Mechanical Engineering, Faculty of Engineering, King Mongkut's Institute of Technology Ladkrabang, Bangkok 10520, Thailand*), has been accepted by *Chinese Journal of Chemical Engineering* (CJChE) at 2014-07-05 and will be published on CJChE in the next year.

Chinese Journal of Chemical Engineering

2014-07-14

Thermal Performance of Tubular Heat Exchanger with Multiple Twisted-tape Inserts*

Suriya Chokphoemphun, Monsak Pimsarn, Chinaruk Thianpong and Pongjet Promvonge**
Department of Mechanical Engineering, Faculty of Engineering,
King Mongkut's Institute of Technology Ladkrabang, Bangkok 10520, Thailand

Abstract The paper presents an experimental investigation on enhanced heat transfer and pressure loss characteristics by using single, double, triple, and quadruple twisted-tape inserts in a round tube having a uniform heat-fluxed wall. The investigation has been conducted in the heat exchanger tube inserted with various twisted-tape numbers for co- and counter-twist arrangements for the turbulent air flow, Reynolds number (*Re*) from 5300 to 24,000. The typical single twisted-tape inserts at two twist ratios, *y*/*w*=4 and 5, are used as the base case, while the other multiple twisted-tape inserts are at *y*/*w*=4 only. The experimental results of heat transfer and pressure drop in terms of Nusselt number (*Nu*) and friction factor (*f*), respectively, reveal that *Nu* increases with the increment of *Re* and of twisted-tape number. The values of *Nu* for the inserted tube is in a range of 1.15–2.12 times that for the plain tube while *f* is 1.9–4.1 times. The thermal enhancement factor of the inserted tube under similar pumping power is evaluated and found to be above unity except for the single and the double co-twisted tapes. The quadruple counter-twisted tape insert provides the maximum thermal performance.

Keywords thermal performance, twisted tape arrangement, turbulator, Nusselt number, friction factor

1 INTRODUCTION

Heat exchanger as equipment to facilitate the convective heat transfer of fluid inside tubes is frequently utilized in many industrial applications, such as chemical engineering process, heat recovery, air conditioning and refrigeration systems, power plant and radiators for automobiles. In general, heat transfer enhancement in heat exchangers can be divided into two methods. One is the active method requiring extra external power sources such as fluid vibration, injection and suction of the fluid, jet impingement and electrostatic fields. The other is the passive method that requires no other power source. The devices in this category are surface coating, rough surfaces, turbulent/swirl flow devices, extended surfaces etc.

Several investigations have been carried out to study the effect of turbulators (turbulent promoters) with different geometries on thermal behaviors in the heat exchanger, for example twisted-tapes [1,2], wire-coils [3,4], dimpled or grooved tubes [5,6], winglet/fins [7,8], combined turbulators [9,10]. However, twisted tapes as one of

Received 2014-xx-xx, accepted 2014-07-05.
* Supported by the Thailand Research Fund (TRF)
** To whom correspondence should be addressed. E-mail: kppongje@kmitl.ac.th

passive turbulators have been applied extensively to enhance convection heat transfer in heat exchanger systems due to the need for finding the way to reduce the size and cost of those systems. For decades, the heat transfer enhancement by twisted-tape insert has been widely investigated both experimentally and numerically. Eiamsa-ard *et al.* [1] reported the heat transfer and pressure loss behaviors in a double pipe heat exchanger fitted with regularly-spaced twisted-tape elements at several space ratios. Promvonge [9] conducted measurements using wire coil in conjunction with twisted tape for heat transfer augmentation and reported that this combination leads to a double increase in heat transfer over the use of wire coil/twisted tape alone.

Krishna *et al*. [11] experimentally investigated the heat transfer characteristics in a circular tube fitted with straight full twist insert with different spacer distances. Influence of the tube equipped with the short-length twisted tape on *Nu*, *f* and thermal performance characteristics for several tape-length ratios was examined by Eiamsa-ard *et al*. [12]. The effect of twisted tape consisting wire-nails and plain twisted-tapes with three different twist ratios fitted in a heat exchanger pipe using water as the test fluid on thermal characteristics was studied experimentally by Murugesan *et al*. [13]. Liao and Xin [14] reported the heat transfer behaviors in a tube with three-dimensional internal extended surfaces and twisted-tape inserts with various working fluids. Chiu and Jang [15] presented the experimental and numerical analyses on thermal–hydraulic characteristics of air flow inside a circular tube with 5 different tube inserts; longitudinal strip inserts both with/without holes and twisted-tape inserts with three different twist angles for inlet velocity ranging from 3 to 18 m/s. Eiamsa-ard and Promvonge [16] conducted an experimental study on turbulent flow and heat transfer characteristics in a tube equipped with two types of twisted tapes: (1) typical twisted tapes and (2) alternate clockwise and counterclockwise twisted-tapes. Nine different clockwise and counterclockwise twisted-tapes were tested in that work and included the tapes with three twist-ratios and three twist-angles. The experiments were performed for Reynolds number of 3000 to 27,000 using water as working fluid. The twin and triple twisted tapes used to generate twin and triple swirl flows in a circular tube were reported by Chang *et al*. [17].

Hong *et al*. [18] performed a numerical simulation of turbulent flow and heat transfer in converging-diverging tubes and converging-diverging tubes equipped with twin counter-swirling twisted tapes. In their work, effect of *Re*, pitch length, rib height, gap distance between twin twisted-tapes and tape number on *Nu*, *f* and thermal enhancement factor (η) were investigated. A simulation of multi-longitudinal vortices in a tube induced by multiple twisted-tapes inserts for the *Re* from 300 to 1800 were examined by Zhang *et al*. [19]. Effect of the combined conical-ring turbulator and twisted tape on heat transfer characteristics and thermal performance was also studied

by Promvonge and Eiamsa-ard [20]. Bharadwaj *et al*. [21] investigated the heat transfer and pressure drop in a spirally grooved tube with twisted-tape insert for laminar to fully turbulent regions. The effect of the direction of twist (left-twist and right-twist) on the thermo-hydraulic characteristics was also reported. Date and Gaitonde [22] developed the correlations for predicting the heat transfer coefficient and friction loss of laminar flow in a tube fitted with regularly spaced twisted-tape elements. Rahimi *et al*. [23] examined the heat transfer and thermal hydraulic performance in a round tube fitted with classic and modified twisted-tape inserts. They found that the jagged twisted tape provides more heat transfer enhancement than other tapes. Eiamsa-ard *et al*. [24] numerically studied the convective heat transfer in a circular tube fitted with loose-fit twisted tapes. Liu *et al*. [25] conducted a numerical investigation on the effect of short-width twisted-tapes inserted in a circular tube on heat transfer behaviors in laminar and turbulent flows.

In the literature review above, many investigations are almost focused on the use of single, double and triple twisted tapes with similar tape-twist direction, apart from the modified twisted-tape while the effect of the tape number, co- and counter-twist arrangements has rarely been reported. Therefore, the utilization of double, triple and quadruple twisted-tapes in various forms of co- and counter-twist arrangements is offered as an enhancement device in the present work. The experiments are performed using the left- and right-twisted tapes arranged in different forms of counter-twisted and co-twisted tape pairs with the *Re* range in turbulent region, where air is used as the test fluid. The effect of the twisted-tape number and the combined counter- and co-swirls on the heat transfer rate, *f* and thermal performance characteristics in a round tube is determined in the current work.

2 EXPERIMENTAL SETUP

A detail of the experimental apparatus used is displayed schematically in Fig. 1. In the apparatus setting above, inlet air at 25 ºC from a 1.5 kW blower was directed through an orifice flow meter and passed in the heat transfer test section. The airflow rate was measured by the orifice meter, built according to ASME standard [26] and calibrated by using a hot-wire anemometer to measure flow velocities across the tube section. Manometric fluid was used in an inclined-manometer with specific gravity (SG) of 0.826 to ensure reasonably accurate measurement of pressure drop across the orifice. The volumetric airflow rate from the blower was adjusted by varying the motor speed of the blower through an inverter. The inner (D) and outer diameters of the copper test tube was, respectively, 50.8 and 54.8 mm, and the tube was 3000 mm long, including the test section of L=1000 mm located at the exit. The test tube was heated by continually winding flexible electrical wire on the outer tube wall. The electrical

output power was controlled by a Variac transformer to obtain a uniform heat-flux along the entire length of the test section. The outer surface of test tube was well insulated to minimize heat loss to the surrounding. The inlet and outlet air temperatures in the test tube were measured by resistance temperature detectors thermocouples (RTD-Pt100) with ±0.1 ºC accuracy are positioned around 50 mm upstream and downstream of the test tube while the surface temperatures (T_w) were measured by 12 K-type thermocouples located equally on both top and side walls along the test section. All 24 K-type thermocouples were embedded in holes drilled from the outer surface and centered in the tube walls with the respective junctions positioned within 1 mm of the inside wall, and axial separation of the thermocouples was 90 mm apart and calibrated within ±0.2 ºC deviation by thermostat before being used. All of the temperatures getting from the system were consistently recorded using a data logger. The pressure drop across the test section for calculation of friction factor was measured at an isothermal condition by a digital manometer with accuracy ±0.5%. Reynolds numbers for air flowing through the test section were controlled in the range of 5300 to 24,000.

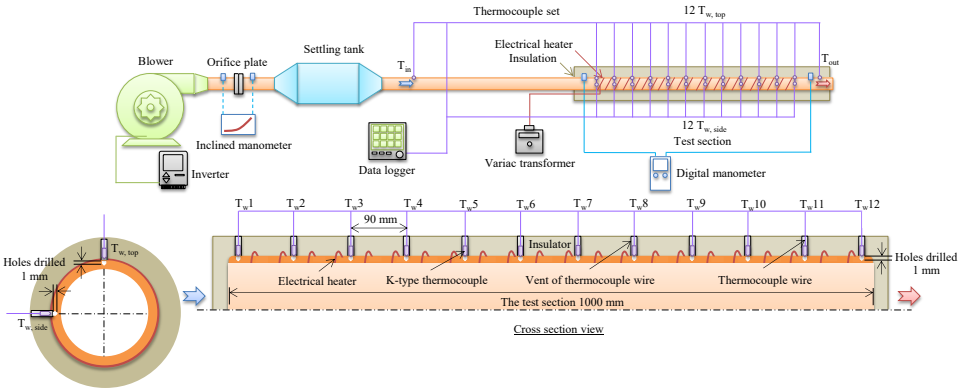

Figure 1 Schematic diagram of experimental apparatus.

Figure 2 shows the photographs of the test tube inserted with various number and arrangement of twisted tapes. In the figure, details on twisted-tape insertions indicating the number of twisted tapes (N) and the arrangement and the designation of each case were provided. All twisted-tapes were inserted in the test section with slightly tight fit and multiple twisted-tapes were attached together by superglue before insertion. The twisted-tapes made of aluminum sheet were 1200 mm long and 0.8 mm thick. The typical single twisted-tape had a width (w) of 42 mm with two different twist lengths (y): 168 and 210 mm (twist ratio, y/w=4 and 5) while the rest were 21 mm wide with 84 mm twist-length (y/w=4). All tapes were twisted in two different directions: left-twist (L_T) and right-twist (R_T), and were arranged in 8 different configurations (2T1, 2T2, 3T1, 3T2, 4T1, 4T2, 4T3 and 4T4) as can be seen in Fig. 2.

The uncertainty calculation based on ref. [27] reveals that the maximum uncertainties of non-dimensional parameters were ±5% for Reynolds number, ±7.6% for Nusselt number and ±9.5% for friction factor. The uncertainty in the axial velocity measurement was estimated to be less than ±5%, and pressure has a corresponding estimated uncertainty of ±5%, whereas the uncertainty in temperature measurement at the tube wall was about ±0.5% (±0.35 ºC).

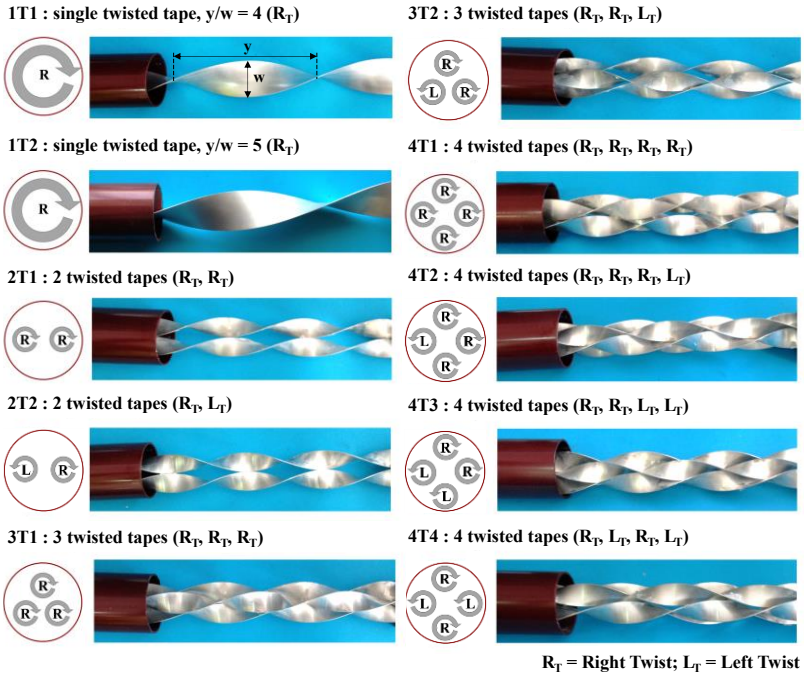

Figure 2 Test tube inserted with various numbers of twisted tapes.

3 DATA REDUCTION

The aim of the current work is to determine the heat transfer rate in a circular tube fitted with multiple twisted-tapes. The independent parameters are Reynolds number (*Re*), the number of twisted tapes (*N*) and twisted-tape arrangements. The Reynolds number is given by

$$Re = UD/\nu \tag{1}$$

The friction factor (*f*) computed by pressure drop across the test tube length (*L*) is written as

$$f = \frac{2}{(L/D)}\frac{\Delta P}{\rho U^2} \tag{2}$$

in which *U* is mean air velocity in the test tube.

In the experiment, air flowed through the test tube under a uniform heat-flux condition. The steady state of the heat transfer rate means that the heat transferred across the test section wall Q_{conv} is equal to the heat absorbed by flowing air Q_a:

$$Q_a = Q_{conv} \tag{3}$$

with

$$Q_{\mathrm{a}} = \dot{m} C_{\mathrm{p,a}} \left(T_{\mathrm{o}} - T_{\mathrm{i}} \right) \tag{4}$$

and the convection heat transfer from test section can be written by

$$Q_{\mathrm{c\,o\,n\,\overline{v}}} hA\left(\widetilde{T}_{\mathrm{w}} - T_{\mathrm{b}} \right) \tag{5}$$

in which

$$T_{\mathrm{b}} = (T_{\mathrm{o}} + T_{\mathrm{i}}) / 2 \tag{6}$$

and

$$\widetilde{T}_{\mathrm{w}} = \sum T_{\mathrm{w}} / 24 \tag{7}$$

where T_w is local wall temperature and evaluated at the outer wall surface of test tube. The average wall temperature was calculated from 24 points of surface temperatures lined equally between the inlet and the exit of test tube. The average heat transfer coefficient (h) and mean Nusselt number (Nu) are estimated as follows:

$$h = \dot{m} C_{\mathrm{p,a}} \left(T_{\mathrm{o}} - T_{\mathrm{i}} \right) / A\left(\widetilde{T}_{\mathrm{w}} - T_{\mathrm{b}} \right) \tag{8}$$

$$Nu = \frac{hD}{k} \tag{9}$$

All of thermo-physical properties of air are determined at the overall bulk air temperature (T_b) from Eq. (6).

To assess the practical use, thermal performance of the enhanced tube is evaluated relatively to the smooth tube at an identical pumping power in the form of thermal enhancement factor (η) which can be expressed by

$$\eta = \left. \frac{h_{\mathrm{s}}}{h_{\mathrm{p}}} \right|_{\mathrm{pp}} = \left. \frac{Nu_{\mathrm{s}}}{Nu_{\mathrm{p}}} \right|_{\mathrm{pp}} = \left(\frac{Nu_{\mathrm{s}}}{Nu_{\mathrm{p}}} \right) \left(\frac{f_{\mathrm{s}}}{f_{\mathrm{p}}} \right)^{-1/3} \tag{10}$$

where h_p and h_s are heat transfer coefficients for plain tube and inserted tube, respectively.

4 RESULTS AND DISCUSSION

4.1 Validation of plain tube

In the present work, the heat transfer and pressure drop of plain tube in terms of Nussult number (Nu) and friction factor (f) are, respectively, verified with the Dittus-Boelter and Blasius correlations [28] respectively for, Nu and f as given in Eqs. (11) and (12):

Dittus - Boelter correlation:

$$Nu = 0.023\, Re^{0.8} Pr^{0.4} \tag{11}$$

Blasius correlation:

$$f = 0.316\ Re^{-0.25} \tag{12}$$

Figures 3a and 3b show that the measured data are in good agreement with the

corresponding correlations. The average deviation of the measured is about 5% for *Nu* and 6% for *f*.

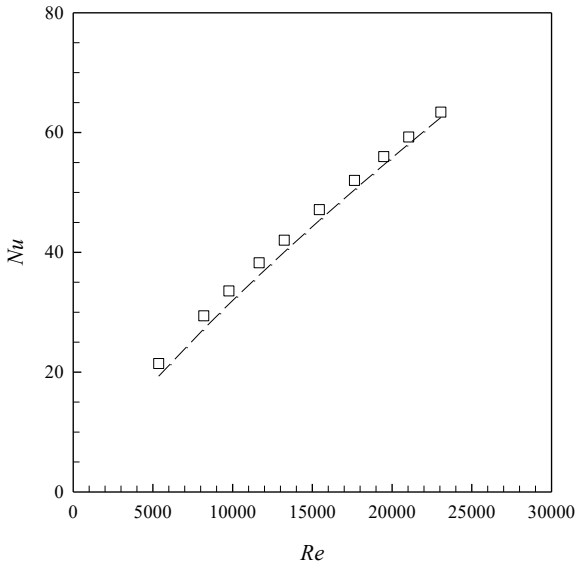

(a)

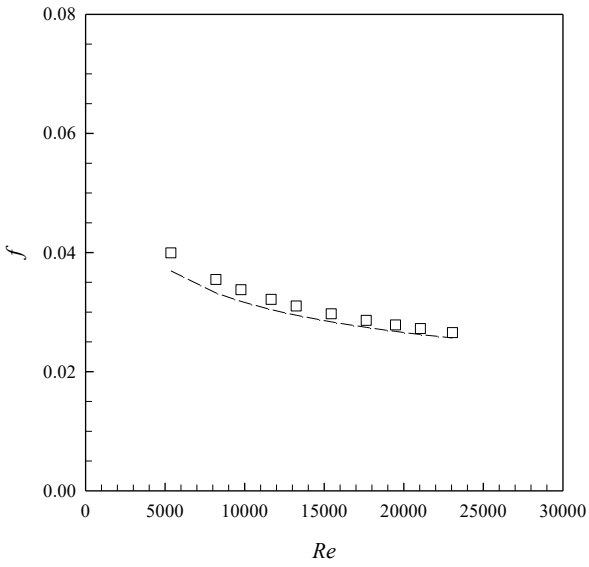

(b)

Figure 3 Verification of (a) *Nu* and (b) *f* for plain tube.

---- correlations; □ exp. data

4.2 Effect of twisted-tape arrangements

The variation of *Nu* and Nusselt number ratio, Nu/Nu_0, with *Re* for the tube with multiple twisted-tape inserts is depicted in Figs. 4a and 4b, respectively. It is visible that all the twisted-tapes yield considerable heat transfer with a similar trend in comparison with plain tube. For single twisted-tape, the heat transfer rate increases with the decreasing twist ratio as already mentioned in the literature. Due to the

increase of swirl intensity imparted to the flow at tube wall, heat transfer rate of the inserted tube is found to be considerably higher than that of plain tube with no insert. This can be attributed to stronger swirl enhancing turbulence intensity, leading to higher convection heat transfer than axial flow in plain tube. Thus, the higher vortex flow, the greater Nusselt number becomes. In scrutiny of Fig. 4, *Nu* obtained from the combined R_T and L_T tapes (called counter-twisted tapes) seems to be higher than that from the R_T-R_T combination, or the L_T-L_T ones (called co-twisted tapes). For double twisted-tapes, the counter-twisted tapes (2T2) perform better than the co-twisted tapes (2T1) and also the triple counter-twisted tapes (3T2) yield higher *Nu* than the triple co-twisted ones (3T1). In quadruple twisted tapes, it is noted that the four counter-swirl pairs, 4T4 and four co-swirl pairs, 4T1 provide, respectively, the highest and lowest heat transfer rate. 4T3 consisting of two counter-swirl pairs performs better than the 4T2 comprising the counter-swirl and co-swirl pairs. In addition, *Nu* obtained from wire-coil insert taken from ref. [3] is included in Fig. 4 for comparison. The wire coil insert provides higher heat transfer rate than the twisted-tape insert at all cases.

The Nusselt number ratio (Nu/Nu_0) defined as a ratio of augmented Nusselt number to that of plain tube shows a decreasing trend with the rise of *Re* as can be seen in Fig. 4b. Under the present measured data, the Nu/Nu_0 values for 4T4, 4T3, 4T2, 4T1, 3T2, 3T1, 2T2, 2T1 and 1T1 tapes are in the range of 1.15 to 2.12 depending on *Re*, while the wire coil yields the Nu/Nu_0 value ranging from 2.08-2.28, higher than the twisted tapes (Fig. 4b).

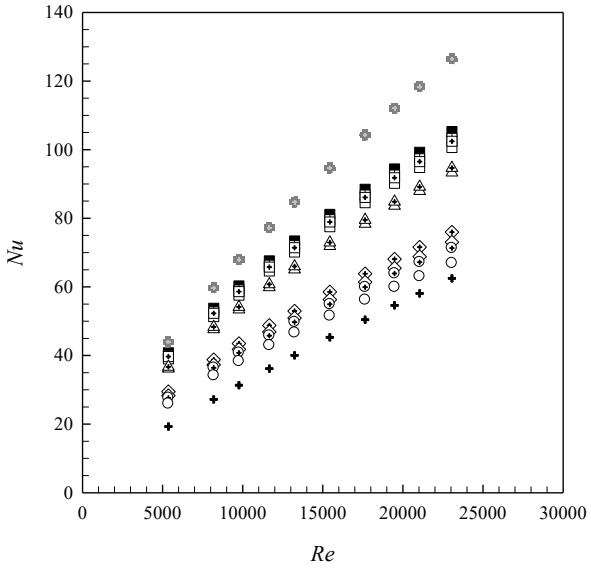

(a)

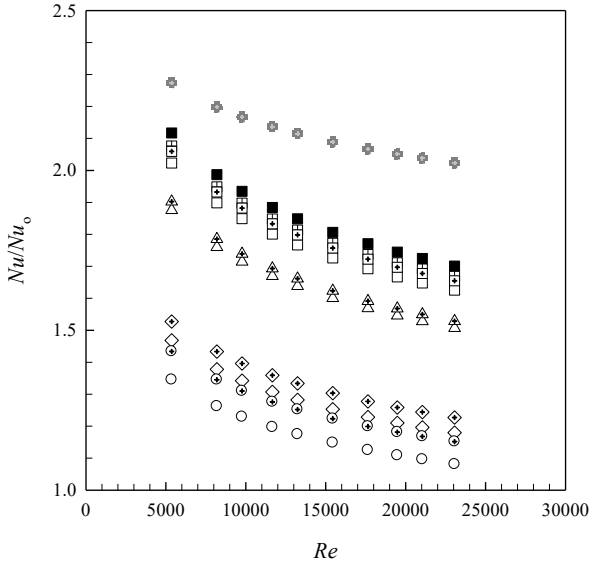

(b)

Figure 4 Variation of (a) *Nu* and (b) *Nu*/*Nu*$_0$ with *Re* for various twisted tapes.

■4T4; ⊞4T3; ⊡4T2; □4T1; ◬3T2; △3T1; ◈2T2; ◇2T1; ⊙1T1, *y*/*w*=4; ○1T2, y/w=5; ✤wire coil [3]; ✚plain tube

The influence of different twisted-tape number and arrangements on f and f/f_0 characteristics against Re is depicted in Figs. 5a and 5b, respectively. It is observed that the application of twisted tapes gives rise to considerably higher f than that of plain tube with no insert. The higher friction loss mainly comes from the increased surface area and higher swirl intensity. The f values for double and triple counter-twisted tapes (2T2 and 3T2) are seen to be higher than those for double and triple co-twisted ones (2T1 and 3T1) and are around 5% and 50% above that for single twisted-tape. For quadruple twisted-tapes, the highest and lowest f values are, respectively, found for four counter-twisted (4T4) and four co-twisted (4T1) tapes while the f of two counter-twisted tapes (4T3) is slightly larger than that of two co-twisted ones (4T2). This indicates a significant effect of multiple twisted-tape arrangements on thermal performance. Also, the f value of the wire coil taken from ref. [3] is substantially higher than that of twisted-tapes. In Fig. 5b, the f/f_0 for twisted tapes is in the range of 1.94 to 4.06 while that for wire coil is ranging from 7.38 to 7.85.

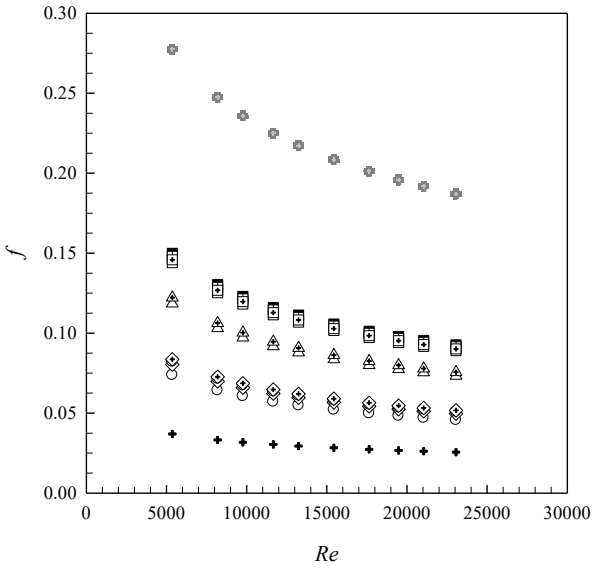

(a)

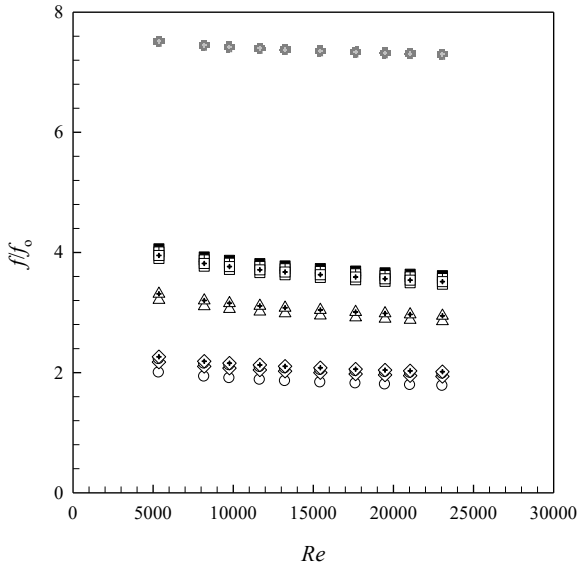

(b)

Figure 5 Variation of (a) *f* and (b) *f*/*f*$_0$ with *Re* for various twisted tapes.

■4T4; ⊞4T3; ⊡4T2; □4T1; ▲3T2; △3T1; ◈2T2; ⊙1T1, *y*/*w*=4; ◇2T1; ○1T2, *y*/*w*=5; ❁wire coil [3]; ✚plain tube

4.3 Effect of twisted-tape number

Figures 6a and 6b display an effect of the number of counter-twisted tapes on *Nu*/*Nu*$_0$ and *f*/*f*$_0$, respectively. It is visible that *Nu*/*Nu*$_0$ increases with the increment of *N*, especially for *N* > 2, but with the reduction of *Re*. The mean *Nu*/*Nu*$_0$ and *f*/*f*$_0$ increases for *N*=4 (4T4), 3 (3T2), 2 (2T2) and 1 (1T1) are, respectively, about 87%, 68%, 35% and 27%; and 278%, 208%, 111% and 107% above the plain tube. This shows the advantage of multiple counter-twisted tapes over the plain tube.

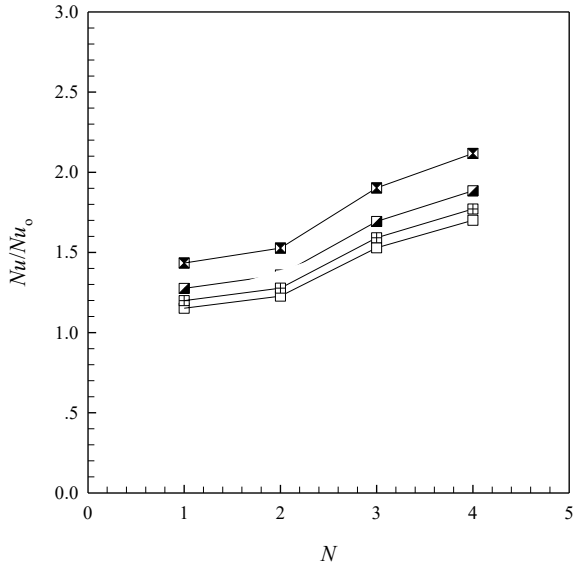

(a)

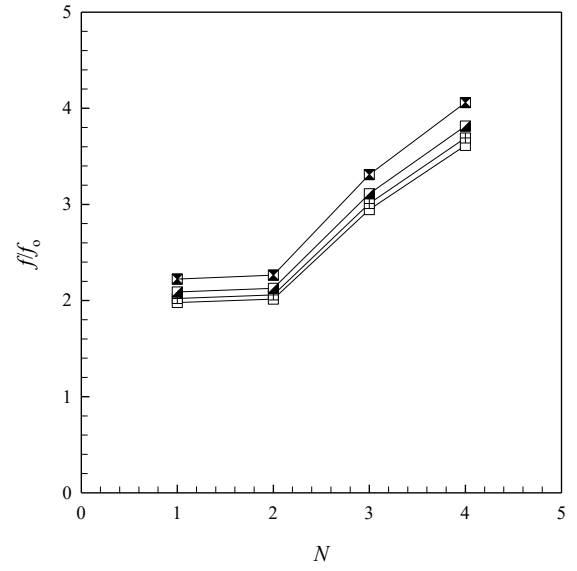

(b)

Figure 6 Effect of N on (a) Nu/Nu_0 and (b) f/f_0.

Re = 5363; Re = 11,660; Re = 17,638; Re = 23,057

The axial wall temperature distribution along the tube at each thermocouple location for a four counter-twisted tape insert (4T4) is depicted in Fig. 7. The wall temperature variation is found to gradually increase downstream of the inlet until $x/D \approx 5 - 6$ and then increased slightly to the exit. However, in the region near the exit, the wall temperature drops slightly from location $x/D \approx 18$ to the outlet, similar trend as found in ref. [2] if it is presented in the form of local Nu_x. The wall temperature and the temperature difference between the inlet and outlet of air at low Re are seen to be higher than those at high Re.

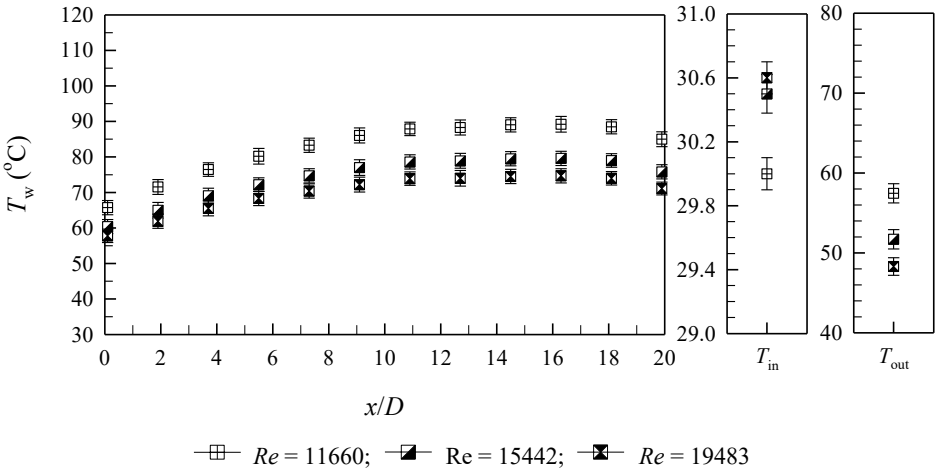

Figure 7 Axial wall temperature distribution along test tube.

In addition, the empirical correlations developed by relating the *Re* and *N* together are compared with experimental data within ±3.5% and ±4.8% for Nusselt number and friction factor, respectively. Correlations for multiple counter-twisted tapes are

$$Nu = 0.092\ Re^{0.65} Pr^{0.4} N^{0.46} \tag{13}$$

$$f = 0.791\ Re^{-0.33} N^{0.873} \tag{14}$$

4.4 Thermal performance assessment

Figures 8 and 9 present the variation of thermal enhancement factor (η) with *Re* and the number of counter–twisted tapes (*N*), respectively. It can be seen in the plots that the η values are generally above unity for all the inserted tubes, except for the single twisted (1T1) and double co-twisted tapes (2T1) at higher *Re* values. η shows downtrend as *Re* increases for all tapes tested. Counter-twisted tapes provide higher η than co-twisted tapes, and the maximum η of about 1.33 is found for quadruple counter-twisted tapes (4T4) at lower *Re*. It is noted that η tends to increase with the increment of *N*. To obtain higher η, the use of counter-twisted tapes at $N>2$ is recommended. The application of counter-twisted tapes leads to the increase in mean η of about 20%, 15% and 5% for $N = 4$ (4T4), 3 (3T2) and 2 (2T2), respectively. In comparison with wire-coil inserts [3], the triple and quadruple counter-twisted tapes perform much higher than the wire-coil. However, η of wire coil is better than using single twisted-tape alone as seen in Fig. 8. The detail on experimental results of multiple counter-twisted tapes is presented in Table 1

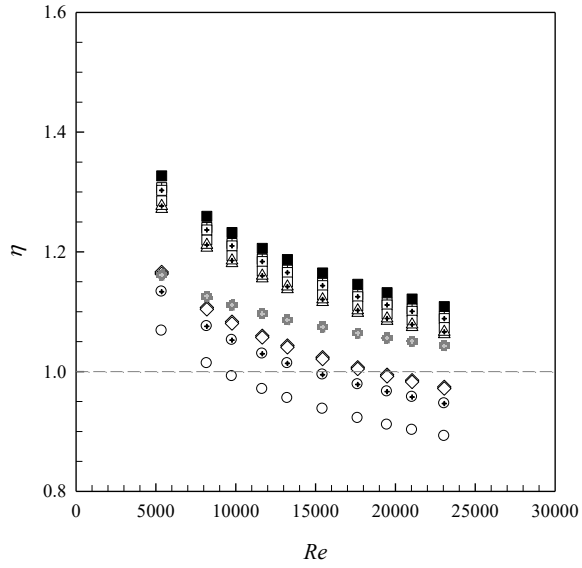

Figure 8 Variation of η with *Re*.

■ 4T4; ⊞ 4T3; ⊡ 4T2; □ 4T1; ⧋ 3T2; △ 3T1; ⧁ 2T2; ◇ 2T1; ⊙ 1T1, *y/w*=4; ○ 1T2, *y/w*=5; ✿ wire coil [3]

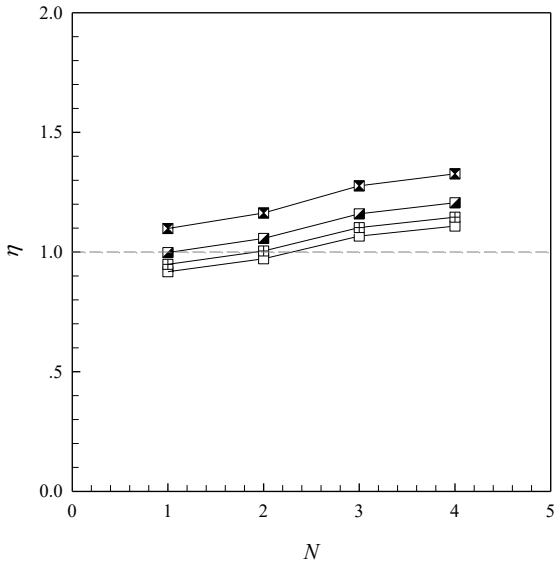

Figure 9 Variation of η with *N*.

Re = 5363; *Re* = 11,660; *Re* = 17,638; *Re* = 23,057

Table 1 Experimental results of multiple counter-twisted tapes.

Case	Results		
	Nu/Nu_0	f/f_0	η
4T4	1.70-2.12	3.61-4.06	1.11-1.33
4T3	1.67-2.08	3.57-4.01	1.09-1.31
4T2	1.65-2.06	3.51-3.95	1.09-1.30
4T1	1.63-2.02	3.47-3.90	1.07-1.29
3T2	1.53-1.90	2.95-3.31	1.07-1.28

3T1	1.51-1.88	2.86-3.21	1.06-1.27
2T2	1.23-1.53	2.01-2.26	0.97-1.16
2T1	1.18-1.47	1.94-2.18	0.95-1.13
1T1	1.15-1.43	1.98-2.22	0.92-1.10

5 CONCLUSIONS

An experimental study has been conducted to examine heat transfer and flow friction characteristics in a circular tube inserted with single, double, triple and quadruple twisted tapes comprised of either co- or counter-twisted tapes for the turbulent regime (*Re* from about 5,300 to 24,000) under a uniform wall heat-flux. For using multiple twisted-tapes, *Nu* is in the range of 1.15-2.12 times while *f* is 1.94-4.06 times that of the plain tube. Both *Nu* and *f* are seen to increase with the increment of *N* and with counter-twisted tape arrangements. η tends to decrease with the increase in *Re* but with decreasing *N*. The highest η is found to be about 1.33 for using quadruple counter-twisted tapes (4T4).

ACKNOWLEDGEMENT

The authors would like to gratefully acknowledge the Thailand Research Fund (TRF) for the financial support of this research.

NOMENCLATURE

A	heat transfer surface area, m^2
C_p	specific heat of fluid, $J \cdot kg^{-1} \cdot K^{-1}$
D	inner diameter of test tube, m
f	friction factor
h	heat transfer coefficient, $W \cdot m^{-2} \cdot K^{-1}$
k	thermal conductivity of fluid, $W \cdot m^{-1} \cdot K^{-1}$
L	length of the test section, m
$\dot{m}$	mass flow rate, $kg \cdot s^{-1}$
N	number of twisted tapes
Nu	Nusselt number ($=hD/k$)
ΔP	pressure drop, Pa
Pr	Prandtl number ($=C_p\mu/k$)
Q	heat transfer rate, W
Re	Reynolds number ($=UD/\nu$)
$\tilde{T}$	mean temperature, K
T	temperature, K
U	mean air velocity, $m \cdot s^{-1}$
w	tape width, m
y	pitch length of twisted tape (180° rotation), m

Greek symbols

η	thermal enhancement factor $(=(Nu/Nu_0)/(f/f_0)^{1/3})$
ρ	fluid density, $kg \cdot m^{-3}$
v	kinematic viscosity, $m^2 \cdot s^{-1}$

Subscripts

a	air
b	bulk
conv	convection
i	inlet
o	outlet
pp	pumping power
p	plain tube
s	swirl flow generator
w	wall

REFERENCES

1 Eiamsa-ard, S., Thianpong, C., Promvonge, P., "Experimental investigation of heat transfer and flow friction in a circular tube fitted with regularly spaced twisted tape elements", *Int. Commun. Heat Mass Transfer*, **33** (10), 1225–1233 (2006).

2 Chang, S.W., Yang, T.L., Liou, J.S., "Heat transfer and pressure drop in tube with broken twisted tape insert", *Exp. Therm. Fluid Sci*, **32** (2), 489–501 (2007).

3 Promvonge, P., "Thermal performance in circular tube fitted with coiled square wires", *Energy Convers. Manage.*, **49** (5), 980–987 (2008).

4 Gunes, S., Ozceyhan, V., Buyukalaca, O., "Heat transfer enhancement in a tube with equilateral triangle cross sectioned coiled wire inserts", *Exp. Therm. Fluid Sci.*, **34** (6), 684–691 (2010).

5 Wang, Y., He, Y.L., Lei, Y.G., Zhang, J., "Heat transfer and hydrodynamics analysis of a novel dimpled tube", *Exp. Therm. Fluid Sci.*, **34** (8), 1273–1281 (2010).

6 Bilen, K., Cetin, M., Gul, H., Balta, T., "The investigation of groove geometry effect on heat transfer for internally grooved tubes", *Appl. Therm. Eng.*, **29** (4), 753–761 (2009).

7 Chokphoemphun, S., Pimsarn, M., Thianpong, C., Promvonge P., "Heat transfer augmentation in a circular tube with winglet vortex generators", accepted by *Chin. J. Chem. Eng.*, (2014) No.2013-0568.

8 Suwannapan, S., Thianpong, C., Promvonge P., "Enhanced heat transfer in a heat exchanger square-duct with discrete V-finned tape inserts", accepted by *Chin. J. Chem. Eng.*, (2014) No.2013-0556.

9 Promvonge, P., "Thermal augmentation in circular tube with twisted tape and wire coil turbulators", *Energy Convers. Manage*., **49** (11), 2949–2955 (2008).

10 Eiamsa-ard, S., Nivesrangsan, P., Chokphoemphun, S., Promvonge, P., "Influence of combined non-uniform wire coil and twisted tape inserts on thermal performance characteristics", *Int. Commun. Heat Mass Transfer*, **37** (7), 850–856 (2010).

11 Krishna, S.R., Pathipaka, G., Sivashanmugam, P., "Heat transfer and pressure drop studies in a circular tube fitted with straight full twist", *Exp. Therm. Fluid Sci.*, **33** (3), 431–438 (2009).

12 Eiamsa-ard, S., Thianpong, C., Eiamsa-ard, P., Promvonge, P., "Convective heat transfer in a

circular tube with short-length twisted tape insert", *Int. Commun. Heat Mass Transfer*, **36** (3), 365–371 (2009).

13 Murugesan, P., Mayilsamy, K., Suresh, S., "Heat transfer and friction factor studies in a circular tube fitted with twisted tape consisting of wire-nails", *Chin. J. Chem. Eng.*, **18** (6), 1038–1042 (2010).

14 Liao, Q., Xin, M.D., "Augmentation of convective heat transfer inside tubes with three-dimensional internal extended surfaces and twisted-tape inserts", *Chem. Eng. J.*, **78** (2–3), 95–105 (2000).

15 Chiu, Y.W., Jang, J.Y., "3D numerical and experimental analysis for thermal–hydraulic characteristics of air flow inside a circular tube with different tube inserts", *Appl. Therm. Eng.*, **29** (2–3), 250–258 (2009).

16 Eiamsa-ard, S., Promvonge, P., "Performance assessment in a heat exchanger tube with alternate clockwise and counter-clockwise twisted-tape inserts", *Int. J. Heat Mass Transfer*, **53** (7–8), 1364–1372 (2010).

17 Chang, S.W., Yu, K.W., Lu, M.H., "Heat transfer in tubes fitted with single, twin and triple twisted tapes", *Exp. Heat Tran.,* **18,** 279–294 (2005).

18 Hong, Y.X., Deng, X.H., Zhang, L.S., "3D numerical study on compound heat transfer enhancement of converging-diverging tubes equipped with twin twisted tapes", *Chin. J. Chem. Eng*., **20** (3), 589–601 (2012).

19 Zhang, X.Y., Liu, Z.C., Liu, W., "Numerical studies on heat transfer and flow characteristics for laminar flow in a tube with multiple regularly spaced twisted tapes", *Int. J. Therm. Sci*., **58**, 157–167 (2012).

20 Promvonge, P., Eiamsa-ard, S., "Heat transfer behaviors in a tube with combined conical-ring and twisted-tape insert". *Int. Commun. Heat Mass Transfer*, **34** (7), 849–859 (2007).

21 Bharadwaj, P., Khondge, A.D., Date, A.W., "Heat transfer and pressure drop in a spirally grooved tube with twisted tape insert", *Int. J. Heat Mass Transfer*, **52** (7–8), 1938–1944 (2009).

22 Date, A.W., Gaitonde, U.N., "Development of correlations for predicting characteristics of laminar flow in a tube fitted with regularly spaced twisted-tape elements", *Exp. Therm. Fluid Sci.*, 3 (4), 373–382 (1990).

23 Rahimi, M., Shabanian, S.R., Alsairafi, A.A., "Experimental and CFD studies on heat transfer and friction factor characteristics of a tube equipped with modified twisted tape inserts", *Chem. Eng. and Process.*, **48** (3), 762–770 (2009).

24 Eiamsa-ard, S, Wongcharee, K., Sripattanapipat, S., "3-D Numerical simulation of swirling flow and convective heat transfer in a circular tube induced by means of loose-fit twisted tapes", *Int. Commun. Heat Mass Transfer*, **36** (9), 947-955 (2009).

25 Liu, W., Yang, K., Liu, Z.C., Ming, T.Z., Fan, A.W., Yang, C., "Mechanism of heat transfer enhancement in the core flow of a tube and its numerical simulation", *Open Transport Phenom. J.*, **2,** 9–15 (2010).

26 ASME, "Standard Measurement of fluid flow in pipes using orifice, nozzle and venture", ASME MFC–3M-1984, United Engineering Center 345 East 47th Street, New York, pp.1–56 (1984).

27 ANSI/ASME, "Measurement uncertainty", PTC 19, Part I, pp.1–1985 (1986).

28 Incropera, F.P., Witt, P.D., Bergman, T.L., Lavine, A.S., *Fundamentals of Heat and Mass Transfer*, John-Wiley & Sons, (2006).

APPENDIX

In order to evaluate the reliability of the experimental facility, the uncertainties of experimental data were determined. The uncertainties of the friction factor and Nusselt number data can be expressed as follows

Friction factor:

$$\frac{\Delta f}{f}=\frac{1}{f}\left[\left\{\frac{\partial f}{\partial(\Delta P)}\Delta(\Delta P)\right\}^2+\left\{\frac{\partial f}{\partial L}\Delta L\right\}^2+\left\{\frac{\partial f}{\partial D}\Delta D\right\}^2+\left\{\frac{\partial f}{\partial(\mathrm{Re})}\Delta \mathrm{Re}\right\}^2\right]^{0.5}$$
$$=\left[\left\{\frac{\Delta(\Delta P)}{\Delta P}\right\}^2+\left\{\frac{\Delta L}{L}\right\}^2+\left\{\frac{3\Delta D}{D}\right\}^2+\left\{\frac{2\Delta \mathrm{Re}}{\mathrm{Re}}\right\}^2\right]^{0.5} \quad (15)$$

where $\Delta(\Delta P)/\Delta P=\Delta h/h$ and $\Delta \mathrm{Re}/\mathrm{Re}=[(\Delta \dot{m}/\dot{m})^2+(\Delta D/D)^2]^{0.5}$

Nusselt number:

$$\frac{\Delta Nu}{Nu}=\frac{1}{Nu}\left[\left\{\frac{\partial}{\partial h}(Nu)\Delta h\right\}^2+\left\{\frac{\partial}{\partial D}(Nu)\Delta D\right\}^2+\left\{\frac{\partial}{\partial k}(Nu)\Delta k\right\}^2\right]^{0.5}$$
$$=\left\{\left(\frac{\Delta h}{h}\right)^2+\left(\frac{\Delta D}{D}\right)^2\right\}^{0.5} \quad (16)$$

where $h=q''/(T_w-T_b)$

$$\frac{\Delta h}{h}=\frac{1}{h}\left[\left\{\frac{\partial h}{\partial q''}\Delta q''\right\}^2+\left\{\frac{\partial h}{\partial T_w}\Delta T_w\right\}^2+\left\{\frac{\partial h}{\partial T_b}\Delta T_b\right\}^2\right]^{0.5}$$
$$=\left[\left\{\frac{\Delta q''}{q''}\right\}^2+\left\{\frac{\Delta T_w}{T_w-T_b}\right\}^2+\left\{\frac{\Delta T_b}{T_w-T_b}\right\}^2\right]^{0.5} \quad (17)$$

where $q''=(1/\pi DL_h)[\dot{m}C_p(T_o-T_i)]$

Graphic Abstract

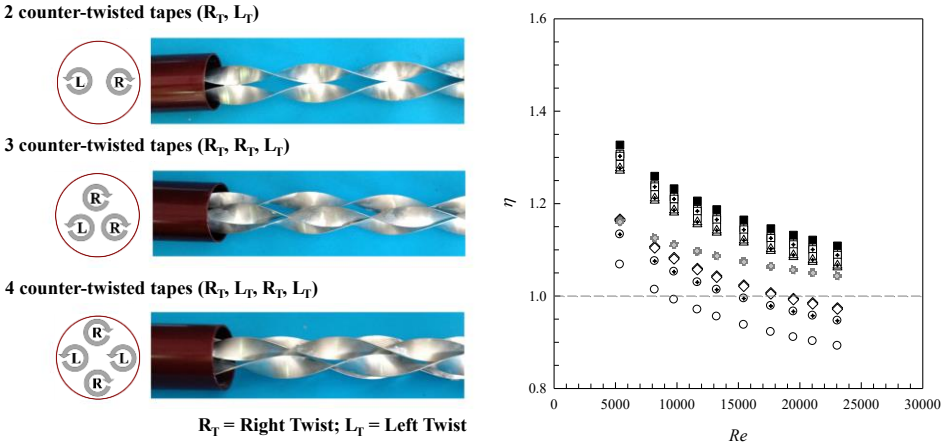

Highlights

- Multiple twisted tapes with co- and counter-twist directions arranged in 8 different forms (2T1, 2T2, 3T1, 3T2, 4T1, 4T2, 4T3 and 4T4) are presented.
- Both the heat transfer and friction factor are increased with the increment of tape number and with counter-twisted tape arrangements providing better thermal performance.
- The empirical correlations for Nusselt number and friction factor for using the multiple counter-twisted tapes are proposed.

Certificate of Acceptance

To whom it may concern:

Article "*Heat Transfer Augmentation in a Circular Tube with Winglet Vortex Generators*" authored by Suriya Chokphoemphun, Monsak Pimsarn, Chinaruk Thianpong, Pongjet Promvonge (*Department of Mechanical Engineering, Faculty of Engineering,King Mongkut's Institute of Technology Ladkrabang, Bangkok 10520, Thailand*), has been accepted by *Chinese Journal of Chemical Engineering* at 2014-04-18 and will be published on CJChE in the next year.

Chinese Journal of Chemical Engineering

2014-06-24

Heat Transfer Augmentation in a Circular Tube with Winglet Vortex Generators*

Suriya Chokphoemphun, Monsak Pimsarn, Chinaruk Thianpong, Pongjet Promvonge**
Department of Mechanical Engineering, Faculty of Engineering,
King Mongkut's Institute of Technology Ladkrabang, Bangkok 10520, Thailand

Abstract The article presents the influence of winglet vortex generators (WVG) placed in the core flow area on thermal performance enhancement of a tube heat exchanger. The experiment was carried out in a uniform wall heat-fluxed tube by varying turbulent airflow for Reynolds number ranging from 5300 to 24,000. In the present work, the WVGs with an attack angle of 30^o were inserted into the test tube at four different winglet pitch ratios (R_P=P/D) and three winglet-width or blockage ratios (R_B=e/D). The experimental results at various R_P and R_B values were evaluated and compared with those for smooth tube and tubes with twisted tape or wire coil. The measurement reveals that the WVGs enhance considerably the heat transfer and friction loss above the plain tube, wire coil and twisted tape. The Nusselt number and friction factor increase with the increment of R_B and Re but with the decreasing R_P. The average Nusselt numbers for the WVGs with various R_B are in the range of 2.03-2.34 times above the plain tube. The thermal performance for the WVGs is found to be much higher than that for the wire coil and twisted tape and is in a range of 1.35-1.59. Also, a numerical investigation is conducted to study the flow structure and heat transfer enhancement mechanisms in the winglet-inserted tube.

Keywords Nusselt number, friction factor, thermal enhancement factor, winglet, vortex generator

1 INTRODUCTION

Passive enhancement techniques by tube inserts are widely used for augmenting the heat transfer rate in a heat exchanger because this method can be easily employed in an existing heat exchanger without requiring an additional power source. Insertion of devices to generate the vortex/swirl flow such as twisted tapes, wire coils, ribs, fins, baffles, winglets etc., in the flow passage to enhance the convective heat transfer rate are the most commonly known in many thermal systems. In general, the objective of enhanced heat transfer is to make the heat exchangers more compact to reduce overall sizes of the heat exchanger, possibly their cost or to reduce the pumping power required for a given heat transfer target, which can result in a saving of operating costs. Therefore, many investigations have been carried out to study the effect of turbulators on heat transfer enhancement in the heat exchanger. The conjugate heat transfer and thermal stress in a tube with coiled wire inserted under a uniform wall heat-flux was numerically investigated by

Received 2013-xx-xx, accepted 2014-04-18.
* Supported by the Thailand Research Fund (TRF)
** To whom correspondence should be addressed. E-mail: kppongje@kmitl.ac.th

Ozceyhan [1], while the heat transfer and pressure drop characteristics in a horizontal double pipe with coiled wire inserts were studied experimentally by Naphon [2]. Promvonge [3] reported a comparative study of effect of square-wire and circular-wire coils on heat transfer and turbulent flow friction characteristics in a uniform heat-fluxed tube.

Rahimi *et al*. [4] examined the heat transfer, friction factor and thermal hydraulic performance in a round tube with the classic and the modified twisted tape inserts. Murugesan *et al*. [5] conducted an experimental work on heat transfer rate and friction factor characteristics in a double pipe heat exchanger fitted with plain twisted tapes and square-cut twisted tapes. Sharma *et al*. [6] investigated the heat transfer coefficient and friction factor in a round tube with twisted-tape inserts in the transition range of flow with Al_2O_3 nanofluid for different twist ratios. Yuxiang *et al*. [7] performed a numerical simulation of turbulent flow and heat transfer in converging-diverging tubes equipped with twin counter-swirling twisted tapes. Influences of the broken twisted tapes with various twist ratios on the heat transfer and friction factor were also studied by Chang *et al*. [8]. The effect of insertion of twisted tape with wire-nails and plain twisted-tapes at three different twist ratios in a double pipe heat exchanger on thermal characteristics was studied experimentally by Murugesan *et al*. [9]. Sivashanmugam *et al*. [10] examined the heat transfer and friction factor characteristics in a tube fitted with right-left helical screw tapes of equal length, and unequal length at different twist ratios. A comparison of the thermal and hydraulic performances between twisted-tape inserts and coil-wire inserts was introduced by Wang and Sunden [11] for both laminar and turbulent flow regimes. Promvonge [12] used wire-coil inserts in conjunction with twisted tapes for heat transfer augmentation in a tube. Bharadwaj *et al*. [13] investigated the heat transfer and pressure drop in a spirally grooved tube with twisted-tape insert for laminar to fully turbulent regions. Promvonge [14] performed a measurement to investigate the effect of the converging and diverging conical-ring arrangements on the heat transfer enhancement in a tube. Durmus [15] employed conical-ring turbulators with different conical angles for enhancing heat transfer in a tube. Promvonge and Eiamsa-ard [16] experimentally studied the effect of the conical-nozzle turbulator combined with the snail entrance on heat transfer rate and flow friction in a heat exchanger tube. The influence of the flow geometry parameters on transient forced convection heat transfer for turbulent flow in a tube with baffle inserts was reported by Tandiroglu [17]. Kongkaitpaiboon *et al*. [18] presented the effect of the circular-ring turbulator on the heat transfer and fluid friction characteristics in a heat exchanger tube.

For winglet applications, Allison and Dally [19] studied experimentally the heat transfer performance of a fin-and-tube radiator with delta-winglet vortex generators by full scale measurements and dye visualization. Tian *et al*. [20] numerically examined the air-side heat transfer and fluid flow characteristics of wavy fin-and-tube heat exchanger with delta winglets; having three-row round tubes in staggered or inline arrangements. Chompookham *et al*. [21] carried out measurements to study the effect of combined wedge ribs and winglet vortex

generators (WVG) on heat transfer and friction loss behaviors for turbulent airflow through a constant heat flux channel. Zhou and Ye [22] experimentally investigated the thermal and flow characteristics in a duct fitted with curved trapezoidal, rectangular, trapezoidal and delta winglets. Sinha *et al*. [23] provided a numerical result pertaining to heat transfer enhancement of a plate-fin heat exchanger using two rows of WVGs with five different strategies on placing the WVGs. Effects of combined ribs and WVGs on convection heat transfer and friction loss behaviors for turbulent airflow through a constant heat-fluxed channel were experimentally investigated by Promvonge *et al*. [24]. Two pairs of WVGs at different attack angles (α) were mounted on the test duct entrance to create longitudinal vortex flows through the test channel. Experiment was conducted to study heat transfer behaviors of a solar air heater channel with combined ribs and delta-winglet type vortex generators (DW) [25]. Ten pairs of DW with three attack angles (α) of 60°, 45° and 30° are introduced and mounted on the lower plate entrance of the tested channel.

According to the literature review above, the application of winglets has been shown more attractive than other vortex-flow devices due to lower pressure loss. However, the winglets cited above, in general, have been used by placing on flat surfaces of ducts or channels and rarely been found to be used in round tubes. To employ winglets in a circular tube, the modification of winglet placements is needed by placing the WVGs repeatedly on the core flow of the tube in the current work. Therefore, the objective of the present work is to examine the influence of the employed WVGs as a turbulence promoter (called turbulator) on enhanced heat transfer and flow characteristics in turbulent flow region, where air is used as the test fluid. The effect of the winglet width and pitch length is determined and the results are compared with the results of the typical twisted-tape at y/w=4 and the wire coil at $R_C=H/d$ = 5 under similar operating conditions. The WVGs are mounted on the core flow with attack angle of 30^o with respect to the main flow direction. The choice of this attack angle is that it provides the optimum thermal performance when compared to other angles of attack as suggested in the literature [24,25]. The larger angle of attack (45^o-60^o) provides higher heat transfer with extreme pressure loss, leading to lower thermal performance while the smaller attack angle (20^o-15^o) yields lower heat transfer rate.

2 EXPERIMENTAL SETUP

The detail of the experimental apparatus used in the present work is displayed schematically in Figure 1. In the apparatus, the air from a 1.5 kW high pressure blower was directed through an orifice flow-meter and passed to the heat transfer test section. The airflow rate was measured by the orifice-meter, built according to ASME standard [26] and calibrated by using a hot-wire anemometer to measure flow velocities across the tube section. Manometric fluid was used in an inclined manometer with specific gravity (SG) of 0.826 to ensure reasonably accurate measurement of pressure drop across the orifice. The desired volumetric airflow rate from the blower was obtained by controlling the motor speed of the blower through an inverter. The inner (D) and outer diameters of the copper test tube was, respectively, 50.8 and 54.8 mm and the tube

was 3000 mm long, included the test section (L) of 1000 mm. The test tube was heated by continually winding flexible electrical wire on the outer tube wall. The electrical output power was controlled by a variac transformer to obtain a uniform heat-flux along the entire length of the test section. The outer surface of the test tube was well insulated to minimize heat loss to surroundings. The inlet and outlet air temperatures in the tube were measured by RTD PT 100 type thermocouples were positioned upstream and downstream of the test tube while the surface temperatures (T_w) were measured by 12 K-type thermocouples on each side are located equally on the top and the side of test tube along the test section. The 24 K-type thermocouples were installed in holes drilled from the rear surface and centered of the tube walls with the respective junctions positioned within 1 mm of the inside wall and axial separation was 90 mm apart. All of the temperature readings from the measurement system were consistently recorded using a data logger. The pressure drop across the test section was measured by a digital manometer. Reynolds numbers for the air flowing through the test section were controlled in the range of 5300 to 24,000.

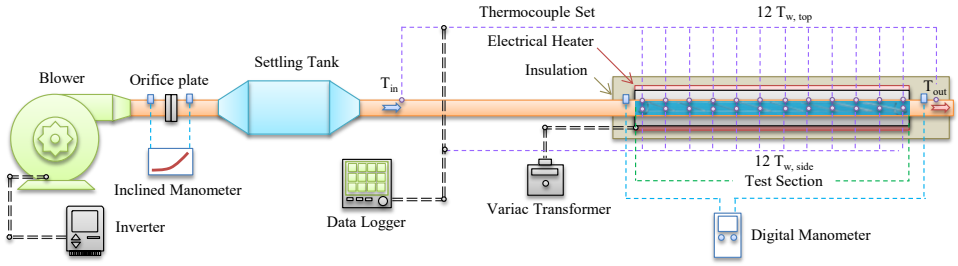

Figure 1 Schematic diagram of experimental apparatus.

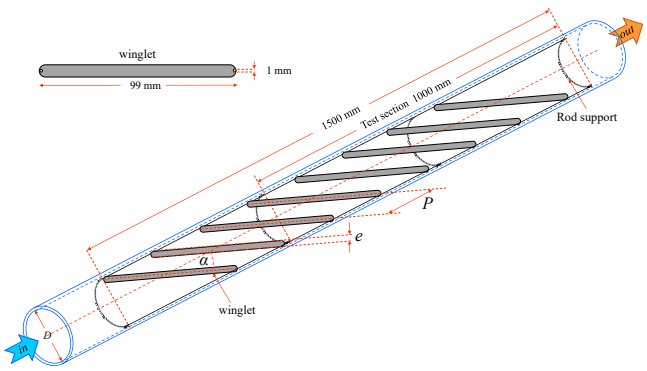

(a)

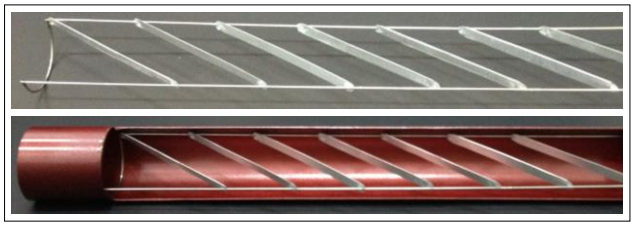

(b)

Figure 2 (a) Test tube fitted with 30º WVGs and (b) photograph of test section.

A detail of the test tube inserted with 30º WVGs is depicted in Fig. 2. All WVGs made of aluminum strip were 0.3 mm thick and 99 mm long with rounded ends and variable width *e*. The WVGs are mounted repeatedly along the core flow at α = 30º with respect to the main flow direction as depicted in Fig. 2a. As seen in figure, the WVG elements were tied together by putting two straight steel wires into the holes drilled on both end areas of the winglets with two semicircular rod-supports on both ends of the inserted. The WVGs were inserted in the test tube with three different winglet widths, e=5, 7.5 and 10 mm (R_B=e/D=0.1, 0.15 and 0.2) and with four pitch lengths; P=25, 50, 75 and 100 mm (R_P=P/D=0.5, 1.0, 1.5 and 2.0).

For comparison, the twisted-tape made of aluminum sheet was introduced and its size was 0.8 mm thick, 42 mm wide (w) and 1200 mm long with twist length (y) of 168 mm (twist ratio, y/w = 4). Also, the wire coil [3] with 3 mm wire thickness (d) and 15 mm coil pitch length (H) at coil pitch ratio, R_C = H/d = 5 was offered and its data were taken from ref.[3].

To quantify the uncertainties of measurements, the reduced data obtained experimentally were determined. The uncertainty in the data calculation was based on ref. [27]. The maximum uncertainties of non-dimensional parameters were ±5% for Reynolds number, ±7.6% for Nusselt number and ±9.5% for friction. The uncertainty in the axial velocity measurement was estimated to be less than ±5%, and pressure has a corresponding estimated uncertainty of ±5%, whereas the uncertainty in temperature measurement at the tube wall was about ±0.5%.

3 DATA REDUCTION

In the present work, the air used as the test fluid flowed through a uniform heat-fluxed and insulated tube. The steady state heat transfer rate is assumed to be equal to the heat loss in the test section, which can be expressed as

$$Q_a = Q_{conv} \tag{1}$$

where

$$Q_a = \dot{m} C_{p,a} \left(T_o - T_i\right) \tag{2}$$

The heat supplied by the electrical winding in the test tube is found to be 3-5% higher than the heat absorbed by the fluid for the thermal equilibrium test due to convection and radiation heat losses from the test section to the surrounding. Thus, only the heat transfer rate absorbed by the fluid is taken for the internal convective heat transfer coefficient calculation. The convection heat transfer in the test tube can be written as

$$Q_{conv} = hA\left(\tilde{T}_w - T_b\right) \tag{3}$$

in which

$$T_b = (T_o + T_i)/2 \tag{4}$$

$$\tilde{T}_w = \sum T_w / 24 \tag{5}$$

where T_w is the local wall temperature evaluated at the outer wall surface of the tested copper tube. The average wall temperature, $\tilde{T}_w$, is calculated from 24 points of surface temperatures lined at

equal interval between the inlet and the exit of the tested tube. The average heat transfer coefficient (h) and the mean Nusselt number (Nu) are estimated as follows:

$$h = \dot{m} C_{\mathrm{p,a}} \left(T_{\mathrm{o}} - T_{\mathrm{i}}\right) / A\left(\tilde{T}_{\mathrm{w}} - T_{\mathrm{b}}\right) \tag{6}$$

The heat transfer is calculated from the Nusselt number which can be obtained by

$$Nu = \frac{hD}{k} \tag{7}$$

The Reynolds number based on tube diameter is given by

$$Re = UD / \nu \tag{8}$$

The friction factor (f) computed by pressure drop across the test tube length (L) is written as

$$f = \frac{2}{\left(L / D\right)} \frac{\Delta P}{\rho U^2} \tag{9}$$

in which U is mean air velocity in the tube. All of thermo-physical properties of the air are determined at the overall bulk air temperature (T_{b}) from Eq. (4).

To assess the practical use of the enhanced tube, the performance of the enhanced tube is evaluated relatively to the smooth tube at an identical pumping power in the form of thermal performance enhancement factor (η) which can be expressed as

$$\eta = (Nu/Nu_0) / (f/f_0)^{1/3} \tag{10}$$

4 NUMERICAL SIMULATION

4.1 Winglet geometry and mathematical modeling

The system of interest is a circular tube inserted with 30° WVGs as shown in Fig. 3. The full-length tube was divided into 3 parts: entry, test section and exit. The detail of the full-length winglet-inserted tube is displayed in Fig. 3a, whereas a module of one periodic flow, computational domain and its grid is shown in Fig. 3b. The periodic flow tube attains a periodical fully developed flow and thermal condition where the velocity field and heat transfer pattern repeats itself from one module to another. The concept of periodical fully developed flow and its solution procedure has been described in ref. [28]. In the periodic flow module, the air enters the tube at an inlet temperature (T_{in}) and flows over a 30° winglet where e is the winglet width, the tube diameter (D) is set to 50 mm, and e/D is known as the blockage ratio (R_{B}). The axial pitch spacing (P) is a distance between the winglet cells, in which P/D is defined as the pitch ratio (R_{P}). To investigate the flow structure and heat transfer mechanism for the WVGs, R_{B} of 0.1, 0.15 and 0.2 is simulated and the results are validated with the measurement in the present work.

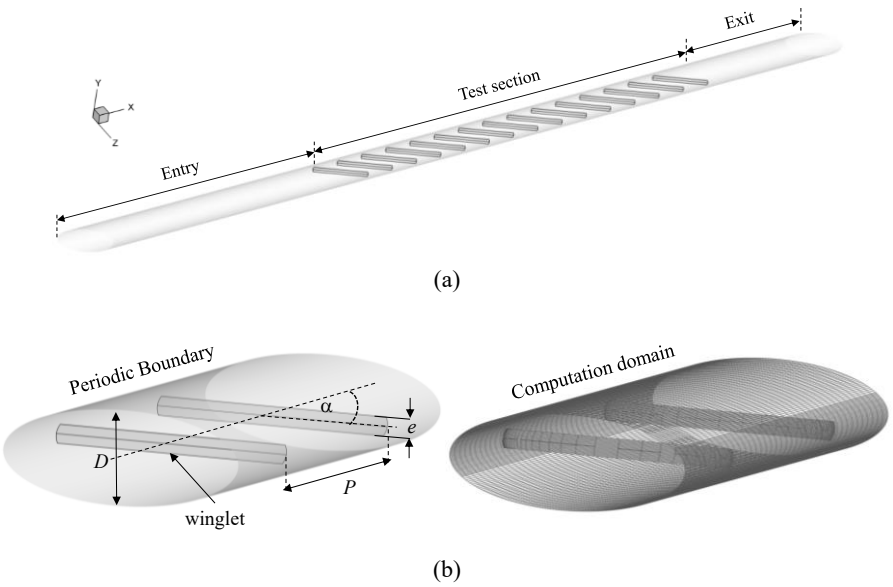

Figure 3(a) Full-length tube geometry and (b) computational domain of periodic flow.

The numerical model for fluid flow and heat transfer in the inserted tube is developed under the following assumptions: steady, three-dimensional, turbulent and incompressible flow; constant fluid properties; and ignored body forces, viscous dissipation and radiation heat transfer. Based on the above assumptions, the tube flow model is governed by the Reynolds averaged Navier–Stokes (RANS) equations with the RNG k-ε turbulence model and the energy equation. The details on mathematical modeling can be found in ref. [29]. In the present simulation, the commercial software ANSYS FLUENT is employed.

4.2 Boundary conditions

For a full-length circular tube fitted with winglets, a uniform air velocity was introduced at the inlet while a pressure outlet condition was applied at the exit. For a periodic flow module, periodic boundaries were used for the inlet and outlet of the flow domain. Constant mass flow rate of air at 300 K was assumed in the flow direction. The physical properties of the air were assumed to remain constant at mean bulk temperature. Impermeable boundary and no–slip wall conditions were implemented inside the tube walls as well as the winglet surface. The constant wall heat flux of the tube was maintained at 600 W/m^2 while the winglet strip was assumed at adiabatic wall condition.

4.3 Grid independence test

The computational domain of a periodic flow module is resolved by regular Cartesian elements or hexahedron elements. A grid independence procedure was implemented by using Richardson extrapolation technique over grids with different numbers of cells, about 32,000, 64,000, 128,000 and 255,000. The variation in Nu and f values is found to be less than 0.3% for the increment of the number of cells from 128,000 to 255,000. With consideration in both computing

time and solution precision, the grid of 128,000 cells was adopted while similar grid density was also applied for the full-length flow model.

4.4 Fully developed periodic condition

To investigate a fully developed periodic condition, the full-length tube fitted with multiple winglets as depicted in Fig. 3a was simulated for Re=10000, R_B=0.2 and R_P=0.1. The fully developed periodic flow and heat transfer in the winglet-inserted tube can be examined by considering the axial Nu_x and velocity distributions. For brevity, both the axial distributions are not displayed here. The simulation revealed that the fully developed periodic condition occurs at about the 5th module/period or at $x/D \approx 5$. In addition, the preliminary study indicates that the fully developed periodic flow condition depends on the winglet width and pitch ratios where the higher R_B and the smaller R_P lead to faster development of the fully periodic flow. Therefore, the concept of fully developed periodic flow can be applied efficiently to turbulent tube flow through winglets. Again, by considering both convergent time and solution precision, only a fully developed periodic flow model (one periodic flow module) is employed in the subsequent computation.

5 RESULTS AND DISCUSSION

5.1 Validation of smooth tube

The present experimental results on the heat transfer and friction characteristics in a smooth wall tube are first validated in terms of Nusselt number (Nu) and friction factor (f). The simulated results of Nu and f for the present smooth tube are, respectively, compared with those from correlations of Dittus-Boelter and Blasius found in the open literature [30] for turbulent flow in circular ducts in Fig. 4.

Dittus and Boelter correlation:

$$Nu = 0.023 Re^{0.8} Pr^{0.4} \tag{11}$$

Blasius correlation:

$$f = 0.316 Re^{-0.25} \tag{12}$$

In Fig. 4, the present simulations agree reasonably well within ±6% with the Blasius correlation and the Dittus-Boelter correlation.

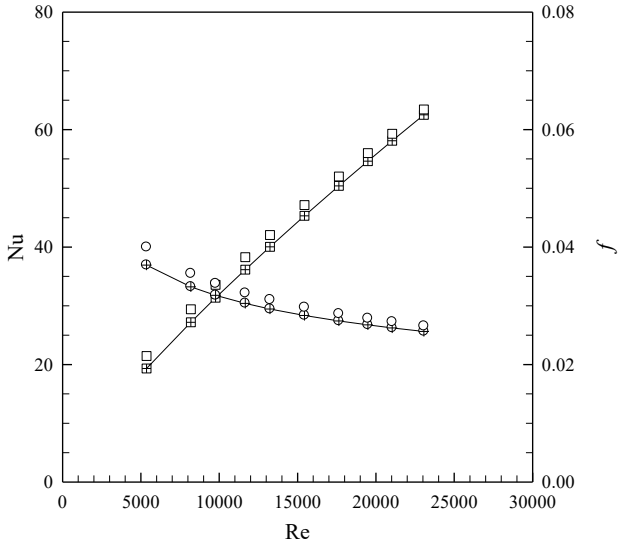

Figure 4 Verification of Nusselt number and friction factor for smooth tube.

⊞ Dittus and Boelter; □ Nu smooth tube; ⊕ Blasius; ○ *f* smooth tube

5.2 Effect of WVGs on heat transfer

The effect of four different pitch ratios (R_P= 0.5, 1, 1.5 and 2) and three blockage ratios (R_B=0.1, 0.15 and 0.2) on the heat transfer is examined and presented in the form of *Nu*. The relationships between heat transfer (*Nu*) and Reynolds numbers (*Re*) of the tube inserted with WVGs are demonstrated in Fig. 5a. According to the figure, WVGs turbulators yield considerable heat transfer enhancement with a similar trend in comparison with the smooth tube, twisted tapes and the wire coil. This is due to the interruption of the flow by the turbulators results in the destruction of thermal boundary layer near the tube wall. The Nusselt number increases with the rise of Reynolds number and the blockage ratio and with the decreasing of the pitch ratio.

The ratio of augmented *Nu* of inserted tube to *Nu* of smooth tube, Nu/Nu_0 plotted against the Reynolds number (*Re*) is displayed in Fig. 5b. In the figure, the Nu/Nu_0 tends to decrease slightly with the rise of *Re* for all cases studied. The heat transfer values of the tube with WVGs are found to be better than that the smooth tube with/without the twisted tapes because the WVGs provide the strong mixing or turbulence intensity leading to destruction of thermal boundary layer and the vortex flow creating better flow mixing between the fluid at the core and the tube wall. Both flow phenomena promote an increase in the tangential and radial turbulent fluctuation or the turbulence intensity, thinning the boundary layer, and therefore cause the rise in heat transfer rate inside a tube. The average increases in *Nu* for using the 30º WVGs with R_P = 0.5, 1, 1.5 and 2 are about 218, 208, 200 and 186%; 234, 222, 215 and 202%; and 251, 240, 229 and 217% at R_B = 0.1, 0.15 and 0.2, respectively while the wire coil and twisted tape inserts yield the mean increase in *Nu* of 212 and 129% above the smooth tube.

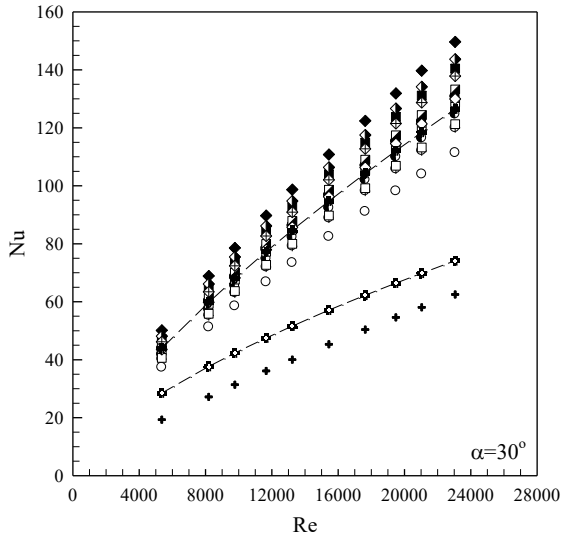

(a)

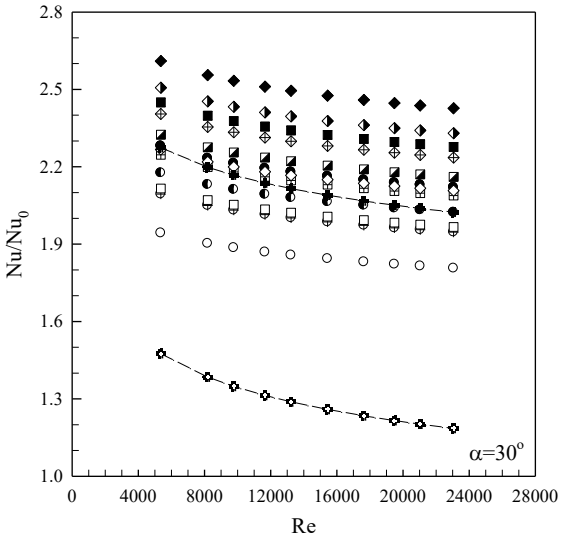

(b)

Figure 5 Variation of (a) Nu and (b) Nu/Nu_0 with Re for WVG inserts.

♦R_B=0.20, R_P=0.5;◊R_B=0.20, R_P=1.0;⊕R_B=0.20, R_P=1.5;◊R_B=0.20, R_P=2.0;■R_B=0.15, R_P=0.5;◪R_B=0.15, R_P=1.0;⊞ R_B=0.15, R_P=1.5;□R_B=0.15, R_P=2.0;●R_B=0.10, R_P=0.5;◐R_B=0.10, R_P=1.0;⊕R_B=0.10, R_P=1.5;○R_B=0.10, R_P=2.0;⧫wire coil, R_C=5; ⧫twisted tape, y/w=4; ⧫smooth tube

The variation of surface temperature along the inserted tube at R_B=0.10, R_P=1.5 for Re=11660 and 15442 is displayed in Fig. 6 where x is the location of thermocouples starting from the entry of test section. In the figure, the surface temperature shows an increase tendency with the increment of x/D for both the Re values and a slight drop at the last two locations ($x/D \approx 18$ and 20) due to the radiation and the exit effect. The wall temperature in the Re = 11660 case is higher than that of Re = 15442 because of lower heat removal from the tube wall.

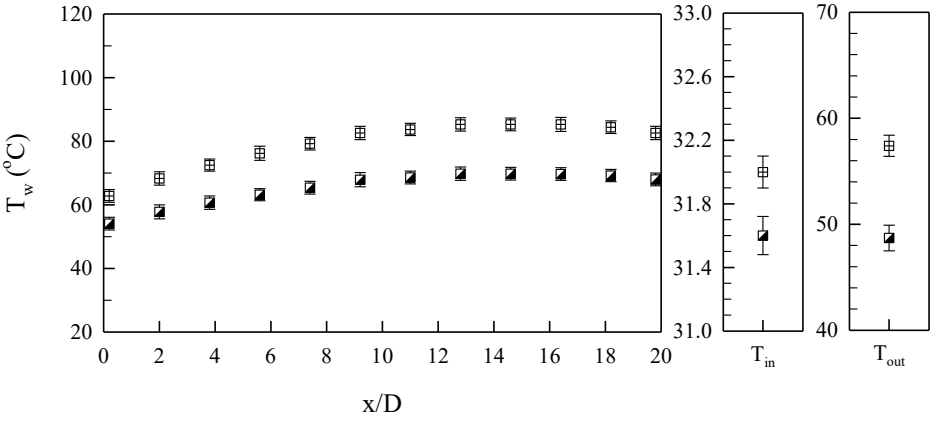

Figure 6 Variation of wall temperature along inserted tube, R_B=0.1 and R_P=1.5.

Re = 11660; Re = 15442

5.3 Effect of WVGs on friction factor

Figure 7a shows the relationship between the friction factor and the Reynolds number obtained with 30º WVGs inserted. It is observed that the friction factor tends to decrease with raising the Reynolds number. The WVG provides a substantial increase in f over the smooth tube, due to the dissipation of dynamic pressure of the fluid due to higher surface area and the reverse/swirl flow. The WVG gives much higher f than that of the twisted tape but considerably lower than the wire coil. f decreases with the decrease of R_B but the rise of R_P.

Figure 7b presents the variation of friction factor ratio (f/f_0) with Re for various R_B and R_P values: f/f_0 tends to increase slightly with the increment of Re for all the WVGs applied and to decrease slightly with the rise of Re for using the twisted tape and wire coil. The maximum f/f_0 of about 5.63 times is seen for the WVG insert at R_B=0.2 and R_P=0.5 while that of about 7.5 times is for the wire coil insert.

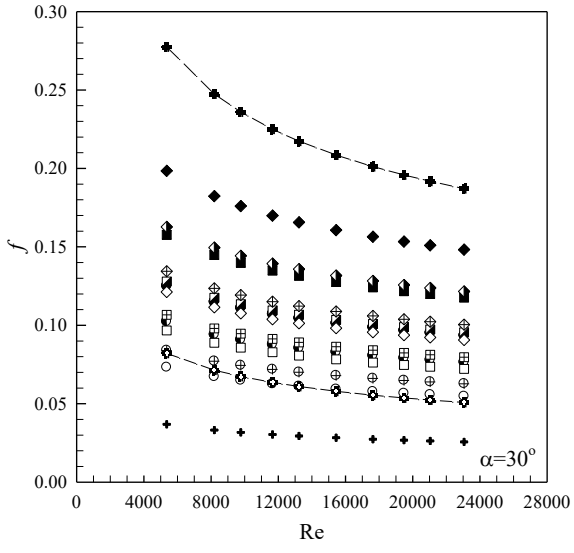

(a)

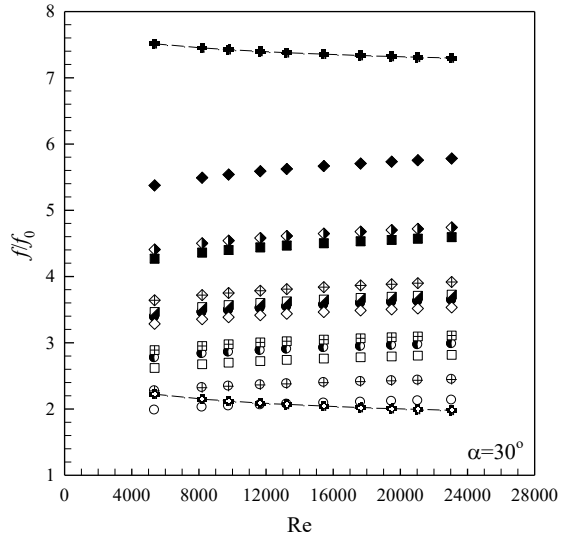

(b)

Figure 7 Variation of (a) *f* and (b) *f*/*f*$_0$ with Re for WVG inserts.

♦R_B=0.20, R_P=0.5;◊R_B=0.20, R_P=1.0;⊕R_B=0.20, R_P=1.5;◇R_B=0.20, R_P=2.0;▮R_B=0.15, R_P=0.5;◪R_B=0.15, R_P=1.0;⊞ R_B=0.15, R_P=1.5;□R_B=0.15, R_P=2.0;●R_B=0.10, R_P=0.5;⬮R_B=0.10, R_P=1.0;⊕R_B=0.10, R_P=1.5;○R_B=0.10, R_P=2.0;⧫wire coil, R_C=5; ⧯twisted tape, *y*/*w*=4; ⧫smooth tube

5.4 Effect of R_P on heat transfer and friction factor

Figure 8a displays the plot of the *Nu*/*Nu*$_0$ against the R_P for various R_B and *Re* values: *Nu*/*Nu*$_0$ tends to decrease with the increment of *Re* and PR. The WVGs at R_P = 0.5, 1, 1.5 and 2 provide the mean increase in *Nu* up to 234, 223, 215 and 202% above the plain tube.

The effect of R_P on *f*/*f*$_0$ is depicted in Fig. 8b: *f*/*f*$_0$ shows a decrease trend with the increment of R_P for all R_B and it is nearly free from *Re*. The maximum friction loss in the present study is found for the WVGs with R_P= 0.5. The mean *f* values for the WVGs at R_P= 0.5 are seen to be higher than those at R_P= 1.0, 1.5 and 2.0 at about 22, 48 and 65%, respectively.

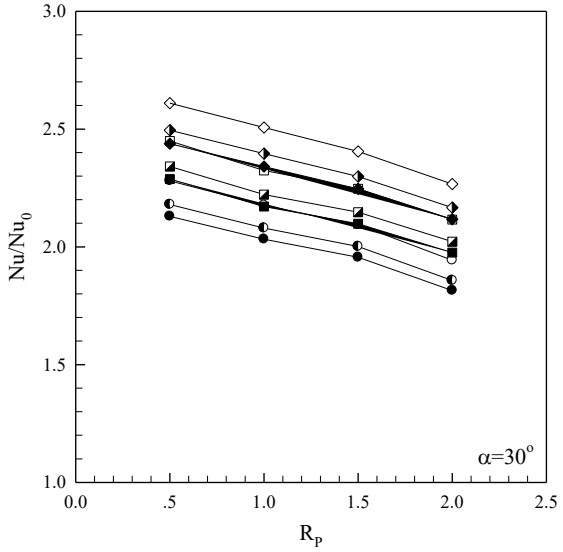

(a)

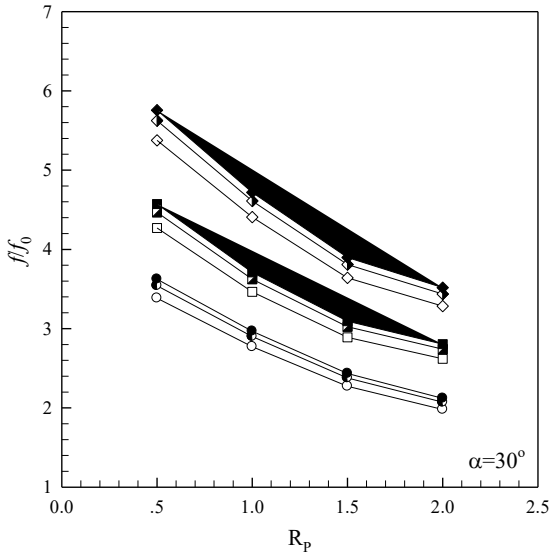

(b)

Figure 8 Variation of (a) *Nu*/*Nu*$_0$ and (b) *f*/*f*$_0$ with R_P for WVG inserts.

◇ R_B=0.20, *Re*=5363; ◆ R_B=0.20, *Re*=13236; ◆ R_B=0.20, *Re*=21042; □ R_B=0.15, *Re*=5363; ◪ R_B=0.15, *Re*=13236; ■ R_B=0.15, *Re*=21042; ○ R_B=0.10, *Re*=5363; ◐ R_B=0.10, *Re*=13236; ● R_B=0.10, *Re*=21042

5.5 Effect of WVGs on thermal performance

In thermal performance evaluation, the thermal enhancement factor (η) under constant pumping power conditions is taken into account by using Eq. (10). The variation of the η with *Re* is depicted in Fig. 9. The η values generally are above unity for the WVG inserts, indicating that the use of WVGs is advantageous over the smooth tube. η tends to decrease with the increase of *Re* and R_B values for all WVG inserts. The maximum η is between 1.45-1.59 for the WVGs with R_B=0.1 and R_P=1.5 while the minimum is between 1.35-1.49 for the one with R_B=0.2 and R_P=0.5. The highest η of 1.59 is found for the WVGs at R_B=0.1 and R_P=1.5 at lower *Re*.

In addition, the empirical correlations for WVGs developed by relating the *Re*, R_B and R_P together are compared with experimental data within ±5% and ±6% for Nusselt number and friction factor, as can be seen in Figs. 10a and 10b, respectively.

$$Nu = 0.1206 Re^{0.75} Pr^{0.4} \left(R_B\right)^{0.2036} \left(R_P\right)^{-0.1008} \tag{13}$$

$$f = 2.5858 Re^{-0.2} \left(R_B\right)^{0.6809} \left(R_P\right)^{-0.3672} \tag{14}$$

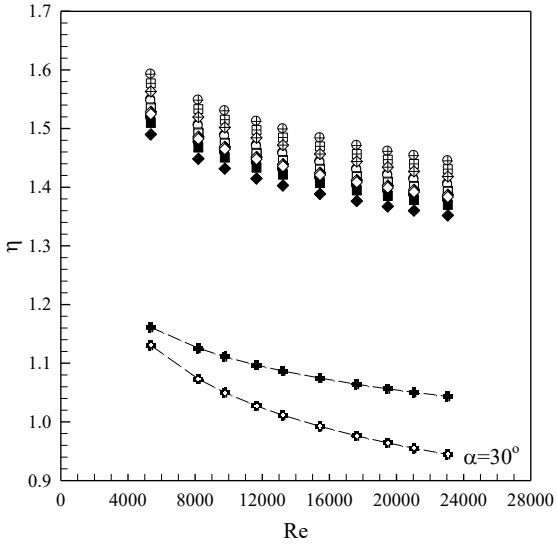

Figure 9 Variation of η with *Re* for WVG inserts.

R_B=0.10, R_P=1.5;R_B=0.10, R_P=1.0;R_B=0.10, R_P=2.0;R_B=0.10, R_P=0.5;R_B=0.15, R_P=1.5;R_B=0.15, R_P=1.0;R_B=0.15, R_P=2.0;R_B=0.15, R_P=0.5;R_B=0.20, R_P=1.5;R_B=0.20, R_P=1.0;R_B=0.20, R_P=2.0;R_B=0.20, PR=0.5;wire coil, R_C=5; twisted tape, y/w=4;

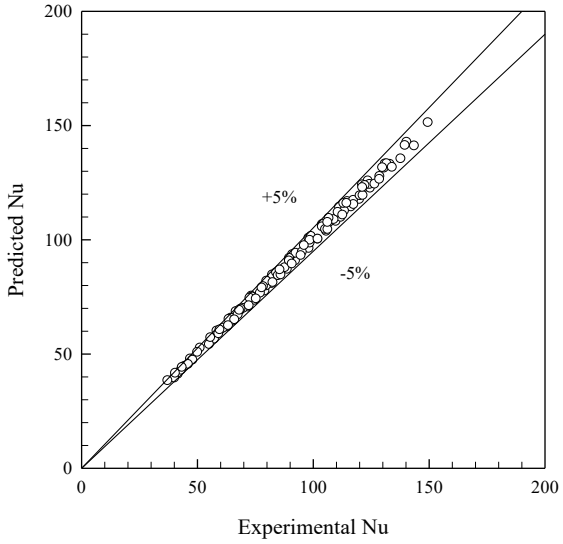

(a)

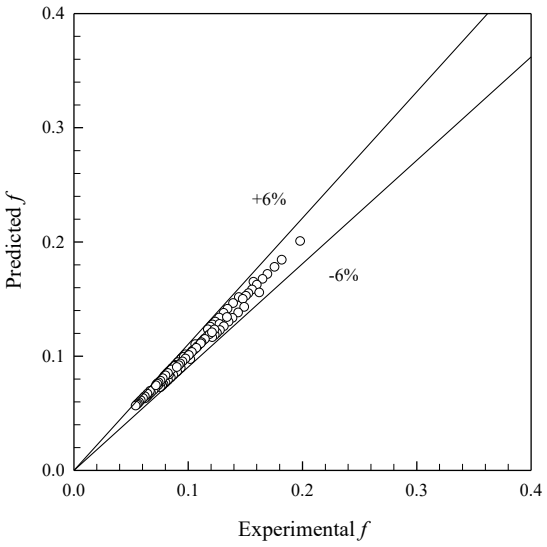

(b)

Figure 10 Variation tests of (a) Nusselt number and (b) friction factor correlations.

5.6 Numerical results of inserted-tube flow

The flow and vortex coherent structure in the inserted tube is displayed by streamlines superimposed with temperature field at various locations in transverse planes as depicted in Fig. 11. The streamlines of the WVG flow model are presented for Re=10,000, R_P=1.0 and R_B=0.2, showing that there are two main counter-rotating vortex flows appear on the lower and upper parts along the tube. The appearance of the two vortex flows can help to increase higher heat transfer in the tube because of higher transport of the fluid from the central core to the near-wall regimes as can be observed from the major change in the temperature field over the tube. This means that the vortex flows provide a significant influence on the temperature field, because it can induce better fluid mixing between the wall and the core flow regions, leading to a high temperature gradient over the heated wall, especially in the downstream winglet-end region.

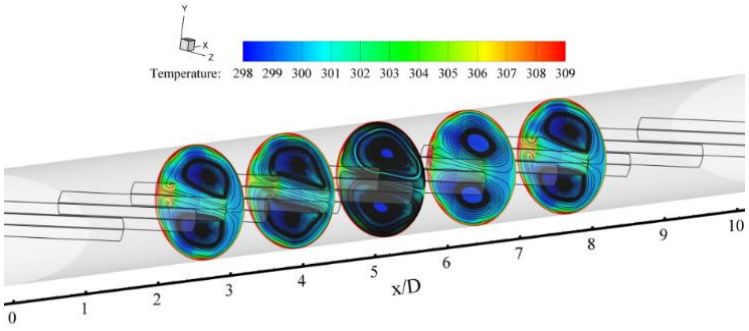

Figure 11 Streamlines and temperature contours in transverse planes for WVGs at Re=10,000, R_P=1.0 and R_B=0.2.

The local Nu contour including the streamlines showing the impingement on the tube wall for Re=10,000, R_P=1.0 and R_B=0.2 is presented in Fig. 12. In the figure, it is apparent that the high Nu

values for the inserted tube are seen in large areas over the tube wall. The peaks can be observed in the sidewall area around the downstream winglet-end where the red area shows the impingement region of the secondary flow providing higher heat transfer rate than other areas. This means that the vortex-induced impingement flow is responsible to heat transfer enhancement in the tube, apart from fast fluid mixing between the core and the near-wall regions.

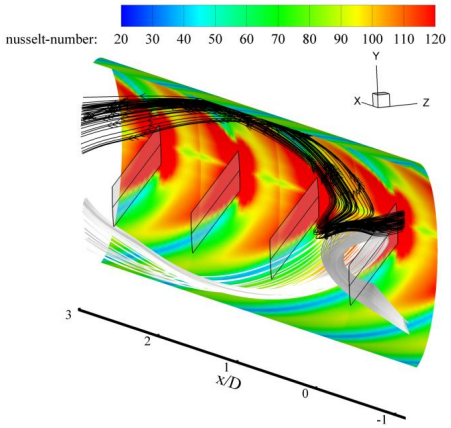

Figure 12 Streamlines of impinging jets on tube wall and *Nu* contours for WVGs at *Re*=10,000, R_P=1.0 and R_B=0.2.

The results of Nusselt number and friction factor from simulation with R_P=1.0 and R_B=0.1, 0.15 and 0.2 are validated by comparison with experimental data under similar operating conditions as shown in Figs. 13a and 13b, respectively. It is worth noting that the numerical results are in good agreement with experimental data. The average deviations of the results are less ±9% for Nusselt number and ±12% for friction factor.

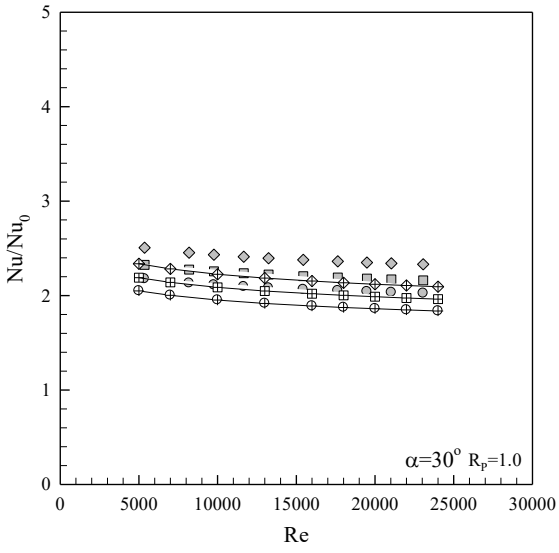

(a)

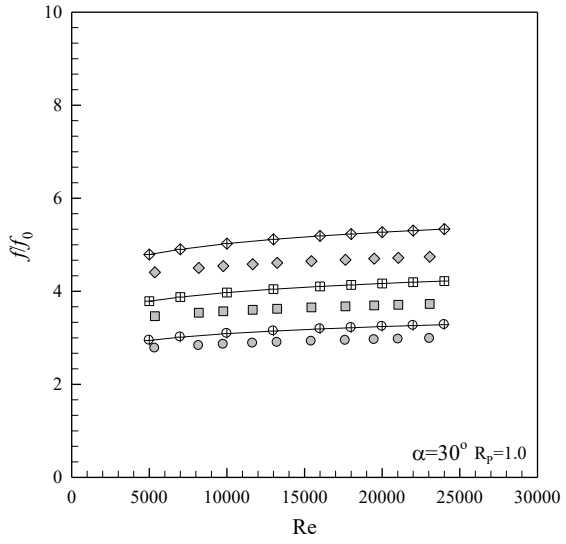

(b)

Figure 13 Variation of (a) Nu/Nu$_0$ and (b) f/f_0 with Re for WVG inserts at R_P=1.0 and R_B=0.2.

◇ R_B=0.20, experimental; ▫ R_B=0.15, experimental; ○ R_B=0.10, experimental; ⊸ R_B=0.20, simulated; ⊟ R_B=0.15, simulated; ⊸ R_B=0.10, simulated

6 CONCLUSIONS

The heat transfer and the friction factor characteristics in a round tube inserted with 30° WVGs at three R_B and four R_P values have been investigated for the turbulent regime, Re=5300-24,000 under a uniform heat-flux condition. In the present study, the following conclusions can be drawn.

- The use of the 30° WVGs leads to considerable heat transfer enhancement over the plain tube at about 186 to 251% depending on the Re, R_B and R_P values.
- The smaller R_P yields higher heat transfer rate than the larger one but the smaller R_B provides an opposite trend.
- The friction factor of the WVGs is found to be 2.07-5.63 times above that of the plain tube. The f tends to decrease with the rise of R_P but with decreasing R_B.
- The η for the WVGs investigated is in a range of 1.35-1.59 which is much higher than that for the coil wire and the twisted tape. The maximum η of around 1.59 is found for the WVGs with R_B=0.1 and R_P=1.5 at lower Re. Thus, the WVG insert is a promising method to improve thermal systems in industrial applications.

ACKNOWLEDGEMENT

The authors would like to gratefully acknowledge the Thailand Research Fund (TRF) for the financial support and also thank Mr. Sombat Tamna, lecturer of the Faculty of Engineering, Thai-Nichi Institute of Technology, Thailand for the support in numerical work of this research.

NOMENCLATURE

A	heat transfer surface area, m^2
C_p	specific heat of fluid, $J \cdot kg^{-1} \cdot K^{-1}$
D	inner diameter of test tube, m
d	wire coil diameter, m
e	winglet width, m
f	friction factor
H	pitch of coil spring, m
h	heat transfer coefficient, $W \cdot m^{-2} \cdot K^{-1}$
I	current, amp
k	thermal conductivity of fluid, $W \cdot m^{-1} \cdot K^{-1}$
L	length of test section, m
$\dot{m}$	mass flow rate, $kg \cdot s^{-1}$
Nu	Nusselt number
P	pitch length, m
ΔP	pressure drop, Pa
Pr	Prandtl number
Q	heat transfer rate, W
R_B	blockage ratio ($=e/D$)
R_C	coil spring pitch ratio ($=H/d$)
R_P	pitch ratio ($=P/D$)
Re	Reynolds number ($=UD/\nu$)
$\widetilde{T}$	mean temperature, K
T	temperature, K
U	mean air velocity, $m \cdot s^{-1}$
w	tape width, m
y	pitch length of twisted tape (180° rotation), m

Greek symbols

η	thermal enhancement factor ($=(Nu/Nu_0)/(f/f_0)^{1/3}$)
ρ	fluid density, $kg \cdot m^{-3}$
ν	kinematic viscosity, $m^2 \cdot s^{-1}$

Subscripts

a	air
b	bulk
conv	convection
i	inlet
o	outlet
pp	pumping power
p	plain tube
s	swirl flow generator

w wall

REFERENCES

1 Ozceyhan, V., “Conjugate heat transfer and thermal stress analysis of wire coil inserted tubes that are heated externally with uniform heat flux”, *Energy Convers. Manage.*, **46** (9-10), 1543–1559 (2005).

2 Naphon, P., “Effect of coil-wire insert on heat transfer enhancement and pressure drop of the horizontal concentric tubes”, *Int. Commun. Heat Mass Transfer*, **33**(6), 753–763 (2006).

3 Promvonge, P., “Thermal performance in circular tube fitted with coiled square wires”, *Energy Convers. Manage.*, **49** (5), 980–987 (2008).

4 Rahimi,M., Shabanian,S.R., Alsairafi,A.A., “Experimental and CFD studies on heat transfer and friction factor characteristics of a tube equipped with modified twisted tape inserts”, *Chem. Eng. Process.*, **48** (3), 762–770 (2009).

5 Murugesan, P., Mayilsamy, K., Suresh, S., “Turbulent heat transfer and pressure drop in tube fitted with square-cut twisted tape”, *Chin. J. Chem. Eng.*, **18** (4), 609–617 (2010).

6 Sharma, K.V., Sundar, L.S., Sarma, P.K., “Estimation of heat transfer coefficient and friction factor in the transition flow with low volume concentration of Al_2O_3 nanofluid flowing in a circular tube and with twisted tape insert”, *Int. Commun. Heat Mass Transfer*, **36** (5), 503-507 (2009).

7 Hong, Y.X., Deng, X.H., Zhang, L.S., “3D numerical study on compound heat transfer enhancement of converging-diverging tubes equipped with twin twisted tapes”, *Chin. J. Chem. Eng*., **20** (3), 589–601 (2012).

8 Chang, S.W., Yang, T.L., Liou, J.S., “Heat transfer and pressure drop in tube with broken twisted tape insert”, *Exp. Therm. Fluid Sci.*, **32** (2), 489-501 (2007).

9 Murugesan, P., Mayilsamy, K., Suresh, S., “Heat Transfer and Friction Factor Studies in a Circular Tube Fitted with Twisted Tape Consisting of Wire-nails”, *Chin. J. Chem. Eng.*, **18** (6), 1038–1042 (2010).

10 Sivashanmugam, P., Nagarajan, P.K., Suresh, S., “Experimental studies on heat transfer and friction factor characteristics of turbulent flow through a circular tube fitted with right and left helical screw-tape inserts”, *Chem. Eng. Commun.*, **195** (8), 977–987 (2008).

11 Wang, L., Sunden, B., “Performance comparison of some tube inserts”, *Int. Commun. Heat Mass Transfer*, **29** (1), 45–56 (2002).

12 Promvonge, P., “Thermal augmentation in circular tube with twisted tape and wire coil turbulators”, *Energy Convers. Manage.*, **29** (1), 45–56 (2002).

13 Bharadwaj, P., Khondge, A.D., Date, A.W., “Heat transfer and pressure drop in a spirally grooved tube with twisted tape insert”, *Int. J. Heat Mass Transfer*, **52** (7–8), 1938–1944 (2009).

14 Promvonge, P., “Heat transfer behaviors in round tube with conical ring inserts, *Energy Convers. Manage*”. **49** (1), 8–15 (2008).

15 Durmus, A., “Heat transfer and exergy loss in cut out conical turbulators”, *Energy Convers. Manage.*, **45** (5), 785–796 (2004).

16 Promvonge, P., Eiamsa-ard, S., “Heat transfer enhancement in a tube with combined conical-nozzle inserts and swirl generator”, *Energy Convers. Manage.*, **47**, 2867–2882 (2006).

17 Tandiroglu, A., “Effect of flow geometry parameters on transient heat transfer for turbulent flow in a circular tube with baffle inserts”, *Int. J. Heat Mass Transfer*, **49** (9–10), 1559–1567 (2006).

18 Kongkaitpaiboon, V., Nanan, K., Eiamsa-ard, S., “Experimental investigation of convective heat transfer and pressure loss in a round tube fitted with circular-ring turbulators”, *Int. Commun. Heat Mass Transfer*, **37** (5), 568–574 (2010).

19. Allison, C.B., Dally, B.B., “Effect of a delta-winglet vortex pair on the performance of a tube-fin heat

exchanger", *Int. J. Heat Mass Transfer*, **50**, 5065–5072 (2007).

20 Tian, L., He, Y., Tao, Y., Tao, W., "A comparative study on the air-side performance of wavy fin-and-tube heat exchanger with punched delta winglets in staggered and in-line arrangements", *Int. J. Therm. Fluid Sci.*, **48**, 1765–1776 (2009).

21 Chompookham, T., Thianpong,C., Kwankaomeng, S., Promvonge, P., "Heat transfer augmentation in a wedge-ribbed channel using winglet vortex generators", *Int. Commun. Heat Mass Transfer*, **37**, 163–169 (2010).

22 Zhou, G., Ye, Q., "Experimental investigations of thermal and flow characteristics of curved trapezoidal winglet type vortex generators", *Appl. Therm. Eng.*, **37**, 241–248 (2012).

23 Sinha, A., Raman, K.A., Chattopadhyay, H., Biswas, G. "Effects of different orientations of winglet arrays on the performance of plate-fin heat exchangers", *Int. J. Heat Mass Transfer*, **57**, 202–214 (2013).

24 Promvonge, P., Chompookham, T., Kwankaomeng, S., Thianpong C., "Enhanced heat transfer in a triangular ribbed channel with longitudinal vortex generators." *Energy Convers. Manage*., **51**, 1242–1249 (2010).

25 Promvonge, P., Khanoknaiyakarn, C., Kwankaomeng,S., Thianpong, C., "Thermal behavior in solar air heater channel fitted with combined rib and delta-winglet", *Int. Commun. Heat Mass Transfer*, **38**, 749–756 (2011).

26 ASME, "Standard Measurement of fluid flow in pipes using orifice, nozzle and venture", ASME MFC–3M-1984, United Engineering Center, New York, pp.1–56 (1984).

27 ANSI/ASME, "Measurement uncertainty", PTC 19, Part I, 1–1985 (1986).

28 Patankar, S.V., Liu, C.H., Sparrow, E.M., "Fully developed flow and heat transfer in ducts having streamwise-periodic variations of cross-sectional area", *ASME J. Heat Transfer*, **98**, 1109–1151 (1998).

29 Promvonge, P., Changcharoen,W., Kwankaomeng S., Thianpong, C., "Numerical heat transfer study of turbulent square-duct flow through inline V-shaped discrete ribs", *Int. Commun. Heat Mass Transfer*, **38** (10), 1392-1399 (2011).

30 Incropera, F.P., Witt, P.D., Bergman, T.L., Lavine, A.S., *Fundamentals of Heat and Mass Transfer*, John-Wiley & Sons (2006).

Graphic Abstract

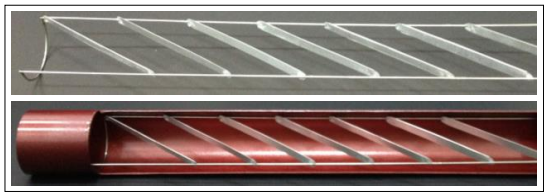

Test tube fitted with 30° WVGs.

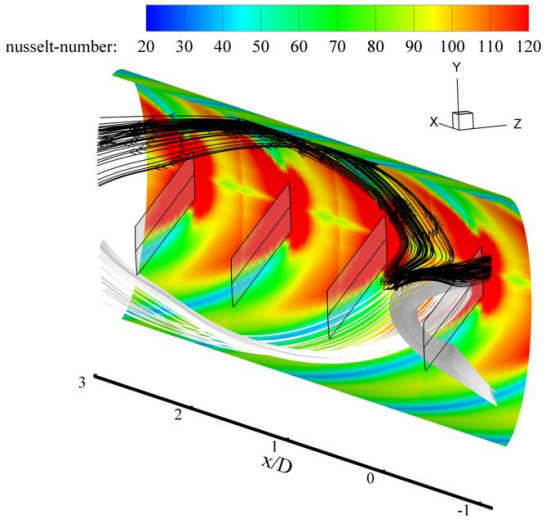

Streamlines of impinging jets on tube wall and Nu contours for WVGs.

Highlights

- An effect of WVG inserts on enhanced heat transfer and flow characteristics in turbulent tube flow is investigated.
- The WVGs with an attack angle of 30° are inserted into the test tube at four different winglet pitch ratios (R_P=P/D) and three winglet-width or blockage ratios (R_B=e/D).
- The empirical correlations for Nusselt number and friction factor for using the WVGs are proposed.
- The thermal enhancement factor for the WVGs is in a range of 1.35-1.59.

KKU International Engineering Conference

Part 2

Edited by
Sujin Bureerat

TRANS TECH PUBLICATIONS

ISBN-13: 978-3-03835-090-3
Advanced Materials Research Vols. 931-932, Part 2
Electronically available at *http://www.scientific.net*

Advanced Materials Research Vols. 931-932 (2014) pp 1188-1192
Online available since 2014/May/09 at www.scientific.net

doi:10.4028/www.scientific.net/AMR.931-932.1188

Heat transfer augmentation in a round tube with 60° Winglet Pair inserts

Suriya Chokphoemphun[1, a], Pattarapan Tongyote[1, b]
Pongjet Promvonge[1, c*] Withada Jedsadaratanachai[1, d]
and Teerapat Chompookham[2, e]

[1]Department of Mechanical Engineering, Faculty of Engineering,
King Mongkut's Institute of Technology Ladkrabang, Bangkok 10520, Thailand
[2]Heat Pipe and Thermal Tools Design Research Unit (HTDR), Faculty of Engineering,
Mahasarakham University, Mahasarakham 44150, Thailand
[a]chok_suriya_@hotmail.com, [b]pattarapan.kmitl@hotmail.com, [c]kppongje@kmitl.ac.th
[d]kjwithad@kmitl.ac.th, [e]teerapat.c@msu.ac.th

Keywords: winglet, counter-vortex, Nusselt number, friction factor, thermal performance

Abstract. The experimental study on heat transfer enhancement in a tubular heat exchanger fitted with 60° winglet pairs is carried out by varying airflow velocity in turbulent region in the test section having a constant wall heat-flux. Effects of three blockage ratios (BR=e/D= 0.1, 0.15 and 0.2) and three pitch ratios (PR=P/D= 1, 1.5 and 2) of the winglet pairs on heat transfer rates in the terms of Nusselt number (Nu) and pressure loss in the form of friction factor (*f*) are examined. The experimental results illustrated that the tube with winglet pair insert provides the heat transfer rate higher than the smooth tube around 1.7 to 2.6 times, depending upon operating conditions. The thermal enhancement factor for using the winglet-pair turbulator is in a range of 1.03 - 1.31.

Introduction

The objective of enhanced heat transfer is to make the heat exchanger more compact to reduce overall sizes of the heat exchanger, possibly their cost or to reduce the pumping power required for a given heat transfer process, resulting in a saving of operating costs. Therefore, many investigations have been carried out to study the effect of inserted devices on heat transfer enhancement in the round tube heat exchanger such as twisted-tapes [1], wire coils [2], conical-ring [3] and delta-wing tape [4] while the winglet [5] and rib [6] are widely used in ducts or channels

According to the literature review above, several vortex-flow generating devices with different geometries have been utilized for enhancing heat transfer rate and thermal performance in tube heat exchangers. Winglets considered as an efficient vortex-generating device due to lowest pressure loss have been widely used by placing on flat surfaces of ducts or channels. However, to apply winglets in a circular tube the modification of winglet arrangements is needed by placing the winglet pairs repeatedly on the central core flow of the tube in the current work.

Experimental Set-up

Test section and winglet pair

The schematic diagram of overall experimental apparatus is shown in Fig. 1. The copper test tube with the inner diameter (D) of 50.8 mm, thickness of 2 mm and length of 3000 mm including the length of the test section (L) of 1000 mm was introduced. The test tube was heated by continually winding flexible electrical wires to provide a uniform heat flux boundary condition over the tube. The outer surface of the test tube was well insulated to minimize any convective heat loss to surroundings and necessary precautions were taken to prevent any leakages from the system.

Details of the test tubes inserted with 60° winglet pairs are demonstrated in Fig. 2. All winglets used in the present work are made of aluminum strip with 0.3 mm thickness. During experiments, the winglets were inserted into the test tube using small steel rods to tie all winglet elements together at three different winglet heights, namely, 5, 7.5 and 10 mm (BR=e/D= 0.1, 0.15 and 0.2) and three different pitch lengths; P=50, 75 and 100 mm (PR=1, 1.5 and 2).

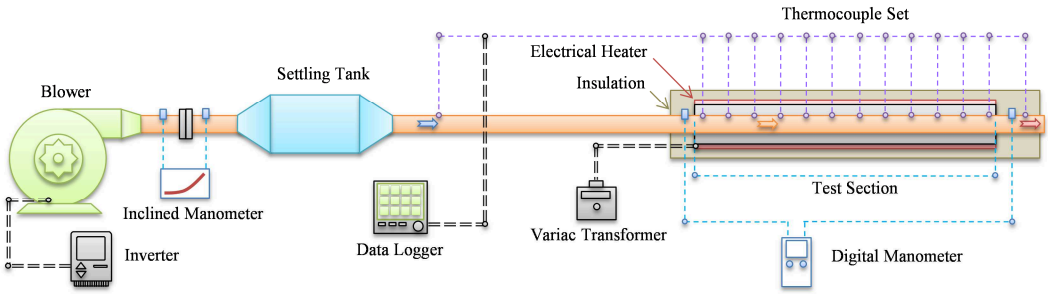

Figure 1. Schematic diagrams of experimental apparatus.

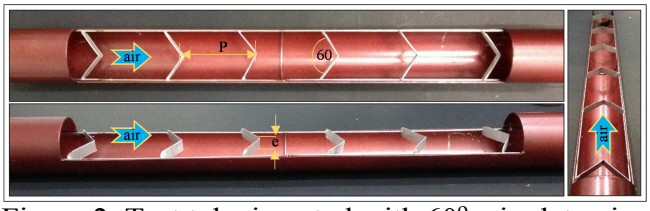

Figure 2. Test tube inserted with 60° winglet pairs.

Experimental procedure

During apparatus setting, the inlet bulk air from a 1.5 kW blower was directed through an orifice flow-meter and passed to the test section. The airflow rate was measured by the flow-meter, built under ASME standard [7] and calibrated by using a hot-wire anemometer to measure flow velocities across the tube section. Manometric fluid was applied in an inclined manometer with specific gravity (SG) of 0.826 to assure the accurate pressure drop measurement across the orifice. The volumetric airflow rates from the blower were adjusted by varying motor speed through an inverter. The electric heater's electrical output power was controlled by a variac transformer to obtain a uniform heat flux along the entire length of the test section. The inlet and outlet air temperatures in the tube were measured by RTD-type thermocouples while the surface temperatures (T_w) were measured by 24 K-type thermocouples located equally along the test section. The temperature and the changes of it were consistently recorded using a data logger. The pressure drop across the test section was measured using a digital manometer. The air flowing were controlled in the range of Re=5,300-24,000.

Experimental uncertainty

To quantify the uncertainties of measurements, the reduced data obtained experimentally were determined. The uncertainty in the data calculation was based on Ref. [8]. The maximum uncertainties of non-dimensional parameters were ±5% for Reynolds number, ±7.6% for Nusselt number and ±9.5% for friction. The uncertainty in the axial velocity measurement was estimated to be less than ±5%, and pressure has a corresponding estimated uncertainty of ±5%, whereas the uncertainty in temperature measurement at the tube wall was about ±0.5%.

Data reduction

The Reynolds number (*Re*) is given by

$$\mathrm{Re} = UD\ /\nu \tag{1}$$

The friction factor (*f*) computed by pressure drop across the length of the test section (*L*) is

$$f = \frac{2}{(L/D)} \frac{\Delta P}{\rho U^2} \tag{2}$$

In the experiment, the steady state of the convective heat transfer rate is assumed to be equal to the heat loss from the test section. The average heat transfer coefficient (h) are estimated as follows:

$$h = \dot{m} C_{p,a} (T_o - T_i) / A(\tilde{T}_w - T_b) \tag{3}$$

The heat transfer is calculated from Nusselt number which can be obtained by

$$\mathrm{Nu} = \frac{hD}{k} \tag{4}$$

For constant pumping power and the relationship between friction and Reynolds number. The thermal enhancement factor (TEF) is given by

$$\mathrm{TEF} = (\mathrm{Nu}/\mathrm{Nu}_0)/(f/f_0)^{1/3} \tag{5}$$

Results and discussion

Validation of plain tube

In the present work, the heat transfer and pressure drop results of plain tube in terms of Nussult number (Nu) and friction factor (f) are, respectively, verified with the Nu and f correlations [9] of Dittus-Boelter and Blasius depicted in Fig. 3. In the figure, the measured data are in good agreement with the correlation's data. The average deviation of the measured is about 5% for Nu and 6% for f.

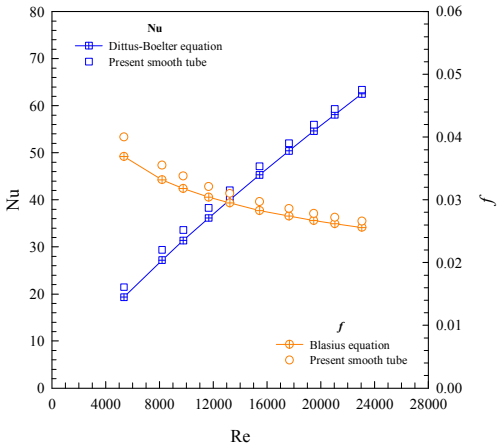

Figure 3. Verification of (a) Nu and (b) f for plain tube.

Effect of 60^o winglet pair on heat transfer and friction factor

The relationships between heat transfer (Nu) and Re of the tube inserted with 60^o winglet pairs are demonstrated in Fig. 4a. From the figure, the heat transfer enhancement values of the tube with winglets are found to be much higher than the smooth tube alone. This is due to the interruption of thermal boundary layer of flow by the turbulators. The Nu increases with the increase of BR but the decrease of PR due to higher turbulence intensity imparted to the flow between winglets elements that leading to a better and rapid mixing of the fluid and resulting in higher temperature gradients near the tube wall. In the present work, the mean Nu values for the winglet pair at BR= 0.1, 0.15 and 0.2 are found to be about 2.05, 2.46 and 2.66; 1.90, 2.24 and 2.45; and 1.70, 2.01 and 2.21 times over the smooth tube for PR = 1, 1.5 and 2, respectively.

Figure 4b presents the variation of friction factor (*f*) with Re values. It is clearly observed in the figure that the *f* tends to decrease with the increment of Re. The winglets provide a substantial increase in *f* over the smooth tube. This can be attributed to the dissipation of dynamic pressure of the fluid due to higher surface area and the act caused by the reverse/swirl flow. The *f* increases with the rise of BR but the decreases of PR. This is because of higher flow blockage from the winglets. In the present work, the mean *f* value for the winglets at BR= 0.1, 0.15 and 0.2 are about 5.29, 9.60 and 13.8; 3.87, 6.74 and 9.43; and 3.08, 5.27 and 7.49 times over the smooth tube for PR = 1, 1.5 and 2, respectively.

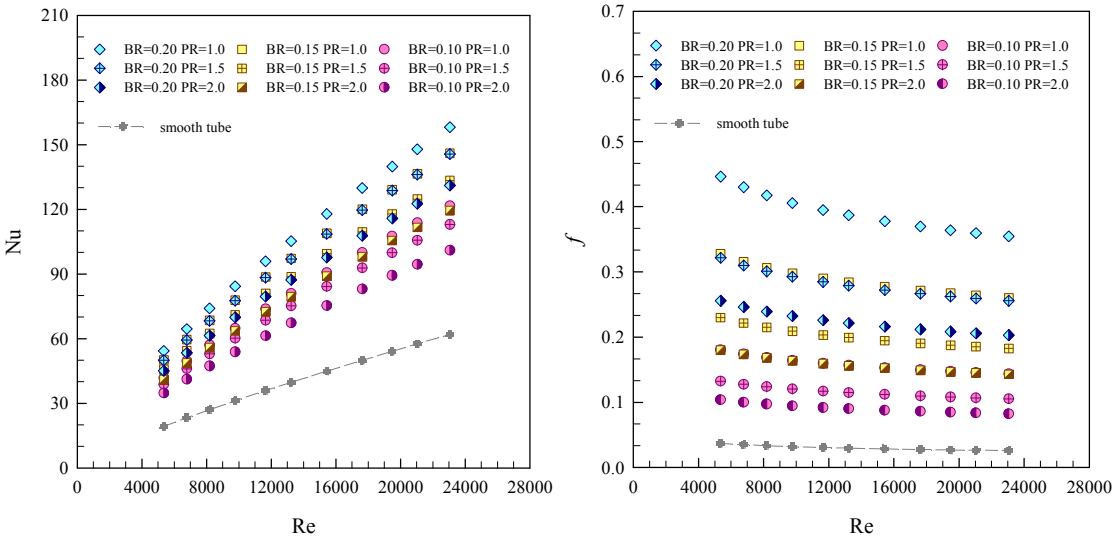

(a) (b)

Figure 4. Variation of (a) Nu and (b) *f* with Re for various 60° winglet pairs.

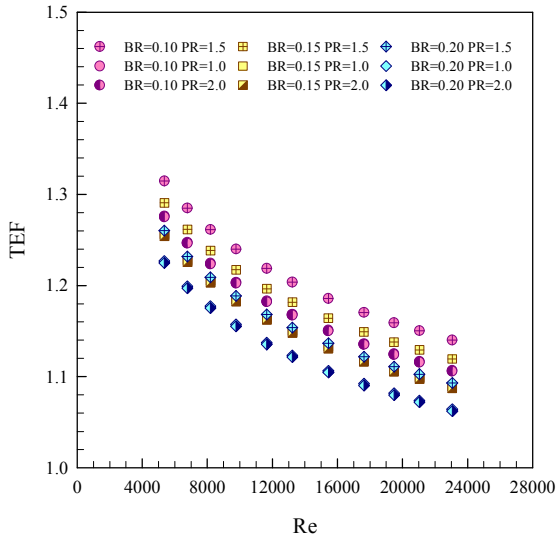

Figure 5. Variation of TEF with Re.

Effect of 60° winglet pairs on thermal performance

Figure 5 shows the variation of the thermal enhancement factor (TEF) with Re at various PR and BR values. It can be seen from the figure that the TEF generally is above unity for all the winglet inserts, indicating that the use of winglet turbulators is advantageous over the smooth tube. The TEF tends to decrease with the increment of Re and the BR for all winglet inserts. At PR=1.5, the TEF values of the winglets are about 1.07-1.31, 1.05-1.29 and 1.03-1.26 for BR=0.1, 0.15 and 0.2, respectively. The maximum enhancement factor of the winglet pairs is 1.31 at Re=5300 for the BR=0.1 and PR=1.5, in the present work.

Conclusions

The heat transfer and the friction factor characteristics in a round tube inserted repeatedly with 60^o winglet pairs at three BR and PR values have been investigated for the turbulent regime, Re=5300 - 24,000 under a uniform heat-flux condition. In the present study, the following conclusions can be drawn.

- The use of the 60^o winglet pairs leads to considerable heat transfer enhancement over the plain tube at about 170 to 266%, depending on the Re, BR and PR values.
- The *f* of using the winglet pairs is found to be 3.08-13.81 times above that of the smooth tube. The *f* tends to decrease with the rise of PRs but with decreasing BRs.
- The TEF for the winglet pairs is in a range of 1.03-1.31. Thus, the winglet insert is a promising method to improve thermal systems in many industrial applications.

Acknowledgements

The authors would like to gratefully acknowledge the Thailand Research Fund (TRF) for the financial support of this research.

References

[1] S.W. Chang, K.W. Yu, M.H. Lu, Heat transfer in tubes fitted with single, twin and triple twisted tapes, Exp. Heat Tran., 18, (2005), 279–294.

[2] P. Promvonge, Thermal performance in circular tube fitted with coiled square wires, Energy Conversion and Management 49 (5) (2008) 980–987.

[3] A. Durmus, Heat transfer and exergy loss in cut out conical turbulators, Energy Conversion and Management 45 (5) (2004) 785–796.

[4] S. Eiamsa-ard and P. Promvonge, Influence of Double-sided Delta-wing Tape Insert with Alternate-axes on Flow and Heat Transfer Characteristics in a Heat Exchanger Tube, Chinese Journal of Chemical Engineering, 19 (3) (2011) 410-423.

[5] T. Chompookham, C. Thianpong, S. Kwankaomeng, P. Promvonge, Heat transfer augmentation in a wedge-ribbed channel using winglet vortex generators, International Communications in Heat and Mass Transfer, 37 (2010) 163–169.

[6] G. Tanda, Heat transfer in rectangular channel with transverse and V-shaped broken ribs. International Journal of Heat and Mass Transfer 47 (2004) 229-243.

[7] ASME, “Standard Measurement of fluid flow in pipes using orifice, nozzle and venture”, ASME MFC–3M-1984, United Engineering Center 345 East 47th Street, New York, (1984), 1–56.

[8] ANSI/ASME, “Measurement uncertainty”, PTC 19, Part I, (1986), 1–1985.

[9] F.B. Incropera, P.D. Witt, T.L. Bergman, A.S. Lavine, Fundamentals of Heat and Mass Transfer, John-Wiley & Sons, (2006).

KKU International Engineering
10.4028/www.scientific.net/AMR.931-932

Heat Transfer Augmentation in a Round Tube with 60^{o} Winglet Pair Inserts
10.4028/www.scientific.net/AMR.931-932.1188

KKU International Engineering Conference

Part 2

Edited by
Sujin Bureerat

TRANS TECH PUBLICATIONS

ISBN-13: 978-3-03835-090-3
Advanced Materials Research Vols. 931-932, Part 2
Electronically available at *http://www.scientific.net*

Advanced Materials Research Vols. 931-932 (2014) pp 1198-1202
Online available since 2014/May/09 at www.scientific.net

doi:10.4028/www.scientific.net/AMR.931-932.1198

Thermal Performance in Circular Tube with Co/Counter-Twisted tapes

Suriya Chokphoemphun[1, a],Chayodom Hinthao[1,b], SmithEiamsa-ard[2, c],
Pongjet Promvonge[1,d*]andChinaruk Thianpong[1,e]

[1]Department of Mechanical Engineering, Faculty of Engineering,
King Mongkut'sInstitute of Technology Ladkrabang, Bangkok10520, Thailand

[2]Department of Mechanical Engineering, Faculty of Engineering,
MahanakornUniversity of Technology, Bangkok10530, Thailand

[a]chok_suriya_@hotmail.com, [b]chayodom.korphai@gmail.com,[c]smith@mut.ac.th,
[d]kppongje@kmitl.ac.th, [e]cthiapong@kmitl.ac.th

Keywords: co-twisted tape,counter-twisted tape,Nusselt number, friction factor, thermal performance

Abstract. Thiswork presents an experimental study on enhanced heat transfer and pressure loss characteristics in a tube having a uniform heat-fluxed wall by using small double and triple co- and counter-twisted tapes at two twist ratios, *y*/*w*=4 and 4.5. The investigation has been conducted for Reynolds number from 5300-20,000. The experimental results of the heat transfer and pressure drop are proposed in terms of Nusselt number and friction factor, respectively.The experimental results reveal thatthe maximum TEF for the triple counter-twisted tapesat smaller twist ratio isabout 1.26.

Introduction

Many investigations have been carried out to study the effect of turbulators with various geometries on heat transfer characteristics in heat exchanger tubes. However, twisted tapes as one of the turbulators have been applied extensively to enhance convection heat transfer in tubular heat exchanger systems due to the need for finding the way to reduce the size and cost of those systems. For decades, the heat transfer enhancement by twisted-tape inserts has been widely investigated both experimentally and numerically. In the earlier papers, heat transfer and pressure loss characteristics of a flow through a circular tube fitted with regularly-spaced twisted-tape elements [1], straight full twisted tape insert with different spacer distances [2], short-width twisted-tapes [3], alternate clockwise and counterclockwise twisted-tapes [4], twin and triple twisted-tapes [5] and multiple twisted-tapes inserts [6]were investigated

In the literature review above, many investigations are almost focused on the use of typical and modified singletwisted tapes and multiple twisted tapes with similar tape-twist direction while the effect of multiple small tapes with loose-fit position and tape-twist direction arrangements has rarely been reported.Therefore, the utilization of double and triple twisted-tapes with co- and counter-twist arrangements is offered as an enhancement device in the present work.

Experimental Set-up

A detail of the experimental apparatus used in the present work is displayed schematically in Fig. 1. In the apparatus, the room air from a 1.5 kW blower was directed through an orifice flow-meter and passed to the heat transfer test section. The airflow rate was measured by the orifice flow-meter, built according to ASME standard [7] and calibrated by using a hot-wire anemometer to measure flow velocities across the tube section. Manometric fluid was used in an inclined manometer with specific gravity (SG) of 0.826 to ensure reasonably accurate measurement of pressure drop across the orifice. The volumetric airflow rate from the blower was controlled as desired by varying the motor speed of the blower through an inverter. The inner (*D*) and outer diameters of the copper test tube was, respectively, 50.8 and 54.8 mm and the tube was 3000 mm long, included the test section

of 1000 mm. The test tube was heated by continually winding flexible electrical wire on the outer tube wall. The electrical output power was controlled by a variac transformer to obtain a uniform heat-flux along the entire length of the test section. The outer surface of the test tube was well insulated to minimize heat loss to surroundings. The inlet and outlet air temperatures in the tube were measured by RTD-type thermocouples while the surface temperatures (T_w) were measured by 24 K-type thermocouples located equally along the test section. All of the temperatures getting from the system were consistently recorded using a data logger. The pressure drop across the test section was measured by a digital manometer. Reynolds numbers for the air flowing through the test section were controlled in the range of 5300 to 20,000.

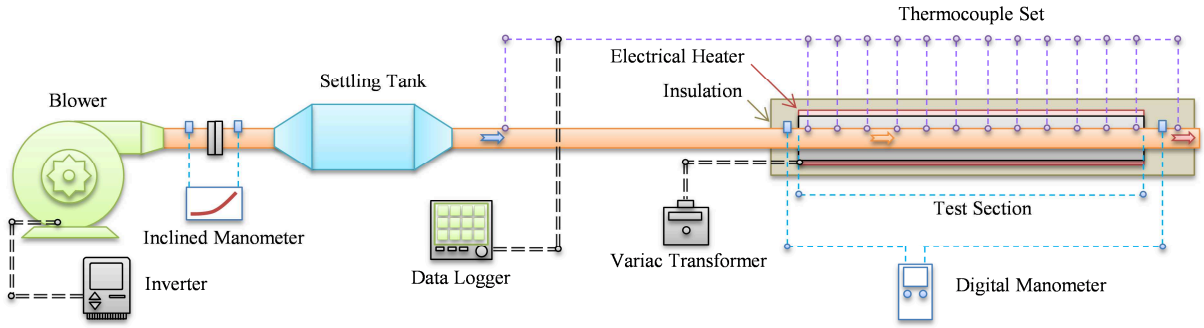

Figure 1 Schematic diagrams of experimental apparatus.

The photographs of the tube inserted with double and triple co- and counter-twisted tapes for all cases studied are shown in Fig. 2. In the figure, details on twisted-tape assembly indicating the number of twisted tapes (N), the arrangement and the designation of each case were provided. All twisted-tapes made of 0.8 mm aluminum sheet were 1000 mm long and 9 mm width (w) with two different twist lengths (y): 32 and 36 mm (twist ratio, y/w = 4 and 4.5). All the tapes were twisted in two different directions: left-twist (L) and right-twist (R), and were arranged in different forms.

To quantify the uncertainties of measurements, the reduced data obtained experimentally were determined. The uncertainty in the data calculation was based on Ref. [8]. The maximum uncertainties of non-dimensional parameters were ±5% for Reynolds number, ±7.6% for Nusselt number and ±9.5% for friction. The uncertainty in the axial velocity measurement was estimated to be less than ±5%, and pressure has a corresponding estimated uncertainty of ±5%, whereas the uncertainty in temperature measurement at the tube wall was about ±0.5%.

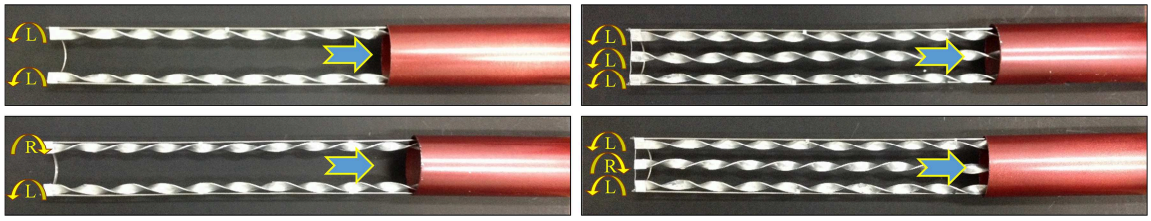

Figure 2 Test tube inserted with various numbers of twisted tapes.

Data reduction

The independent parameters are Reynolds number (Re), the number of twisted tapes (N),twist ratio (y/w) and twisteddirections. The Reynolds number is given by

$$\mathrm{Re}=UD/\nu \tag{1}$$

The friction factor (f) computed by pressure drop across the test tube length (L) is written as

$$f=\frac{2}{(L/D)}\frac{\Delta P}{\rho U^2} \tag{2}$$

in which U is mean air velocity of the test tube.

In the experiment, air flowed through the test tube under a uniform heat-flux condition. The steady state of the heat transfer rate is assumed to be equal to the heat loss from the test section which can be expressed as:

$$Q_a = \dot{m}C_{p,a}(T_o - T_i) = Q_{conv} = hA(\tilde{T}_w - T_b) \quad (3)$$

where T_w is the local wall temperature and evaluated at the outer wall surface of the test tube. The averaged wall temperature was calculated from 24 points of surface temperatures lined equally between the inlet and the exit of the test tube. The average heat transfer coefficient (h) and the mean Nusselt number (Nu) are estimated as follows:

$$h = \dot{m}C_{p,a}(T_o - T_i)/A(\tilde{T}_w - T_b) \quad (4)$$

The heat transfer is calculated from the Nusselt number which can be obtained by

$$\mathrm{Nu} = \frac{hD}{k} \quad (5)$$

All of thermo-physical properties of the air are determined at the overall bulk air temperature (T_b). To assess the practical use of the enhanced tube, the performance of the enhanced tube is evaluated relatively to the smooth tube at an identical pumping power in the form of thermal performance enhancement factor (TEF) which can be expressed as

$$\mathrm{TEF} = (\mathrm{Nu}/\mathrm{Nu}_0)/(f/f_0)^{1/3} \quad (6)$$

Results and discussion

Validation of plain tube

In the present work, the heat transfer and pressure drop results of plain tube in terms of Nussult number (Nu) and friction factor (f) are, respectively, verified with the Nu and f correlations [9] of Dittus-Boelter and Blasius. The measured data are in good agreement with the correlation's data. The average deviation of the measured is about 5% for Nu and 6% for f.

Effect of twisted-tape on heat transfer

The variation of Nusselt number ratio, $\mathrm{Nu}/\mathrm{Nu}_0$ with Re for the tube with multiple twisted-tape inserts is depicted in Fig. 3(a).The Nu increases with decreasing the twist ratio and the increment of N.Due to the increase of swirl intensity imparted to the flow at the tube wall, the heat transfer rate of the inserted tube is found to be considerably higher than that of the plain tube. This can be attributed to the strong swirl enhancing the flow turbulence intensity, leading to higher convection heat transfer than the axial flow in the plain tube. Thus, the higher vortex flow, the greater Nu becomes. The $\mathrm{Nu}/\mathrm{Nu}_0$ defined as a ratio of augmented Nu to Nu of plain tube shows a decrease trend with the rise of Re for all cases studied as can be seen in Fig. 3(a). Under the present measured data, the $\mathrm{Nu}/\mathrm{Nu}_0$ values for the LL, LR, LLL and LRL tapes are, respectively, in a range of 1.02-1.30, 1.05-1.34, 1.14-1.45 and 1.19-1.52 at y/w=4 and 1.01-1.29, 1.04-1.32, 1.11-1.41 and 1.15-1.47 at y/w=4.5 depending on the Re value.

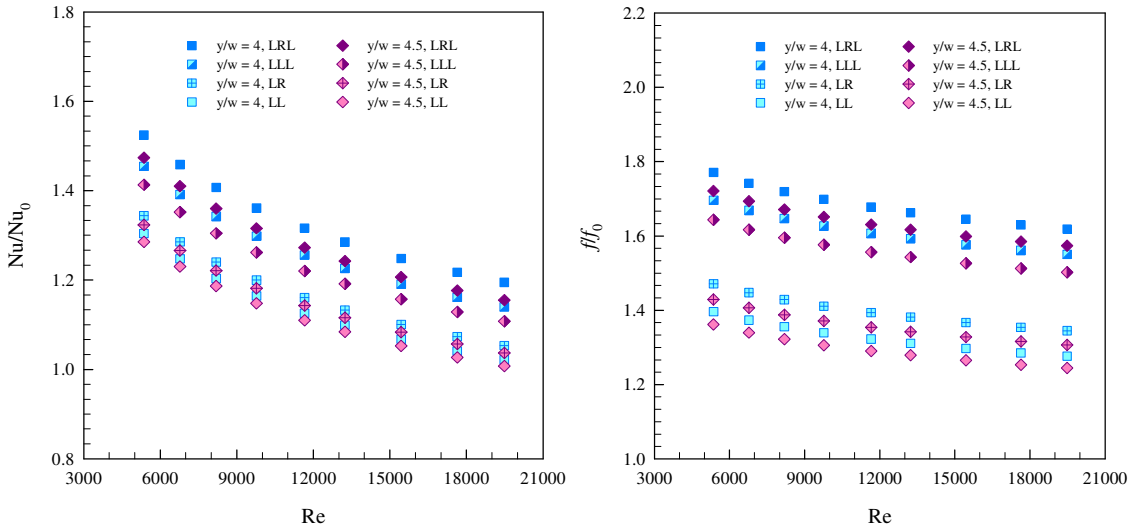

(a) (b)

Figure 3 Variation of (a) Nu/Nu_0 and (b) f/f_0 with Re for various twisted tapes.

Effect of twisted-tape on friction factor

The influence of different twisted-tape number and arrangements on the f/f_0 characteristics against the Re is depicted in Fig. 3(b). It is interesting to note in the figure that the application of twisted tapes gives rise to the f considerably higher than that of the plain tube with no insert. The higher friction loss mainly comes from the increased surface area and higher swirl intensity. The f/f_0 decreases with the increment of y/w and the reduction of N. The f/f_0 values for the counter-twisted tapes (LR and LRL) are seen to be higher than those for the co-twisted ones (LL and LLL). It can be observed that the f/f_0 tends to decrease with the increment of Re. The f/f_0 values for the LL, LR, LLL and LRL tapes are, respectively, in a range of 1.28-1.40, 1.35-1.47, 1.55-1.70 and 1.62-1.77 fory/w=4 and of 1.24-1.36, 1.31-1.43, 1.50-1.64 and 1.57-1.72 fory/w=4.5.

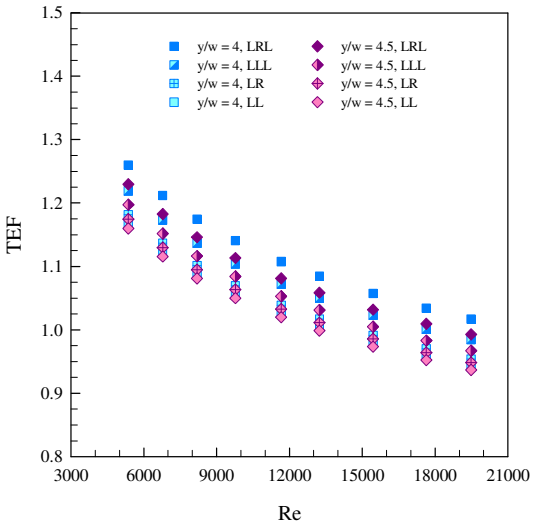

Figure 4 Variation of TEF with Re.

Performance assessment

Figure4 presents the variation of the thermal enhancement factor (TEF) with the Re. In the figure, the TEF tends to decrease with the increase of Re for all the tapes studied. The counter-twisted tapes provide higher TEF than the co-twisted tapes and the maximum TEF of about 1.26 is found for the triple counter-twisted tapes (LRL) at y/w=4. It is interesting to note that the TEF tends to increase with the increment of N.

Conclusions

An experimental study has been conducted to examine the heat transfer and flow friction characteristics in a circular tube inserted with small double and triple twisted tapes arranged in different forms of the co-twisted and counter-twisted tapes for the turbulent regime,Re from about 5300 to 24,000 under a uniform wall heat-flux. The Nu is in the range of 1.01-1.52 times while the f is 1.24-1.77 times above the plain tube. Both the Nu and f are seen to be increased with the increment of N and with the counter-twisted tape arrangements. The TEF tends to reduce with the increase in Re and the decrease of the number of twisted tapes.

Acknowledgements

The authors would like to gratefully acknowledge the Thailand Research Fund (TRF) for the financial support of this research.

References

[1] S. Eiamsa-ard, C. Thianpong, P. Promvonge, Experimental investigation of heat transfer and flow friction in a circular tube fitted with regularly spaced twisted tape elements, Int. Commun. Heat Mass Transfer, 33 (10), (2006), 1225–1233.

[2] S.R.Krishna, G. Pathipaka, P. Sivashanmugam, Heat transfer and pressure drop studies in a circular tube fitted with straight full twist, Exp. Therm. Fluid Sci., 33 (3), (2009), 431–438.

[3] W. Liu, K. Yang, Z.C. Liu, T.Z. Ming, A.W. Fan, C. Yang, Mechanism of heat transfer enhancement in the core flow of a tube and its numerical simulation, Open Transport Phenom J., 2,(2010), 9–15.

[4] S. Eiamsa-ard, P. Promvonge, Performance assessment in a heat exchanger tube with alternate clockwise and counter-clockwise twisted-tape inserts, Int. J. Heat Mass Transfer, 53 (7–8), (2010), 1364–1372.

[5] S.W. Chang, K.W. Yu, M.H. Lu, Heat transfer in tubes fitted with single, twin and triple twisted tapes, Exp. Heat Tran., 18, (2005), 279–294.

[6] Xiaoyu Zhang, Zhichun Liu, Wei Liu, Numerical studies on heat transfer and flow characteristics for laminar flow in a tube with multiple regularly spaced twisted tapes, Int. J. Therm. Sci., 58, (2012), 157–167.

[7] ASME, “Standard Measurement of fluid flow in pipes using orifice, nozzle and venture”, ASME MFC–3M-1984, United Engineering Center 345 East 47th Street, New York, (1984), 1–56.

[8] ANSI/ASME, “Measurement uncertainty”, PTC 19, Part I, (1986), 1–1985.

[9] F.B. Incropera, P.D. Witt, T.L. Bergman, A.S. Lavine, Fundamentals of Heat and Mass Transfer, John-Wiley & Sons, (2006).

KKU International Engineering
10.4028/www.scientific.net/AMR.931-932

Thermal Performance in Circular Tube with Co/Counter-Twisted Tapes
10.4028/www.scientific.net/AMR.931-932.1198

AUTHOR BIOGRAPHY

Name : Mr.Suriya Chokphoemphun

Date of Birth : 26 August 1984

Address : House No.201, Pradistpana Road, Nangrong sub-district, Nangrong district, Buriram province, 31110, Thailand
Tel.087-717-1543

Education :

2003 High school
Nangrong School

2006 Bachelor degree of engineering (Mechanical Engineerig)
Suranaree University of Technology
Academic Advisor : Assoc. Dr.Tawit Chitsomboon
Thesis Advisor : Dr.Teerachat Pornpiboon
Bachelor thesis title : Energy Audit

2009 Master degree of engineering (Mechanical Engineerig)
King Mongkut's Institute of Technology Ladkrabang
Academic Advisor : Assoc. Dr.Pongjet Promvonge
Thesis Advisor : Assoc. Dr.Pongjet Promvonge
Master thesis title : Experimental study on rice husk combustion in a fluidized bed with longitudinal vortex generators

Research experience/expertise fields : Applied Heat Transfer, Thermo-fluid

Scholarships

2007 Teaching Assistant Scholarship, King Mongkut's Institute of Technology Ladkrabang

2008 Teaching Assistant Scholarship, King Mongkut's Institute of Technology Ladkrabang

2009 The Royal Golden Jubilee Ph.D. program (Grant No. PhD/0143/2552), Thailand Research Fund (TRF)

Publications

International Journal

1. Chokphoemphun, S. Pimsarn, M. Thianpong, C. and Promvonge, P. "Heat Transfer Augmentation in a Circular Tube with Winglet Vortex Generators."

has been accepted by *Chinese Journal of Chemical Engineering*. at 2014-04-18

2. Chokphoemphun, S. Pimsarn, M. Thianpong, C. and Promvonge, P. "Thermal Performance of Tubular Heat Exchanger with Multiple Twisted-tape Inserts." has been accepted by *Chinese Journal of Chemical Engineering*. at 2014-07-5
3. Chokphoemphun, S. Tongyote, P. Promvonge, P. Jedsadaratanachai, W and Chompookham, T. 2014. "Heat transfer augmentation in a round tube with 60° Winglet Pair inserts." *Advanced Materials Research*. 931-932 : 1188-1192.
4. Chokphoemphun, S. Hinthao, C. Eiamsa-ard, S. Promvonge, P. and Thianpong. C. 2014. "Thermal Performance in Circular Tube with Co/Counter-Twisted tapes." *Advanced Materials Research*. 931-932 : 1198-1202.

National Journal

1. Chokphoemphun, S. Chompookham, T. and Promvonge. P. 2014 "Heat Transfer Enhancement in a Tube Heat Exchanger with a V-Shape Winglet Turbulator." *KKU Research Journal*. 19(2) :

International Conference

1. Chokphoemphun, S. Skullong S. and Promvonge. P. 2011 "Thermal Characteristics in Square Channel with 45° U-Shaped Ribs." *1st International Symposium on Technology for Sustainability (ISTS)*. 26-29 January 2012, KMITL, Bangkok, Thailand
2. Chokphoemphun, S. Chompookham, T. Skullong, S.and Promvonge. P. 2012. "Heat Transfer in Solar Air Heater Channel with Inline 45° Wavy-Ribs." *International Conference on Green and Sustainable Innovation (ICGSI)*. 24-26 May 2012, Chiang Mai, Thailand.
3. Chokphoemphun, S. Skullong, S. Chompookham, T. Limkul T. and Promvonge. P. 2012. "Turbulent Heat Transfer in a Channel with Rib-Groove Turbulators." *The 3rd TSME International Conference on Mechanical Engineering (ICoME)*. October 2012, Chiang Rai, Thailand.
4. Chokphoemphun, S. Tongyote, P. Chompookham, T. Skullong, S. Promvonge P. and Jansangsuk. D. 2013. "Experimental study on Heat transfer augmentation in a round tube with V-shaped ribs." *International Conference on Interdisciplinary Research and Development in ASEAN*

Universities (ICIRD). 8-10 August 2013, Imperial Mae Ping Hotel, Chiang Mai, Thailand.

5. Hinthao, C. Chokphoemphun, S. Promvonge, P. Thianpong, C. Skullong, S. Chingtoaytong W. and Chompookham. T. 2013. "Heat transfer augmentation in square duct with 30° V-finned tape inserts." *Joint Symposium on Mechanical-Industrial Engineering, and Robotics (MIER).* 14-17 November 2013, Centara Duangtawan Hotel, Chiang Mai, Thailand.